Characterisation of MYB and TRKB as candidate targets in *CYLD* cutaneous syndrome

Naomi Kathryn Sinclair

Thesis submitted for the degree of Doctor of Philosophy

Newcastle University

Faculty of Medical Sciences

Institute of Genetic Medicine

December 2017

Abstract

CYLD cutaneous syndrome is a rare, autosomal dominant inherited disease in which an individual is predisposed to developing multiple cutaneous tumours; namely cylindromas, spiradenomas and trichoepitheliomas, due to germline mutations in the tumour suppressor gene *CYLD.* However at present there are no curative treatments other than repetitive surgery to control tumour burden. Therefore, an overarching theme of this thesis was to identify potential therapeutic targets that could possibly translate into treatment strategies in the clinic.

The first strategic target, c-MYB, was explored, as overexpression of c-MYB was previously shown in sporadic cylindromas due to the presence of the fusion protein MYB-NFIB. It was demonstrated that inherited cylindromas did not express the MYB-NFIB fusion protein. However, using immunohistochemistry c-MYB was shown to be overexpressed in inherited tumours and that gene silencing of *MYB* caused a reduction in cell viability. A novel finding, transcriptomic and protein analysis also revealed that keratinocytes expressed the alternate MYB 9B isoform.

A second strategic target, Trk, was explored using RNA-seq of CYLD defective tumours. Exploration of Trk signalling in these tumour cells found that the truncated TrkB.T1 isoform of the TrkB receptor is overexpressed in the tumours, alongside the receptors cognate ligand BDNF. Overexpression of TrkB.T1 in the HaCaT, keratinocyte cell line, indicated that TrkB.T1 increased cell survival. BDNF stimulation of TrkB.T1 overexpressing cells caused Stat3 phosphorylation, and in primary cylindroma tumour cells BDNF stimulation increased the nuclear localisation of Stat3.

Finally, a three-dimensional spheroid cell culture method was established and characterised using immunofluorescence, as 3D *in vitro* models better reflect the *in vivo* environment. The cultures were found to have an expression pattern similar to their *in vivo* counterparts and were shown to be sensitive to inhibitory Stat3 targeting, supporting the translational relevance of this work in the hope of bringing targeted therapies for *CYLD* cutaneous syndrome to the clinic.

Dedication

This thesis is dedicated to my Gramps

Acknowledgements

First and foremost, I would like to thank my principal supervisor Dr. Neil Rajan for giving me the opportunity to undertake this project, and for his guidance and support throughout the past 5 years. I have thoroughly enjoyed being a part of the establishment of your research group and working in such a supportive environment; I don't think I'll ever get my own tissue culture room again! I would also like to thank my second supervisor Professor David Elliott for his encouragement and helpful suggestions throughout this project. In addition, I am grateful to our collaborators, including members of the group of Professor Goran Stenman (University of Gothenburg, Sweden), who undertook the FISH and MYB knockdown studies in Chapter 3. Finally, I am indebted to the patients who generously donated tissue samples and enabled this research.

I also have to extend my thanks to my colleagues in the IGM who have made my time in the lab such an enjoyable experience. I am thankful to all those who have shared our office and lab home over the past few years, but special thanks goes to Kirsty Hodgson, Dr. Majid Arefi, Dr. Ella Dennis, Robert Jackson, Beth Gibson, and Thais De Las Heras Ruiz, for always being there for much needed coffee breaks, chats, and cake supplies.

Finally, a special thank you goes to my family. I am forever grateful for your unwavering support and encouragement, however you can now stop with 'is it done yet?' Also many thanks go to Arran and his family, I know this thesis would have taken twice as long without your support. Arran your positivity, love and patience have got me here and yes, we can go now.

Declaration

I, Naomi Sinclair, declare that no portion of the work compiled in this thesis has been submitted in support of another degree or qualification at this or any other University or Institute of Learning. This thesis includes nothing that is the work of others, nor the outcomes of work done in collaboration, except where otherwise stated.

Naomi Sinclair

Table of Contents

List of Figures

List of Tables

Abbreviations

2D/3D	Two/Three dimensional
αα	Amino acid
ACC	Adenoid cystic carcinoma
AMV	Avian myeloblastosis virus
ATP	Adenosine triphosphate
BCC	Basal cell carcinoma
BCL	B-cell lymphoma protein
BDNF	Brain derived neurotrophic factor
BSS	Brooke-Spiegler syndrome
CAP-Gly	Cytoskeleton-asociated protein glycine-rich domain
CD	Cluster of differentiation
cDNA	Complementary DNA
CK	Cytokeratin
CPCC	Cylindroma primay cell culture
Ct	Cycle threshold
CTD	Carboxy terminal domain
CYLD	Cylindromatosis tumour suppressor gene
DAPI	4',6-Diamidino-2-phenylindole
DKK2	Dickkopf 2
DMBA	7,12-Dimethylbenz(a)anthracene
DMEM	Dulbecco's modified eagle medium
DMSO	Dimethyl sulfoxide
DNA	Deoxyribonucleic acid
dNTPs	Deoxynucleotide triphosphates
DSL	Delta-Serrate-Lag
DTT	Dithiothreitol
DUB	Deubiquitinating enzyme
Dvl	Dishevelled
ECM	Extracellular matrix
ERK	Extracellular signal-related kinase
FC	Familial Cylindromatosis
GFP	Green fluorescent protein

GSK3-β	Glycogen synthase kinase 3-β
HaCaT	Immortalised keratinocyte cell line
HCC	Hepatocellular carcinoma
H&E	Haematoxylin and Eosin
HDAC	Histone deacetylase
HEK293T	Human embryonic kidney cell line
HeLa	Ovarian cancer cell line
HRP	Horse-radish peroxidase
HSC	Haematopoietic stem cell
HSE	Heat shock element
IFN	Interferon
Ig	Immunoglobulin
IκB	Inhibitor of NF-κB
IKK	IκB kinase
IL	Interleukin
JAG2	Jagged 2
JNK	c-Jun NH_2-terminal kinase
K63	Lysine 63
Kb	kilobases
KSFM	Keratinocyte serum-free media
LB	Lysogeny Broth
LPS	Lipopolysaccharide
LOH	Loss of heterozygosity
LSE	Living skin equivalent
MAPK	Mitogen activated protein kinase
MBS	MYB binding site
MIB2	Mind-bomb homologue 2
miRNA	MicroRNA
MKK	MAPK kinase
MFT	Multiple trichoepithelioma
MYB	Myeloblastosis
NEMO	NF-kB essential modulator
NFκB	Nuclear factor kappa-light-chain-enhancer of activated B cells

NGF	Nerve growth factor
NIK	NF-kB inducing kinase
NLK	Nemo like kinase
NRD	Negative regulatory domain
NT	Neurotrophin
NTR	Neurotrophin receptor
NTRK	Neurotrophic tyrosine kinase
OCT	Optimal cutting temperature compound
PAGE	Polyacrylamide gel electrophoresis
PBS	Phosphate buffered saline
PCR	Polymerase chain reaction
PLC	Phospholipase C
PMSF	Phenylmethylsulfonyl fluoride
Poly-HEMA	Poly-2-hydroxyethyl methacrylate
RANK	Receptor activator for NF-kB
qPCR	Quantitative PCR
RNA	Ribonucleic acid
SDS	Sodium dodecyl sulphate
SH	Src homology
SHH	Sonic hedgehog
SH-SY5Y	Neuroblastoma cell line
STAT3	Signal transducer and activator of transcription 3
TAK1	TGF-β-activated kinase 1
TBST	Tris-buffered saline Tween-20
TE	Trichoepithelioma
TGF-β	Transforming growth factor-β
TNF	Tumour necrosis factor
TPA	12-O-tetradecanoylphorbol 13-acetate
TRAF	TNF receptor-assocaited factor
TRK	Tropomyosin receptor kinase
Ub	Ubiquitin
USP	Ubiquitin specific protease
UTR	Untranslated region

UV	Ultraviolet
Wnt	Wingless

Chapter 1

General Introduction

1 Chapter 1: General Introduction

1.1 Inheritance of *CYLD*-defective tumours: an overview

1.1.1 *CYLD*-defective tumour syndromes

Familial cylindromatosis (FC; OMIM 313270) is a rare autosomal dominant inherited skin tumour syndrome. First described in 1842 by Henry Ancell (Ancell, 1842), affected individuals are predisposed to developing multiple benign tumours, namely cylindromas, in the head and neck region (Figure 1-1) (Rajan, Langtry*, et al.*, 2009). Due to the development of the tumours at hair bearing sites of the body, it is thought that these neoplasms are of hair follicle origin (Massoumi, Podda*, et al.*, 2006; Sellheyer, 2015), although histogenesis of the tumours is an ongoing debate. In 2000, germline mutations in the tumour-suppressor gene, *CYLD,* were found to be the underlying cause of the condition in humans (Bignell *et al.*, 2000) (discussed in more detail in section 1.2)

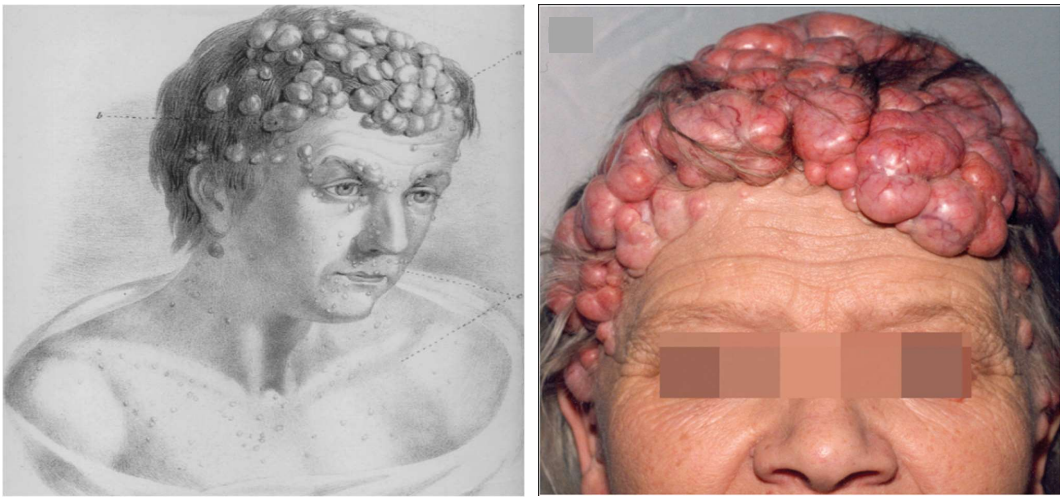

Figure 1-1: Clinical presentation of cylindroma.
An image of the first patient reported in the medical literature with cylindromas by Henry Ancell in 1842; a 52-year-old female with a strong family history of cutaneous tumour development (Image on left). Alongside a present day image of a female patient from a North East family, who presented with multiple cylindromas (Image on right).

Cylindromas are also found in two other inheritable skin tumour predisposition syndromes, multiple familial trichoepithelioma (MFT; OMIM 601606) and Brooke-Spiegler syndrome (BSS; OMIM 605041). Whilst FC is characterized by the presentation of multiple cylindromas, lower numbers of cylindroma coexist in patients affected by

MFT, with predominantly small, benign facial tumours called trichoepithelioma; hair follicle tumours, that are aggregates of basaloid cells and present as skin-coloured papules mainly on the perinasal skin (Alsaad *et al.*, 2007; Navarrete-Dechent *et al.*, 2016; Salhi *et al.*, 2004). Meanwhile BSS is considered an overlap between the two conditions, characterized by the development of multiple skin appendage tumours, including cylindromas, trichoepitheliomas and spiradenomas; tumours that are related to cylindromas that present as blue-black nodules mainly on the trunk and limbs (Obaidat *et al.*, 2007; Uede *et al.*, 2004). Patients may also present with tumours that have features of both cylindroma and spiradenoma that are called spiradenocylindroma, accordingly (Michal *et al.*, 1999; Rajan, Burn*, et al.*, 2011). The other tumour variants arising in these conditions have also been found to be manifestations of mutated *CYLD* (Table 1-1), and have recently been reviewed by (Rajan and Ashworth, 2015; Verhoeft *et al.*, 2016). In addition, milia are another phenotypic variant feature that may arise in carriers of *CYLD* mutations. These are benign, white, small skin cysts, which are seen on the face of affected individuals and can be the only presenting feature. However unlike cylindroma, milia are reported in other genetic disorders (Rutter and Judge, 2009). Therefore in the absence of other factors, they are not a determining indicator of germline *CYLD* mutations (Rajan and Ashworth, 2015).

CYLD cutaneous syndrome has been proposed as an encompassing term for the aforementioned syndromes (Rajan, Langtry*, et al.*, 2009). All three diseases are unified at the genetic level with the inheritance of germline *CYLD* mutations, and as such the diseases are considered to be clinical manifestations of an overlapping phenotypic spectrum of a single disease entity (Lee D. A. *et al.*, 2005; Oranje *et al.*, 2008; Rajan, Langtry*, et al.*, 2009; Welch *et al.*, 1968). Indeed based on the current understanding of CYLD mutations genotype-phenotype correlations have been difficult to establish (Grossmann *et al.*, 2013; Nagy *et al.*, 2015), as all three clinical phenotypes, FC, MFT or BSS can develop in affected individuals from within the same family, despite sharing the same mutation (Rajan, Langtry*, et al.*, 2009). Tumours of the skin appendages, such as cylindromas can also occur sporadically, although they tend to appear as solitary tumours in contrast to the multiple lesions that are affiliated with the aforementioned hereditary conditions.

	Familial cylindromatosis (FC)	Brooke-Spiegler syndrome (BSS)	Multiple familial trichoepithelioma (MFT)
Associated tumour	Predominantly cylindromas	Cylindromas Spiradenomas Spiradenocylindroma Trichoepitheliomas	Predominantly trichoepitheliomas
CYLD mutation	All types of *CYLD* mutation i.e. frameshift, splice-site, missense, nonsense,		
Associated skin appendage (consensus)	Hair follicle	Hair follicle Eccrine and apocrine glands (spiradenomas)	Hair follicle

Table 1-1: Tumour presentation associated with *CYLD* cutaneous syndrome

1.1.2 Clinical presentation of *CYLD*-defective tumours

The average age of onset for *CYLD* cutatenous syndrome in patients with germline *CYLD* mutations is 16 years of age (Rajan, Langtry*, et al.*, 2009). Although there are reports of the first tumours developing as early as 5 years of age (Almeida *et al.*, 2008) and as late as 42 years of age (Martins and Bartolo, 2000). Sporadic, non-inherited neoplasms generally develop later in life (Gerretsen *et al.*, 1993). In inherited conditions penetrance is estimated to be near 100% (Gerretsen *et al.*, 1995), whilst a female preponderance has been described in individuals with *CYLD* mutations (Sicinska *et al.*, 2007; Szepietowski *et al.*, 2001; van Balkom and Hennekam, 1994), analysis of large familial pedigrees supports equal penetrance in both males and females (Gerretsen *et al.*, 1995; Rajan, Langtry*, et al.*, 2009). However in the study by Rajan *et al.* it was shown that in a cohort of 26 affected individuals with germline *CYLD* mutations, of whom 14 were women and 12 were men, tumour burden of the scalp warranted complete scalp excision in 4 females compared to 1 male. This suggests that there may be increased expressivity of *CYLD* mutations presenting as a more severe phenotype in females (Rajan and Ashworth, 2015; Rajan, Langtry*, et al.*, 2009). A number of observations including: the development of tumours occurring just after puberty, when there are significant hormonal changes within the body; the increased occurrence of the tumours at hair bearing sites of the body that are susceptible sites for hormonal stimulation (Figure 1-2), such as the pubic region and areas of the scalp predisposed to androgenic alopecia; report of a women's condition becoming worse during pregnancy and after starting hormone replacement therapy, are all indicators

that hormones may influence the underlying mechanisms for tumourigenesis in these inherited conditions, and possibly presentation in males and females (Rajan, Langtry*, et al.*, 2009). Indeed, although the data is limited due to the small sample numbers, immunohistochemical analyses of the oestrogen and progesterone receptors showed that in 13 cases of cylindroma, expression was negative (Albores-Saavedra *et al.*, 2005). Whilst another group reported positive staining of oestrogen receptor-β in 2 out of 3 cases of spiradenoma, the progesterone receptor in 3 out of 3 cases of spiradenoma, and androgen receptor positivity in 1 case of spiradenoma (Kariya *et al.*, 2005). With the present understanding of these rare syndromes being incomplete, particularly as to how a loss of CYLD initiates tumour formation, this is an area that may require more attention in the future.

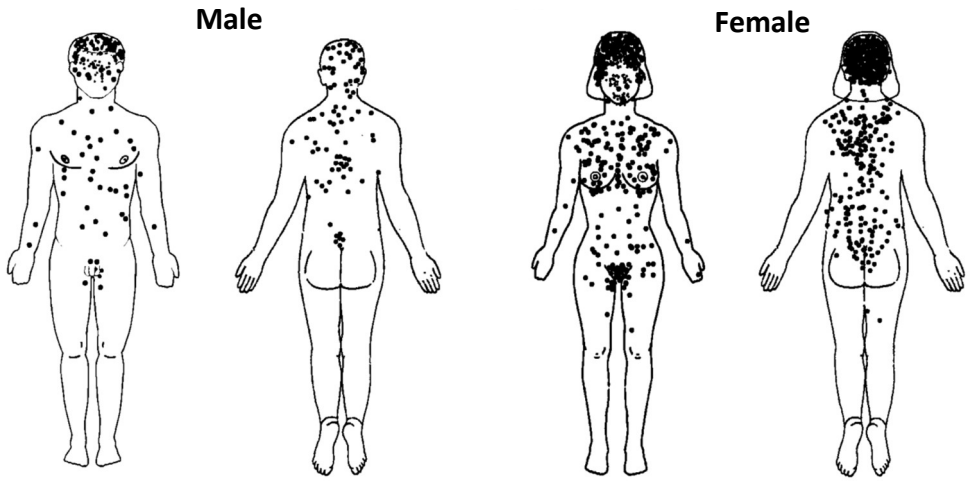

Figure 1-2: Tumour distribution maps.
Pictograms displaying the location of tumours in 14 female and 12 male patients, illustrating the predominance of tumours on the scalp but also at other locations of the body such as the torso and groin (Images from (Rajan, Trainer*, et al.*, 2009).

The distribution of the tumours is predominantly in the head and neck region, mainly the scalp for cylindroma and spiradenoma, and on the face for trichoepitheliomas. However the tumours also present on the trunk of the body and in the genital area in significant numbers (Figure 1-2) (Rajan, Langtry*, et al.*, 2009). With the high incidence of tumour formation on the face and scalp others had postulated that ultraviolet (UV) radiation could be responsible for tumour initiation (Massoumi, Chmielarska*, et al.*, 2006; Massoumi and Paus, 2007), due to the DNA damage caused by UV that is recognized in other forms of skin cancer (Kim Y. and He, 2014; Narayanan *et al.*, 2010). However the frequency with which tumours also arise on sites that are either less exposed to ultraviolet rays from the sun such as the torso, or protected skin such as

the pubic and perineal region, indicate that mechanisms independent of UV radiation are responsible for tumour formation, but that is not to say that it may not have a contributory role to malignant transformation of exposed tumours.

Cylindroma tumours are benign slow growing appendages, but become more frequent in number and increase in size over a patient's lifetime. The tumours appear as pink nodules, with blood vessels visible on the tumour surface. They are generally painless and can grow to a considerable size, measuring up to 3-5cm in diameter (Dubois *et al.*, 2017). When a significant number of cylindromas present on the scalp, the tumours can coalesce into a confluent mass, hence the historical term for the condition of Turban tumour (Evans, 1954). On the other hand spiradenomas are painful nodular tumours, which can also be deep-seated within the dermis and are generally encapsulated. They can grow to be as large as 5-10cm in their diameter and can require a substantial blood supply. In comparison trichoepitheliomas are smaller lesions, usually no more than 2-5mm across (images of the described tumours shown in Figure 1-3) (Dubois *et al.*, 2017). Cylindromas can develop blue foci within them and become painful, which may represent cystic degeneration and associated formation of spiradenoma within the same tumour (Rajan and Ashworth, 2015).

Despite the typically benign nature of *CYLD*-defective tumours, these skin appendage tumours can have a significant impact on the quality of life of patients affected by BSS, FC or MFT, both physically and psychologically. Aside from being a highly disfiguring condition, with additional scarring from repetitive surgeries, leading to reports of low mood and depression (Parren *et al.*, 2014; van Balkom and Hennekam, 1994), *CYLD*-defective tumours that develop at pressure points such as on the back are susceptible to compression, which is not only painful but can lead to pressure necrosis and consequently ulceration, bleeding and chronic discharge. In addition painful tumours in the pubic and perineal regions can cause sexual dysfunction whilst growth of the tumours on the external ear can occlude the auditory canal and result in deafness (Dubois *et al.*, 2017; Rajan, Langtry*, et al.*, 2009). Furthermore aside from the skin, there are rare incidences of patients with BSS developing cylindroma of the breast (Mahmoud *et al.*, 2009) and lung (Vernon *et al.*, 1988), in addition to an association between patients with BSS and the development of salivary gland tumours in a small proportion of patients (Jungehulsing *et al.*, 1999)

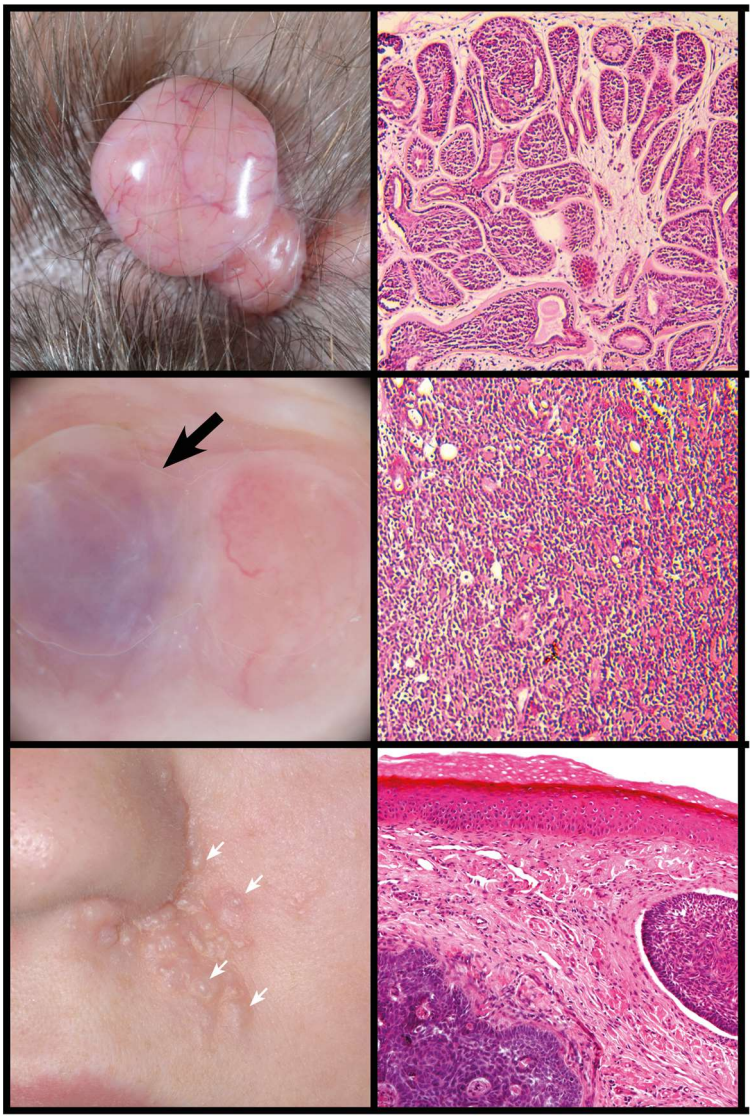

Figure 1-3: Histology of *CYLD*-defective tumours.
Examples of the three types of *CYLD*-defective tumours that arise within CYLD cutaneous syndrome, as they present in patients and H&E staining showing each of the tumours pathology. (Top) a cylindroma is shown with arborizing blood vessels, and the typical island structure of basaloid cells. (Middle) a spiradenoma that is characteristically blue-purple colour underneath the skin, and disorganised sheets of basophilic cells. (Bottom) trichoepitheliomas arising as skin coloured papules and displaying islands of basaloid cells that contain abortive hair cysts. (Images from (Dubois *et al.*, 2017)

1.1.3 Histology of *CYLD*-defective tumours

The term cylindroma was determined by the histological appearance of the tumours; well-defined nests of basaloid cells that resemble cylinders when cut in cross-section (Figure 1-3) (Rajan and Ashworth, 2015). These tumour cell islands are arranged in a jigsaw pattern, and are surrounded by a thick, eosinophilic, hyaline membrane, considered a basement membrane-like zone as it consists of extracellular matrix proteins such as Collagens IV and VII, and Laminin 5 (Bruckner-Tuderman *et al.*, 1991; Tunggal *et al.*, 2002). The tumour islands contain two groups of cells: peripheral palisading basophilic cells, with small dark nuclei, representing relatively

undifferentiated epithelial tumour cells, whilst centrally the cells are larger and paler resembling ductal or secretory cells (Massoumi and Paus, 2007). In between the tumour islands thin bands of stroma are occasionally seen. In comparison to cylindromas, spiradenomas appear more disorganised in their structure (Figure 1-3), and are instead comprised of a dense mass of sheets or cords of epithelial cells, with obvious vessel and tubular structures throughout, and globules of basement membrane material present within the neoplastic nodules (Obaidat *et al.*, 2007). A main difference between the tumour types is the association of a lymphocytic infiltrate with spiradenomas (Michal *et al.*, 1999).

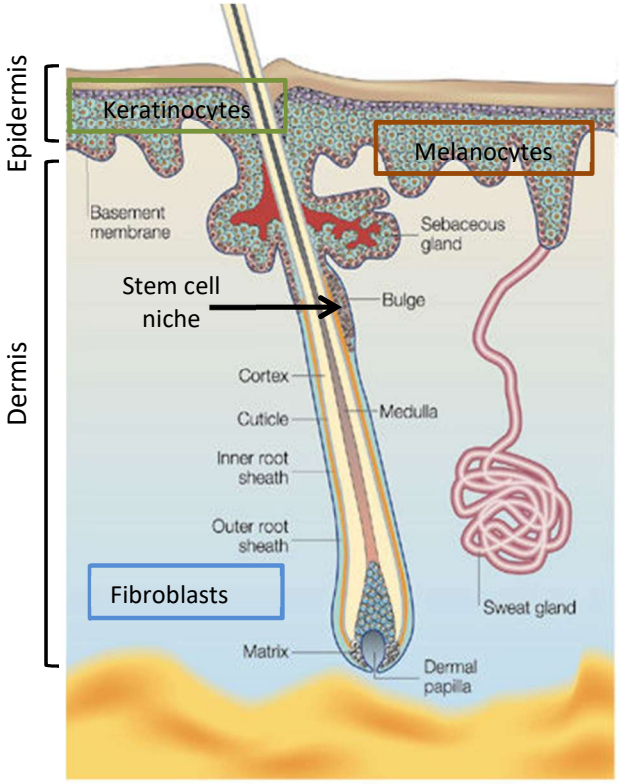

Figure 1-4: An overview of the hair follicle.
The hair follicle is considered a mini organ within the skin. It consists of the hair follicle itself, the sebaceous gland (for sebum production) and apocrine gland (for scent at particular body sites (not shown). The eccrine gland (sweat gland in image) is distinct from the hair follicle unit and is required for thermoregulation. The outer root sheath of the follicle is contiguous with the basal epidermal layer, which separates the epidermis and dermis compartments of the skin. The bulge region is where the epidermal stem cells reside, which migrate along the outer root sheath to the dermal papilla and give rise to transit-amplifying matrix cells that terminally dfferntiate to generate the different cell types of the hair follicle. Thus maintaining the hair follicle through its cyclical growth phases. At the bottom of the hair follicle is the hair bulb, which consists of the dermal papilla where interactions between the mesenchymal cells and surrounding epithelial matrix cells leads to new hair formation. Adapted from (Fuchs and Raghavan, 2002).

1.1.4 Cell of origin of *CYLD*-defective tumours

There has been much debate over the cell of origin of *CYLD*-defective tumours, and whether the tumours are derived from the follicular, apocrine or eccrine lineages. The appendages of the skin (Figure 1-4), which arise from progenitor cells committed to such differentiation lineages, such as the hair follicles, sebaceous glands, and sweat glands, each contain epidermal stem cells that replenish and maintain these compartments, yet these stem cells have been shown to be functionally interconvertible (Arwert *et al.*, 2012; Blanpain and Fuchs, 2006). These stem cells therefore are prime candidates in which early tumourigenic events may take place, such as the loss of CYLD, and consequently lead to tumour development due to aberrations in cellular differentiation.

Both apocrine and eccrine patterns of differentiation in cylindroma and spiradenoma have been found (Cotton and Braye, 1984; Crain and Helwig, 1961; Michal, 1996; Penneys and Kaiser, 1993; van der Putte, 1995). The striking histological similarity between cylindromas and salivary gland cancers such as adenoid cystic carcinoma (ACC) (Albores-Saavedra *et al.*, 2005; Crain and Helwig, 1961; Fusco *et al.*, 2016), alongside the reported development of salivary gland tumours in BSS patients (Headington *et al.*, 1977; Jungehulsing *et al.*, 1999) had led to earlier speculation that the tumours were eccrine derivatives. However in more recent years, further investigation of *CYLD*-defective tumours with immunohistochemical analyses of cylindromas and spiradenomas, has led Massoumi *et al*. (Massoumi, Podda, *et al.*, 2006) and Sellheyer (Sellheyer, 2015) to argue that stem cells of the hair follicle are the more likely tumour cell of origin. This is evidenced by the fact that hair-specific differentiation markers such as hair Keratins 17, 71 and 75 are expressed in cylindroma (Massoumi, Podda*, et al.*, 2006), alongside expression of the hair stem cell marker CD200 (Sellheyer, 2015) in cylindromas and spiradenomas, all of which are absent in the eccrine glands. Furthermore the multipotent nature of hair follicle stem cells (Ohyama, 2007), and the fact that the tumours do not present on the palms or soles of the feet, areas of the skin that are recognized to have the highest density of eccrine (sweat) glands but are devoid of pilo-sebaceous units (including the hair follicle and sebaceous gland) and apocrine glands (Massoumi, Podda*, et al.*, 2006), alongside the reported hair defects in a conditional mouse model, with epidermis-targeted

expression of catalytically deficient *CYLD* expression due to K14-Cre-mediated deletion of exon 9 (Jin Y. J. *et al.*, 2016), all together provide convincing evidence in support of the hair follicle hypothesis.

1.1.5 Malignant transformation of *CYLD*-defective tumours

The majority of *CYLD*-defective tumours are benign, however there are rare incidences (< 50) reported in the literature of cylindroma and spiradenoma undergoing malignant transformation to cylindrocarcinoma and spiradenocarcinoma respectively (Bansal *et al.*, 2012; Borik *et al.*, 2015; Durani *et al.*, 2001; Gerretsen *et al.*, 1993; Kazakov, Zelger*, et al.*, 2009; Kostler *et al.*, 2005). There is a greater tendency for malignant transformation in the inherited tumour conditions, like BSS, compared to sporadic neoplasms, probably due to the increased number of tumours present (Gerretsen *et al.*, 1993). As would be expected malignancy occurs in more elderly patients with an age range of 43 -96 years (Durani *et al.*, 2001; Kazakov, Zelger*, et al.*, 2009). Cutaneous clinical features that are associated with transformation are ulceration, bleeding, rapid growth and an increase in surface vascularity (Durani *et al.*, 2001; Gerretsen *et al.*, 1993), although it should be acknowledged that these are also features that can be seen in benign tumours (Rajan and Ashworth, 2015). Histologically, malignant cells are distinct from the residual benign tumour often present within the same specimen (Gerretsen *et al.*, 1993). Malignant cylindroma cells lose the defining histological characteristics of benign growths such as the jigsaw pattern of growth and hyaline sheaths, as well as having high mitotic counts and pleiomorphic cells (Gerretsen *et al.*, 1993; Kuklani *et al.*, 2009).

Malignant tumours of the scalp have been found to invade locally into the skull plate and the brain (Durani *et al.*, 2001; Tripathy *et al.*, 2015). Although local infiltration is reported in benign cases too (Serracino and Kleinschmidt-Demasters, 2013). Tumours may also metastasise to a variety of organs and tissues including the lungs, liver, thyroid, stomach and bone (Bansal *et al.*, 2012; Kazakov, Zelger*, et al.*, 2009; Kuklani *et al.*, 2009). One of the largest reviews of malignant cylindromas by Gerretsen et al. showed that out of 24 malignant cases, 15 were cylindromas from individuals affected by BSS and 9 were sporadic lesions. Furthermore 9 of the 15 inherited cases metastasized, most commonly to the lymph nodes and liver, and as a direct result caused death in 6 of these patients, demonstrating the aggressive nature of the

malignancy (Gerretsen *et al.*, 1993).

Aside from cylindromas and spiradenomas, there have also been a handful of reports of malignant transformation of trichoepitheliomas into basal cell carcinomas (BCC) in both the inherited and sporadic settings (Kallam *et al.*, 2016; Melly *et al.*, 2012). As BCC is the most common form of cancer the occurrence of BCC may be coincidental, as was evidenced in one of the cases in which a BCC and trichoepithelioma (TE) were found to be separate lesions on the face (Kallam *et al.*, 2016). Meanwhile another rare event in these normally benign tumours are reports of a trichoepithelioma variant called trichoblastoma also undergoing malignant transformation into a trichoblastic carcinoma (Lee K. H. *et al.*, 2008; Schulz *et al.*, 2005).

1.1.6 Genetics of *CYLD*-defective tumours

Initial genetic linkage analysis studies in two families with BSS, which are based on tracking the inheritance pattern of specific genetic markers that are matched between family members, led to mapping of the locus for the susceptibility gene to chromosome 16q12-13 and revealed the likely loss of a tumour suppressor gene as the underlying cause for the rare condition (Biggs *et al.*, 1996), with the locus further refined in 19 families by Takahashi *et al.* (Takahashi M. *et al.*, 2000). Subsequently germline mutations in a gene encoding for an ubiquitin-specific protease were found in 21 cylindromatosis families and somatic mutations found in 6 cylindromas, leading to the identification of the causative tumour-suppressor gene *CYLD* (cylindromatosis) (Bignell *et al.*, 2000). Four years later the same gene was found to be responsible for multiple familial trichoepithelioma (Zhang X. J. *et al.*, 2004).

Carriers of *CYLD* mutations are rare, with an occurrence rate of ~1:100,000, although the prevalence is difficult to estimate due to such variation in the phenotypic manifestation of the mutations of *CYLD* (Rajan and Ashworth, 2015). In patients who have inherited germline *CYLD* mutations, tumour formation occurs as a result of a loss of heterozygosity (LOH) of the remaining wild-type allele, which is seen in 70% of tumours (Bignell *et al.*, 2000), whilst the others have acquired somatic mutations (Grossmann *et al.*, 2013). This genetic pattern for the development of these tumours follows the principles of Knudson's two hit hypothesis model for cancer initiation (Knudson, 1971), whereby a cell requires a mutation in each allele of a tumour

suppressive gene. In inherited conditions a mutated copy of the gene is already present in the cells, and the second copy can become mutated or lost through somatic events causing a cell to become neoplastic. In BSS, FC and MFT this leads to loss of the tumour-suppressor gene *CYLD.*

Mutations in the *CYLD* gene have been identified in patients with BSS, FC and MFT, with around 108 germline mutations reported to date (Fujii *et al.*, 2017; Grossmann *et al.*, 2013; Verhoeft *et al.*, 2016). There is bias in the location of *CYLD* mutations, the vast majority (99%) of germline mutations having been found in the C terminal two-thirds of the gene, encompassing exons 9-20, as shown in Figure 1-5 (Nagy *et al.*, 2015). This includes the catalytic domain of the deubiquitinase protein encoded for by *CYLD* (Blake and Toro, 2009). A mutation has however been reported in exon 5, near the start of the coding region of the gene (Nasti *et al.*, 2009). Indeed several hotspot mutation sites that have been identified in *CYLD:* 1112C>A (S371), 2272C>T (R758) and 2806C>T (R936), which correspond to exons 9, 17 and 20, respectively, and are the most frequently reported having been found in 14, 10 and 13 families, respectively (Verhoeft *et al.*, 2016). The mutations of *CYLD* are mainly deleterious consisting of frameshift (44%), nonsense (25%), splice site (11%) and missense (11%) mutations, with small numbers of germline deletions also occurring (Nagy *et al.*, 2015; Verhoeft *et al.*, 2016). The collation of known germline *CYLD* mutations in a bid to evaluate genotype-phenotype correlations in 2015 by Nagy *et al.* demonstrated that nonsense mutations are associated with the most phenotypic diversity, meanwhile missense mutations have been associated with the least diversity, as 73% of mutations are found only in patients affected by MFT (Nagy *et al.*, 2015).

The majority of mutations are predicted to encode premature termination codons, which consequently result in a truncated protein product and loss of the catalytic activity of CYLD (Blake and Toro, 2009). There are incidences in which patients affected by BSS and MFT were found to lack mutation of *CYLD* (Grossmann *et al.*, 2013). This may be a reflection of the methods used such as direct sequencing in specific regions, which would have meant that some alterations of *CYLD* would be undetectable. There may be rare intronic variants that may effect splicing of *CYLD* (Kazakov, Thoma-Uszynski*, et al.*, 2009) or large rearrangements of *CYLD* including large deletions (Vanecek *et al.*, 2014), which may explain an apparent absence of causal mutation for

the presented disease in these patients.

Aside from undetermined *CYLD* mutations, it may also be that other unidentified genetic events may have a role to play in how the condition manifests. This is exemplified when a patient's ancestry is taken into account. Whilst *CYLD* mutations have been described in European, African and Asian populations, there are unaccounted for differences in disease severity and phenotypes despite commonality in the genetic loss of *CYLD*. For example the confluent growth of tumours on the scalp in those affected by familial cylindromatosis is almost exclusively reported in patients of white European origin, meanwhile patients of African or Asian origin suffer a severe facial multiple trichoepithelioma phenotype which infrequently affects the scalp; this phenotype is more uncommon in white European patients (Rajan and Ashworth, 2015). Likewise even in those that share the same recurrent mutation there can be a vast difference in the severity of the phenotype as demonstrated in two European families, where a Romanian pedigree had large tumours compared to a few trichoepitheliomas in an unrelated English pedigree (Nagy *et al.*, 2013). This suggests that there may also be unknown population specific modifier genes that produce a certain phenotype.

Despite at present not being able to predict a clinical phenotype or disease severity from the type of *CYLD* mutation, there is not yet a single study in which the whole of the *CYLD* gene has been sequenced in the tumours. Therefore as we embark on the next-generation sequencing era it is thought that previously undetermined alterations to *CYLD* and other potential genetic changes associated with this disease can be detected, which can be used to inform treatment strategies, genetic counselling and management of this collection of cutaneous tumour conditions.

1.1.7 Treatment of *CYLD*-defective tumours

At present surgical excision of the tumours is the mainstay treatment strategy to control tumour burden; in some cases this can necessitate whole scalp removal (Rajan, Trainer*, et al.*, 2009). Some of the surgical techniques include primary excision, curettage, and laser resurfacing (Rajan, Trainer*, et al.*, 2009). This means in a condition in which multiple tumours are developing throughout an affected individual's lifetime, repetitive surgical procedures are required, which only adds to the morbidity of the

disease. Furthermore recurrence rates after excision are around 35% (Crain and Helwig, 1961). Therefore alternative non-surgical interventions are warranted; gaining further insight into the biology of the tumours and understanding the function of CYLD may yield attractive therapeutic targets. To this end a clinical trial with a topical treatment of salicylic acid was undertaken (Oosterkamp *et al.*, 2006). As an inhibitor of NF-κB activation, by prevention of IκB degradation, it aimed to target the increased activity of NF-κB that is caused by the loss of CYLD function (see section 1.2.3.1). However the trial showed only modest results with complete remission seen in only 2 of 12 cylindromas (Oosterkamp *et al.*, 2006). A case report in which a combination of oral aspirin and Adalimumab (a TNF-α neutralizing antibody) were used in the treatment of trichoepithelioma, which additionally blocked TNF activation of NF-κB, showed a gradual improvement of the condition (Fisher and Geronemus, 2006). However the patient also had concurrent laser resurfacing so it was difficult to conclude the extent of the effectiveness of the treatment. More recently tropomyosin receptor kinase (Trk) signalling has been identified as a therapeutic target. Evidenced by transcriptomic data and the oncogenic dependency of primary cylindroma cultures on Trk (Rajan, Elliott*, et al.*, 2011). Therefore with further understanding of perturbed signalling pathways alternative treatment options may be found.

1.2 CYLD

The human *CYLD* gene is approximately 56kb in length and is composed of 20 exons, the first 3 of which are non-coding. The remaining 17 exons encode for the protein product CYLD, a deubiquitinating enzyme, which is 956$\alpha\alpha$ (amino acids) in length (Bignell *et al.*, 2000). Alternative splicing occurs in non-coding exon 3, and in the small, nine-nucleotide, exon 7, which produces a shorter isoform of 953$\alpha\alpha$. This splice variant, like the full-length transcript, is ubiquitously expressed yet little is known about its function (Bignell *et al.*, 2000). However knock-in mouse studies in which the short CYLD$^{ex7/8}$ variant, which lacks exons 7 and 8, is selectively expressed, appear to suggest that this splice form has regulatory roles in immune responses (Hovelmeyer *et al.*, 2007; Srokowski *et al.*, 2009). CYLD is an evolutionarily conserved gene with homologues identified in common model organisms such as *Drosophila melanogaster* and *Caenorhabditis elegans* (Hadweh *et al.,* 2018). CYLD expressed in many tissues, including the fetal brain, testis and skeletal muscle, with lower levels observed in the

heart, liver, lung, kidney, spleen and ovary (Bignell *et al.*, 2000). Within the skin, the highest level of CYLD expression is found in the inner root sheath of the hair follicle (Massoumi, Podda*, et al.*, 2006), and it has been shown in mice to be elevated in the catagen phase of the hair cycle, in which there is proliferation cessation (Moriwaki *et al.*, 2007). Whilst this reinforces the idea that hair follicle stem cells are the cells of origin of cylindroma (Massoumi, Podda*, et al.*, 2006), it should be noted that eccrine sweat glands also express CYLD, which again brings into debate the origin of the tumours (Zuo *et al.*, 2007). The ubiquitous expression of CYLD does bring into question why the inherited conditions manifest so specifically in the skin and implies other tissue specific events are responsible for tumour formation.

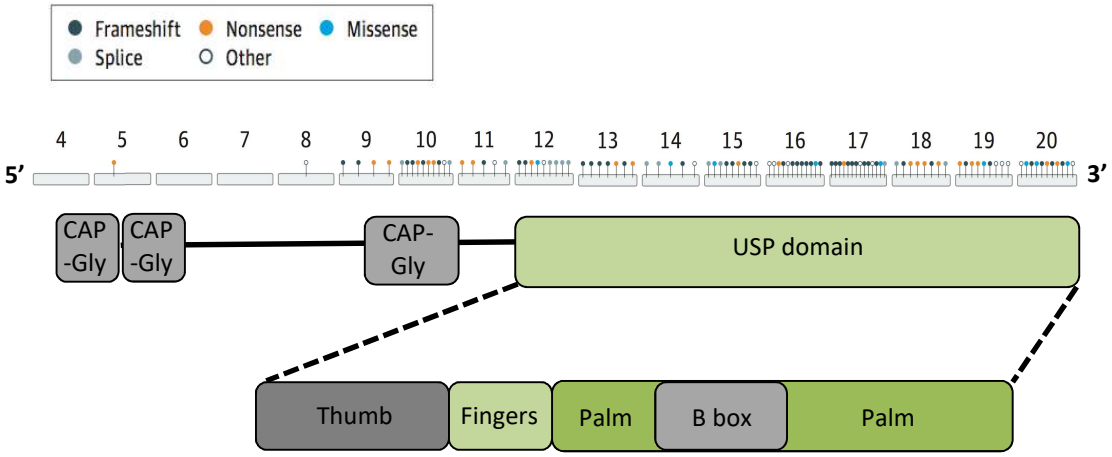

Figure 1-5: An overview of the *CYLD* gene and protein structure.
The exons of the *CYLD* gene are shown (numbered 4-20), starting at exon 4, as this is the exon from which translation is initiated. The coloured sticks represent the known mutations of *CYLD*, with a key for the type of mutation shown above (top diagram). The domains of the protein structure are shown beneath the exons by which they are encoded. The catalytic domain of CYLD is sub divided into the regions labelled. Together these subdomains allow for disruption of ubiquitin bonds and give specificity to the types of ubiquitin attachments the protein acts upon. The B-box domain is a unique feature of CYLD.

1.2.1 The structure of CYLD

The CYLD protein has three main functional motifs (Figure 1-5), these are comprised of 3 cytoskeleton-associated protein glycine-rich (CAP-Gly) domains at the N terminus, a proline rich region that is thought to constitute a Src homology 3 (SH3)-binding domain, and a catalytic ubiquitin-specific protease (USP) domain which mediates CYLD's deubiquitinating function (Bignell *et al.*, 2000; Komander *et al.*, 2008). The CAP-Gly domains are important in the regulation of microtubule dynamics and function, with CYLD having been shown to interact directly with microtubules and tubulin, implying functions outside of the catalytic domain (Gao *et al.*, 2008; Yang and Zhou,

2016). The first CAP-Gly domain in particular was shown to be necessary for cell migration (Gao *et al.*, 2008). There are four subdomains that make up the USP of CYLD: Thumb, Palm, Fingers, and an important additional insert within the palm domain, the zinc-finger-like B box domain (Komander *et al.*, 2008). Highly conserved within the USP family of deubiquitinating enzymes, the Thumb and Palm regions are responsible for engaging and attacking the bond between ubiquitin moieties and lysine residues, due to the palm incorporating the catalytic triad of Cysteine 601, Histidine 871 and Aspartic acid 889 (Komander *et al.*, 2008). Whilst for some defined USP motifs homology is conserved, the determination of the structure of the USP domain revealed unique properties of CYLD within this region, which are highly divergent from other USP family members. The most telling being that the Fingers subdomain is much smaller in CYLD compared to other USPs, together with secondary structural alterations near to the catalytic site underpinning CYLD's specificity for Lysine (K) 63-linked ubiquitin chains over K48-linked chains (Komander *et al.*, 2008). Alongside this the B-box domain was shown to be necessary for sub cellular localization of CYLD to the cytoplasm (Komander *et al.*, 2008; Xie *et al.*, 2017).

1.2.2 The function of CYLD

As demonstrated by the structure of CYLD, the function of this protein is as a deubiquitinating enzyme (DUB), intended to hydrolyse and reverse the attachment of K63-linked and Met-1 (linear) -linked polyubiquitin moieties from a variety of substrates (Komander *et al.*, 2009; Sato Y. *et al.*, 2015). Despite this it is unclear whether CYLD is exclusively specific for these ubiquitin linkages, as CYLD has been reported to have shown activity towards K48-linked ubiquitn chains also, suggesting that specificity may be dependent on the target protein (Reiley W. W. *et al.*, 2006). The post-translational modification of ubiquitylation is an important regulatory mechanism that influences many cellular processes such as: DNA repair, cell cycle, signal transduction, endocytosis of membrane proteins, and protein degradation (Haglund and Dikic, 2005). Ubiquitins (Ubs) are small proteins that can attach to substrates as single molecules or as polymeric chains that are linked through either of the 7 Lysine residues (K6, K11, K27, K29, K33, K48 and K63) or Met1. This ubiquitin code can affect the stability and protein-protein interactions of a target substrate depending on the number and the residue by which ubiquitin moieties are linked (Ikeda and Dikic, 2008;

Komander and Rape, 2012). For example the attachment of K48 linked ubiquitin chains are thought to highlight a protein to the proteasome for degradation (Clague and Urbe, 2010), on the other hand K63 linked ubiquitin chains are thought to be involved in other proteasome-independent functions such as, receptor endocytosis, DNA repair and signal transduction (Yau and Rape, 2016). Increasingly proteins tagged with K63 linked ubiquitin are being recognised to have a role in cancer (Dwane *et al.*, 2017), meanwhile linear ubiquitin chains are involved in the regulation of immune and apoptotic signalling (Rittinger and Ikeda, 2017).

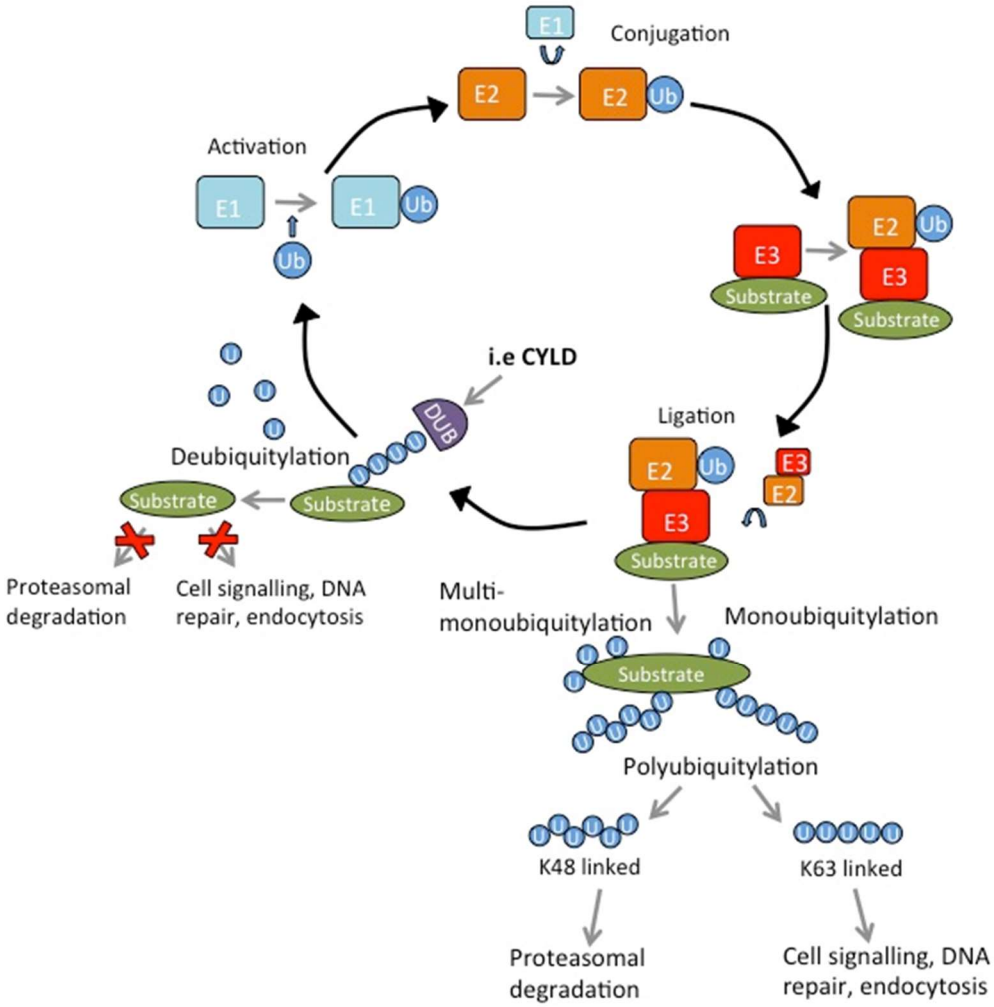

Figure 1-6: The cycle of ubiquitylation and deubiquitination.
The process of ubiqutiylation is a reversible process that involves the attachment of ubiquitin moieties to a substrate. Depending on the composition and assembly of the ubiquitin molecules, either as single entities or in polyubiquitin chains, different fates are determined for the substrate, such as degradation or cell signalling interactions. The process requires the activity of three enzymes: E1, the activating enzyme, which activates the c-terminus of ubiquitin for nucleophilic attack. E2, the conjugating enzyme, that carries activated ubiquitin to the substrate, where it is then transferred by E3, the ligase enzyme, to the lysine residue to which it will attach. The E3 ligases displaying specificity in their substrate interactions. Deubiquitinating enzymes (DUB) then cleave the bond between ubiquitin moieties and substrates to terminate the ubiquitin signal.

The conjugation of ubiquitin to its specific substrate is a three-step enzymatic cascade that starts with C-terminal activation of the ubiquitin protein via an ubiquitin-activating enzyme (E1), which then transfers the ubiquitin to an ubiquitin-conjugating enzyme (E2), which in turn interacts with an ubiquitin-protein ligase (E3) to bring the substrate and ubiquitin moiety together (Figure 1-6) (Pickart and Eddins, 2004). Ubiquitination is a reversible process, and CYLD has been shown to regulate various signalling pathways via the cleavage of K63 linked polyubiquitin chains (as will be discussed in section 1.2.3). The molecular studies of CYLD to date have shown that CYLD is a structurally unique DUB, and with the majority of mutations in CYLD found in the catalytic USP domain abolishing DUB activity, it is clear that the loss of this specific deubiquitinating function of CYLD is important in the initiation of tumourigenesis.

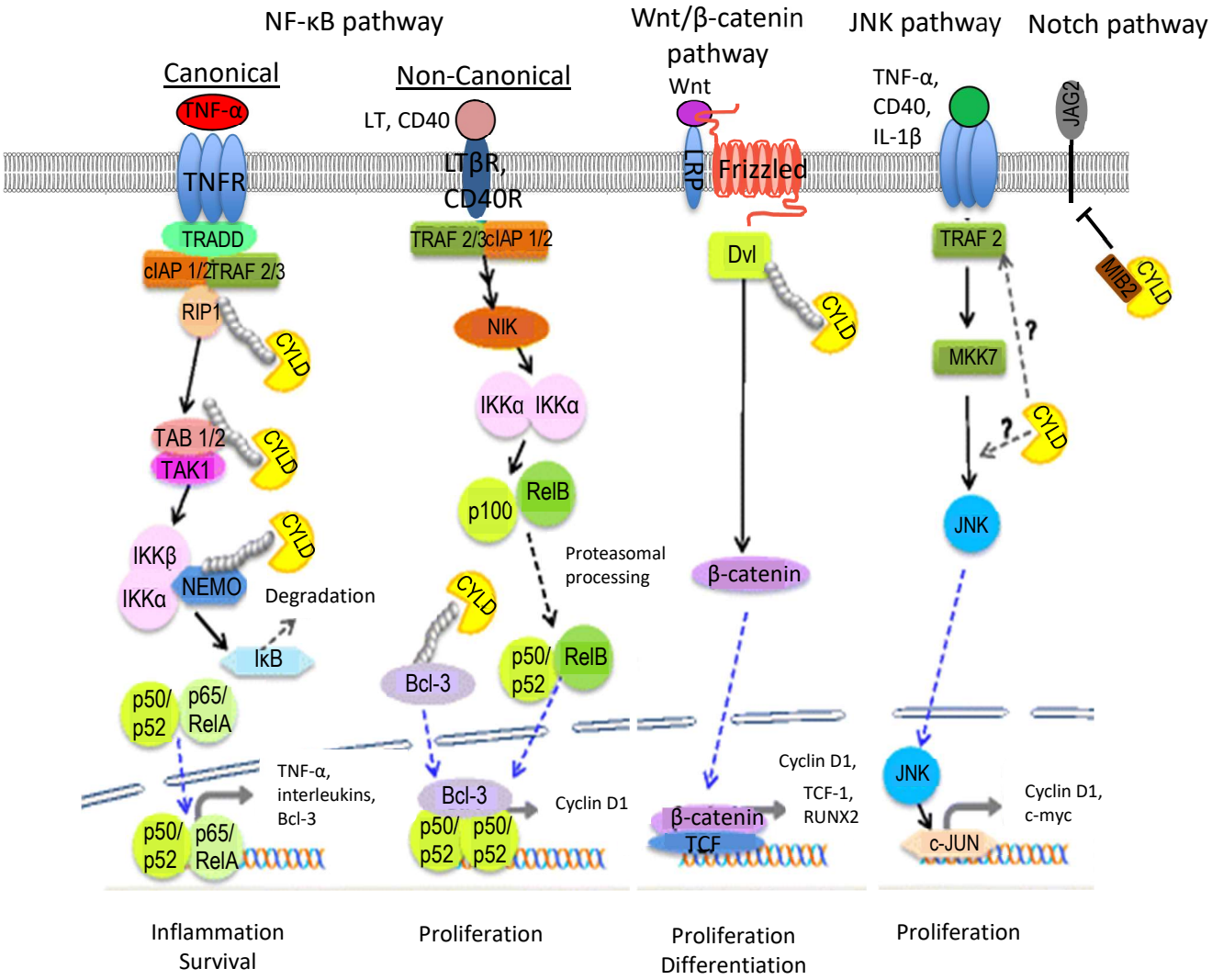

Figure 1-7: Signalling pathways associated with CYLD

Figure 1-7: Signalling pathways associated with CYLD (from previous page).
CYLD has been found to negatively regulate the NF- κB, Wnt, JNK and Notch signalling pathways. CYLD prevents downstream signalling and activation of target genes via deubiquitylation of target substrates. In the Notch pathway in a role independent of its catalytic function CYLD stabilises MIB2 to attenuate signalling. Blue arrows indicate nuclear translocation of the substrate. Figure adapted from (Verhoeft *et al.*, 2016).

1.2.3 CYLD regulation of cell signalling

In efforts to understand the pathogenesis of *CYLD*-defective tumours, CYLD has been found to be involved in the negative regulation of a number of key signalling pathways (Figure 1-7), as detailed below. In addition Trk signalling is discussed in results chapter 3. As many of these pathways have already been defined to have a role in many cancer types, these findings reinforced the proteins role as a tumour suppressor, as reviewed by (Blake and Toro, 2009; Verhoeft *et al.*, 2016). However despite increased knowledge of the mutation status of CYLD and disease linkage, understanding of the molecular mechanisms that promote the formation of multiple tumours still remains incomplete.

1.2.3.1 Regulation of NF-κB signalling by CYLD

NF-κB signalling was indicated as a target of CYLD when it was discovered that a loss of CYLD resulted in the upregulation of NF-κB in an RNA interference screen of DUB enzymes (Brummelkamp *et al.*, 2003). NF-κB is a family of transcription factors, consisting of five members: p65/RelA, RelB, c-Rel, p52/p100 and p50/p105, whose activation results in the induction of a variety of inflammatory, developmental, cell survival and proliferation genes (Shih *et al.*, 2011). The oncogenic potential of this signalling pathway is therefore well recognised, with aberrant activation of NF-κB seen as a 'driver' of oncogenesis in cancers such as diffuse large B-cell lymphoma (DLBCL), hepatocellular carcinoma (HCC) and prostate (Karin, 2009). NF-κB can be activated via a variety of stimuli, such as tumour-necrosis factor-α (TNF-α), interleukin-1 (IL-1), and lipopolysaccharide (LPS), through their corresponding receptors. These signals induce a rapid and reversible inflammatory or immune response through activation of the canonical pathway, which is dependent on NF-κB essential modulator (NEMO). In contrast stimuli such as CD40 and receptor activator for NF-κB (RANK), induce a slower and irreversible developmental response typically through the non-canonical pathway, which is instead dependent on NF-κB-inducing kinase (NIK) (Shih *et al.*, 2011; Zhang Q. *et al.*, 2017).

NF-κB is usually kept inactivated in the cytoplasm by inhibitor of NF-κB (IκB) proteins, preventing it from entering the nucleus and interacting with the DNA. When stimulated, downstream events such as recruitment and auto-ubiquitination of TNF receptor-associated factors (TRAFs), TRAF2 and TRAF6, activate the IκB kinase (IKK) complex causing phosphorylation of IκB, leading to its subsequent polyubiquitination and degradation by the proteasome. Alternatively in non-canonical signalling NIK activates an IKK complex, which in turn phosphorylates the IκB domain of p100 for proteolytic processing to p52. In both instances this then leaves NF-κB dimers free to translocate to the nucleus, where they can activate the transcription of a variety of target genes that facilitate cell proliferation and survival (Hoesel and Schmid, 2013; Karin *et al.*, 2002).

CYLD is a negative regulator of the NF-κB signalling pathway and has been found to interact with a number of proteins involved in mediating NF-κB activation (Sun S. C., 2010). These include NEMO (IKKγ), a non-catalytic regulatory subunit of the IKK complex, and other upstream activating proteins such as TRAF2 and TRAF6 (Trompouki *et al.*, 2003), receptor-interacting protein 1 (RIP1) (Wright *et al.*, 2007), and transforming growth factor-β-Activated Kinase 1 (TAK1) (Reiley W. W. *et al.*, 2007). Essentially due to the prevention of ubiquitylation by CYLD of K-63 linked polyubiquitin chains to substrates that are upstream of IKK, activation of NF-κB cannot occur due to a lack of activation of IKK, as the ubiquitin tags facilitate protein interactions and the assembly of signalling complexes to transmit the signal (Kovalenko *et al.*, 2003). However the negative regulation of IKK by CYLD could be conditional upon the stimulating receptor, after it was found that the knockdown of CYLD in HEK293 cells and HeLa cells did not promote IKK activation in response to TNF-α stimulation, but IKK was activated in response to LPS and IL-1β (Reiley W. *et al.*, 2004). CYLD also interacts and negatively regulates TAK1, via the cleavage of unanchored K-63 polyubiquitin chains by which TAK1 is activated, preventing subsequent phosphorylation of IKK-β, another component of the IKK complex, and inhibiting activation of IKK (Xia *et al.*, 2009). Also in co-operation with the E3 ubiquitin ligase Itch, the CYLD-Itch complex is capable of blocking TAK1 activation via the removal of K-63 ubiquitin by CYLD, and catalysing TAK1 degradation via the addition of K-48 ubiquitin by Itch, thus preventing the induction of proinflammatory cyotokines and regulating inflammation (Ahmed *et*

al., 2011).

CYLD has also been implicated in the regulation of non-canonical NF-κB signalling. Studies using *CYLD*$^{-/-}$ mice found that CYLD was required to remove K63-linked ubiquitin chains from B- cell lymphoma protein-3 (Bcl-3) (Massoumi, Chmielarska*, et al.*, 2006). Bcl-3 is a homolog of IκBα, which is a transcriptional co-activator of NF-κB p50 and p52 homodimers (Lenardo and Siebenlist, 1994). In normal conditions regulatory deubiquitination by CYLD prevents Bcl-3 from entering the nucleus and interacting with NF-κB subunits, inhibiting transcription and attenuating NF-κB signalling. Conversely, *CYLD*$^{-/-}$ mice were highly susceptible to chemically or UV light-induced skin tumours, that were caused by nuclear accumulation of Bcl-3 and subsequent CyclinD1 expression leading to increased proliferation (Massoumi, Chmielarska*, et al.*, 2006). Further to this Bcl-3 promotion of cell proliferation and oncogenesis through activation of CyclinD1 transcription has been shown in a variety of tumour types for example breast (Cogswell *et al.*, 2000), melanoma (Massoumi *et al.*, 2009) and hepatocellular carcinoma (Tu *et al.*, 2016).

Therefore it has been postulated that the loss of CYLD regulation may modulate different effects by the different NF-κB family members. Indeed TNF-α treatment, stimulating canonical NF-κB signalling, inhibited the proliferation of both *CYLD*$^{+/+}$ and *CYLD*$^{-/-}$ keratinocytes, yet led to significantly higher activation of an NF-κB responsive luciferase reporter (Massoumi, Chmielarska*, et al.*, 2006). Hence non-canonical p50-Bcl-3 and p52-Bcl-3 activation may contribute to tumour formation through increased proliferation, whilst canonical TRAF2-dependent NF-κB signalling may instead be responsible for immune or inflammatory responses to promote cell survival and support tumourigenesis. Interestingly an immune lymphocytic infiltrate is observed in spiradenoma tumours (Michal *et al.*, 1999). Although in this *CYLD*$^{-/-}$ mouse model the role of canonical NF-κB signalling requires further clarification, to explain how dysregulation of canonical NF-κB signalling contributes to *CYLD*-defective tumourigenesis.

1.2.3.2 Regulation of MAPK/JNK signalling by CYLD

CYLD is also a modulator of the c-Jun NH_2-terminal Kinase (JNK) signalling pathway. A member of the mitogen-activated protein kinase (MAPK) family, the JNK pathway has

roles in regulating cell proliferation, survival, and apoptosis. As these processes are hallmarks of tumourigenesis, this pathway is constitutively active in many cancers (Bubici and Papa, 2014). In response to cytokine activation, a downstream signalling cascade through TRAF2 to MAPK kinases, such as MKK7 and MKK4 leads to the activation of JNK and subsequent downstream targets such as c-Jun and c-Fos (Davis R. J., 2000). MKK7 in particular is required for JNK activation by inflammatory cytokines (Tournier *et al.*, 2001). CYLD through its modulation of TRAF2 ubiquitylation negatively regulates the activation of MKK7 and thus prevents phosphorylation of JNK, attenuating further signalling. It was shown however that this signalling inhibition by CYLD is receptor dependent. In CYLD knockdown studies in HEK293 cells, TNF-α stimulation showed a preferential activation of JNK instead of IKK. In addition CD40, LPS and IL-1β were also capable of more prominent JNK activation in contrast to IKK, suggesting JNK is a key downstream target of CYLD (Reiley W. *et al.*, 2004). In addition a study by Millani de Marval *et al.* using a mouse model, in which catalytically deficient CYLD expression was driven by the Cytokeratin 14 (CK14) promoter, found that JNK/AP-1 (Activator protein-1) activity was essential for chemically induced tumour formation in mutant CYLD mice, and that CYLD could also suppress AP-1 activity through regulation of c-Jun and c-Fos ubiquitylation (Miliani de Marval *et al.*, 2011).

TAK1 also has a role in activation of JNK-p38MAPK signalling through phosphorylation and activation of MKK6 and is regulated by K63-ubiquitination (Wang C. *et al.*, 2001). This pathway is crucial to T-cell development and innate immune responses (Liu H. H. *et al.*, 2006). These functions, in addition to the role of TAK1 in the NF-κB pathway, may also be mechanisms by which de-regulation of these pathways can contribute to the pathogenesis of *CYLD*-defective tumours.

1.2.3.3 Regulation of Wnt/β-catenin signalling by CYLD

The Wingless (Wnt)/β-catenin pathway is another signalling cascade in which components are negatively regulated by CYLD. Wnt/β-catenin signalling is critical in development and tissue homeostasis, especially for self-renewal of the skin and skin appendage formation (Lim X. and Nusse, 2013; Reddy *et al.*, 2001), which again can be frequently dysregulated in cancer (as reviewed by (Zhan *et al.*, 2017) and may be another way in which a loss of CYLD function can cause tumour formation. Particularly as hyperactive Wnt signalling, represented by nuclear β-catenin, was demonstrated in

tumours from cylindromatosis patients (Tauriello *et al.*, 2010). Dishevelled (Dvl) acts directly downstream of the Wnt receptor, Frizzled, and allows for transduction of the Wnt signal by disrupting the β-catenin inhibitory complex to prevent degradation of β-catenin. Consequently β-catenin is free to locate to the nucleus to promote target gene transcription. CYLD was found to regulate K63 ubiquitylation of Dvl. In the absence of functional CYLD, sustained K-63 ubiquitylation of Dvl facilitates signal transduction through polymerization of Dvl, and recruitment of the β-catenin inhibitory complex to the membrane. This allows for accumulation of the transcription factor ß-catenin, leading to enhanced levels of transcription of its target genes (Tauriello *et al.*, 2010). Furthermore a study by Rajan *et al.* found that expression of Dickkopf 2 (DKK2), a negative regulator of the Wnt pathway, is reduced in spiradenomas possibly due to the methylation of the *DKK2* promoter, and correlated with the increased tumour disorganisation found in these tumours. The potential pathogenic role of this pathway was emulated *in vitro* with primary cylindroma cells conferring a survival advantage when *DKK2* was silenced (Rajan, Burn*, et al.*, 2011). However the influence of CYLD in this aspect of Wnt signalling regulation is yet to be resolved.

1.2.3.4 Regulation of Notch signalling by CYLD

Notch signalling is involved in the development and homeostasis of a number of tissues including the skin (Williams *et al.*, 2011), mediating a number of cell fate decisions such as stem cell self-renewal, differentiation and cell cycle progression (Wilson A. and Radtke, 2006). Interestingly Notch receptors and their ligands show a restrictive pattern of expression to areas that are undergoing both early and late stages of differentiation within the hair follicles and interfollicular epidermis skin compartments (Nowell and Radtke, 2013; Powell *et al.*, 1998), indicating that perturbations to this pathway could influence the normal differentiation associated with the activity of this pathway within these skin compartments. This may result in a pathogenic role for this pathway, as has been shown in human cancers such as myeloma and leukaemia (Liu N. *et al.*, 2013; Takeuchi *et al.*, 2005).

The Notch signalling cascade functions in a cell-cell contact-dependent manner. Signalling is initiated by expression of the Delta-Serrate-Lag (DSL) family of ligands on a

signal-sending cell interacting with Notch receptors expressed on a signal-receiving cell. This results in cleavage of the Notch receptor and translocation of the intracellular part of the receptor to the nucleus where it acts as a transcriptional co-activator to drive gene expression. The DSL ligand relies on ubiquitylation to facilitate the signalling interaction with a signal-receiving cell (Le Bras *et al.*, 2011). Mind-Bomb homologue 2 (MIB2)/skeletrophin is an E3 ubiquitin ligase, which specifically interacts with the DSL ligand Jagged-2 (JAG2) to enhance Notch signalling by mediating endocytosis of JAG2 (Takeuchi *et al.*, 2005). CYLD is thought to attenuate Notch signalling by stabilising MIB2, in a non-catalytic dependent manner. This stabilisation disrupts autoubiquitylation and processing of MIB2 demonstrated by an increase in lower molecular weight ubiquitylated MIB2 products in the presence of exogenous CYLD expression, and consequently leads to a reduction in JAG2 expression (Rajan *et al.*, 2014). Indeed Notch signalling was found to be activated in *CYLD*-defective tumours and primary cylindroma cells were sensitive to γ-secretase inhibitors, which suppress Notch signalling through disabling cleavage of the Notch receptor and release of the intracellular domain. These results therefore suggest that the cells may have an oncogenic dependency on this signalling pathway (Rajan *et al.*, 2014).

1.2.4 Physiological functions of CYLD

CYLD is recognised to have diverse physiological functions, which mainly revolve around the critical regulatory role of CYLD in NF-κB signalling. Examples include negative regulation of innate immune responses to both bacterial and viral infection. For instance CYLD was shown to suppress the induction of proinflammatory mediators by inhibition of NF-κB activation in response to *Escherichia coli* pneumonia infection, protecting the host from inflammatory tissue damage and sepsis (Lim J. H. *et al.*, 2008). In a similar manner CYLD was found to deubiquitinate Myeloid differentiation factor (MyD88) to regulate immune responses induced by nontypeable *Haemophilus influenza* (NTHi) (Lee B. C. *et al.*, 2016). As MyD88 is an adaptor molecule for Toll-like receptors (TLR's), K63-linked polyubiquitylation of MyD88 is induced by NHTi infection to trigger TLR dependent NF-κB signalling and initiate an inflammatory response. In addition TLR stimulation promotes upregulation of CYLD in an autoregulatory feedback mechanism to deubiquitinate TRAF6 and TRAF7, causing attenuation of NF-κB mediated immune responses (Jono *et al.*, 2004; Yoshida *et al.*, 2005). Separately CYLD was also shown to negatively regulate virus-induced production of type 1 interferon

(IFN) cytokines (Friedman *et al.*, 2008). The proposed mechanism involving CYLD deubiquitination of a cytoplasmic viral RNA sensor, retinoic acid-induced gene 1 (RIG-1), and IKK-related kinases TRAF family member-associated NF-kB activator (TANK) binding kinase 1 (TBK1) and IKK-ε, causing inhibition of the interferon regulatory factor 3 (IRF3) pathway (Friedman *et al.*, 2008; Zhang M. *et al.*, 2008).

Other regulatory roles for CYLD in spermatogenesis and osteoclastogenesis were identified in *CYLD* knockout mouse studies. The loss of CYLD caused attenuation of the early wave of germ cell apoptosis, which is critical to germ cell homeostasis in the spermatogenesis process, due to increased activation of NF-κB and consequently heightened expression of anti-apoptotic genes (Wright *et al.*, 2007). On the other hand in bones the loss of CYLD caused deregulation of the homeostatic control of osteoclastogenesis, resulting in over production of osteoclasts, due to the loss of negative regulation of RANK ligand (RANKL) induced NF-κB signalling and deubiquitination of TRAF6 to inhibit signalling (Jin W. *et al.*, 2008).

1.2.4.1 Regulation of microtubule dynamics and associated activities by CYLD

More recently an accumulating body of evidence has demonstrated that CYLD is involved in the regulation of a number of cellular processes, independent of NF-kB signalling, including cell cycle progression, cell migration and ciliogenesis due to interacting with microtubules (as reviewed by (Yang and Zhou, 2016)). Microtubules are filamentous structures comprised of tubulin polymers providing a cytoskeleton to cells to give the cells shape, as well as mediating activities such as intracellular trafficking, cell division and motility. As stated in section 1.2.1 the CAP-Gly domains of CYLD are mainly responsible for microtubule interactions (Gao *et al.*, 2008), suggesting deubiquitylase independent functions of CYLD that may be important to tumour formation. Indeed, CYLD has been found to enhance microtubule stability through inhibition of HDAC6 deacetylase activity. Consequently this was found to lead to increased acetylation of a-tubulin and a delay in G_1/S transition of the cell cycle in both melanoma cells and keratinocytes (Wickstrom *et al.*, 2010). Whilst others have shown that CYLD is a critical regulator of microtubule dynamics and cell polarization during angiogenesis. This was evidenced by silencing of *CYLD* in human umbilical vein endothelial cells (HUVECS) causing microtubules to spend an increased amount of time in a paused state, impairing normal switching between growth and shortening phases,

and causing randomised centrosome localisation leading to cell migration defects (Gao *et al.*, 2010). In addition CYLD interacts with microtubule binding proteins such as End binding 1 (EB1) to regulate microtubule-related activities, however this was found to be dependent on the deubiqutiylase activity of CYLD and not the CAP-Gly domains (Li D. *et al.*, 2014). This therefore indicates that the different domains of CYLD may mutually affect each other or act synergistically in their regulation of cellular processes especially as microtubule-associated proteins undergo ubiquitylation (Gilberto and Peter, 2017; Yang, Liu*, et al.*, 2014). Interplay between these two functional domains of CYLD is yet to be clarified, however the regulation of microtubule activity may have an underlying role in the pathogenicity of *CYLD* mutations in *CYLD* cutaneous syndrome, particularly as a cylindroma phenotype has been reported in patients harbouring mutations in exon 5 which partly encodes for the Cap-Gly domains (Nasti *et al.*, 2009).

Furthermore CYLD has been found to promote ciliogenesis, as several symptoms were observed in *CYLD* knock out mice or mice expressing truncated CYLD that are associated with cilia abnormalities, such as male infertility (Wright *et al.*, 2007), osteoporosis (Jin W. *et al.*, 2008), impaired lung maturation (Trompouki *et al.*, 2009) and polydactyly (extra digits on the foot) and cilia defects in the skin, kidney, trachea and sperm (Yang, Ran*, et al.*, 2014). Primary cilia are microtubule-based structures that present on the surface of eukaryotic cells to sense chemical and mechanical signals from the environment (Goetz and Anderson, 2010). Further investigation found CYLD interacted with centrosomal proteins, including Centrosomal protein of 70kDa (Cep70), which was deubiquitinated by CYLD (Yang, Liu*, et al.*, 2014), and Centrosome-associated protein 350 (Cap350) (Eguether *et al.*, 2014). These interactions are important for positioning of CYLD at the centrosome and localisation of Cep70 at the basal bodies of cilia to promote their organisation and the elongation of microtubules for ciliogenesis (Eguether *et al.*, 2014; Yang, Liu*, et al.*, 2014). In addition the inhibition of HDAC6 by CYLD is involved in regulation of cililary length (Yang, Liu*, et al.*, 2014).

Cilia formation is intrinsically linked with cell cycle progression, through connections with the centrosome, and has been shown to be essential for signal transduction through recognised oncogenes and tumour suppressors such as Sonic hedgehog/

Patched 1 (Shh/Ptch1), Platelet-derived growth factor receptor-α (PDGFR-α), and Von Hippel-Landau (VHL) (Michaud and Yoder, 2006; Schneider *et al.*, 2005). Therefore it has been postulated by others that defective ciliogenesis and cilia functioning may contribute to tumourigenesis due to unrestrained growth, however whether this is due to the presence or absence of primary cilia remains contested (Castresana, 2015; Michaud and Yoder, 2006; Moser *et al.*, 2009). Intriguingly the Shh/Ptch1 signalling pathway, which is a primary driver of basal cell carcinoma (Bonilla *et al.*, 2016), another skin tumour that is thought to originate from hair follicle stem cells and is a malignancy into which trichoepithelioma has been reported to transform (Kallam *et al.*, 2016), has been identified as an upstream regulator of *CYLD* expression (discussed in more detail in section 1.2.5) (Kuphal *et al.*, 2011). In addition a number of the pathways that CYLD regulates have also been found to be cilia-related for example, Wnt (Gerdes *et al.*, 2007), Notch (Ezratty *et al.*, 2011) and Transforming growth factor-β (TGF-β) (Clement *et al.*, 2013). Therefore it would be interesting to further investigate whether perturbation of normal cilia formation and function due to a loss of CYLD has pathological implications in CYLD cutaneous syndrome.

CYLD has also been implicated as a regulator of mitotic entry, after it was shown that CYLD depletion in HeLa cells caused a premitotic arrest phenotype, which was dependent on CYLD deubiquitination, as the arrest phenotype was not restored by a catalytically inactive mutant of CYLD (Stegmeier *et al.*, 2007). The fluctuating pattern of CYLD protein levels during the cell cycle; reduced on mitosis exit and accumulating during S phase, were observed to be similar to other mitotic regulators such as Polo like kinase 1 (PLK1). Subsequently it was found that CYLD interacted with PLK1 and the authors speculated that K63 deubiquitination regulated PLK1 activity. This result therefore implies a paradoxical, tumour promoting function of CYLD, which was suggested to be a possibility for the benign nature of CYLD-defective tumours, as the loss of functional CYLD would lead to a proliferative disadvantage and restricted growth (Stegmeier *et al.*, 2007). Alternatively though other deubiquitinating enzymes may afford redundancy in the importance of this cell-cycle regulatory role of CYLD in different tissues. Conversely CYLD has been shown to inhibit Aurora-B independently of its deubiquitinating function but still requiring the C-terminus (Sun L. *et al.*, 2010). As the Aurora-B kinase is important in regulating chromosomal segregation and

promotes cell cycle progression, it is frequently found to be over-expressed in cancer (Tang *et al.*, 2017). Therefore as a tumour-suppressive mitotic regulatory role of CYLD, deregulation by a loss of CYLD could promote tumour growth.

1.2.5 Regulation of CYLD

In *CYLD*-defective tumours mutations cause a loss of CYLD function, however CYLD expression and function can be regulated by both transcriptional and post-translational modifications. At the promoter level *CYLD* transcription is regulated by NF-κB signalling in autoregulatory feedback mechanisms to suppress NF-κB activation; supported by genomic sequence analysis, which found NF-κB binding sites in the promoter region of *CYLD* (Jono *et al.*, 2004). Other proteins that are recruited to the *CYLD* promoter include BAF57, an ATP-dependent protein complex required for chromatin structure modification, which can be mutated in a vaiety of tumour types. In human breast carcinoma cells the overexpression of BAF57 was found to trigger up-regulation of CYLD by recruitment to the promoter region, to induce apoptosis and cell cycle arrest causing reversal of the transformed phenotype (Wang L. *et al.*, 2005). Meanwhile in melanoma cells the transcriptional repressor Snail is recruited to the *CYLD* promoter in response to BRAF-mediated activation of extracellular signal-related kinase (ERK), to facilitate the growth and metastasis of melanoma (Massoumi *et al.*, 2009). Similarly in the context of basal cell carcinoma Snail mediated the repression of *CYLD* expression and caused increased cell proliferation, except that in this cell context Snail was induced by the transcription factor Glioma-associated onocogene 1 (GLI1) downstream of Shh signalling. The loss of CYLD in these cells was rescued by the inhibition of GLI1 (Kuphal *et al.*, 2011).

Phosphorylation is another modification that is capable of controlling the activity of CYLD. For example in response to cell stimuli such as TNF-α, TRAF2 undergoes self-ubiquitylation to activate JNK signalling. Reiley et al. found that this coincided with phosphorylation of CYLD, which required IKKγ, to inactivate the catalytic activity of CYLD to allow for temporary accumulation of ubiquitin chains and subsequent downstream signalling (Reiley W. *et al.*, 2005). Furthermore in breast cancer cells the phosphorylation of CYLD, at Serine 418, by IKK-ε again suppressed CYLD activity and in

turn increased NF-κB activation. Thus demonstrating a potential mechanism for IKK-ε driven oncogenesis in breast cancer (Hutti *et al.*, 2009)

There is evidence that CYLD itself may be ubiquitylated to promote its degradation. The human papilloma virus (HPV) encoded E6 protein was shown under hypoxic conditions, to act as an E3 ubiquitin ligase, responsible for Lys48 ubiquitylation of CYLD and induction of NF-κB activation to drive HPV-infected malignancies (An *et al.*, 2008). Also in the regulation of Notch signalling and the interaction between CYLD and MIB2, ubiquitylation of CYLD by MIB2 is thought to target CYLD for degradation as a self-regulatory measure to control the autoubiquitylation of MIB2 (Rajan *et al.*, 2014).

Finally the micro-RNA, miR-181b-1 has been shown to target and repress CYLD. In a transducible model of cellular transformation, using the mammary epithelial cell line MCF-10A, the expression of signal transducer and activator of transcription 3 (STAT3) was induced upon transformation. Consequently this led to the establishment of an inflammatory feedback loop involving STAT3 mediated upregulation of miR181b-1 which directly targeted CYLD to suppress it's expression and cause increased NF-κB activation to maintain the inflammatory response required for a sustained transformed state (Iliopoulos *et al.*, 2010).

1.2.6 CYLD and other human malignancies

Despite the tissue tropism of tumour formation to the skin in CYLD cutaneous syndrome, it is evident that CYLD has an effect on cancer pathogenesis outwith of the skin, from the aforementioned various roles of CYLD and mechanisms of regulation Therefore the study of CYLD biology and the effects of CYLD dysfunction in *CYLD*-defective tumours gives us the opportunity to gain greater insight into not just the pathology of this rare benign tumour syndrome, but also of more common malignancies and the contribution of deubiquitinating enzymes, which could then inform on targeted treatment strategies for these cancers.

Although at a low frequency, the loss of CYLD through genetic mutation and a LOH has been observed in other tumour types including head and neck squamous cell carcinoma, lung adenocarcinoma and stomach adenocarcinoma (Verhoeft *et al.*, 2016) human atlas (60)). The two regions in which mutations of CYLD cluster, identified by

large-scale studies for cancer sequencing, correspond to coding exons for the functional domains of CYLD; the catalytic residues of the C-terminus and the CAP-Gly domains at the start of the coding region with mutations predominantly encoding for premature stop codons (Rajan and Ashworth, 2015).

The alternative mechanism employed in different cancers to the truncating mutations, like those observed in *CYLD*-defective tumours, is repression of CYLD expression. Further to the examples described in section 1.2.5, repression of CYLD is seen in T-cell acute lymphoblastic leukaemia (T-ALL), in which crosstalk between Notch and NF-κB signalling promotes survival of T-ALL cells, with Hes1 the transcriptional repressor target of Notch, driving the repression of CYLD and activation of IKK and NF-κB (Espinosa *et al.*, 2010). Similarly in multiple myeloma mutation or deletion of *CYLD* was associated with enhanced disease aggression due to aberrant Wnt activation (van Andel *et al.*, 2017). Finally CYLD expression is downregulated in HCC, which due to increased NF-κB activity and the ensuing inflammation promotes carcinogenesis (Urbanik *et al.*, 2011). Indeed in mouse liver models in which CYLD is lost, constitutive activation of TAK1 initially leads to hepatocyte apoptosis, disrupting liver homeostasis and causing inflammation and fibrosis as potential compensatory survival mechanisms, which results in the development of tumours (Nikolaou *et al.*, 2012).

1.2.7 *CYLD* transgenic models

A number of transgenic mouse models have been developed to aid with the characterisation of CYLD (Table 1-2), as demonstrated by the examples given in the functions of CYLD section previously. However to date none of the CYLD-deficient mouse models spontaneously develop *CYLD*-defective tumours such as cylindroma. Nonetheless these models have provided further insight into CYLD function, and intriguingly marked differences in the phenotypes of complete *CYLD*-knockout mice and mice ubiquitously expressing truncating *CYLD* mutations that closely mimic human mutations have been observed. *CYLD*-knockout mice are viable but show an increased susceptibility to chemically induced tumour formation. Indeed the topical application of 7, 12-dimethylbenz(a)anthracene (DMBA) followed by 12-O-tetradecanoylphorbol-13 acetate (TPA) in $CYLD^{-/-}$ mice led to the development of squamous cutaneous papillomas, with increases seen in the number, frequency and size of tumours

compared to wild-type littermates (Massoumi, Chmielarska*, et al.*, 2006). Likewise the treatment of another *CYLD*$^{-/-}$ mouse model with azoxymethane (AOM) and dextran sulphate sodium (DSS), to induce mutations and inflammation in the colon epithelium, led to the development of an increased number of colorectal tumours compared to wild-type mice (Zhang J. *et al.*, 2006). Conversely the ubiquitous expression of truncated CYLD leads to perinatal lethality due to incomplete lung development and leads to a lack of oxygenation (Trompouki *et al.*, 2009). This discrepancy between the models may possibly be explained by compensatory mechanisms that may exist in knockout mice. On the other hand truncated CYLD may act in a dominant-negative manner, interfering with compensatory networks and deubiquitylase activities, as it is still capable of binding to target substrates and maintains the CAP-Gly domain on which some deubiquitylase activities may be dependent. In support of this theory a mouse with deletion of exons 7 and 8 of CYLD that abrogates the TRAF2 and NEMO binding site is viable, suggesting that this domain may be responsible for mediating dominant-negative effects that account for the lethal phenotype (Hovelmeyer *et al.*, 2007). Further investigation of these models may lead to explanations of the pathogenic effects exerted by CYLD truncation.

Due to viability issues with the truncated CYLD mouse models, more recent studies have tried to circumvent this by creating conditional knock in models to express mutant *CYLD* in a particular tissue. Intriguingly mouse models in which mutant *CYLD* expression has been targeted to the skin have again shown diverging phenotypes. Mice that conditionally expressed a catalytically deficient form of CYLD driven by the CK14 promoter (K14-CYLD^{m}) displayed no obvious developmental abnormalities, other than mild epidermal hyper-proliferation. However in contrast to *CYLD*$^{-/-}$ mice, they were susceptible to developing highly malignant and metastatic skin tumours, some displayed clinical features of SCC when exposed to DMBA/TPA treatment (Miliani de Marval *et al.*, 2011). Yet mice that expressed a truncated form of CYLD, due to deletion of exon 9, and whose expression of truncated CYLD was exclusive to K14-positive hair follicles and basal epidermal cells (*CYLD* $^{E\Delta9/E\Delta9}$) were born alive, but in contrast to K14-*CYLD*^{m} mice developed skin, hair and dental abnormalities, as well as being prone to developing basaloid tumours and sebaceous adenomas in response to DMBA/TPA treatment. The study also identified c-Myc as a potential driver of tumour

development (Jin Y. J. *et al.*, 2016). These results importantly highlighted that the expression of truncated CYLD by its endogenous promoter must be essential for the observed defects within the context of the hair follicle compartment. However the lack of spontaneous skin tumour development limits the use of these models for drug discovery strategies, and indicates that there may be biological differences between humans and mice in the role of CYLD in the hair follicle or that other tumour initiating events are required to promote tumour formation. Interestingly cylindromas and trichoepitheliomas are reported in a Gli1 over-expressing mouse model (Nilsson *et al.*, 2000), suggesting interplay between the Shh signalling network and CYLD may be such a hair follicle tumour promoting event, especially as this signalling pathway is important for hair follicle development (Rishikaysh *et al.*, 2014). However expression of Gli1 was under the K5 promoter, which may reflect differences in biology.

1.3 Research aims and objectives

A lack of treatment options for CYLD cutaneous syndrome, other than repetitive surgery, warrants the need for further understanding of *CYLD*-defective tumours to identify potential therapeutic targets for alternate treatment strategies for patients with this genetic condition. Further understanding may also provide molecular insight into the promotion of tumorigenesis in other cancers in which CYLD is mutated or repressed. Previous work has highlighted the many signalling pathways in which CYLD is involved, with MYB and TrkB having been identified as targets of interest due to their overexpression in *CYLD*-defective tumours. The overall aim of this thesis therefore, was to identify and characterise targetable downstream targets of signalling pathways, such as MYB and TrkB, which are perturbed by a loss of functional CYLD, alongside developing a 3D culture model in which to explore these targets with compounds that may be therapeutically beneficial to patients.

***CYLD* genotype**	**Region targeted**	**Tumour induction**	**Phenotypic observations**	**Reference**
CYLD$^{-/-}$	Exon 1 deletion	Not described	Viable, with altered T-cell development	Reiley *et al.* 2006
CYLD$^{-/-}$	Exon 2 and 3 deletion	Increased susceptibility to chemically induced colonic tumours	Viable no obvious phenotype until 10 months old, with inflammatory infiltrates in organs such as the liver, spleen and lungs	Zhang *et al.* (2006)
CYLD$^{-/-}$	Exon 4 deletion	Skin papillomas	Viable with no apparent phenotype	Massoumi *et al*. (2006)
CYLD$^{-/-}$	Exon 7 deletion	Not described	Viable, with increased expression of a short splice variant of *CYLD.* Also an accumulation of mature B lymphocytes in secondary lymphoid organs	Hovelmeyer *et al.* (2007)
CYLD$^{E\Delta 9/\Delta 9}$	Exon 9 deletion-catalytically deficient	Not described	Died shortly after birth due to abnormal development of lungs that failed to inflate. Also were smaller than wild-types with kinked tails	Trompouki *et al.* (2009)
K14-CYLD^{m}	Lacks last 21 αα (1-932)0 catalytically deficient	Tumours with clinical features of SCC, which metastasised to lymph nodes	Viable with mild epidermal hyperproliferation	Miliani de Marval *et al.* (2011)
K14Cre-CYLD$^{E\Delta 9/\Delta 9}$	Exon 9 deletion-catalytically deficient	Sebaceous adenoma and basaloid tumours	Viable with hair and dental growth defects	Jin *et al. (*2016)

Table 1-2: CYLD transgenic mouse models.

Chapter 2

Materials and Methods

2 Chapter 2: Materials and Methods

2.1 General Principles

2.1.1 Ethical Approval

Ethical approval had been granted from the local ethical review board (REC 06/1059) and written informed consent obtained from patients for the patient samples used in this study.

2.2 Molecular Biology

2.2.1 Collection of tissue for extractions

Surplus skin and tumour tissue taken from patients undergoing routine surgery was obtained and snap frozen in liquid nitrogen and stored at -80°C. Tissue was mounted with OCT embedding reagent and sectioned on a cryostat (Leica), cutting at a thickness of 30µm with 10 sections collected per sample.

2.2.2 RNA extraction from tissue

Prior to commencing extractions the working area was prepared to reduce possible RNase contamination. All work surfaces and pipettes were wiped with RNAse Zap (Ambion) and filter tips were used for all pipetting steps.

Total RNA was extracted from tumour and skin tissue samples using the AllPrep® DNA/RNA/miRNA Universal kit (Qiagen) according to the manufacturer's protocol. Tissue sections were lysed in 600µl Buffer RLT containing β-mercaptoethanol and guanidine isothiocyanate to denature RNAses and DNAses, with disruption of the samples using a pestle and homogenisation via repeated pipetting through a 1ml tip. Samples were then centrifuged for 1 minute at x13000rpm to pellet the debris and the supernatant transferred to a DNA Mini spin column for extraction of DNA. The flow through from this column containing the RNA was then transferred to an eppendorf. To extract the RNA 150µl of chloroform was added, before centrifugation at 4°C at x15000rpm for 3 minutes. The upper aqueous phase was removed and treated with 80µl Proteinase K in the presence of 350µl of 100% ethanol to remove protein contaminants. Samples were left to incubate at room temperature for 10 minutes

before 750µl of 100% ethanol was added and the sample transferred to an RNeasy mini spin column. The columns were centrifuged for 15 seconds at x13000rpm to bind the RNA to the column membrane. The columns were washed with Buffer RPE before on column DNase digestion, 80µl of DNase I mixed with Buffer RDD was applied and the columns were left at room temperature for 15 minutes. The sample columns then underwent a series of washes with 500µl of each of Buffer FRN, Buffer RPE and 100% ethanol added in turn to the column with centrifugation at x13000rpm for 15 seconds in between, before a final centrifugation step for 2 minutes to ensure the removal of all ethanol. The RNA was then eluted in 30µl of RNase-free water, with three elutions per sample. All samples were stored at-80°C.

2.2.3 RNA extraction from cells

Similar to the column based method above, total RNA was extracted directly after trypsinisation from cell pellets using the RNeasy® Mini kit (Qiagen) according to the manufacturer's protocol. Briefly, cell pellets were lysed in 600µl Buffer RLT containing β-mercaptoethanol, before being centrifuged at x15000rpm for 10 minutes and the supernatant added to 600µl of 70% ethanol. The mixture was then put through an RNeasy spin column, with subsequent washing with 700µl Buffer RWT and 500µl Buffer RPE and centrifugation steps at x13000rpm for 1 minute in between, before a final centrifugation step for 2 minutes to ensure the removal of all ethanol. The RNA was then eluted in 30µl RNase-free water, with three elutions per sample. All samples were stored at -80°C.

2.2.3.1 DNase treatment of RNA

As the RNA extraction protocol above did not include a DNase digestion step this was carried out after extraction using the TURBO DNA-*free*™ kit (Ambion). A volume of RNA equivalent to 1µg was added to 10X TURBO DNase buffer (x0.1 of RNA volume) and 1µl of DNase. The samples were mixed and incubated for 30 minutes at 37°C in a thermoshaker. Subsequently 2µl of DNase inactivation reagent was added to also remove divalent cations that can catalyse RNA degradation when heated. The samples were then left at 26°C for 5 minutes in a thermoshaker, before centrifugation at x13000rpm and the RNA supernatant removed and stored at -80°C or taken forward for generation of cDNA.

2.2.4 Determination of RNA concentration

The concentration of RNA samples was quantified using a fluorometric quantitation method. This works on the principle that a fluorescent dye (specific for the molecule of interest) upon binding with RNA in the sample-dye solution produces a fluorescent signal, which is directly proportional to the concentration of RNA in the solution. The level of fluorescence is then detected by a fluorometer and converted into a concentration value using RNA standards of known concentration and a curve-fitting algorithm.

The Qubit® RNA Broad Range assay kit was used alongside the Qubit® 2.0 fluorometer (both Life Technologies). Samples were prepared according to the manufacturer's protocol. In brief a buffer/dye working solution was prepared by diluting dye reagent 1:200 in assay buffer in a volume appropriate to cover the number of samples and standards to be assayed. RNA sample was diluted 1:100 in a buffer/dye working solution (2µl to 198µl), alongside two RNA standards (0ng/µl and 10ng/µl) diluted 1:20 in the buffer/dye working solution (10µl to 190µl). These were then incubated at room temperature for 2 minutes before taking concentration readings.

2.2.5 Analysis of RNA integrity

Once extracted the integrity of the RNA was assessed to ensure the samples had not degraded and were of a quality suitable for sequencing and other downstream applications. The RNA 6000 Nano Kit alongside a 2100 Bioanalyzer instrument was used for analysis (both Agilent Technologies). This is an electrophoretic assay, with 1µl of RNA sample added to a microfluidic chip primed with a gel containing a fluorescent dye. RNA fragments are separated and internal markers of known size are used to generate a standard curve of migration time versus fragment size, to which the samples are referenced. A digitised image then displays the RNA bands and an integrity number (RIN) calculated based on the preservation of the 18S and 28S ribosomal bands (Figure 2-1). For sequencing purposes, samples that had a RIN >8 were included (see section 2.7).

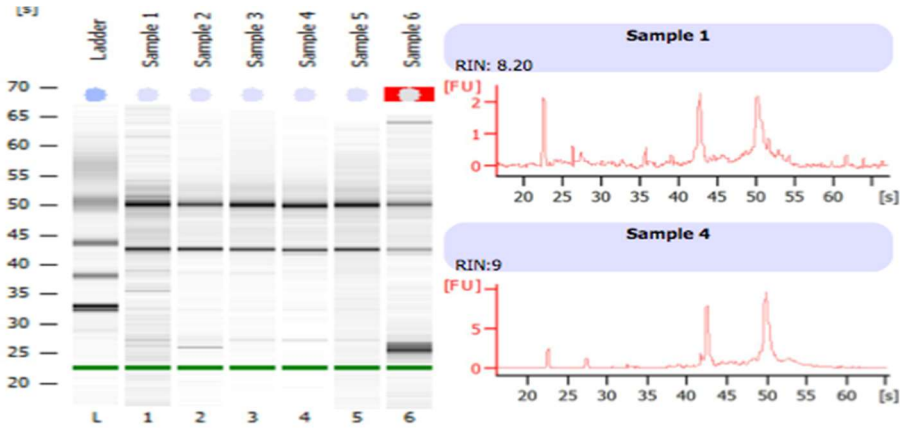

Figure 2-1: An example of the digitized gel image or electropherogram showing intact 18S and 28S ribosomal peaks within the RNA samples after a Bioanalyzer run.

2.2.6 Generation of cDNA by reverse transcription

cDNA was generated from RNA using the SuperScript® II Reverse Transcriptase kit (Invitrogen). For each sample 1µg of RNA was reverse transcribed in a total reaction volume of 20µl (reaction mix shown in Table 2-1). Firstly sample RNA, RNase-free water, Random Primers (Promega) and dNTP mix (Promega) were added together to give a total volume of 12µl. The reaction mix was then heated for 5 minutes at 65°C in a heat block. Next 5x First Strand Buffer, DTT, and RNase-free water were added, to bring the total volume to 19µl. The reaction mix was left at 25°C for 2 minutes in a heat block, before finally adding the reverse transcriptase SuperScript® II enzyme. The reactions were run in a thermal cycler following the programme shown in Table 2-2. Once generated the cDNA was diluted 1:50 with water to achieve a working concentration. The cDNA was then stored at -20°C.

Reaction Component	Volume
RNA sample (input 1μg)	*X*μl (max 10.5μl)
Random Primers (250ng)	0.5μl
dNTP mix (each 10mM)	1μl
5X First Strand Buffer	4μl
DTT (0.1M)	2μl
SuperScript® II Enzyme	1μl
ddH_2O	Make up to 20μl

Table 2-1: Reaction mixture composition for cDNA generation

Temperature	Time
25°C	10 minutes
42°C	50 minutes
70°C	15 minutes
4°C	Hold

Table 2-2: Thermocycler program for cDNA generation

2.2.7 Polymerase chain reaction (PCR) for TrkB (*NTRK2*) isoforms for cloning

The cDNA from a cylindroma tumour and the SHSY-5Y cell-line treated with retinoic acid was used for amplification of transcripts of each of the *NTRK2* isoforms *NTRK2*.FL and *NTRK2*.T1 respectively, for cloning purposes (see section 2.6). Primers were designed based on sequences obtained from Ensembl (www.ensembl.org) (Table 2-3). Each of the *NTRK2* transcripts was amplified using a proofreading KOD polymerase (Novagen®) in a total reaction volume of 20μl (reaction mix shown in Table 2-4) and reactions were run in a thermal cycler following the conditions in Table 2-5.

Primer	Transcript ID of sequence	Forward/ Reverse	Sequence	Amplicon Size
NTRK2		Forward	5'-ATGTCGTCCTGGATAAGGTGGCAT-3'	-
NTRK2.FL	ENST00000376214	Reverse	5'-CTAGCCTAGAATGTCCAGGTAGAC-3'	2517bp
NTRK2.T1	ENST00000395882	Reverse	5'-CTACCCATCCAGTGGGATCTTATG-3'	1433bp

Table 2-3: Primers used for amplification of the *NTRK2* gene for cloning of TrkB isoforms

Reaction Components	Volume
KOD Hot Start Master Mix	10μl
Forward Primer	0.6μl
Reverse Primer	0.6μl
cDNA	2μl
DMSO	1μl
ddH_2O	5.8μl

Table 2-4: Reaction mixture composition for *NTRK2* PCR for cloning of TrkB isoforms

Step/Cycles	Temperature	Time
Polymerase activation	95°C	2 minutes
Denaturation	95°C	20 seconds
Annealing	50°C FL/ 55°C T1	10 seconds
Extension	70°C	1 minute
(Repeat for x40 cycles)		

Table 2-5: Thermocycler PCR program for cloning of TrkB isoforms

2.2.8 Agarose gel electrophoresis

PCR products were run and visualised on a 1% agarose gel containing GelRed™nucleic acid stain. The gel was produced by adding 1g of agarose to 100ml of TAE buffer, heating the mixture until bubbling and left to solidify. PCR product samples (20µl) were mixed with 6X loading dye (4 µl) prior to loading onto the gel. Gels were run for one hour at 100V in 1X TAE buffer to separate the PCR amplicons. A 1Kb ladder (Promega) was run alongside the PCR product samples to determine if the correct amplicon size was obtained.

2.2.9 Gel extraction and DNA purification

DNA was extracted from agarose gels and purified using a QIAquick gel extraction kit

(Qiagen) according to the manufacturer's protocol. DNA fragments were visualised using a UV light box and the DNA fragment of interest excised from the gel with a scalpel. The gel fragment was placed in an eppendorf and weighed to allow for correct calculation of the buffer volume for extraction, with 300µl Buffer QG added per 100mg of gel. The agarose gel was incubated in Buffer QG at 50°C for 10 minutes to dissolve the gel. For DNA fragments that were less than 500bp and greater than 4kb, isopropanol was added to increase the yield. The sample was then added to a QIAquick spin column to bind the DNA and centrifuged for 1 minute at x13000rpm (all subsequent centrifugation steps carried out in the same way). The column was washed with 500µl Buffer QG to remove any residual traces of agarose, before being incubated with 750µl Buffer PE for 5 minutes to remove salts that may interfere with downstream ligations for cloning. DNA was finally eluted from the column in 30µl of Buffer EB and DNA stored at -20°C.

2.2.10 Quantitative reverse transcription polymerase chain reaction (qPCR)

2.2.10.1 Principles of qPCR

Quantitative PCR is a technique that utilises the amplification of specific DNA target sequences by traditional PCR, whilst using fluorescent dyes or fluorescently-tagged probes to detect and measure the amount of DNA generated during each cycle of the PCR reaction. As the amount of fluorescence measured is proportional to the accumulation of PCR product as the reaction progresses the amount of DNA can be quantified. Therefore the higher the starting level of the target sequence the fewer PCR cycles needed to generate a significant level of DNA.

There are two types of fluorescence detection methods that can be used in qPCR. Fluorescent dyes, such as SYBR® Green I, are non-specific DNA binding dyes that intensely fluoresce when they intercalate within the double stranded DNA produced during the PCR reaction. Alternatively probe-based chemistry, such as a Taqman® probe, uses fluorescently tagged oligonucleotide probes that are specifically designed for a particular DNA sequence. The 5' end of the probe contains a fluorophore such as 6FAM (6-carboxyfluorescein), which when excited by a light source from the thermal cycler transfers energy to the quencher such as TAMRA (tetramethylrhodamine) attached at the 3' end leading to suppression of any fluorescence signal. However

upon binding of the probe to the specific DNA region to which they are designed, during the elongation phase the 5' to 3' exonuclease activity of the Taq polymerase cleaves the fluorophore releasing it from the quencher leading to an increase in fluorescence which reflects amplification of the target amplicon. This method increases specificity, as it requires hybridization of the probe to the target sequence to generate a fluorescent signal.

2.2.10.2 qPCR with SYBR® green

The primers used (Table 2-6) were designed using Primer3 software (version 4.0.0), and targeted the terminal exons unique to each isoform. Sequences that ran across the intron-exon boundary were selected to ensure non-amplification of potential contaminating genomic DNA, and designed to flank exons unique to the 3' end of each *NTRK2* isoform transcript. For *NTRK2.FL* this was exon 24 and for *NTRK2.T1* this was exon 16. A master mix was prepared for each set of primers, and individual reactions were set-up in a 96 well format with a final volume of 25μl. The components of each reaction mix are shown in Table 2-7 below. For each sample, each primer pair was run in triplicate.

Primer	Forward/Reverse	Sequence	Amplicon Size
TrkB.FL (full length)	Forward Reverse	5'-TGGGAGATTTTCACCTATGG-3' 5'-AAGGGCCCTAGCCTAGAATG-3'	247bp
TrkB.T1 (truncated)	Forward Reverse	5'-TGGGATTTTGCCTTTTGGTA-3' 5'-CCCCAGATAAGCAGCACTTC-3'	225bp
GAPDH	Forward Reverse	5'-CGACCACTTTGTCAAGCTCA-3' 5'-AGGGGTCTACATGGCAACTG-3'	228bp

Table 2-6: Primers used for amplification of the *NTRK2* isoforms for qPCR

Reaction Components	Volume per well
2x SYBR® Green JumpStart™ Taq ReadyMix™	12.5μl
Forward Primer	1μl
Reverse Primer	1μl
cDNA	5μl
ddH_2O	5.5μl

Table 2-7: Reaction mixture composition for *NTRK2* isoforms for qPCR

Once plates had been set-up and sealed, they were centrifuged at 2000rpm for 1 minute to ensure all reagents were at the bottom of the well and to remove air bubbles. Plates were then run on a Chromo4™ Real-Time PCR Detector System

(Biorad) with Opticon Monitor™ software (BioRad), using the thermal cycling conditions shown in Table 2-8.

Step/Cycles	Temperature	Time
Polymerase activation	95°C	2 minutes
Denaturation	95°C	30 seconds
Annealing	60.2°C	30 seconds
Extension	72°C	30 seconds
(Repeat for x40 cycles)		
	4°C	Hold

Table 2-8: Thermocycler PCR program for *NTRK2* isoforms for qPCR

PCR products were initially analysed on a 2% agarose gel, to confirm amplification of a single product of the correct size, as well as the generation of a melting curve during the qPCR run. In the amplification plots a threshold was set and Ct values determined. The relative normalized gene expression was calculated using the $2^{-\Delta Ct}$ method, and gene expression was normalised to GAPDH. Experiments were repeated three times.

2.2.10.3 qPCR with Taqman® probes

For qPCR using Taqman probes the Taqman Gene Expression Mastermix was used. A master mix was prepared for each set of primers (Table 2-9), and individual reactions were set-up in a 96 well format with a final volume of 20µl. The components of each reaction mix are shown in Table 2-10. For each sample, each primer pair was run in triplicate. Once plates had been set-up and sealed, they were centrifuged at x2000rpm for 1 minute to ensure all reagents were at the bottom of the well and to remove air bubbles. Plates were then run on a 7500 Fast Real-Time PCR system (Applied Biosystems) with 7500 software v.2.0.5 (Applied Biosystems), using the thermal cycling conditions shown in Table 2-11. In the amplification plots a threshold was set and Ct values determined. The relative normalized gene expression was calculated using the $2^{-\Delta Ct}$ method and gene expression was normalised to PUM1. Experiments were repeated three times. PUM1 was chosen for normalisation due to previous analysis of the microarray dataset comparing the expression values of 15 housekeeping genes between tumours and perilesional skin. PUM1 was selected due to this gene having the smallest standard deviation as a percentage of the mean expression signal value, which was consistent between both the tumour and control samples.

Gene Name	Probe ID
BDNF	Hs00380947_m1
PUM1	Hs00472881_m1

Table 2-9: Taqman Probes for qPCR

Reaction Components	Volume per well
2x TaqMan® gene expression MasterMix	10μl
20X TaqMan® Gene expression primer and probe	1μl
cDNA (diluted 1:3)	1μl
ddH_2O	8μl

Table 2-10: Reaction mixture composition for Taqman probe qPCR

Step/Cycles	Temperature	Time
Uracil-DNA glycosylase incubation	50°C	2 minutes
AmpliTaq Gold® activation	95°C	10 minutes
Denaturation	95°C	15 seconds
Annealing/ Extension (Repeat for x40 cycles)	60°C	1 minute

Table 2-11: Thermocycler PCR program for Taqman probe qPCR

2.3 Cloning

2.3.1 Preparation of competent cells

*E.*coli *DH5-alpha* cells (Stratagene) were streaked from a glycerol stock onto an LB agar plate and incubated at 37°C overnight. A single colony was selected and used to inoculate 10mls of LB media without any selection antibiotic, which was incubated at 37°C overnight on a shaking platform at 220rpm. 1ml of the starter culture was added to 100mls of LB media and incubated at 37°C with vigorous shaking and checked over a few hours until the absorbance at 600nm gave a reading of 0.6. The cells were harvested by firstly placing the cells on ice for 10 minutes before centrifuging at x6000rpm for 10 minutes in a pre-chilled centrifuge. Following this cells were

resuspended in 25mls of ice-cold, 100mM calcium chloride ($CaCl_2$) and incubated on ice for 20 minutes. The cells were again centrifuged as before then resuspended in 5mls of $CaCl_2$ and 1ml of 100% glycerol added. The cells were divided into 100μl aliquots and stored at -80°C.

2.3.2 Purification of plasmid DNA

Plasmid DNA was purified using the QIAprep® Spin Miniprep Kit (Qiagen) according to the manufacturer's protocol. In brief, overnight bacterial cultures were pelleted by centrifugation at x3000rpm for 5 minutes. Bacterial cells were then resuspended in a series of buffers, firstly 250μl of Buffer P1 containing RNase A (100μg/ml) and LyseBlue reagent. The cells are then lysed under alkaline conditions with 250μl of Buffer P2 added which turns the sample blue to ensure a homogenous solution, prior to adding 350μl of Buffer NE to neutralise and precipitate the cellular debris in a high salt concentrate buffer, followed by separation of the DNA via centrifugation for 10 minutes at x13000rpm. The plasmid DNA was then isolated through adsorption onto a silica membrane of a spin column, which was subsequently washed with Buffer PB then Buffer PE to remove endonucleases and residual salts respectively. The purified plasmid DNA was finally eluted in 50μl Buffer EB by centrifugation and stored at -20°C.

2.3.3 Glycerol stocks

From the 5ml overnight bacterial cultures generated from selected colonies, 1ml of culture was transferred to an eppendorf and centrifuged at x5000rpm for 1 minute to pellet the cells. The supernatant was discarded until and the pellet resuspended in 50μl 100% glycerol to make stocks. These were stored at -80°C and used to further amplify the plasmids in *E.*coli *DH5-alpha* cells for lentiviral transfection into human HEK293T and HaCaT cells.

2.3.4 Generation of mutant *pLEX*-CYLD

The lentiviral expression vector *pLEX*-CYLD was previously generated by Dr Neil Rajan, and incorporated wild-type CYLD into the lentiviral vector *pLEX*-MCS. Glycerol stocks of transformed *E.*coli *DH5-alpha* were grown and plasmid DNA prepared as explained above.

2.3.4.1 Site-directed mutagenesis

Site directed mutagenesis is a technique that is used to investigate the relationship

between the structure and biological activity of proteins, DNA and RNA, thus helping to characterise the mechanisms of known disease causing mutations. It allows for targeted alterations, such as base substitutions, insertions or deletions to be made in double stranded plasmid DNA, with the use of primers that are designed with the desired mutation incorporated and flanked by sequences that are complementary to the template DNA. Therefore with thermal cycling the primers anneal to the vector DNA and are extended to integrate the mutation into the newly synthesised plasmid DNA. The product from this PCR reaction is then subjected to enzymatic digestion, to isolate the mutant product from the parental template, using the restriction endonuclease *Dpn* I. This enzyme specifically recognises a methylated GATC sequence present on DNA or plasmids isolated from *E.coli* strains such as the template plasmid. The mutant plasmid can then be transformed into competent bacteria (see below).

Patient specific mutations of CYLD: *c.*2460*del*C, *c.*2290- 2294*del*, *c.*2806 C>T and p.C601S (which corresponds to a *g* > *c* change at position 1803 in the nucleotide sequence) were incorporated in to the previously generated expression vector pLEX-*CYLD*, using the QuikChange Lightning Site-Directed Mutagenesis Kit (Agilent Technologies). Primer pairs were designed to incorporate the *CYLD* mutations using the QuikChange primer design program and guidelines (available at www.agilent.com/genomics/qcpd), and synthesised by Eurofins. The mutations were positioned in the middle of the primer sequence (as shown in Table 2-12). The first reaction set-up used PCR amplification to incorporate the desired mutations into the wild-type template (Tables 2-13 & 2-14). This was followed by incubation of the amplified reactions with 2µl of *Dpn* I restriction enzyme at 37°C for 5 minutes, to digest the non-mutated DNA template.

CYLD mutation	Sense (SN) or Antisense (ASN)
c.2460*del*C	SN: 5'-AGCAGTTTTGTAAAACCTGAACACTCAAGTCCACCTTC-3' ASN: 5'-GAAGGTGGACTTGAGTGTTCAGGTTTTACAAAACTGCT-3'
c.2290_2294*del*5AAACT	SN: 5'-GATGCCTCGATTTGGAAAAGACTTTATTTAAAAAAATTTTTCCTTCTCTG-3' ASN: 5'-CAGAGAAGGAAAAATTTTTTTAAATAAAGTCTTTTCCAAATCGAGGCATC-3'
c.2806 C>T	SN: 5'-ATCACAAAGCAGTCTTCATGCACAGCCTTGGATTC-3' ASN: 5'-GAATCCAAGGCTGTGCATGAAGACTGCTTTGTGAT-3'
p.C601S	SN: 5'-ATCCAGGGTCATTACAATTCTTCTTACTTAGACTCAACCTTATTC-3' AN:5'-GAATAAGGTTGAGTCTAAGTAAGAAGAATTGTAATGACCCTGGAT-3'

Table 2-12: Primer sequences for site-directed mutagenesis of *pLEX*-CYLD

The letters that are underlined in red represent the bases between which the deletion has occurred. The bases in red represent the bases that have been altered for another base.

Reagent	Volume (μl)
10x Reaction Buffer	5μl
p*LEX*-CYLD dsDNA	1μl
Mutation Primer F	*X*μl *(*μl required for 125ng)
Mutation Primer R	*X*μl (μl required for 125ng)
dNTP mix	1μl
QuikSolution reagent	1.5μl
QuikChange Lightning Enzyme	1μl
ddH_2O	Make up to 50μl

Table 2-13: Reaction mixture composition for site-directed mutagenesis

Step/Cycles	Temperature	Time
Initial denaturation	95°C	2 minutes
Denaturation	95°C	20 seconds
Annealing	60°C	10 seconds
Extension	68°C	7 minutes
(Repeat for x18 cycles)		
Final extension	68°C	5 minutes

Table 2-14: Thermocycler program for site-directed mutagenesis

2.3.4.2 Transformation of competent cells with mutant *pLEX*-CYLD

XL10-Gold ultracompetent cells (45μl aliquot) were thawed on ice, then incubated with 2μl β-mercaptoethanol mix (provided in kit) on ice for 2 minutes. Subsequently 2μl of the *Dpn* I treated DNA was added to the reaction mix and left on ice for 30 minutes. The cells were then heat shocked at 42°C for 30 seconds, then returned to ice for 2 minutes. The cells were then agitated at 225rpm for an hour at 37°C with 500μl of NZY^+ media, before being spread onto agar plates, containing the selective antibiotic Ampicillin, and left to incubate at 37°C overnight. Single colonies were picked from selective agar plates and used to inoculate 5mls of NZY^+ media containing ampicillin, before being cultured overnight at 37°C on a shaking platform at 220rpm. Plasmid DNA was extracted from bacterial cultures (section 2.3.2) and DNA sent for sequence verification (section 2.3.6). Once verified *E.*coli *DH5-alpha* cells were transformed in the same manner to generate stocks.

2.3.5 Generation of p*LEX*-TrkB.FL and p*LEX*-TrkB.T1

2.3.5.1 Blunt PCR cloning

Both TrkB.FL and TrkB.T1 isoforms were amplified and the resulting PCR products purified (section 2.2.7). The StrataClone blunt PCR cloning kit (Agilent Technologies) was used to ligate the TrkB DNA products into the pSC-B-amp/kan vector supplied, by exploiting the activity of Topoisomerase I to ligate the PCR product into DNA arms that contain *lox*P recognition sequences on the opposite ends. This linear product, once transformed into competent cells expressing *Cre* recombinase, can undergo *Cre*-mediated recombination of the vector and linear molecule containing the PCR product to create circular DNA (Figure 2-2). The ligation reaction mix is included in Table 2-15 and the components were added in the order in which they are displayed. The reaction was incubated for 5 minutes at room temperature before being placed onto ice.

Reagent	Volume (μl)
10x Reaction Buffer	5μl
p*LEX*-CYLD dsDNA	1μl
Mutation Primer F	*X*μl *(*μl required for 125ng)
Mutation Primer R	*X*μl (μl required for 125ng)
dNTP mix	1μl
QuikSolution reagent	1.5μl
QuikChange Lightning Enzyme	1μl
ddH_2O	Make up to 50μl

Table 2-15: Reaction mixture composition for blunt PCR cloning

StrataClone solopack competent cells (50μl aliquot) were thawed on ice, before adding 2μl of the cloning reaction mix and incubating on ice for 20 minutes. The cells were then heat shocked at 42°C for 45 seconds, then returned to ice for 2 minutes. The cells were then agitated at 225rpm for an hour at 37°C with 250μl of LB (lysogeny broth) media, before being spread onto agar plates containing the selective antibiotic Ampicillin, and left to incubate at 37°C overnight. Single colonies were picked from selective agar plates and used to inoculate 5mls of LB media containing ampicillin, before being cultured overnight at 37°C on a shaking platform at 220rpm. Plasmid DNA was extracted from bacterial cultures (section 2.3.2) and the DNA used for subsequent restriction digests and ligations.

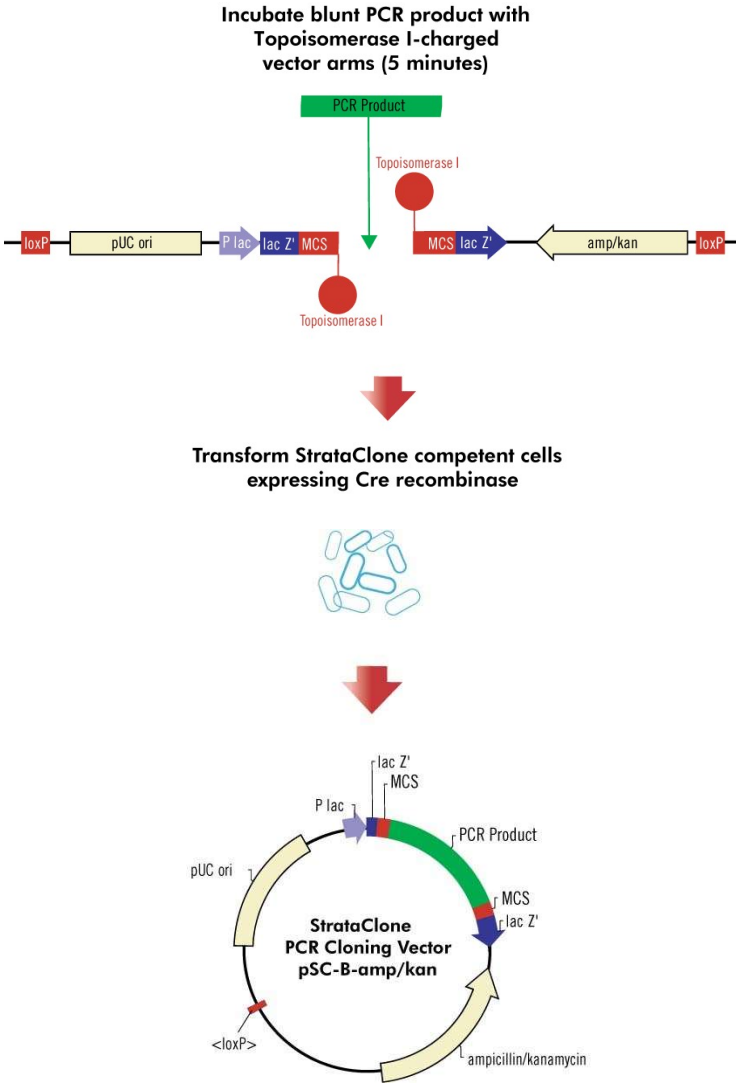

Figure 2-2: An overview of the Strataclone Blunt PCR cloning method.

2.3.5.2 Restriction enzyme digests

Both the pSC-B-amp/kan and *pLEX*-MCS vectors carried restriction enzyme sites and underwent restriction digests to enable downstream insertion of desired inserts and for the analysis of positive clones. A double digest was carried out for all digest reactions using the restriction enzymes BamHI and XhoI (New England BioLabs). The most compatible buffer for both enzymes was selected for, which for these reactions was NEBuffer 3 (New England BioLabs). The reaction mix is shown in Table 2-16. The reactions were incubated for 1 hour at 37°C, before being resolved on a 1% agarose gel.

Reaction Components	Volume
Restriction enzyme (BamHI) (10U)	0.5μl
Restriction enzyme (XhoI) (10U)	1μl
NEBuffer (10X)	2.5μl
BSA	2.5μl
DNA/plasmid (500ng)	*n* μl
ddH_2O	Upto 25μl

Table 2-16: Reaction mixture composition for restriction enzyme digests.

2.3.5.3 Ligation reactions

The digested DNA underwent agarose gel electrophoresis and the fragments of interest were cut out and purified. The purified digested DNA was then ligated in different ratios of vector to insert in a 20μl ligation reaction mix, which included 1μl T4 DNA ligase (Promega) and 2μl of Reaction Buffer (10X). The reaction was left for 20 minutes at room temperature before being left at 70°C for 5 minutes. The ligation mixture was then used to transform competent *E.*coli *DH5-alpha* cells, which were then spread onto agar plates containing the selective antibiotic Ampicillin and left for at least 18 hours at 37°C. Colonies were numbered, selected and each cultured in 200μl of LB media in a 96 well plate overnight on a shaking platform at 220rpm. The cells were pelleted by centrifugation at x1000rpm for 5 minutes before sterile tips were dipped into the pellets and transferred into a 96 well plate for PCR screening. The recipient PCR plate contained 10μl of PCR mastermix in each well, containing primers for each of the TrkB isoforms; Exons 15-18 for TrkB.FL and Exons 15-16 for TrkB.T1 (section 4.2.1). The plate was placed into a thermal cycler to run the PCR reactions and the products run on a 1% agarose gel. Colonies that were identified as positive for the insert were then used to inoculate 5mls of LB media containing ampicillin, before being cultured overnight at 37°C on a shaking platform at 220rpm. Plasmid DNA was extracted from bacterial cultures (section 2.3.2) and subject to digestion again to confirm the presence of the insert. Once confirmed the p*LEX-TrkB.FL and* p*LEX-TrkB.T1* products were sent for sequence and orientation verification.

2.3.6 Sequence verification of plasmids and PCR product inserts

Plasmid DNA for both CYLD and TrkB was sent for sequencing (Eurofins Genomics) with primers that covered the entire gene and flanking sequence from the insertion site of the plasmid (primer sequences included in Appendix), to verify the sequence and check the orientation of the product before proceeding with cell transduction experiments. Sequences were visualised in Sequencher v5.1 (Genecodes Corporation) (Figure 2-3).

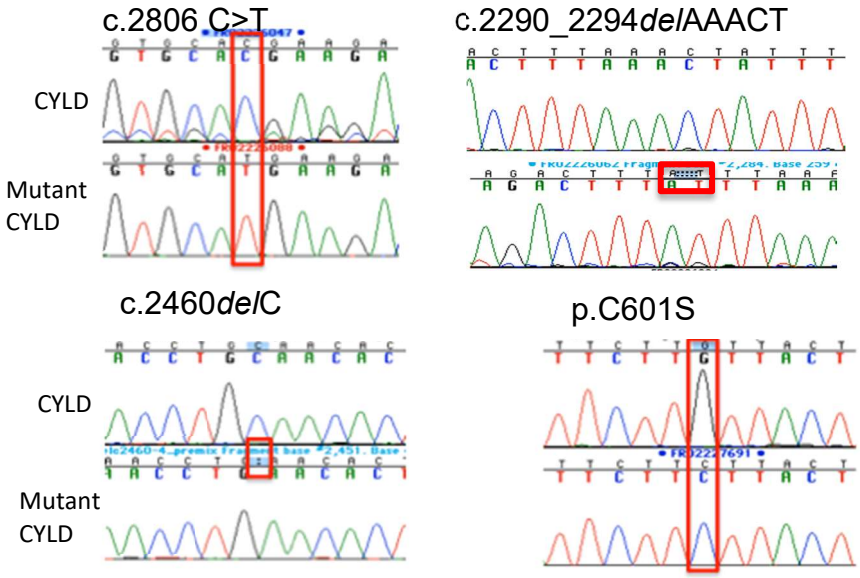

Figure 2-3: Chromatogram examples of sequencing of mutant pLEX-*CYLD* vectors.

2.4 Western Blotting

The levels of protein expression in cell lysates and tissue samples were measured using western blotting. The technique has four stages as follows: firstly protein denaturation, which involves boiling protein samples in the presence of a reducing agent such as β-mercaptoethanol or dithiothreitol (DTT) to break down tertiary protein structures such as disulphide bonds. Secondly the samples are prepared with sodium dodecyl sulphate (SDS), an ionic detergent that covers the protein with a negative charge to create a homogenous mass to charge ratio, which allows for electrophoretic separation according to molecular weight by SDS-PAGE. Thirdly proteins are transferred to a PVDF membrane and probed with antibodies, which are lastly visualised with the use of horseradish peroxidase (HRP) conjugated antibodies. The peroxidase catalysing the oxidation of luminol in the presence of chemical enhancers to produce a chemiluminescence signal that can be detected.

2.4.1 Preparation and extraction of protein lysates from tissue

Tissue samples, snap frozen after surgery in liquid nitrogen, were mounted in OCT embedding reagent and sectioned using a cryostat. Samples were cut at a thickness of 30μm, with 10-20 sections collected per sample and placed into a 1.5ml eppendorf on dry ice. The tissue sections were firstly washed in 1ml ice cold PBS with phosphatase inhibitors, such as PhosSTOP™ tablets (Roche), then briefly centrifuged at 4°C to pellet the tissue. The tissue was lysed in 150-200μl of Phosphosafe™ lysis buffer and samples left at room temperature for 5 minutes before being transferred to a Precellys® bead tube (Bertin). The samples were then homogenized at x6500rpm for 30 seconds using the Precellys® Evolution homogeniser (Bertin) with the sample lysate then being transferred into a 1.5ml eppendorf. The beads were washed with a further 100μl of lysis buffer, which was added to the homogenized lysate. The samples were then centrifuged at 14000rpm for 15 minutes at 4°C. The supernatant was removed and samples were either taken forward to determine the protein concentration or stored at -80°C.

2.4.2 Preparation and extraction of protein lysates from cells

Cells were trypsinised (section 2.6.4) and cell pellets collected. Any surplus media was removed before resuspending the cell pellet in 50-200μl (dependent on the pellet size and the vessel trypsinised) of Phosphosafe™ lysis buffer. The sample was then transferred to an eppendorf and centrifuged at x14000rpm for 15 minutes at 4°C. Following this the supernatant was collected and both the pellet and lysate were stored at -80°C or the lysate was taken forward to determine the protein concentration.

2.4.3 Determination of protein concentration- Qubit

The concentration of protein in sample lysates was quantified using a fluorometric quantitation method as explained in section 2.2.4. The level of fluorescence is detected by a fluorometer and converted into a concentration value using protein standards of known concentration and a curve-fitting algorithm.

The Qubit® Protein Assay kit was used alongside the Qubit® 3.0 fluorometer (both Life Technologies). Samples were prepared according to the manufacturer's protocol. In brief a buffer/dye working solution was prepared by diluting dye reagent 1:200 in

assay buffer in a volume appropriate to cover the number of samples and standards to be assayed. Protein lysate was diluted 1:100 in the buffer/dye working solution (2µl to 198µl), alongside three protein standards (0ng/µl, 200ng/µl, 400 ng/µl) diluted 1:20 in the buffer/dye working solution (10µl to 190µl). These were then incubated at room temperature for 15 minutes before taking readings.

2.4.4 Determination of protein concentration- BCA assay

Alternatively protein concentrations were quantified using a BCA kit (Pierce, ThermoFisher Scientific) according to manufacturer's instructions. Briefly, sample lysates were first diluted 1:20 in distilled water, before 25µl of sample was added to 200µl of working reagent (50:1, Part A:Part B) in a 96 well microplate, with samples set up in duplicate wells. An albumin standard supplied with the kit was serially diluted (0.025mg/ml-2mg/ml) with water and a constant proportion of lysis buffer, with each standard also included in duplicate on the plate. Plates were incubated for 30 minutes at 37°C before determining the colourimetric absorbance at 562nm on a plate reader. A standard curve was generated from the mean absorbance values of the standards and sample concentrations were interpolated, before correcting for dilution factor.

2.4.5 SDS-PAGE (Sodium Dodecyl Sulphate-Poly Acrylamide gel electrophoresis) and membrane transfer

Protein samples were prepared with an appropriate volume of lysate that equated to 25 µg of protein would be run in each lane of a gel. The samples were also prepared with 4X LDS (lithium dodecyl sulphate) loading buffer (Invitrogen), 10X reducing agent (Invitrogen) and water to make the final volume upto 30µl. Protein samples were boiled at 70°C for 10 minutes, then separated under reduced conditions using the NuPAGE® gel electrophoresis system on 3-8% Tris-Acetate gels (Invitrogen) in 1X Tris-Acetate SDS running buffer (Invitrogen). Alongside the samples 7µl of PageRuler™ Plus prestained protein stanadrd was used for molecular weight markers (Thermofisher Scientific). Following this proteins were transferred onto PVDF membranes using the Trans-Blot® Turbo™ blotting system (Bio-Rad) according to the manufacturer's protocol. This is a semi-dry rapid transfer system in which the PVDF membranes are soaked in 100% methanol before being equilibrated in 1X transfer buffer for a couple of minutes. The membrane, protein gel, and sponges are then assembled into a transfer cassette and proteins transferred at 25V for 10 minutes.

2.4.6 Protein detection

After protein transfer the membranes were blocked in 5% (w/v) non-fat milk powder in Tris buffered saline with Tween 20 (TBST) (50mM Tris pH7.4, 200mM NaCl, 0.1% (v/v) Tween 20) for 1 hour at room temperature. Membranes were subsequently probed with primary antibody overnight at 4°C with rotary agitation, with all antibodies used prepared in 5% (w/v) non-fat milk powder in TBST. Antibodies used are listed in Table 2-17. After primary antibody exposure, the blot was washed three times, for 5 minutes with TBST. Membranes were then left to incubate with HRP-conjugated goat anti-rabbit (Cell Signalling Technologies) or goat anti-mouse (Cell Signalling Technologies) secondary antibody diluted in 5% (w/v) non-fat milk powder in TBST, for 1 hour at room temperature with agitation. Membranes were washed as previously described before visualisation using enhanced chemiluminescence (ECL) detection reagents (GE Healthcare) and exposure onto photographic film (FujiFilm Corporation).

Protein	Antibody type	Clone	Isotype	Dilution	Supplier	Cat no.
Primary Antibodies for WB						
CYLD	Monoclonal	D1A10	Rabbit IgG	1:1000	Cell Signalling	#8462
TrkB	Monoclonal	80E3	Rabbit IgG	1:1000	Cell Signalling	#4603
p-Stat3 (Tyr705)	Monoclonal	D3A7	Rabbit IgG	1:2000	Cell Signalling	#9145
p-Stat3 (Ser727)	Polyclonal	-	Rabbit	1:1000	Cell Signalling	#9134
Stat3	Monoclonal	124H6	Mouse IgG2a	1:1000	Cell Signalling	#9139
p-Src (Tyr416)	Monoclonal	D49G4	Rabbit IgG	1:1000	Cell Signalling	#6943
p-Src (Tyr 527)	Polyclonal	-	Rabbit	1:1000	Cell Signalling	#2105
p-Src (Ser17)	Monoclonal	D7F2Q	Rabbit IgG	1:1000	Cell Signalling	#12432
Src	Monoclonal	36D10	Rabbit IgG	1:1000	Cell Signalling	#2109
p-Akt (Ser473)	Monoclonal	D9E	Rabbit IgG	1:2000	Cell Signalling	#4060
Akt	Polyclonal	-	Rabbit	1:1000	Cell Signalling	#9272
BDNF	Monoclonal	#35928	Mouse IgG1	1:1000	R&D Systems	MAB248
Bcl-xL	Monoclonal	54H6	Rabbit IgG	1:1000	Cell Signalling	#2764
CyclinD1	Monoclonal	92G2	Rabbit IgG	1:1000	Cell Signalling	#2978
c-Myb	Monoclonal	D2R4Y	Rabbit IgG	1:1000	Cell Signalling	#12319
β-Actin	Monoclonal	D6A8	Rabbit IgG	1:1000	Cell Signalling	#8457
GAPDH	Monoclonal	14C10	Rabbit IgG	1:1000	Cell Signalling	#2118
Secondary Antibodies						
Anti-Rabbit HRP-linked antibody	-	-	IgG	1:5000	Cell Signalling	#7074
Anti-Mouse HRP-linked antibody	-	-	IgG	1:5000	Cell Signalling	#7076

Table 2-17: Antibodies used for Western Blotting.

2.5 Histological Techniques

2.5.1 Tissue processing and sectioning

2.5.1.1 Tissue fixation and embedding

Surplus skin and tumour tissue taken from patients undergoing routine surgery was obtained and the tissue samples were fixed the in 4% PFA for 2 hours to overnight at 4°C, depending on the specimen size. Once fixed the tissue samples were washed in PBS to remove excess fixative. The tissue was then dehydrated in graded alcohols (30%-100%) followed by xylene, before finally being immersed in molten paraffin wax at 60°C and the wax changed a further two times. The tissue was then embedded in paraffin wax and set into moulds to create a block.

2.5.1.2 Tissue sectioning (wax)

Tissue blocks were sectioned using a microtome (Leica) at a thickness of 5-8μm and orientated onto Superfrost™ Plus slides (VWR). Tissue sections were floated on water atop of the slides, warmed to 37°C using a hotplate, and left to flatten out. Excess water was removed and sections were left to dry at 40°C overnight to ensure sections adhered well to the slide.

2.5.1.3 Tissue sectioning (frozen)

Tissue specimens were embedded in OCT and sectioned using a Cryostat (Leica). Tissue sections were cut at 5-8μm and mounted onto Superfrost Plus slides (VWR). Slides were left to dry on dry ice before being stored short-term at -20°C until required.

2.5.2 Haematoxylin and Eosin staining

For analysis of tissue morphology, sections were stained with haematoxylin- a purple stain to visualize the nuclei of cells, and eosin- a pink counterstain to visualize the cytoplasm. Briefly slides were de-waxed in xylene for 2 x 10 minutes with a change of xylene, submerged in graded alcohols (100%-30%) then distilled water, 5 minutes in each, to rehydrate the slides, before being put in haematoxylin solution for 30 seconds. Following this slides were briefly dipped in distilled water, before 3-4 dips in the bluing solution Scott's Tap water. Again the slides were briefly washed in distilled water before being submerged in eosin for 30 seconds, followed by a brief wash in water and dips back up the graded alcohols, before sitting in 100% Ethanol for 2 x 5

mins and then placed in xylene for 2 x 5 minutes. Finally the slides were mounted with DPX mounting medium (Fisher) and cover-slipped.

2.5.3 Immunohistochemistry (IHC) using DAB

Solutions:

Sodium Citrate Buffer (pH6.0): 5.84g sodium citrate to 2L of distilled H20

2.5.3.1 IHC immunostaining protocol

Tissue section slides were firstly incubated in an oven at 60°C for 30 minutes to melt the paraffin wax, the wax was then removed by submerging the slides in fresh xylene for 10 minutes, which was then repeated. The sections were then rehydrated in graded alcohols (100%-30%) for 5 minutes each and finally immersed in distilled water. Tissue sections were placed in sodium citrate buffer (pH6.0) in a pressure cooker, for antigen retrieval, with sections left at full pressure for 8-16 minutes. Slides were then washed three times in tris buffered saline (TBS) for 3 minutes before the sections were circled with a hydrophobic barrier pen, ensuring that the sections were not allowed to dry out. The EnVision™ + Dual Link System-HRP kit (Dako) was applied for immunohistochemical staining. Peroxidase blocking solution was applied to the sections for 5 minutes to prevent endogenous peroxidase activity, followed by three washes in TBS for 3 minutes. Sections were subsequently incubated with primary antibody, prepared in antibody diluent (Dako) to the concentrations specified in Table 2-18, for 1 hour at room temperature or overnight at 4°C, followed by three washes in TBS for 3 minutes. An HRP-labelled polymer conjugated with secondary antibodies was then applied to the sections for 1 hour at room temperature before washing three times in TBS for 3 minutes. Antibody binding was visualized with liquid DAB (3,3'-Diaminobenzidine) staining, prepared according to the manufacturer's instructions (Dako). The slides were rinsed in distilled water three times for 3 minutes followed by nuclear counterstaining with haematoxylin (diluted 1:5 in distilled water), dehydration in graded alcohols and clearing in xylene. The slides were finally mounted under cover slips with DPX mounting medium (Thermofisher Scientific) and left to dry overnight.

2.5.3.2 Analysis and protein quantification of DAB staining

Slides were inspected under a microscope, before being scanned on a SCN400 slide scanner (Leica) (Newcastle Biobank service). For quantification five representative

immunohistochemistry images were taken at 20X magnification, of a tissue section from each tumour sample and control perilesional skin areas. ImageJ software (v 1.48; https://imagej.nih.gov/ij) was used to quantify DAB staining in the images. RGB values were restricted to the colour of DAB in the images were used to distinguish areas that were DAB-positive and the area quantified. This was then compared to the total area of the assessed image to generate a ratio of positive staining. The mean average of the ratios was taken from across all 5 images to generate a ratio per sample. This was repeated for the control areas for comparison.

2.5.4 Immunofluorescence (IF) on frozen sections

Solutions:

Washing Reagent 1: 1x PBS- 5 PBS tablets (fisher) into 1L distilled H_2O)

Washing Reagent 2: 0.1% Triton X-100- 100ul Triton X-100 (maker), 0.2% BSA- 0.2g BSA (fisher) per 100mL 1x PBS

Block/Antibody diluent: 0.3% Triton X-100- 300ul Triton X-100, 0.5% BSA- 0.5g BSA per 100mL 1x PBS

2.5.4.1 IF immunostaining protocol

Spheroid section slides were initially thawed at room temperature for 5 minutes before being placed in sodium citrate buffer (pH6.0) in a pressure cooker, for antigen retrieval, with sections left at full pressure for 6-8 minutes. The slides were then washed for 10 minutes in PBS before the sections were circled with a hydrophobic barrier pen, ensuring that the sections were not allowed to dry out. The sections were incubated for an hour at room temperature in 50-100µl of blocking solution (0.3% Triton X-100, 0.5%BSA in PBS). Primary antibodies were prepared in antibody diluent (0.3% Triton X-100, 0.5%BSA in PBS) to the concentrations specified in Table 2-18, and sections incubated with 50-100µl of primary antibody overnight at 4°C. Subsequently slides were washed three times in 0.1% Triton X-100, 0.2% BSA in PBS solution for 10 minutes, before sections were incubated with 50-100µl Alexafluor® conjugated secondary antibodies (Jackson Laboratories) prepared in the same antibody diluent as the primary and filtered. Slides were left to incubate for an hour at room temperature in the dark. After which the slides were washed as previously described, then excess

liquid was removed and sections were mounted with coverslips using 20-30µl of Vectashield Antifade mounting medium with DAPI included for a nuclear stain (Vector Laboratories). Images of the slides were then taken using a UV Zeiss Axioimager microscope and images captured with a monochrome digital camera (Zeiss) connected to a computer running Zeiss Axiovision 4.7 software.

Protein	Use	Antibody type	Clone	Isotype	Dilution	Supplier	Cat no.
Primary Antibodies for immunohistochemical techniques							
p-Stat3 (Tyr705)	IHC	Monoclonal	D3A7	Rabbit IgG	1:200	Cell Signalling	#9145
STAT3	IHC/IF/ICC	Monoclonal	124H6	Mouse IgG2a	1:600/ 1:1600	Cell Signalling	#9139
TrkB	IHC/IF	Monoclonal	80G2	Rabbit IgG	1:200	Cell Signalling	#4607
CK17	ICC	Monoclonal	EPR1624Y	Rabbit IgG	1:100	Abcam	Ab51056
c-MYB	IHC	Monoclonal	SPM175	Mouse IgG2a	1:50	Abcam	Ab17851
Secondary Antibodies							
Affinipure Goat Anti-Mouse, Alexa Fluor® 594 conjugate		-	-	IgG	1:200	Jackson ImmunoResearch	115-585-146
Affinipure Goat Anti-Rabbit, Alexa Fluor® 488 conjugate		-	-	IgG	1:200	Jackson ImmunoResearch	111-545-144

Table 2-18: Antibodies used for Immunohistochemical techniques

2.5.5 Immunocytochemistry (ICC) on cell culture chamber slides

Solutions:

Antibody diluent: 0.1% Triton X-100 - 5µl Triton X-100 into 5mls 1x PBS

Washing Reagent 1: 1x PBS- 5 PBS tablets (fisher) into 1L distilled H_2O)

2.5.5.1 ICC immunostaining protocol

Storage PBS was removed form each well of the chamber slide and 500µl of ice-cold methanol added for 10mins to allow for permeabilisation of cell membranes, before wells were rinsed with PBS. To each well 500µl of 2% normal goat serum in PBS was added and left at room temperature for 20 minutes, with agitation on a rocker. Following this 200µl of primary antibody, diluted in 0.1% Triton X-100 solution (5µl Triton X-100 in 5mls PBS) to the concentration specified in Table 2-18, was added to each of the wells and the slides left overnight at 4 C. Subsequently wells were washed three times in PBS for 10 minutes on a rocker, before adding 200µl of filtered, Alexafluor® conjugated secondary antibodies (Jackson Laboratories) diluted in PBS, to each well. The slides were then left at room temperature for an hour and kept in the dark. After which the slides were washed as previously described, the chamber well

casing and excess liquid was removed and sections were mounted with coverslips using 20-30µl of Vectashield Antifade mounting medium with DAPI included for a nuclear stain (Vector Laboratories). Images of the slides were then taken using a UV Zeiss Axioimager microscope and images captured with a monochrome digital camera (Zeiss) connected to a computer running Zeiss Axiovision 4.7 software.

2.6 Cell culture

2.6.1 Cell line maintenance

All cell culture procedures and experiments were carried out under aseptic conditions using a class II vertical laminar flow biological safety cabinet. The HaCaT and HEK-293T cell lines were used in this study. HEK293T cells, are a derivative of the human embryonic kidney cell line (Graham *et al.*, 1977) but are transformed with SV40 T antigen (DuBridge *et al.*, 1987), and are routinely used in research due to their high transfection efficiency. HaCaTs are a spontaneously immortalised human keratinocyte cell line with a transformed phenotype, but remains non-tumouregenic and maintains full epidermal differentiation capacity (Boukamp *et al.*, 1988). Cells lines were routinely cultured on standard tissue culture plasticware, flasks and plates, at 37°C in a humidified atmosphere in a 5% CO_2 incubator. HEK293-T cells were maintained in DMEM (with phenol red) (Invitrogen, cat no: 21969-500) supplemented with 10% FBS, 1% Penicillin (100U/ml) Streptomycin (100µg/ml), 1% L-glutamine (2mM) and 1ml Amphotericin B (0.5µg/ml) (all Gibco, Invitrogen). HaCaT cells were maintained in EpiLife™ medium (Gibco, cat no: MEPI500CA) supplemented with 1% 100X human keratinocyte growth supplement (containing growth promoting additives including recombinant epidermal growth factor, insulin and bovine pituitary extract; cat no: S0015), 0.2% Penicillin (20U/ml) Streptomycin (20µg/ml), 1% L-glutamine (2mM) and 0.2ml Amphotericin B (0.1µg/ml) (all Gibco, Invitrogen). Media was replaced every 48 hours.

2.6.2 Cylindroma primary cell culture (CPCC)

Tumour tissue obtained from surgery was stored in complete DMEM (as above) for transport of the samples and processed within 1-2 hours. Firstly any remaining overlying epidermis and fat were removed before the cylindroma tumour sample was cut up into 1-2mm pieces with scalpels in a petri dish. The tissue pieces were then

transferred to a sterile 15ml tube in 2-3mls of complete DMEM and centrifuged at x900rpm for 5 minutes. All subsequent centrifugation steps were carried out with these settings. Once the media had been decanted the tissue pieces underwent enzymatic digestion to gain a single cell suspension; firstly being resuspended in 5mls of 2.5% Trypsin (Gibco) for an hour at 37°C, followed by centrifugation and resuspension in 5mls of Collagenase (1mg/ml) (Sigma) for 95 minutes at 37°C, with periodic agitation of tubes in a waterbath. Tumour samples were centrifuged again then resuspended in 10mls of complete DMEM to inhibit any further enzymatic digestion. The cells were then filtered through a 40µm filter before being counted with a Neubauer chamber haemocytometer (section 2.6.6). Once counted, cells were seeded for experiments (see below), and the remaining cells cryopreserved (section 2.6.5). Cells were seeded onto plasticware that had been coated with Type I collagen at a concentration of 0.661µl/cm^2 using a collagen coating matrix kit (Gibco cat no: R011K). Primary cells cells were maintained in defined Keratinocyte Serum-Free Media (K-SFM) (Invitrogen, cat no: 10744-019) supplemented with 1ml 10X growth supplement, containing recombinant growth factors but not bovine pituitary extract, 1ml Penicillin (20U/ml) Streptomycin (20µg/ml), 1% L-glutamine (2mM) and 0.2ml Amphotericin B (0.1µg/ml) (all Gibco, Invitrogen). Media was replaced every 48 hours with a 50:50 exchange of fresh media.

2.6.3 Thawing of cell lines and primary cells

Cells were removed from -80°C storage and thawed in a 37°C bead bath. The cell suspension was transferred into a sterile falcon tube and centrifuged at 200xg for 5 minutes to remove the cryoprotective DMSO media. The pelleted cells were then resuspended in 7mls of pre-warmed complete growth media and transferred to a 75cm^2 flask and placed in an 5% CO_2 incubator at 37°C.

2.6.4 Routine passaging of cells

Cells were passaged every 3-7 days depending on how quickly cells reached confluency. The cell growth media was removed and the cell monolayer was washed with sterile phosphate buffered saline (PBS) (Gibco). For HaCaTs and primary cells, the cells were initially incubated with Versene (an EDTA solution) (Gibco) for 5 minutes at 37°C. Cells were then incubated with 0.5% Trypsin-EDTA for 5-15 minutes at 37°C. An equivalent volume of complete DMEM growth media was then added to neutralise the

Trypsin-EDTA and detached cells were collected and centrifuged to pellet the cells. The supernatant was discarded before cells were resuspended in complete growth media and passaged as required.

2.6.5 Cryopreservation of cells

To maintain stocks of cells, cultured cells were routinely cryopreserved in cryoprotective media consisting of 90% FBS (v/v) (Gibco) and 10% DMSO (v/v) (dimethyl sulphoxide) (ThermoFisher). Cells were trypsinised and resuspended in cryoprotective media. The cell suspension was divided into 1ml aliquots in cryogenic vials (ThermoFisher) and stored at -80°C for long-term storage.

2.6.6 Cell counting

Cells that had been trypsinised were counted prior to experiments using a Neubauer chamber haemocytometer. Cell pellets were resuspended in complete DMEM growth media and a 10µl aliquot of cell suspension was added to 10µl of trypan blue to discount dead cells. This cell suspension was then placed onto the haemocytometer and cells were counted in the two central grids; the liquid was of 0.1mm depth covering a 1mm square and therefore had a volume of 10^{-4} ml. The number of cells per ml was calculated and the cells then diluted to the required number for seeding.

2.6.7 Culturing of cells on chamber slides

Primary cells were counted and seeded onto glass cell culture chamber slides (8 wells per slide) (BD Falcon Biosciences) at a density of 10 x 10^4 cells/well. Wells had been collagen coated prior to seeding. Cell slides were cultured for 5- 7 days before cells were treated with 100ng/µl BDNF and 25ng/µl IL-6 diluted in 200ul of KSFM media, for 30 minutes at 37**°**C in a 5% CO_2 incubator. Following treatment of the cells, media was removed and cells were fixed in 4% PFA for 30 minutes before being washed with PBS and stored in fresh PBS at 4**°**C until required.

2.6.8 3D cell culture on scaffolds

Polystyrene tissue culture scaffolds (Alvetex) were first hydrated with 100% ethanol before being alternately washed with 70% ethanol and PBS twice before finally being coated with 32.5µl of Type1 collagen and 200µl KSFM. Scaffolds were left for 1 hour in the hood. Both primary cells and HaCaTs were seeded onto scaffolds. After cells had been counted, 3 x 10^6 cells were pelleted by centrifugation and resuspended in 200µl

of KSFM. Scaffolds were transferred into 6 well plates and the cell suspension was added drop wise onto the scaffold until covered. Scaffolds were then incubated for 1 hour at 37°C in a 5% CO_2 incubator. After, the wells were topped up with 5mls KSFM, slowly added down the wall of the well to gently flood the scaffold. Scaffolds were then left for 4 weeks with media changes every 2-3 days.

2.6.9 Cell viability assay

The viability of the cells was assessed using the CellTiterGlo® luminescent cell viability assay (Promega), which quantitates the amount of ATP present as a marker of metabolically active 'alive' cells, and thus generates a luminescent signal that is directly proportional to the number of cells present.

Cells that had been transfected were seeded at 1 x 10^4 cells/well into the central 60 wells of a 96 well white tissue culture plate, with clear well bases. At least 10 wells were seeded per sample. Plates were left in a 5% CO2 incubator at 37C for 72 hours. The bottoms of the wells of the plates were taped over before growth media was removed and a 1:1 ratio of 40µl of fresh complete media and 40µl of CellTiterGlo® solution was added to each well. Plates were then run on a Luminoskan (Thermo Scientific) to measure luminescence. The machine followed a program of plate shaking for 2 minutes followed by incubation for 10 minutes in the dark before taking measurements of luminescence as luminescent units (RLU) for each well. Control wells with no cells were included (in triplicate) to establish background luminescence. Experiments were repeated at least three times. Data was normalised and the mean value of the three replicates for each cell type plotted in GraphPad Prism v6.0 (GraphPad Software Inc).

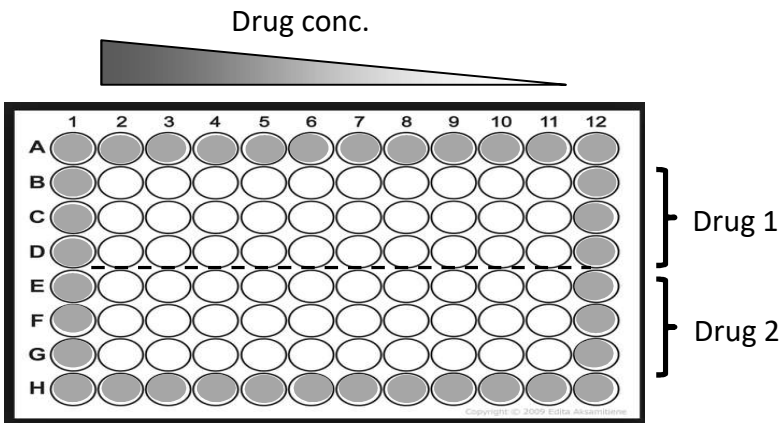

Figure 2-4: 96 well set-up for drug assays.

2.6.10 Drug assays

Cells that had been grown on 3D tissue scaffolds for 4 weeks had 2mm discs of the scaffold punched out, using a 2mm Harris uni-core (GE Healthcare) and placed into the inner 60 wells of a 96 well plate. The cells were maintained for 2 weeks in a final volume of 280µl of KSFM with inhibitors diluted in DMSO, with a final concentration of 0.1% DMSO. Each drug was prepared as a 10X stock solution at a range of concentrations in KSFM media. 28µl of drug at the specified concentration was added per well and media changes were performed every 48 hours. After 2 weeks the cells were assayed using CellTiterGlo®. Alternatively inhibitors were added to the growth media at the desired concentration to treat cells cultured in 6 well plates. Cells were incubated for 48 hours before being assayed by Western blot.

2.6.11 Colony forming assay

Cells that had been transfected were seeded at 2 x 10^3 cells per well into 6 well tissue culutre plates. Cells were grown for 8 days for colony formation before being fixed with 4% PFA for 30 minutes, washed with PBS and stained with 2mls of 0.57% sulphorhodamine in 1% acetic acid per well for 30 minutes. Cells were then washed in 1% acetic acid three times, left to dry overnight before being scanned. Plate images were analysed using Image J software (v 1.48; https://imagej.nih.gov/ij) to quantify staining in the images. RGB values were restricted to the colour of sulphorhodamine to distinguish areas that were positively stained and colony counts and total cell area were determined. Data was normalised and the mean value of the three replicates plotted in GraphPad Prism v6.0 (GraphPad Software Inc).

2.6.12 Lentiviral mediated gene over-expression and silencing

2.6.12.1 Lentivirus packaging and production

Lentiviral vectors were used to deliver the pLEX and pGIPz shRNA vectors (Figure 2-5), for CYLD (shCYL1 and shCYL2) and TrkB isoforms, to the cell lines. Both pLEX-MCS empty vector and non-silencing shRNA vectors were used as controls (Thermo Scientific Openbiosystems). Lentiviral vectors were first packaged using a Trans-Lentiviral packaging mix (Thermo Scientific Openbiosystems), containing the genes required for viral particle formation on 5 different vectors. A liposomal transfection technique was used to transfect HEK293T cells with a specified ratio of packaging mix

vectors to the lentiviral vectors in serum-free DMEM medium, with media changed to fully supplemented DMEM the next day. Cells were left for a further 48 hours before lentiviral-containing media was harvested. Media was cleared of cell debris by centrifugation followed by filtration (0.45μM). Polybrene was added (4μg/ml final concentration) to optimise transfection efficiency, and the lentivirus was aliquoted and stored at -80°C.

2.6.12.2 Lentiviral transduction of cell lines

HaCaT and HEK293T cells were grown to 50%-70% confluence in 6 well plates before being transduced with 2mls lentiviral media for 24 hours. The media was then replaced with supplemented DMEM for HEK293T or EpiLife for HaCaTs and the cells grown for a further 48 hours. Puromycin selection was used (upto 5ug/ml) to obtain successfully transduced cells, with the shCYLD vectors also monitored for GFP expression.

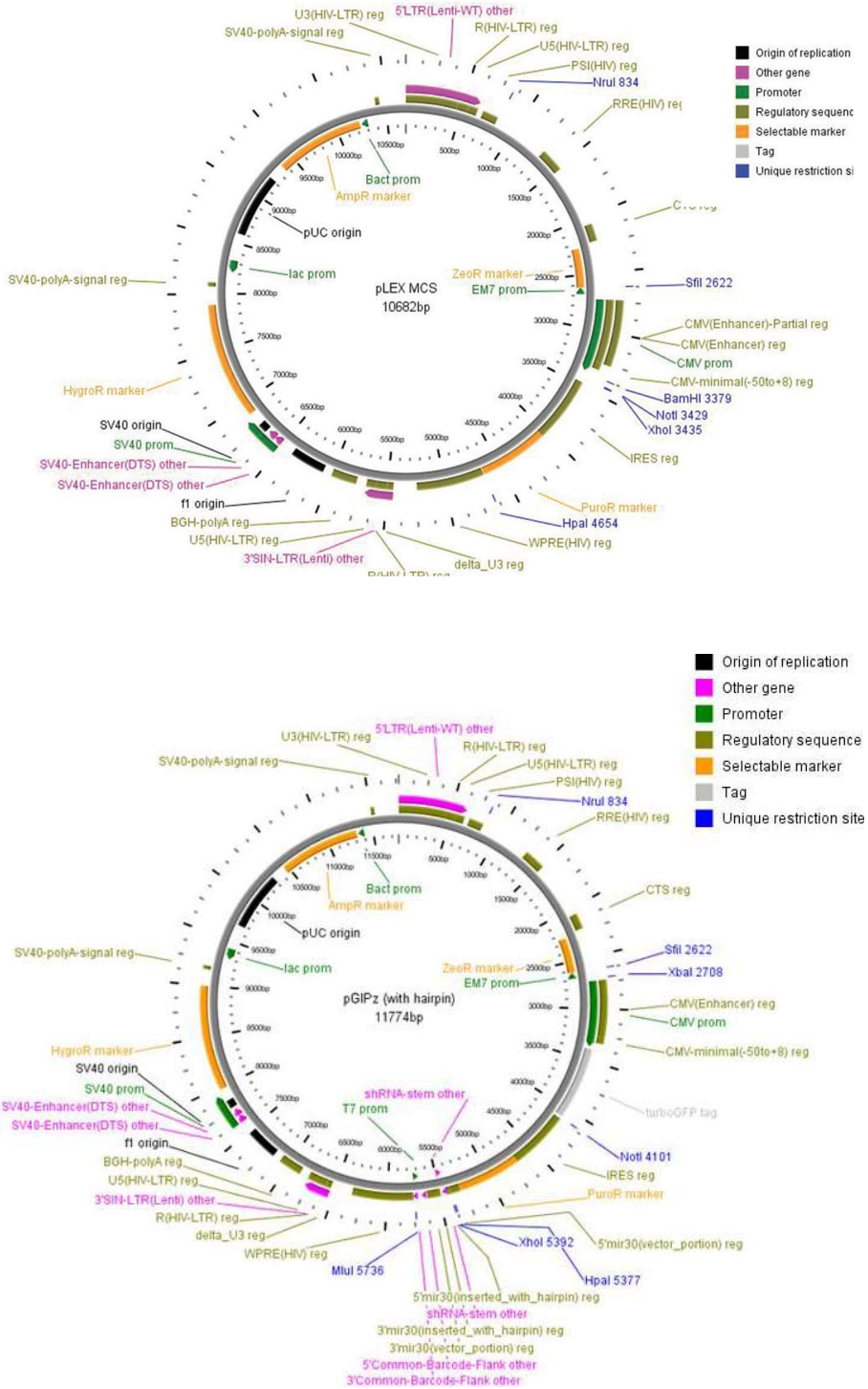

Figure 2-5: Lentiviral vectors pLEX-MCS and pGIPz.

The pLEX MCS and pGIPz vectors (both Open Biosystems) contain elements for lentiviral transduction and generation of stable cell lines. The gene of interest ligated into pLEX-MCS or a shRNA (shRNAmir) expression are under the control of the CMV promoter. Alongside other elements that are common to both of the vectors, including 5'LTR (5' long terminal repeat), ampicillin resistance (bacterial selectable marker), IRES-Puro resistance, (mammalian selectable marker), SIN-LTR (3' self inactivating long terminal repeat), WPRE (enhances the level of gene expression) and pUC Ori (high copy replication in E.coli). In addition the pGIPz vectors have Turbo GFP (marker to track shRNAmir expression).

2.7 RNA-seq

RNA was extracted from snap frozen *CYLD*-defective tumours and perilesional control skin, quantified and RNA integrity checked as stated in sections 2.2.2 and 2.2.5. The samples were then sent to AROS Applied Biotechnology A/S (Denmark) for library preparation and RNA sequencing analysis. cDNA libraries were prepared from 200ng of RNA using the TruSeq stranded mRNA library prep kit (Illumina). During this procedure mRNA species within the samples are purified through poly-A selection, using poly-T oligo-attached magnetic beads, followed by fragmentation using divalent cations and heat. The RNA fragments were then sequentially subjected to first and second strand cDNA synthesis by random priming, 3' adenylation and adaptor ligation, and finally PCR amplification to enrich for DNA fragments with adaptors attached at both ends ready for hybridisation of the cDNA library on to a flow cell for sequencing. Paired-end sequencing was performed on an Illumina Hiseq 2500 machine using version 4 chemistry, giving a minimum of 84 million 100 base pair, paired end reads per sample.

RNA-seq FASTQ files were processed and analysed by Mr Robert Stones (Newcastle University). The quality of the sequencing reads was checked using FastQC software. The reads were then aligned to the human reference genome GRCh38 using TopHat2 (Kim, 2013). This is a program that is designed to identify exon-exon splice junctions in its alignment of reads to the genome. Differential gene expression between tumours and perilesional controls was performed using Cufflinks and CuffDiff (Trapnell, 2012). This is an algorithm designed to estimate the expression of a transcript by counting the number of fragments generated by it and learns how read counts vary for each gene across replicates and uses these variance estimates to calculate the significance of observed changes in expression (Trapnell, 2012), with outputs tabulated in a spreadsheet. BED files generated form this pipeline were visualised in integrated genomic viewer v2.3 (IGV) and GTF files were visualised in the UCSC genome browser.

2.8 Statistical analyses

All statistical tests were performed using GraphPad Prism Version 6.0 software (GraphPad Software Inc.). Paired and unpaired t-tests were used where stated, with a *p*- value of <0.05 considered significant.

Chapter 3

Investigation of the transcription factor MYB in *CYLD*-defective tumours

3 Chapter 3: Investigation of the transcription factor MYB in *CYLD*-defective tumours

3.1 Introduction

3.1.1 Chapter Aims

Taking in to consideration the recognised histological similarities of cylindromas and adenoid cystic carcinoma (ACC), a salivary gland malignancy in which *MYB-NFIB* fusion expression is considered a molecular hallmark; in addition to *MYB-NFIB* fusion transcripts, and in the absence of fusions activation of MYB, having been identified in sporadic cases of cylindroma, the overall objective of the work in this chapter was to characterise the expression of *MYB*, including *MYB-NFIB* fusion transcripts, in inherited *CYLD*-defective tumours. The main aims were:

- To assess whether inherited cylindromas express the *MYB-NFIB* transcript
- To characterise the expression of MYB in inherited CYLD defective tumours
- To determine whether CYLD regulates MYB expression using *in vitro* silencing and overexpression assays
- To explore whether NF-κB regulates MYB expression using *in vitro* drug inhibition assays

3.1.2 The MYB family of transcription factors

The highly conserved *MYB* family of genes includes three members A-*MYB*, B-*MYB (*also known as *MYBL1 and MYBL2* respectively), and the most widely studied proto-oncogene c-*MYB* (hereafter referred to as *MYB* for the gene and MYB for the protein*)*. Each of the genes encode for nuclear proteins that act as transcriptional activators, with *MYB* in particular having a key role in regulating the proliferation and differentiation of the stem and progenitor cell niches in bone marrow, colonic crypts and the adult brain (Ramsay and Gonda, 2008). The three family members share extensive amino acid sequence homology and the structure of the MYB proteins has three main functional regions, including DNA-binding domains, a transactivating domain and a leucine-rich negative regulatory domain (NRD) (Figure 3-1) (Oh and Reddy, 1999). The major translational product of *MYB* is a 75kDa nuclear protein,

which has a short half-life of around 30 minutes (Bies and Wolff, 1997). However alternative splicing of the gene can produce a number of protein isoforms that have altered structures, and are discussed in more detail below.

The DNA binding domain of the protein is constructed of three tandem 50 amino acid repeats (R1-3), and deletion analysis showed that R2 and R3 are required for the interaction between MYB and DNA (Howe *et al.*, 1990; Saikumar *et al.*, 1990), with MYB operating through recognition of the DNA sequence t/cAACt/gG known as the MYB binding site (MBS) (Ramsay and Gonda, 2008). However there are reports of MYB activation of gene transcription that is independent of DNA binding, such as activation of heat shock protein 70 (HSP70). Experiments revealed that MYB was capable of activating HSP70 through a heat shock element (HSE) within the promoter, but the HSE did not contain a MYB binding site, suggesting that alternate activation mechanisms such as interactions with other transcription factors or sequestration of promoter repressors by MYB facilitate gene activation (Foos *et al.*, 1993; Kanei-Ishii *et al.*, 1994). Additionally the DNA-binding domain of MYB was found to share strong structural similarity to the SANT (Swi3, Ada2, N-Cor and TFIIIB) domain, variants of which are found in the subunits of several regulatory chromatin-remodelling complexes and is responsible for the recognition of histone tails (Boyer *et al.*, 2004).

To induce target gene transcription that is DNA-binding dependent, the transactivation domain is required and involves the recruitment of co-activators CREB-binding protein (CBP) and p300 (Dai P. *et al.*, 1996). MYB can also cooperate with other transcription factor families such as ETS and CEBP (CAAT enhancer binding protein) to enhance the transcription of target genes (Oh and Reddy, 1999). There have been a number of studies using various approaches, such as knockdown or over-expression of *MYB* as well as microarrays, to determine the targets of MYB, mainly using haematopoietic cells or cancer cell lines. More than 80 target genes have been identified and include other transcription regulators such as *E2F4* and *STAT5A*, as well as genes involved in cell cycle progression, proliferation and survival such as c-*Myc*, Cyclin B1 (*CCNB1)*, c-*Kit*, and *Bcl-2* (Bengtsen *et al.*, 2015; Lang *et al.*, 2005; Liu F. *et al.*, 2006; Lorenzo *et al.*, 2011; Quintana *et al.*, 2011; Zhao L. *et al.*, 2011). Together these studies have contributed to understanding how MYB functions and the cellular processes that it

augments, but as is highlighted in section 1.1.4 the specificity of which target genes are activated is very much dependent on the cell context.

Figure 3-1: A schematic diagram of the protein structure of MYB and v-MYB.
The major functional domains of c-MYB are shown in the top illustration. This includes the highly

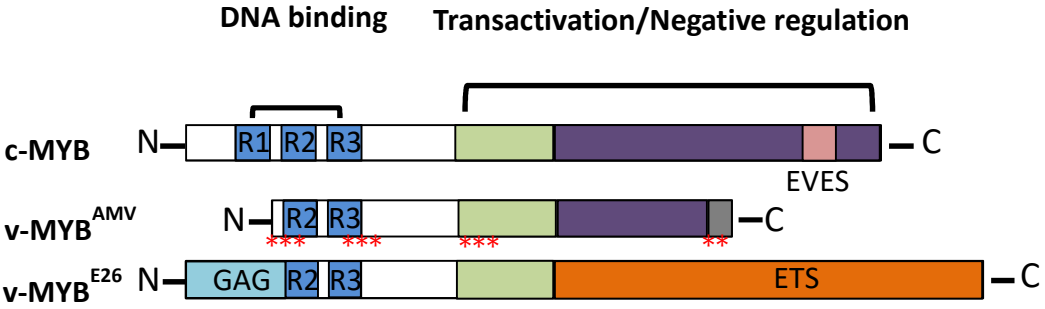

conserved DNA binding domain at the N-terminus, with the three, tandem amino acid repeats shown in blue. The transactivation domain in the middle is shown in green, with the negative regulatory domain in purple. The EVES motif (pink) includes sites for inter-protein interactions to modify the transcriptional activity of MYB. Below are the structures of the viral MYB oncogenes for comparison. v-MYB^{AMV} is truncated at both the N and C terminals, and contains 11 point mutations (red stars) which contribute to the oncogenic transformation of the protein. Equally v-MYB^{E26} is truncated at both terminals but is fused with viral Gag and ETS proteins to form an active three-component fusion protein capable of transformation. Domains are not drawn to scale. (Image adapted from (Ramsay and Gonda, 2008).

3.1.3 The proto-oncogene *MYB*

The proto-oncogene *MYB* was first identified as the mammalian homologue of the transforming v-*MYB* oncogenes of the avian myeloblastosis virus (AMV) and E26 virus that induced erythroid and myeloid leukaemias, respectively, in chickens (Figure 3-1) (Beug *et al.*, 1979; Leprince *et al.*, 1983). Subsequently *MYB* was identified as a common integration site for other avian and murine retroviruses that caused leukaemia, due to the retroviral insertions of *MYB* translating into proteins with N- and C-terminal truncations which led to the disruption of key regulatory domains, and ultimately resulted in over-expression or inappropriate expression of MYB proteins with transforming capabilities (Ramsay and Gonda, 2008). Indeed duplication, genomic rearrangement and aberrant expression of *MYB* has been reported in various human malignancies, and is associated with poorly differentiated tumours, including different forms of leukaemia (Clappier *et al.*, 2007; Lahortiga *et al.*, 2007; Prinzhorn *et al.*, 2016), breast cancer (Kauraniemi *et al.*, 2000; Li Y. *et al.*, 2016), colon cancer (Hugo *et al.*, 2006; Ramsay, Thompson, *et al.*, 1992), melanoma (Hijiya *et al.*, 1994), ACC (Bell *et al.*, 2016; Fehr *et al.*, 2011; Ho *et al.*, 2013), and oesophageal adenocarcinoma (Brabender *et al.*, 2001).

In contrast to v-*MYB* and despite the association of MYB with several tumour types, the cellular counterpart *MYB* was found to only be capable of weak transformation of cells *in vitro* (Fu and Lipsick, 1997), in addition to being incapable of inducing leukaemia when over-expressed in all tissues of transgenic mice (Furuta *et al.*, 1993). To this end comparisons have been made between the actions of v-MYB and the normal functioning of MYB proteins to try and elucidate the oncogenic switches in MYB activity. In addition to N- and C-terminal truncations (Grasser *et al.*, 1991), there are 11 mutations that have been acquired in v-*MYB* of AMV. Those mutations that are situated in the DNA binding domain have been shown to abrogate the protein interactions between MYB and regulatory proteins and affect binding to target genes (Ivanova *et al.*, 2007; Leverson and Ness, 1998; Tahirov *et al.*, 2002; Wilczek *et al.*, 2009). Furthermore v-MYB and MYB were found to regulate largely distinct sets of target genes, implying that they are qualitatively different (Liu F. *et al.*, 2006; Zhou and Ness, 2011). Due to some of the target genes of MYB being associated with proliferation and differentiation, it is thought that in general the persistent over expression of MYB leads to a blockade of anti-oncogenic differentiation and therefore maintains the cancer cells in an immature oncogenic proliferative state (George and Ness, 2014; Ramsay and Gonda, 2008). Indeed disrupting the function of v-MYB in transformed cells leads to a shift from proliferation to differentiation (Beug *et al.*, 1987). Of note however is the interesting observation that in luminal breast cancer, comprised of differentiated, mature luminal cells, MYB is highly expressed and may actually have a tumour suppressor role, as over-expression may be beneficial due to stabilisation of p53 (Thorner *et al.*, 2010). This finding again suggests that the cell context is influential in the functioning of MYB. Overall the evidence so far has unveiled some of the potential mechanisms behind the transformation potential of MYB, but yet it still remains to be clarified how exactly *MYB* becomes oncogenic, and which of its target genes are responsible for cell transformation.

3.1.4 Function of MYB

Many studies involving *MYB* have focussed on its function in haematopoietic cells, due to the induction of leukaemia by v-MYB and after it was shown that the loss of *MYB* in homozygous null mutant mice was embryonically lethal at day 15 due to catastrophic defects in the development of the blood cell lineages, thus demonstrating the critical role of the protein in haematopoiesis (Mucenski *et al.*, 1991). More recently the

conditional knockout of *MYB* has shown the importance of MYB as a key regulator of self-renewal and multi-lineage differentiation in adult haematopoietic stem cells (HSCs) (Lieu and Reddy, 2009). Additionally studies have supported a requirement of MYB to lineage commitment in T and B cell development (Allen R. D., 3rd *et al.*, 1999; Greig *et al.*, 2010). Furthermore differing thresholds of *MYB* expression levels are needed at distinct stages of differentiation (Emambokus *et al.*, 2003; Sakamoto *et al.*, 2006) for normal development, with the highest levels of expression in the immature progenitor cells, which reduces as the cells differentiate (Oh and Reddy, 1999; Ramsay and Gonda, 2008; Zhou and Ness, 2011). In T-cells *MYB* expression can be activated by external signals, such as IL-2, and being a downstream effector of signalling pathways such as PI3K-Akt, protecting the cells from apoptosis (Lauder *et al.*, 2001). Meanwhile identified target genes such as CyclinB1 show a role for MYB in G2/M cell cycle progression, and demonstrate a mechanism by which MYB regulates haematopoiesis (Nakata *et al.*, 2007). Whilst others have found that the protein interactions of MYB are also critical to its function, especially the association of MYB with p300. In mice harbouring a form of MYB with a mutation in the transactivation domain, the interaction with p300 was disrupted leading to perturbed development and increases in the number of cycling HSCs, suggesting that this interaction is a key proliferation regulator (Sandberg M. L. *et al.*, 2005).

Equally though MYB has been shown to be involved in other high turnover cell compartments such as the intestinal crypts and neurogenic regions of the brain (Ramsay and Gonda, 2008). The epithelium lining of the intestinal crypts, much like the haematopoietic system, has a hierarchical structure of cell turnover, with the stem cells of the crypt base giving rise to progenitor cells which terminally differentiate to migrate to the crypt apex in the lumen. A number of *MYB* mouse mutant and knockout models were used to show that MYB is essential to the homeostasis of the crypts with MYB loss causing reduced crypt length and proliferation, alongside perturbation of lineage differentiation with a bias to just one cell type (Malaterre *et al.*, 2007). More recently MYB was also shown to control the expression of intestinal stem cell genes like Lgr5 (Cheasley *et al.*, 2011). Malaterre and colleagues also identified that the loss of MYB caused a reduction in proliferation of neural stem/progenitor cells and caused

a reduction in the expression of key target genes *PAX6* and *SOX2,* suggesting that MYB was important in neurogenesis (Malaterre *et al.*, 2008).

3.1.4.1 The role of MYB in the skin and hair follicle

It is thought that *CYLD* defective tumours are derived from the hair follicle (Massoumi, Podda*, et al.*, 2006), and in studies regarding the development of mouse hair follicles it was found that MYB was abundantly expressed in hair follicles postnatally at P5, mainly within the outer root sheath under the bulge region (Vesela *et al.*, 2014). This area is associated with transient-amplifying cells of the hair matrix leading the authors to conclude that MYB may be required in the activation of quiescent hair follicle stem cells leaving the niche. Although it was observed that there was no MYB expression at P21 (Vesela *et al.*, 2014). Interestingly others have found that targeted deletion of MYB in CK14 (keratinocyte marker) positive cells caused a reduction in epidermal thickness and keratinocyte proliferation but not differentiation (Sampurno *et al.*, 2015). Furthermore the loss of MYB resulted in perturbed collagen 1 production from fibroblasts due to a reduction in TGFβ-1 expression in the keratinocytes, demonstrating a role for MYB in the signalling axis between the two cell populations of the skin (Sampurno *et al.*, 2015). Therefore from the above evidence it is clear that *MYB* expression is widespread and this evidence highlights the important functional role of MYB in the normal development of a variety of tissues including the skin. Taken alongside the different malignancies *MYB* has also been associated with, it suggests that the cell/tissue context is influential to the role of MYB; targeting different genes not only in different cell types but also cells at different maturity and even cell cycle stages (Zhou and Ness, 2011).

3.1.5 Regulation of MYB

A myriad of regulatory mechanisms are involved in the regulation of MYB at both the protein and mRNA level. The recognition of C-terminal domain truncations of both forms of v-MYB led to the suggestion that this deleted region of MYB may function as a negative regulator of its own actions. Particularly as it had been demonstrated that the loss of the C-terminal led to increases in the transcriptional, transformation and DNA binding activities of MYB (Gonda *et al.*, 1989; Ramsay, Ishii*, et al.*, 1992; Sakura *et al.*, 1989), supporting that this region is indeed important for modulating the activity of MYB. A number of structural motifs including a leucine zipper motif are found in the

NRD, and are thought to be involved after it was shown that swapping of one or more leucines to proline residues resulted in increased transactivation and transformation activity (Kanei-Ishii *et al.*, 1992). In addition an isoform of MYB lacking the leucine zipper domain exhibits enhanced transactivational activities (Woo *et al.*, 1998). The precise mechanism remains unresolved, but such proposals include the existence of an auto-regulatory loop, as MYB is capable of forming homodimers via the leucine zipper and is a target of itself (Nomura *et al.*, 1993), or through interactions with proteins such as p67 and p160 (Favier and Gonda, 1994). Likewise the EVES motif is found in the NRD and was shown to interact with the DNA binding domain in the N-terminus (Dash *et al.*, 1996). Similarly this motif was found in the transcriptional co-activator p100, which also interacted with MYB and could modify its transcriptional activity (Dash *et al.*, 1996). Thus intra- and inter-molecular interactions are both involved in the regulation of MYB.

Although perhaps the least understood post-translational modifications are another level of regulation that have the ability to alter the activity of MYB. For example in response to Wnt-1 signalling, MYB is targeted for proteasomal degradation through NEMO-like kinase (NLK) phosphorylation-dependent ubiquitination via the ubiquitin ligase Fbxw7-α (Kanei-Ishii *et al.*, 2004; Kanei-Ishii *et al.*, 2008). Meanwhile phosphorylation can also alter the DNA binding capacity of MYB (Cures *et al.*, 2001; Luscher *et al.*, 1990). Similarly acetylation affects the transactivation capacity of MYB activity (Tomita *et al.*, 2000), possibly by enhancing the affinity of MYB for CBP (Sano and Ishii, 2001), and finally sumoylation modifies its stability and transactivation capacity (Bies *et al.*, 2002), again by interfering with the interaction of MYB with other co-activators such as p300 (Molvaersmyr *et al.*, 2010).

A blockade of transcription at the mRNA level, due to the presence of an attenuation sequence, exists in the first intron of *c-MYB,* which has to be overcome by RNA polymerase II to enable cells to express full-length transcripts (Bender *et al.*, 1987). The differentiation of haematopoietic cells or the induction of differentiation through compounds such as histone deacetylase (HDAC) inhibitors causes the re-establishment of elongation arrest and leads to down-regulation of c-*MYB* expression levels (Ramsay *et al.*, 1986; Thompson *et al.*, 1998). Recently a mechanism was proposed for

overcoming the elongation blockade, involving the NFκB subunits p50 and p65 interacting with a RNA stem-loop and poly-T RNA tract that follows it, which is encoded for by the attenuator sequence in intron 1 of c-*myb.* The binding of p50 and p65 lending themselves to the recruitment of other co-factors such as P-TEFb (positive transcription elongation factor), a complex involving CDK9 (cyclin dependent kinase) and CyclinT1, allowing for Serine-2 phosphorylation of the CTD (carboxy-terminal domain) of RNA polymerase II and stimulation of c-MYB transcription elongation (Pereira *et al.*, 2015). In addition NFκB enhancer elements have been found to reside in Intron 1 of the murine *MYB* gene (Suhasini and Pilz, 1999), and NFκB binding sites in the human c-*MYB* promoter (Lauder *et al.*, 2001). Taken together these studies suggest that *MYB* is a target of NFκB family members and that NFκB may be able to regulate the *MYB* gene in a variety of ways. Whilst mutation of the elongation attenuation region of *MYB* has been found to be a common oncogenic mechanism in colorectal cancer, where sequence analysis of primary colorectal tumours revealed mutations in the poly-T tract allowing for greater gene expression (Hugo *et al.*, 2006). Similarly this regulatory mechanism has been shown in breast cancer as the elongation of *MYB* transcripts has been found to be dependent upon the presence of ligand-bound ERα (oestrogen receptor-alpha), which can relieve the transcriptional attenuation in intron1 (Drabsch *et al.*, 2007). Indeed *MYB* was identified as a direct target of ERα (Frasor *et al.*, 2003) and subsequent studies have shown that the high *MYB* expression levels are a driver of proliferation in $ER\alpha^+$ but not $ER\alpha^-$ breast cancer (Drabsch *et al.*, 2007). Similar to the action of NFκB in the continuation of *MYB* transcription, independent of hormone, ERα forms a complex with P-TEFb then upon oestrogen ligand binding this complex is recruited to the transcriptional pausing site (Mitra *et al.*, 2012).

Finally miRNAs (microRNAS) have been found to post-transcriptionally regulate the expression of *MYB.* In haematopoietic cells, miR-15a was found to directly bind to the 3'UTR (untranslated region) of *MYB* resulting in down regulation of *MYB* expression. Additionally miR-15a caused G_1 cell cycle arrest when over expressed in the K562 leukemic cell line which was partially rescued by the expression of a c-*MYB* construct that wasn't subject to miR-15a regulation (Zhao H. *et al.*, 2009). Equally MYB was shown to regulate miR-15a expression suggesting a negative autoregulatory feedback

loop (Zhao H. *et al.*, 2009). Likewise miR-150 has been suggested to be a regulator of MYB protein translation in models of skeletal muscle differentiation and Burkitt lymphoma (Chen S. *et al.*, 2013; Kaspar *et al.*, 2015).

It is clear that the function of MYB and regulation of *MYB* expression are complex and that each is controlled on many levels through a myriad of mechanisms involving a host of protein interactions. All of which, can be influenced by the cellular context. The apparent contradictory role of MYB in both stimulating proliferation and differentiation emphasises that MYB can regulate different sets of genes and alter its activities in response to different cellular circumstances. Further research is still needed though to decipher the context-specific transcription factor code, the post-translational modifications and protein-protein interactions that regulate the activity of MYB (Ness, 2003).

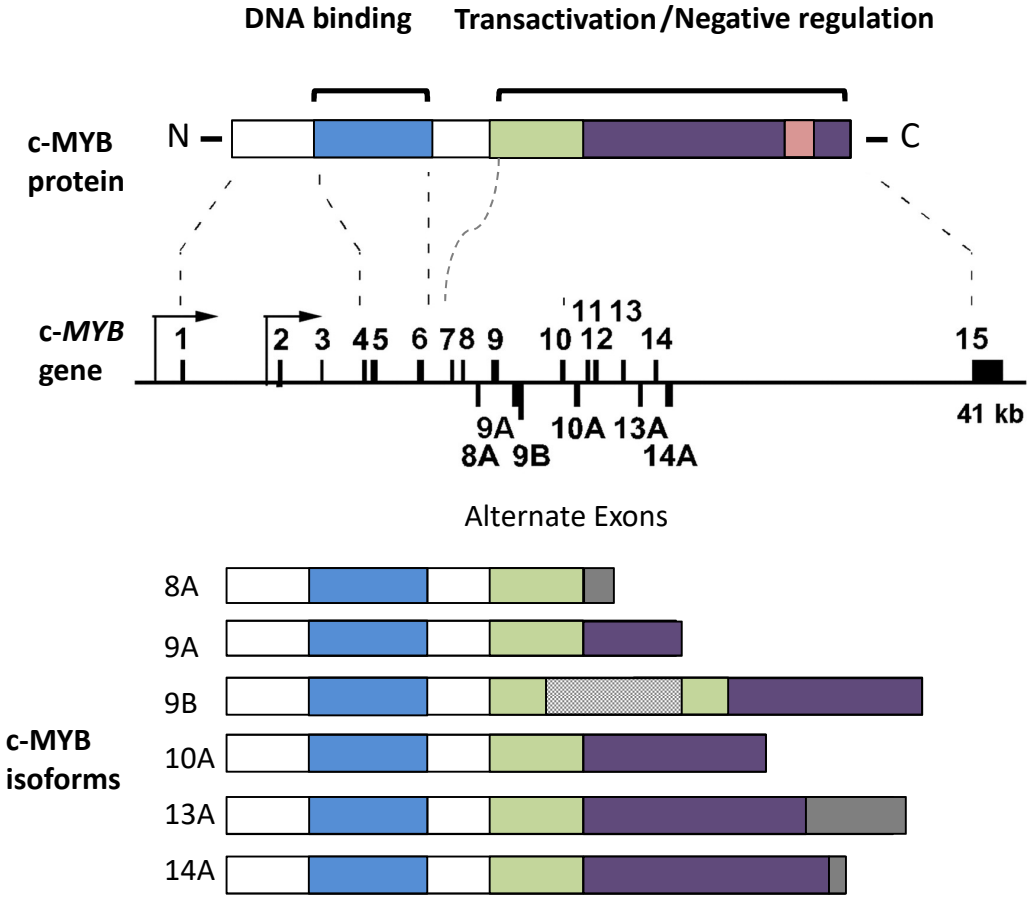

Figure 3-2: A schematic diagram of the isoforms of human c-MYB in relation to the *MYB* gene and protein structure.

The structure of the c-MYB protein (top) is shown and the corresponding exons that encode for the different domains of the protein below. Exons 4-6 encoding the DNA binding domain, while exons 7-15 encode for the C-terminal domains involved in transactivation, specificity and regulation. Six alternatively spliced isoforms of the gene exist in humans, all with alternate C-terminals isoforms 8A, 13A and 14A are fused with extra amino acids (indicated in grey), whilst 9A and 10A have a truncated C-terminus, Lastly isoform 9B has an insertion of 121 amino acids in the transactivational domain (indicated by grey striped box). Domains are not drawn to scale. (Diagram adapted from (O'Rourke and Ness, 2008).

3.1.6 Alternative splicing of c-*MYB* and the protein isoforms of MYB

The *MYB* gene is comprised of 15 exons but is subject to extensive alternative splicing through the use of 6 alternative exons, 8A, 9A, 9B, 10A, 13A, 14A (Figure 3-2). The complexity of MYB splicing is further increased due to exons 8 and 9 including cryptic splice donor sites, generating a short (8') form of exon 8 lacking 9 nucleotides and a short (9S) form of exon 9 lacking 85 nucleotides (Close *et al.*, 2004; Zhou and Ness, 2011) The exon 8' form can be spliced to either alternate exon 8A which are commonly seen together, or exon 9 (Close *et al.*, 2004) The exon 9S form can be spliced to either

alternate exons 9A or 9B or exon 10 (Zhou and Ness, 2011). All of the exons that can be alternatively spliced are located in the region of the gene that encodes for the transcriptional activation and regulatory functions of MYB. Therefore incorporation of these exons leads to the production of many splice variants that can encode for MYB isoforms with differing C-terminal structures, and distinct transcriptional activities that could activate unique sets of target genes (Zhou and Ness, 2011).

The work of O'Rourke and Ness analysed the alternately spliced transcripts of human *MYB* in primary haematopoietic and leukemic cells and cell lines. They showed that the transcripts containing exon 9A or 10A encode proteins that are prematurely truncated. However in the case of exon 10A it retains a part the negative regulatory domain of the c-terminus. Meanwhile exons 8A, 13A or 14A again create transcripts with a unique c-terminus by fusing MYB with an extra 34, 100 or 10 amino acids, respectively (O'Rourke and Ness, 2008). Additionally quantitative assays showed the expression patterns of the *MYB* variants to be considerably different between the cell types, and in particular increased *MYB* levels in the leukaemia patient samples. This was suggestive of a tightly regulated programme of alternative splicing of *MYB*, creating cell-type specific ratios of the different transcripts that are important to the regulation of haematopoiesis in normal cells, which when uncontrolled can promote oncogenesis (O'Rourke and Ness, 2008).

Indeed recently it was demonstrated that in adult T-cell leukaemia (ATL) *MYB* expression was dysregulated and it was over expression of the c-MYB isoform 9A in particular that was a driver of the malignancy (Nakano *et al.*, 2016). Likewise alternate transcripts that include exon 9B (confusingly the avian and murine forms are referred to as exon 9A) encode for a protein that is 89kDA, due to the insertion of 121 additional amino acids in the middle of the transcriptional activation domain of MYB (O'Rourke and Ness, 2008). When over-expressed this isoform has been shown to have increased transactivational activities in avian and human cells (O'Rourke and Ness, 2008; Woo *et al.*, 1998), and was capable of transformation of avian cells (Woo *et al.*, 1998). In addition cell viability was increased when the isoform was over-expressed in murine cells (Kumar A. *et al.*, 2003). Alongside this down-regulation of isoform 9B in BCR/ABL transformed cells, suppressed the proliferation and colony forming

capabilities of these cells as well as reducing their sensitivity to Imatinib (Manzotti *et al.*, 2012). Attempts to understand the role of this isoform has led to the generation of a p89 c-MYB knockout mouse model but this showed no apparent phenotype, which is in stark contrast to the embryonic lethality at day 15 seen in p75 c-MYB knockouts, and suggests that the expression of the predominant p75 isoform of c-MYB can compensate for the loss (Baker *et al.*, 2010; Mucenski *et al.*, 1991). So as with the other isoforms, further studies are required to elucidate the differing functions of the transcripts and their downstream target genes to fully understand their role.

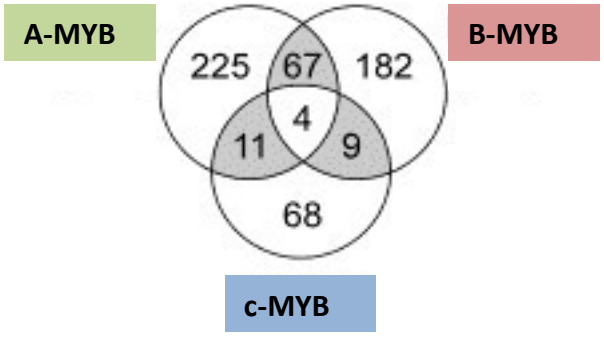

Figure 3-3: The differential activities of A-MYB, B-MYB and c-MYB.
The Venn diagram summarises the number of genes that were activated following expression of each MYB protein. This highlights the specificity in the gene sets that are activated (>two fold) by each of the MYB proteins, with very little overlap seen between them. Of the 65,000 genes that were represented on the array, only 4 genes were activated in response to all 3 MYB family members. MCF7 cells were infected by adenoviruses expressing each of the MYB family members and assayed using the Affymetrix U95A-E Gene chips. Diagram was taken from (Ness, 2003) and based on results from (Rushton *et al.*, 2003).

3.1.7 The other MYB family members: A-*MYB* and B-*MYB*

The other family members A-*MYB* and B-*MYB* also encode transcription factors, which share a high degree of sequence homology, largely in the DNA binding domain. Therefore all three members of the family can bind the same DNA sequences and activate the same promoters in reporter gene assays (Rushton and Ness, 2001). However microarray assays have found each member to activate its own unique set of endogenous genes when over-expressed in MCF7 cells, suggesting that each member has its own distinct interacting partners and functions in a context-specific manner (Figure 3-3) (Rushton *et al.*, 2003). As with the c-MYB isoforms it appears to be the variation in the C-terminus structure that determines the unique functional roles of these family members, as only the DNA binding domain was shown to be interchangeable in domain swapping experiments (Rushton and Ness, 2001). On the contrary a study by Bergholtz et al found that small conserved differences of the DNA-

binding domain fine-tuned the specificity of each family member. Whilst A-MYB and c-MYB functioned similarly, B-MYB was found to form complexes with less stability and had a lower tolerance for variations within the MBS (Bergholtz *et al.*, 2001). Furthermore differences in specificity between A-, B- and c-MYB maybe explained by studies that have found sub domains within the transactivation domain between A-MYB and c-MYB (Lei *et al.*, 2004), and likewise B-MYB was found to have a c-terminus with functional subdomains different to A-MYB and c-MYB, that acted as both positive and negative regulators of its transcription activation (Nakagoshi *et al.*, 1993; Oh and Reddy, 1998).

There is some overlap in the expression of all three family members, with some cell types particularly within the bone marrow, capable of expressing more than one family member. The expression pattern of A-*MYB* compared to B-*MYB* is more restrictive as it is found in select tissue compartments such as the developing mammary gland and testis (Toscani *et al.*, 1997), central nervous system and B-lymphocytes (Trauth *et al.*, 1994). Meanwhile B-*MYB* is more ubiquitously expressed (Oh and Reddy, 1999), with very early developmental arrest observed in mice when this gene is knocked out (Tanaka Y. *et al.*, 1999). The expression of B-*MYB* plays an important role in the cell cycle by inducing the transcription of genes that promote entry in to the S and M phases of the cycle. Conversely B-*MYB* repression induces premature senescence (Martinez and Dimaio, 2011). Indeed B-MYB has been found to have an important role in maintaining the undifferentiated phenotype of keratinocytes and enhancing their proliferation (Maruyama *et al.*, 2014). Due to the control B-*MYB* can exert on cell behaviour it is therefore not surprising that it has also been suggested to have a role in tumourigenesis as the over-expression of B-*MYB* is associated with a poorer prognosis in neuroblastoma (Raschella *et al.*, 1999) and breast cancer (Thorner *et al.*, 2009). Similarly A-MYB has been shown to be a potential interchangeable oncogenic driver with c-MYB in adenoid cystic carcinoma (Brayer *et al.*, 2016).

3.1.8 *CYLD*-defective tumours and Adenoid cystic carcinoma

A cancer of the secretory glands, ACC is commonly found in the salivary glands of the head and neck and in rare incidences the breast. A slow growing tumour, it is aggressive and can lead to metastasis (Drier *et al.*, 2016). However with restricted treatment options, especially for patients with metastatic disease, of surgery and/or

radiation therapy, research has been focused at the molecular level to discover targets for curative and non-operative treatment approaches (Adelstein *et al.*, 2012; Stenman *et al.*, 2014). MYB over-expression has been found to be a key alteration in ACC development, and in a sub-set of ACCs a molecular hallmark is the chromosomal translocation t(6;9)(q22-23;p23-24), which results in the fusion of the oncogene *MYB* with the transcription factor gene *NFIB* (Nuclear Factor I B) (Ho *et al.*, 2013; Mitani *et al.*, 2010; Persson *et al.*, 2009; Stenman *et al.*, 2014). The genomic rearrangement causes constitutive activation of *MYB,* due to the loss of miRNA binding sites in the 3'UTR, which negatively regulate *MYB* expression. The fusion protein MYB-NFIB, however retains the DNA-binding and transactivation domains, and is therefore capable of activating MYB target genes and thus promote oncogenesis (Persson *et al.*, 2009; Stenman *et al.*, 2010). With alternative splicing and variable breakpoints in both *MYB* and *NFIB,* a number of fusion transcript variants have been identified with the most common consisting of *MYB* exon 14 linked to *NFIB* exons 8c or 9 (Persson *et al.*, 2009; Persson *et al.*, 2012). More recently analysis of MYB in ACC found the *MYB-NFIB* fusion to only disrupt the 3'UTR in a third of cases, and proposed that the high levels of *MYB* expression found in ACC were due to chromosomal 'regulatory rearrangements' that juxtapose super-enhancer regions to the *MYB* locus. Here the enhancers interact with the *MYB* promoter and MYB itself then binds the enhancers to establish a positive feedback loop and augment its own expression (Drier *et al.*, 2016).

Interestingly the *MYB-NFIB* fusion transcript provides a genetic link between ACC and cylindroma, with sporadic cases of dermal cylindromas having also been found to express fusion transcripts or show increased activation of MYB in the absence of such fusions, although at a lower frequency (Fehr *et al.*, 2011). Meanwhile other striking similarities between ACC and cylindroma have been observed. Histologically the two tumour types share a cylindrical pattern arrangement of multiple lobules of tumour cells. Alongside this others have reported areas of ACC-like differentiation arising in spiradenocylindroma and spiradenomas (Petersson *et al.*, 2009). There have also been somatic CYLD mutations reported in ACC, although due to the very low frequency (4%) it is unlikely that CYLD contributes to ACC tumourigenesis (Daa *et al.*, 2013; Stephens *et al.*, 2013). Conversely there are incidences of patients with germline *CYLD* mutations who develop multiple cylindromas also developing membranous basal cell adenomas

(MBCA), another salivary gland tumour with morphological similarities to cylindroma (Jungehulsing *et al.*, 1999). Finally the overlap between ACC and cylindroma is indicated further with both tumour types over-expressing TrkC (Ivanov *et al.*, 2013; Rajan, Elliott*, et al.*, 2011). It was found that TrkC expression levels were increased up to 100-fold compared to normal salivary tissue, and that in the presence of its cognate ligand NT-3 it stimulated pro-invasive signalling and behaviour, providing a link between TrkC and cancer progression in ACC (Ivanov *et al.*, 2013). The conclusions from these studies therefore warranted further investigation of MYB in inherited *CYLD*-defective tumours.

3.2 Chapter specific materials and methods

3.2.1 Nester RT-PCR

Nested PCR is a modified approach to traditional PCR that is used to reduce the amplification of non-specific products by running two successive rounds of PCR amplification. The product from the first round is used as the template for the second round, with the separate rounds using different primer sets. The second set of nested primers is designed to only amplify a target within the intended product from the first round of amplification, therefore increasing the specificity of the PCR reaction.

3.2.1.1 Sample preparation

Total RNA was extracted from five 10μm sections obtained from snap frozen cylindroma tumour samples using the RNeasy Mini-kit (Qiagen). Subsequently 2000ng of extracted RNA was converted to cDNA using Superscript First-strand synthesis system (Invitrogen) as explained in section 2.2.6, to give a final concentration of 100ng/μl in the final 20μl reaction volume.

3.2.1.2 RT-PCR

RT-PCR was carried out according to the validated protocol in (Persson *et al.*, 2009). Each reaction was set up on a 96 well plate according to Table 3-1, with a total reaction volume of 25μl/well. Both rounds of PCR followed the same cycling program and were run under the conditions according to Table 3-2. Final PCR products were then run out on a 2% agarose gel at 100 volts for 1 hour to visualise the presence of an amplification product. For all samples each RT-PCR was repeated in triplicate.

Reaction component	Per reaction
MyTaq™ HS Mix	12.5μl
Primer F (20μM)	0.6μl
Primer R (20μM)	0.6μl
Nuclease-free water	10.3μl
Template (100ng) or from PCR1	1 μl

Table 3-1: Reaction mixture for nested RT-PCR.

Step/Cycles	Temperature	Time
Initial denaturation	94°C	2 minutes
31 cycles	94°C	30 seconds
	60°C	30 seconds
	72°C	45 seconds
Final extension	72°C	8 minutes

Table 3-2: Thermocycling conditions for nested RT-PCR

3.2.2 Fluorescence *in situ* hybridisation (FISH)

FISH is a technique widely used to detect genomic rearrangements by using fluorophore-labeled probes that specifically hybridise to the part of a chromosome with a high degree of sequence complementarity, which can then be visualised with a fluorescent microscope to indicate the location of the target DNA. A dual colour split FISH probe is designed with two different coloured fluorophores to detect gene translocations. FISH analysis for the detection of *MYB* gene rearrangements, was very kindly carried out by the group of Prof. Goran Stenman (University of Gothenburg, Sweden). FFPE sections (5μm) from 10 cylindroma tumours were probed using a dual colour *MYB* split FISH probe (Abnova, Taiwan), according to manufacturer's instructions. Flourescence signals were imaged and analysed using the Isis FISH imaging system v5.5 (MetaSystems GmbH, Germany) and at least 50 nuclei were scored from each tumour.

3.2.3 Gene silencing in cell culture

3.2.3.1 RNA inteference

RNA interference is a post-transcriptional process mediated by short interfering RNA (siRNA) that leads to gene silencing. siRNAs are double-stranded RNA (dsRNA) duplexes that are 20-25bp in length with 3' dinucleotide overhangs, formed by the cleavage of long dsRNAs by the RNA endonuclease Dicer enzyme. Upon entry into the cell siRNA is incorporated into the RNA-induced silencing complex (RISC), whereby the siRNA is unwound and one of the RNA strands is selected and the partner strand degraded. The selected 'guide strand' stays within the complex regulating gene expression via hybridising to their complementary nucleotide sequence within the target mRNA, initiating mRNA fragmentation and degradation by activated

endonucleases and thus preventing translation into proteins. This is a mechanism that has been exploited in the laboratory using synthetic siRNAs that are designed accordingly to 'knock down' the expression of a target gene of interest.

The use of short-hairpin RNAs (shRNAs) works on the same principles as above. shRNAs are double-stranded RNA duplexes that are 19-22bp in length linked by a short loop. The main difference to siRNA is the requirement of an expression vector to deliver the artificial RNA molecule to the nucleus of the cells to allow for shRNA expression. Once integrated into the genome, the shRNA is then transcribed by RNA polymerases and processed by the RNA endonuclease Drosha, before finally being exported into the cytoplasm. Here further processing of the loop structure by Dicer occurs before being loaded into RISC and following the same downstream processing leading to silencing of the target gene.

3.2.3.2 siRNA transfection of primary cylindroma cell cultures

siRNA gene silencing experiments in primary cylindroma cells were kindly carried out by the group of Prof. Goran Stenman (University of Gothenburg, Sweden). Briefly primary cylindroma cells were cultured in assay plates, until at the desired confluency for transfection. Cells were then transfected with 50nM Stealth RNAi™ MYB siRNAs (HSS106819 and HSS106821) (Thermo Fisher Scientific), using Lipofectamine RNAiMAX transfection reagent in antibiotic-free medium (Life Technologies) according to the manufacturer's instructions. A non-targeting siRNA was used as a negative control. In line with the manufacturer's guarantee to yield >70% gene knockdown, efficient knockdown was confirmed by qPCR and Western blotting for each siRNA duplex used. Experiments were performed in triplicate and cells were treated with siRNA for the time periods indicated.

3.2.3.3 shRNA transfection of cell lines

Lentiviral vectors were used for the delivery of CYLD shRNAs to HEK293T and HaCaT cells for gene silencing experiments. See Materials and Methods section 2.6.12 for the generation and packaging of lentiviral vectors and cell transduction.

3.2.4 Cell proliferation assay

As part of the knockdown experiments, these assays were also kindly carried out by the group of Prof. Goran Stenman (University of Gothenburg, Sweden). Cell

proliferation was assayed using alamarBlue® reagent (Thermo Fisher Scientific), according to the manufacturer's instructions. This assay measures cell proliferation by using an oxidation-reduction indicator which results in a colour change from blue (oxidised) to red (reduced) in response to the metabolic activity of cell growth, which can be quantified by taking absorbance readings. In brief alamarBlue® reagent was added directly to the cells to be assayed at a 1:10 dilution, before being left to incubate at 37°C. Readings were taken using a VICTOR-3 multilabel reader (Perkin-Elmer).

3.2.5 Treatment of cells with NF-κB inhibitors

Primary cylindroma cells were plated out into 6 well plates at a density of 1.5 $x10^5$ cells/well. Cells were left for 24 hours before being treated with DMSO, TPCA-1 or BMS345541 for 48 hours and subsequently trypsinised and collected for lysates. DMSO only controls were included at the larger dilution volume of the two drugs.

3.3 Results

3.3.1 Familial *CYLD*-defective tumours do not express *MYB-NFIB* fusion transcripts

As the fusion oncogene *MYB-NFIB* has previously been described in sporadic cylindromas (Fehr *et al.*, 2011), a validated nested RT-PCR approach was used to detect the presence of fusion transcripts in inherited *CYLD*-defective tumours. A panel of 13 cylindroma tumours, from five patients, were screened for the most common *MYB-NFIB* fusion transcript variants (Table 3-3) (as described by (Fehr *et al.*, 2011; Persson *et al.*, 2009). As a positive control cDNA generated from a fusion-positive (*MYB*exon14–*NFIB*exon8c) ACC was used, as this fusion variant was one of the more commonly detected fusion transcripts (sample gifted from Prof. Goran Stenman, University of Gothenburg, Sweden). None of the tumour samples were found to express any of the *MYB-NFIB* fusion transcript variants tested for, as indicated by the lack of amplified fragments in Figure 3-4.

In collaboration with the Prof. Stenman, 10 additional inherited *CYLD* defective tumours (FFPE samples), which included cylindroma, spiradenoma and spiradeno-cylindroma, were also screened using nested RT-PCR as above, for the expression of the same *MYB-NFIB* fusion transcript variants. All 10 tumours were also found to be negative for each transcript variant. Additionally fluorescence *in situ* hybridisation (FISH) analysis with a dual-colour MYB break apart probe, was carried out by Prof. Stenman and colleagues, on the same 10 tumour samples to identify any rearrangements of the *MYB* locus. A fusion-positive ACC was used as a control. In support of the findings of the RT-PCR experiments, no rearrangements or copy number gains/amplifications involving the *MYB* locus were identified in any of the inherited tumour samples, as indicated by the fused red/green signals in the FISH analysis which represent an intact *MYB* allele (Figure 3-5). Together these results indicate that inherited tumours do not express *MYB-NFIB* fusion transcripts. (Prof. Stenman and colleagues at the University of Gothenburg, Sweden, performed the FISH analysis included in this results section).

Gel label	Primer Pair (2nd round PCR)	Fusion transcripts
1	*MYB* Exon6-876 *NFIB* Exon9-1952	*MYB*exon8-*NFIB*exon9
2	*MYB* Exon9-1334 *NFIB* Exon9-1952	*MYB*exon10-*NFIB*exon9
3	*MYB* Exon 11-1554 *NFIB* Exon9-1952	*MYB*exon12-*NFIB*exon9
4	*MYB* Exon 12-1693 *NFIB* Exon9-1952	*MYB*exon14-*NFIB*exon9
5	*MYB* Exon 12-1693 *NFIB* Exon8c-1067	*MYB*exon14-*NFIB*exon8c

Table 3-3: *MYB-NFIB* fusion primer pairs and their corresponding fusion transcript. Fusion primer pairs with numbers corresponding to the fusion transcript variant screened for and numbering for the lanes of the gel showing the nested RT-PCR result (below).

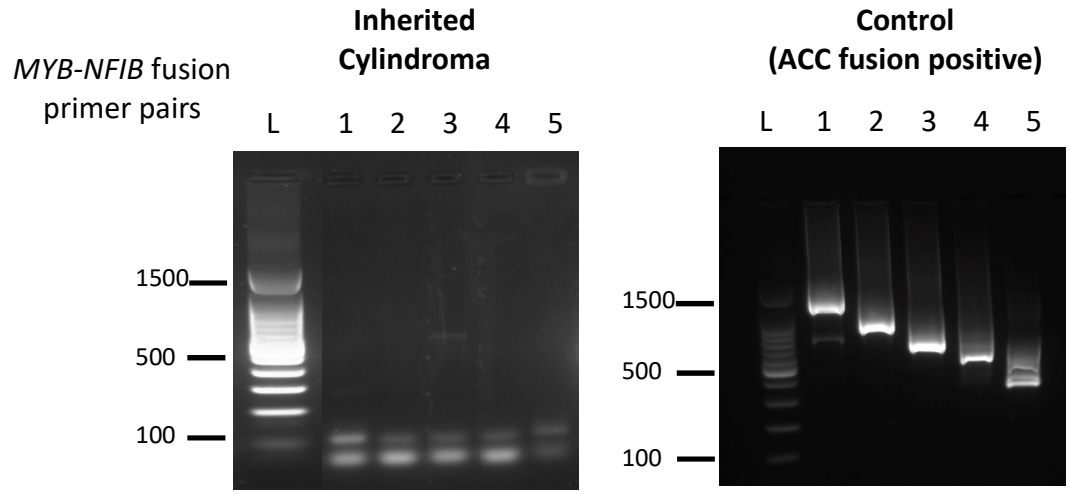

Figure 3-4: *MYB-NFIB* fusion transcripts were not detectable in inherited cylindromas using nested RT-PCR.

Representative agarose gel images from RT-PCR analysis of each of the five *MYB-NFIB* fusions (Table 3-3) screened for in a panel of inherited cylindroma tumour samples (left panel *n*=13). The expected PCR-fragments from the fusion-positive (*MYB*exon14–*NFIB*exon8c) ACC control are also shown for comparison (right panel). Lane numbering corresponds to Table 3-3 above (Data representative of *N*=3 independent experiments).

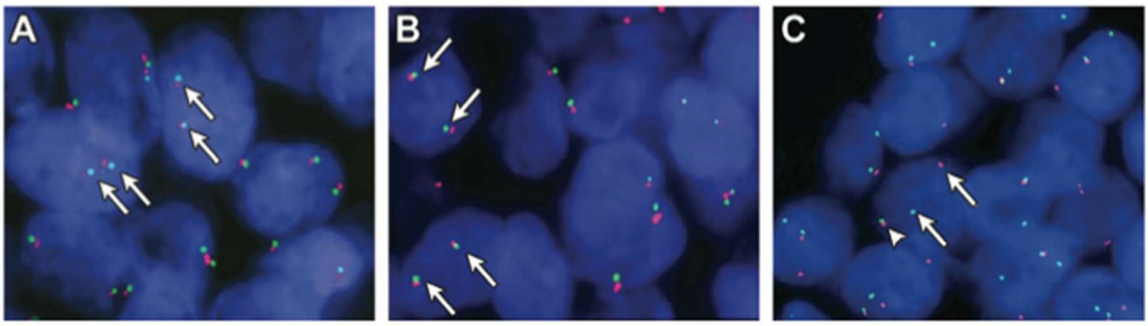

Figure 3-5: *MYB-NFIB* fusion transcripts were not detectable in inherited cylindromas using FISH.

(A & B) FISH analysis of two inherited cylindromas, each showing two non-rearranged copies of *MYB* in each cell nucleus (arrows indicate fused red/green signals) (C) FISH analysis of an adenoid cystic carcinoma that is *MYB-NFIB* fusion-positive (control), showing rearranged copies of *MYB,* the split signal consistent with a *MYB* gene fusion (arrows indicate separated red and green signals; arrowhead, intact *MYB* allele). Figure taken from (Rajan *et al.*, 2016) and produced by collaborators at the University of Gothenburg, Sweden.

3.3.2 MYB protein is overexpressed in inherited *CYLD*-defective tumours

In both ACC and sporadic cylindromas small sub-sets of tumours were found to have MYB activation despite a lack of fusion transcripts (Fehr *et al.*, 2011; Persson *et al.*, 2012). Due to the lack of fusion transcripts in the inherited *CYLD*-defective tumours, the expression of MYB protein was assessed using immunohistochemistry to further investigate. Tissue sections from 16 tumours including both cylindromas and spiradenomas, were probed with MYB antibody, visualised with DAB and quantified. Samples were considered MYB positive if >15% of cells demonstrated MYB expression. In both the cylindromas (Figure 3-6A) and the spiradenomas (Figure 3-6B) MYB expression was shown to have a nuclear localisation (Figure3-6A&B; Black and White arrows in inset), which varied in intensity throughout the tissue sections. In both tumour types there was a scattered pattern of MYB expression, which was not restricted to the basal cells of the tumour cell islands as immuno-positive cells were seen throughout some of the islands in the cylindroma samples. In comparison in control perilesional (*CYLD* +/-) and normal skin (*CYLD* +/+) MYB demonstrated a cytoplasmic localisation in the majority of cells (Figure 3-6C & D). Positive nuclear MYB expression was also observed within the hair follicles surrounding the dermal papilla (Figure 3-6E). Semi-quantitative analysis of the immunostaining intensity using ImageJ software showed that out of the 16 tumours analysed, 11 tumours (69%) were considered MYB-positive (Figure 3-7A). Furthermore there was a significant increase in MYB expression in the *CYLD*-defective tumours when compared to control perilesional epidermis (CYLD +/-) (p = 0.031) (Figure 3-7B).

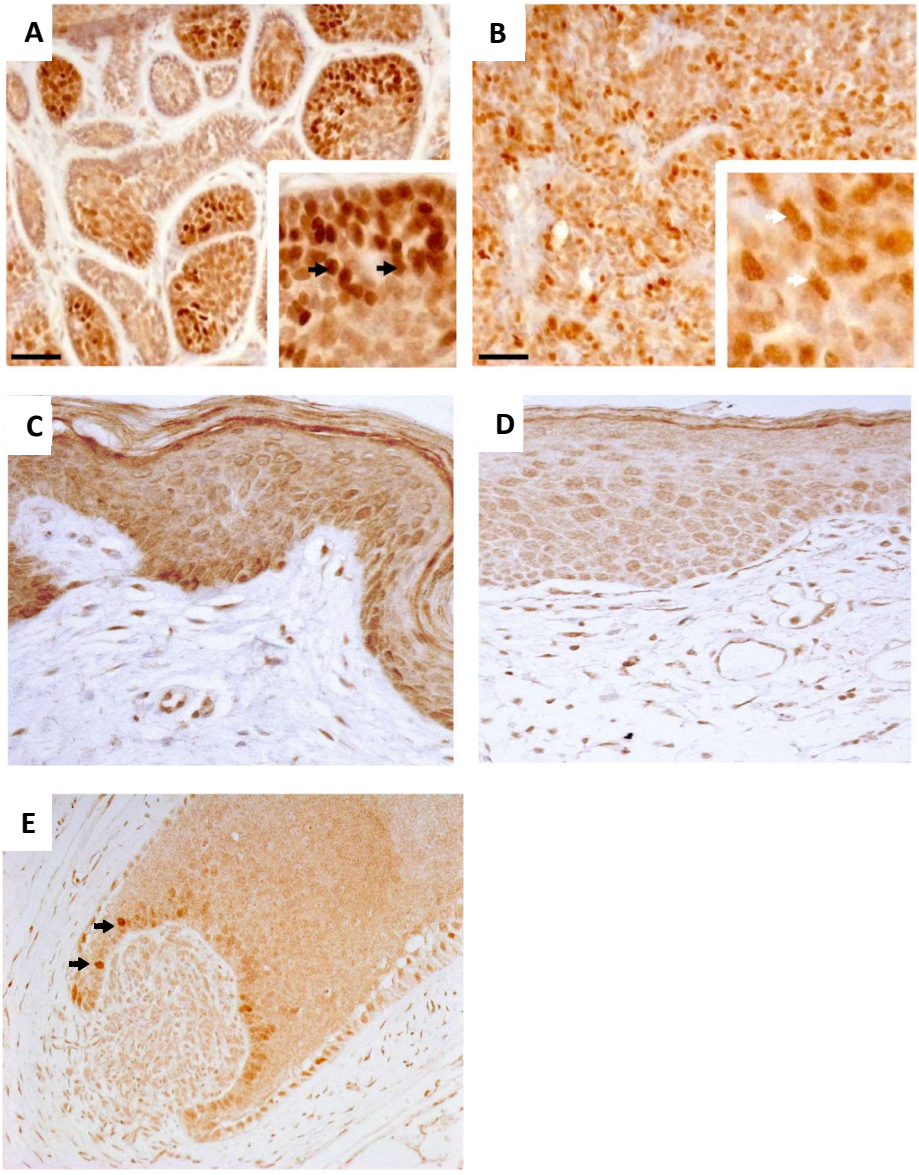

Figure 3-6: MYB protein expression is increased in inherited CYLD-defective tumours as assessed by IHC.

(A & B) MYB protein expression in (A) cylindromas and (B) spiradenomas demonstrating nuclear localisation (black arrows inset (A) and white arrows inset (B)). (C & D) MYB protein expression in control perilesional skin from a *CYLD* mutation carrier (C) and age matched control unaffected skin (D) demonstrating cytoplasmic nuclear localisation. (E) MYB protein expression in hair follicles demonstrating nuclear localisation surrounding the dermal papilla (black arrows). Scale bars represent 50μm.

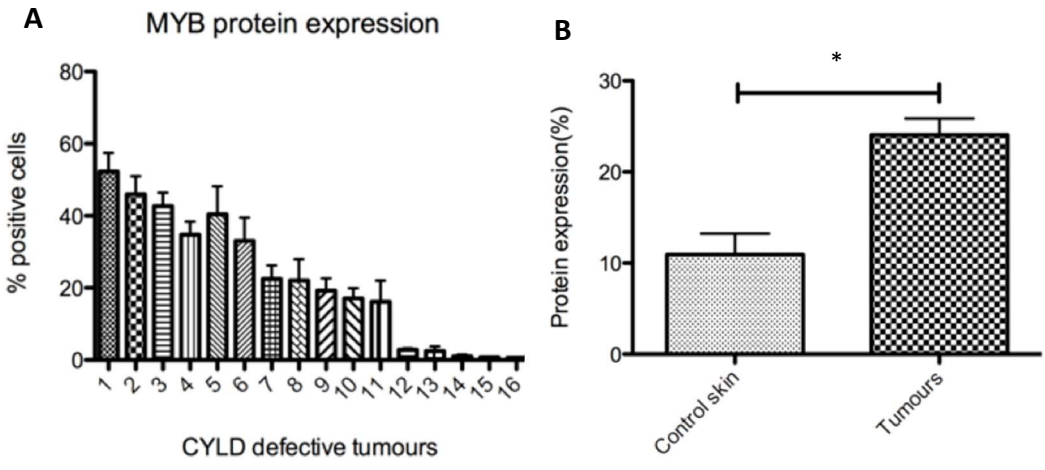

Figure 3-7: Quantification of MYB protein expression in *CYLD*-defective tumours.
(A) Semi-quantitative analysis of the immunostaining intensity of MYB showed that 11 /16 (69%) samples analysed were MYB positive. (B) Protein expression of MYB was significantly increased in *CYLD*-defective tumours compared to control perilesional skin (*CYLD* $^{+/-}$) (* p <0.05, unpaired t-test)

3.3.3 A *MYB* gene expression signature is found in inherited *CYLD*-defective tumours

Microarray gene expression studies, in a pool of *CYLD*-defective tumours (*n*=32) and perilesional skin controls (*n*=10), had previously been performed by Dr. Neil Rajan (Rajan, Elliott*, et al.*, 2011). Using this dataset the expression of *MYB* and selected MYB target genes from the published literature were analysed by Dr. Neil Rajan, and the results have been included as further supporting evidence of the expression of MYB and of the work within this chapter to offer insight into its activity within the tumours. Differentially expressed MYB target genes in *CYLD*-defective tumours compared to controls were determined with a threshold for statistical significance of $p < 0.05$ after correction for multiple hypothesis testing. To visualise the expression of each of the genes (*n*=48) at an individual sample level, normalised signal values were plotted on a heat map, following logarithmic transformation (Figure 3-8) and as described in (Rajan et al., 2016). Clustering by Euclidean distance separated the majority of tumours, including all cylindromas and spiradenomas, from control skin with the exception of two trichoepitheliomas (tumours 1 and 30).

In this independent dataset, *MYB* was shown to be overexpressed in the tumours (fold-change increase = x 2.04). Gene targets that were found to be overexpressed included BIRC3 (fold-change increase = x 3.93) and Bcl-2 (fold-change increase = x 2.34) (Table 3-4), which are both anti-apoptotic proteins. In contrast the expression of some gene targets that have previously been reported to be overexpressed in certain malignancies, such as *CCNE1 (*Cyclin E1) in colorectal cancer (Cheasley *et al.*, 2011), and *CD34* in ACC (Persson *et al.*, 2009), were downregulated in *CYLD*-defective tumours; *CCNE1* fold-change increase = x 0.55, *CD34* fold-change increase = x 0.50 (Table 3-4). These results again highlight the cell-specific nature of MYB activity, whilst also suggesting that MYB may contribute to tumourigenesis in the tumour cells by preventing apoptosis.

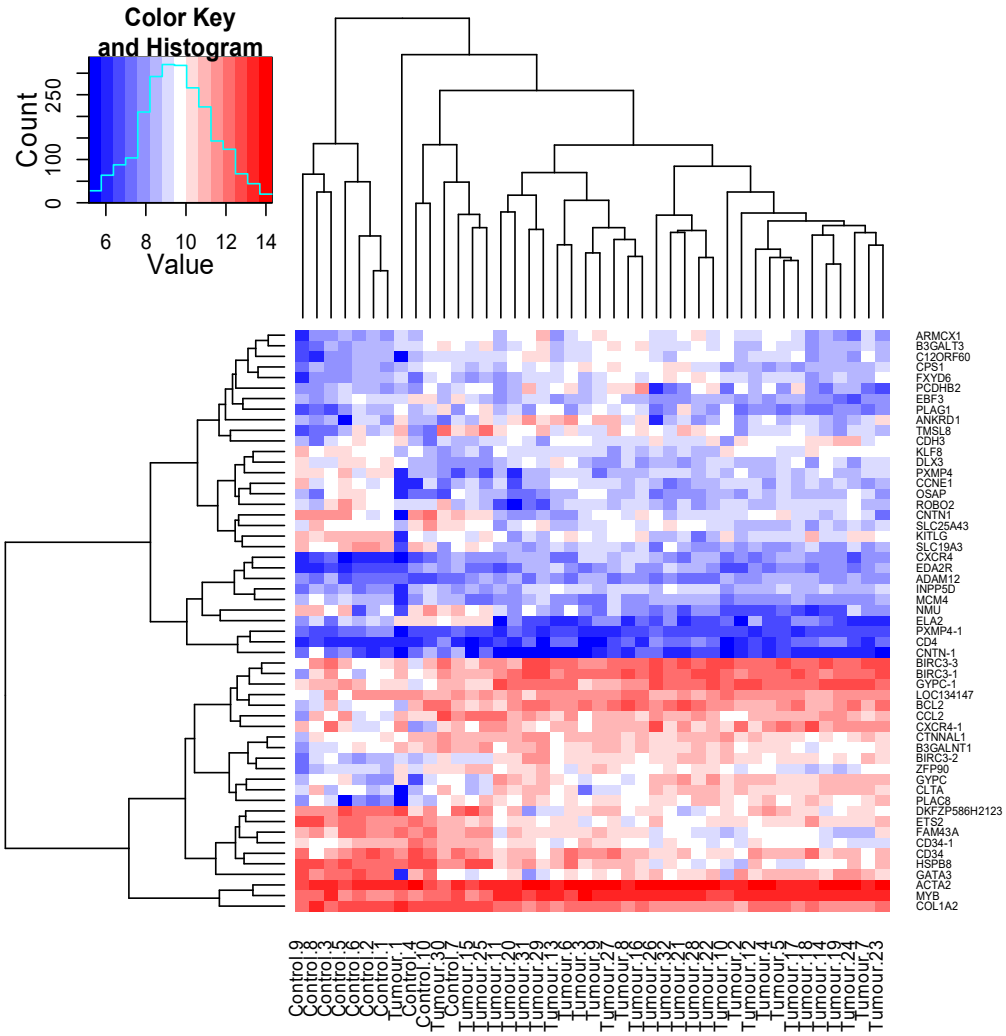

Figure 3-8: The expression of *MYB* and *MYB* target genes in *CYLD*-defective tumours and perilesional skin.

A heat map plot illustrating the expression levels of *MYB* and known MYB target genes in 32 *CYLD*-defective tumours and 10 controls (samples indicated at the bottom of the heat map). Differentially expressed genes were determined (p <0.05) between tumours and controls, and transcript expression levels at a single sample level are displayed on the heat map; red, over-expressed transcripts; blue, under-expressed transcripts; gene names indicated on the right-hand side of the figure; where data from multiple transcripts for a single gene were available are indicated with a numerical suffix (n = 8*).* Clustering by similarity is shown, determined by Euclidean distance.

Gene	Fold change	Gene name	ILMN Probe ID
BIRC3	3.93	Baculoviral IAP repeat-containing 3	ILMN_1776181
GYPC	2.70	Glycophorin C (Gerbich blood group)	ILMN_1668039
PLAC8	2.61	Placenta-specific 8	ILMN_2093343
ANKRD1	2.58	Ankyrin repeat domain 1 (cardiac muscle)	ILMN_1716264
BCL2	2.34	B-cell CLL/lymphoma 2	ILMN_2246956
CXCR4	2.34	Chemokine (C–X–C motif) receptor 4	ILMN_2320888
TMSL8	2.31	Thymosin β15a	ILMN_1681737
MYB	2.04	V-myb myeloblastosis viral oncogene homologue (avian)	ILMN_1711894
FXYD6	1.99	FXYD domain containing ion transport regulator 6	ILMN_1768812
C12orf60	1.98	Chromosome 12 open reading frame 60	ILMN_2234710
ARMCX1	1.90	Armadillo repeat containing, X-linked 1	ILMN_2180677
CLTA	1.82	Clathrin, light chain (Lca)	ILMN_1695420
ZFP90	1.80	Zinc finger protein 90 homologue (mouse)	ILMN_1684628
PCDHB2	1.76	Protocadherin β2	ILMN_2227757
CD4	1.76	CD4 molecule	ILMN_1727284
PLAG1	1.75	Pleiomorphic adenoma gene 1	ILMN_2287653
CCL2	1.60	Chemokine (C–C motif) ligand 2	ILMN_1720048
B3GALT3	1.58	β1,3-*N*-acetylgalactosaminyltransferase 1	ILMN_1787595
EDA2R	1.58	Ectodysplasin A2 receptor	ILMN_1767233
CDH3	1.54	Cadherin 3, type 1, P-cadherin (placental)	ILMN_1704294
CPS1	1.52	Carbamoyl-phosphate synthetase 1, mitochondrial	ILMN_1792748
ADAM12	1.50	ADAM metallopeptidase domain 12	ILMN_1726266
INPP5D	1.47	Inositol polyphosphate 5-phosphatase, 145 kDa	ILMN_1744212
B3GALNT1	1.45	β1,3-*N*-acetylgalactosaminyltransferase 1	ILMN_2325347
CMBL	1.39	Carboxymethylenebutenolidase homologue (*Pseudomonas*)	ILMN_1709634
CTNNAL1	1.39	Catenin (cadherin-associated protein), α-like 1	ILMN_2136446
ACTA2	1.33	Actin, α2, smooth muscle, aorta	ILMN_1671703
KLF8	0.66	Kruppel-like factor 8	ILMN_1788793
MCM4	0.65	Minichromosome maintenance complex component 4	ILMN_2412860
PXMP4	0.64	Peroxisomal membrane protein 4, 24 kDa	ILMN_1664025
COL1A2	0.61	Collagen, type I, α2	ILMN_2104356
DLX3	0.57	Distal-less homeobox 3	ILMN_1789357
CCNE1	0.55	Cyclin E1	ILMN_2374425
OSAP	0.54	Chromosome 4 open reading frame 49	ILMN_2072101
SLC25A43	0.54	Solute carrier family 25, member 43	ILMN_2142284
CD34	0.50	CD34 molecule	ILMN_2341229
ROBO2	0.49	Roundabout, axon guidance receptor, homologue 2	ILMN_2189306
EBF3	0.48	Early B-cell factor 3	ILMN_1707232
KITLG	0.45	KIT ligand	ILMN_1746232
PAMR1	0.43	Inactive serine protease PAMR1	ILMN_1658356
FAM43A	0.38	Family with sequence similarity 43, member A	ILMN_1706015
ELA2	0.38	Elastase 2, neutrophil	ILMN_1706635
GATA3	0.34	GATA binding protein 3	ILMN_2406656
HSPB8	0.32	Heat shock 22 kDa protein 8	ILMN_1791280
ETS2	0.32	V-ets erythroblastosis virus E26 oncogene homologue 2 (avian)	ILMN_1720158
CNTN1	0.31	Contactin 1	ILMN_1661852
NMU	0.25	Neuromedin U	ILMN_2162253
SLC19A3	0.23	Solute carrier family 19, member 3	ILMN_1716359

Table 3-4: Differentially expressed MYB target genes in *CYLD*-defective tumours compared to perilesional control skin.

The fold changes (FC) of transcripts are included for differentially expressed genes with a threshold of $p < 0.05$. Red indicates genes that are overexpressed and blue indicates genes that have reduced expression in CYLD-defective tumours compared to control. (For genes with more than one transcript as indicated on the heat map the highest value is shown).

3.3.4 MYB overexpression promotes the proliferation of primary *CYLD*-defective cylindroma cells

To investigate the biological significance of MYB over-expression in inherited *CYLD*-defective tumours *MYB* mRNA expression was silenced using two siRNAs in cultured primary *CYLD*-defective cylindroma cells. Cells were cultured from three different primary tumours, which had been taken from two patients whom were undergoing surgical excision. Analysis by qPCR of *MYB* mRNA expression following 48 hours of siRNA treatment showed successful knockdown of *MYB* by both siRNAs (Figure 3-9A). This result was confirmed by MYB protein expression also being reduced following 72 hours of siRNA treatment (Figure 3-9B). Primary cell cultures were treated with *MYB* siRNA for 6 days, and it was shown that in each of the three primary *CYLD*-defective cell cultures the silencing of both *MYB* mRNA and protein levels led to a significant decrease in cell proliferation ($p = < 0.001$) (Figure 3-9C). This result suggests that MYB expression is important in the regulation of proliferation in *CYLD*-defective cylindromas. (Prof. Stenman and colleagues at the University of Gothenburg, Sweden, generated the data included in this results section).

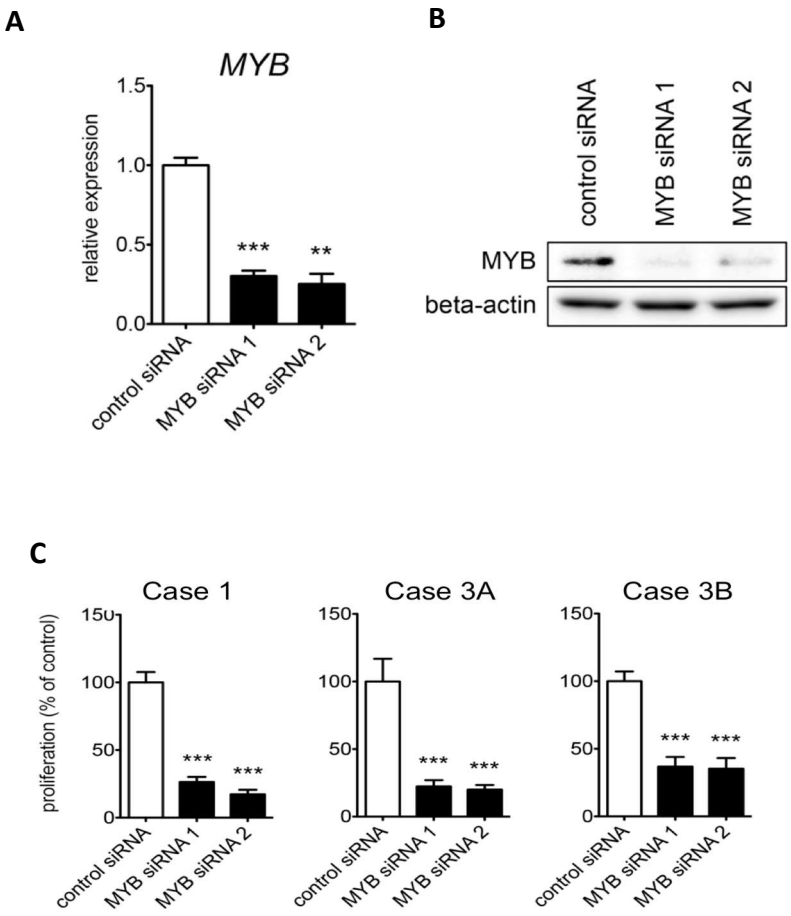

Figure 3-9: Silencing MYB expression reduces the proliferation of primary *CYLD*-defective cylindroma cells.

(A) RT-qPCR analysis of MYB mRNA expression in cultured cells from case 1, following 48 hours of MYB siRNA treatment. (B) Western blot analysis of MYB protein expression in cultured cells form case 1, following 72 hours of MYB siRNA treatment (Data representative of 3 independent experiments) (C) Effect of MYB knockdown on the proliferation of cultured primary cylindroma cells, following 6 days of MYB siRNA treatment. Cells were derived from three individual tumours. (Data are the mean and error bars represent SEM of n=3 experiments. **p <0.01 ***p <0.001.) Figure taken from (Rajan *et al.*, 2016) and produced by collaborators at the University of Gothenburg, Sweden.

3.3.5 CYLD can regulate MYB expression in HEK293T and HaCaT cell lines

In order to recapture the cellular context of the tumours and to determine if a loss of CYLD directly affected MYB expression, *CYLD* mRNA expression was silenced using two shRNAs, shCYL1 and shCYL2, in HEK293T and HaCaT cells alongside the relevant negative non-scrambled shRNA control (NSC). The haematopoietic cell line Jurkat, was included as a positive control for MYB. In both cell lines a conflicting result is seen in response to each of the shRNAs. Conversely in the HEK293T cells compared to control MYB levels decrease when CYLD expression is repressed using shCYL1, but increase when shCYL2 is used (Figure 3-10A). In HaCaTs the opposite result is seen with shCYL1 increasing the level of MYB expression and shCYL2 decreasing it (Figure 3-10B). CYLD expression is reduced by each shRNA but there is no detectable difference in the efficiency of the transduction between the two shRNAs in either cell line. Intriguingly however the band for MYB in the HaCaT cells occurs above the 85kDA protein ladder marker, in contrast to the 75kDA MYB band seen in the HEK293T cells. This suggests differential splicing between the two cell types and that the prominent isoform expressed in keratinocytes is isoform MYB 9B (89kDA).

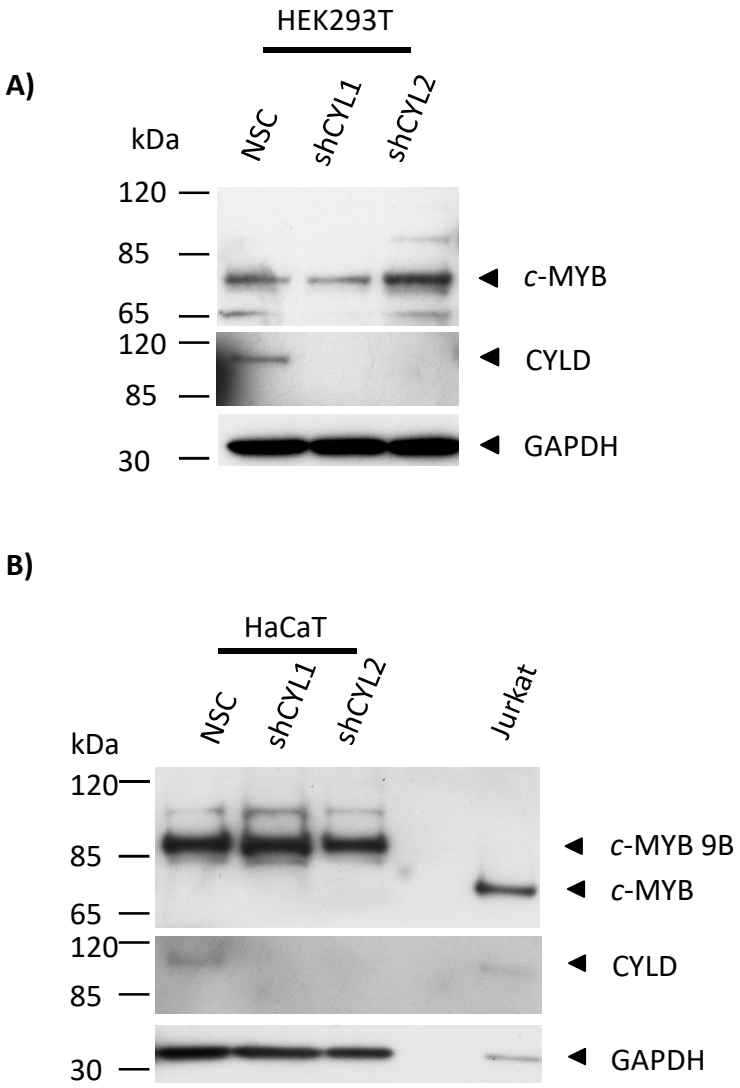

Figure 3-10: Silencing *CYLD* expression affects MYB protein expression in HEK293T and HaCaT cells.

(A&B) Western blot showing the effect of CYLD knockdown using two shRNA constructs on MYB protein levels in the HEK293T cell line (A) or the HaCaT cell line (B). The Jurkat cell line was used as a positive control for MYB. The Western blot shown is representative of 3 independent repeats (A) and 2 independent repeats (B). GAPDH was used as a loading control.

3.3.6 Overexpression of catalytically inactive or truncated CYLD affects MYB expression in the HEK293T cell line

Due to the conflicting results from the shRNA silencing experiments, the up-regulation of MYB in *CYLD*-defective tumours was instead further investigated in overexpression studies. Lysates from HEK293T cells over-expressing either wild-type *CYLD*, catalytically inactive (p.C601S) or truncated *CYLD* harbouring patient specific mutations, were probed with an anti-MYB antibody to determine whether the loss of CYLD accounted for the increase in the expression of MYB. Empty vector was used as a negative control (Figure 3-11). For all *CYLD* mutants except c.2290-94*del*5, there was no observed change in MYB protein expression when compare to wild-type CYLD or empty vector. A slight decrease in the expression of MYB protein was seen in cells overexpressing c.2290-94*del*5 mutated *CYLD,* however this may be due to the reduced level of overexpression and is contrary to the hypothesis of mutant *CYLD* causing an increase in the expression of MYB. These results indicate that the loss of functional CYLD alone is not the determining factor for increased MYB expression in the tumours, and that other indirect mechanisms that are independent of CYLD catalytic activity have a role in driving the increased expression of MYB.

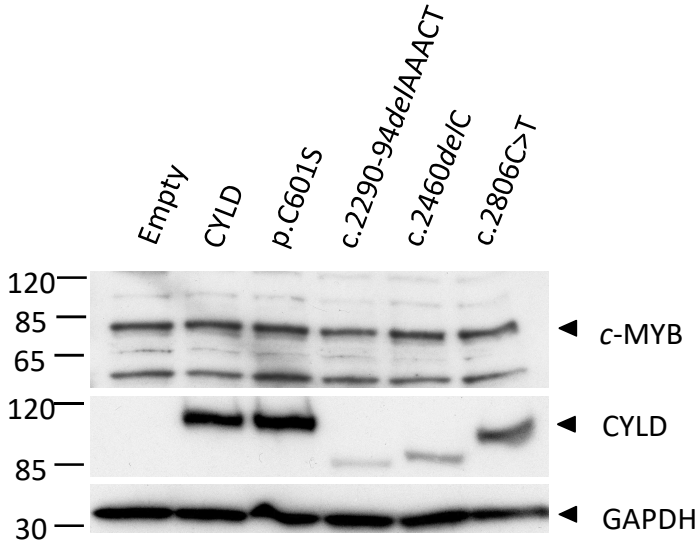

Figure 3-11: Overexpression of wild-type, catalytically inactive or truncated CYLD in HEK293T cells does not affect MYB protein expression.

Cell lysates were generated from cells overexpressing wild-type, catalytically inactive or truncated CYLD, run on a membrane and probed with MYB and CYLD antibodies. GAPDH was used as a loading control. The Western blot shown is representative of 3 independent repeats.

3.3.7 *MYB* isoform *MYB 9B* is upregulated in inherited *CYLD*-defective tumours

RNA-seq data was utilised to look at the expression of alternatively spliced isoforms of MYB in a number of cylindroma tumours (*n*=16), with aligned and exon junction sorted reads visualised using the UCSC genome browser and IGV. When comparing the tumours to control perilesional skin (*n*=4; from mutated *CYLD* carriers*)* it was observed that expression of the MYB gene was increased (Figure 3-12), as indicated by the scale of the Y-axis and the difference in the height of the read-depth peaks. The RNA-seq data supporting what had been shown at the protein level with IHC. The mapping of the RNA-seq reads to exon junctions (see Figure 3-13) demonstrated that there was also an increase in the tumours of alternate exon inclusion in the MYB transcripts compared to the controls (Figure 3-12 & 13), as indicated by the number and thickness of the red arcs in the IGV software. In particular it was shown that there were an increased number of reads at the 5' and 3' splice junctions for exon 9B in the tumours (Table 3-5). In addition it was observed that whilst constitutive exon 10 predominantly followed exon 9 in the majority of transcripts, the alternate exon 9S was also occasionally used exclusively in the tumours. In fact for many of the alternate exons very low read numbers or no reads at all were recorded at alternate exon junctions in control skin samples.

Following the findings at the mRNA level and the observations from the HaCaT cell line for MYB isoforms, tumour lysates from 4 patients were probed for MYB to determine the presence of isoforms at the protein level. Normal skin lysates (*CYLD* $^{+/+}$) from 3 patients were used as controls. In agreement with the HaCaT result, in normal skin the prominent isoform that was detected was MYB 9B (89kDa) with variable levels of expression between samples (Figure 3-14). There was also variabliity in the tumour lysates as MYB was not detectable in all the samples, but in those samples in which MYB was present (3/6) MYB expression was increased compared to controls. Interestingly wild-type MYB (75kDA) was present in the tumour lysates in which MYB 9B had been seen. In addition the same samples were probed for TrkB and intriguingly the tumours with increased MYB protein levels also showed strong TrkB.T1 expression (Figure 3-14).

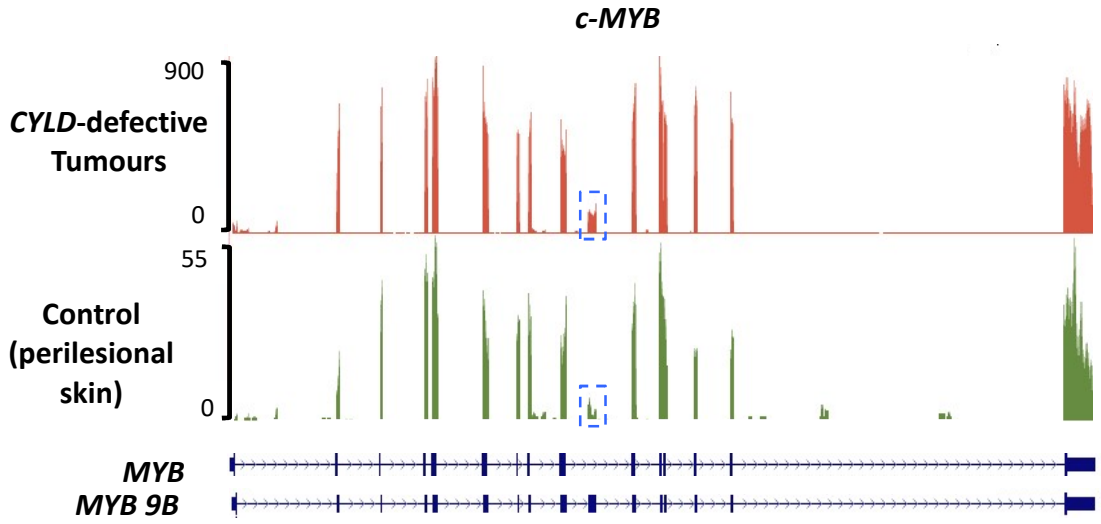

Figure 3-12: UCSC genome browser view of the *MYB* gene showing aligned RNA-seq reads from a panel of *CYLD*-defective tumours (red track) and perilesional skin controls (green track).

The height of the peaks illustrating the number of reads which align to the exons of the MYB gene, with a scale given on the Y-axis (note the scales are different on each axis to reflect the difference between *CYLD*-defective tumours and perilesional skin controls). The blue dashed line rectangles highlight the increased inclusion of exon 9B in the tumour samples.

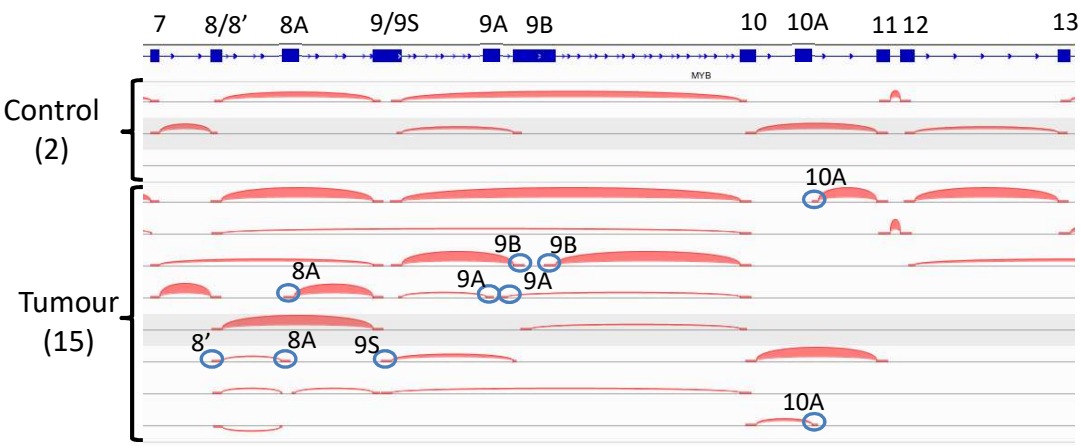

Figure 3-13: IGV view of the MYB gene showing aligned exon junctions of RNA-seq reads in a panel of *CYLD*-defective tumours and perilesional skin controls.

(A) IGV view illustrating the inclusion of alternatively spliced exons of MYB from the alignment of RNA-seq reads by exon junctions. The red arcs represent the alignment of RNA-seq reads between the 5' and 3' splice junctions of the exons and the thickness of the red arcs is reflective of the number of reads that aligned to that region. Blue circles are to highlight the alternate exons.

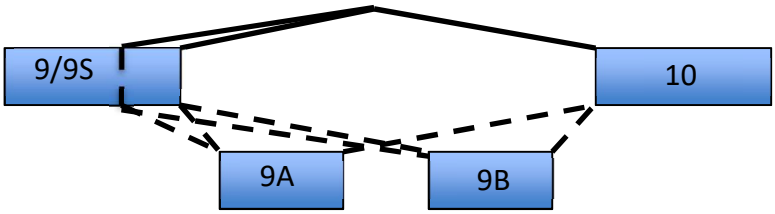

Sample	Exon 9/10	9/9A	9A/10	9/9B	9B/10	9S/10	9S/9A	9S/9B
Control (1)****	4	-	-	-	-	-	-	-
Control (2)*	27	-	-	-	-	-	-	-
Control (3)***	36	-	-	-	-	-	-	-
Control (4)	28	-	-	6	8	-	-	-
1*	144	-	-	41	88	-	-	20
2**	470	-	-	130	108	-	-	-
3***	391	-	-	104	141	-	-	-
4	81	-	-	33	27	-	-	-
5**	350	6	7	99	96	-	-	5
6**	144	-	-	27	45	10	-	-
7****	627	-	-	134	219	11	-	-
8****	497	-	-	196	240	28	-	2
9*	282	1	9	48	80	6	-	-
10***	466	-	-	106	93	12	-	-
11***	443	-	-	96	105	11	-	-
12***	249	-	-	72	67	4	-	-
13*	447	-	-	83	96	14	-	-
14**	166	1	5	64	38	9	-	-
15	471	1	8	198	104	8	-	14
16	215	-	-	102	35	-	-	4

Table 3-5: RNA-seq exon junction read depth counts for MYB exon 9 and alternate exons 9S, 9A and 9B from a panel of *CYLD*-defective tumours and perilesional skin controls.

Schematic diagram above the table displays the possible alternative splicing events. Stars included in the sample column of the table denote samples that have been taken from the same patient, with the samples assigned an equivalent number of stars to indicate matched samples (i.e samples Control (2), 1, 9 and 13 are from the same patient)

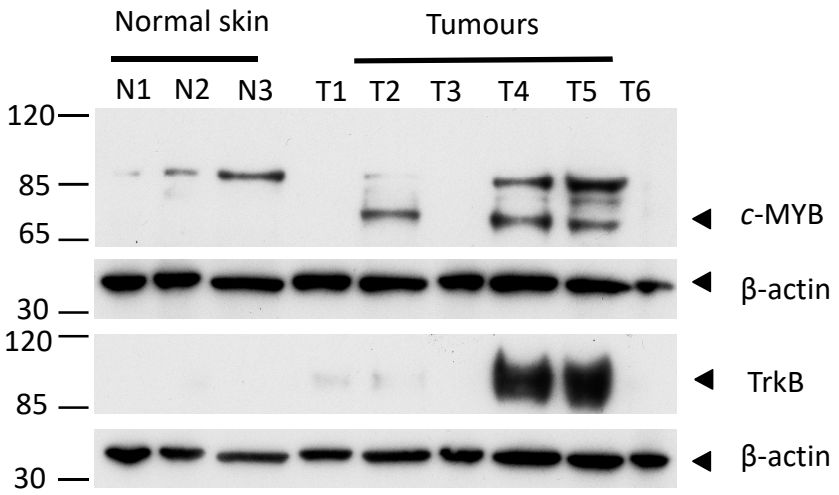

Figure 3-14: Expresssion of both MYB and MYB9B isoforms is increased in CYLD-defective tumours compared to normal skin controls.

Lysates from tumours A Western blot showing the expression of MYB and TrkB isoforms in a panel of cylindroma tumours and normal skin controls. Tumours 2, 4 and 5 are from the same patient. β-actin was used as a loading control. The Western blot shown is representative of 2 independent repeats.

3.3.8 Inhibition of NF-κB does not perturb MYB expression in primary cylindroma cells *in vitro*

NF-κB signalling is dysregulated in *CYLD*-defective tumours due to the loss of CYLD (Brummelkamp 2003), meanwhile MYB has been found to be a target of NF-κB signalling (Lauder, 2001, Pereira, 2015). Therefore the aim was to investigate by inhibition of NF-κB whether this was a molecular mechanism through which *MYB* expression is driven in the tumours. HaCaT cells and two cylindroma primary cell cultures (CPCC), derived from two tumours from different individuals, were treated with the NF-κB inhibitors TPCA-1 and BMS345541. Cell cultures were treated with 1μM and 5μM of TPCA-1 and BMS345541 for 48 hours, with DMSO only included as a control. When MYB protein expression was analysed by Western blotting all cell culture samples showed that with increasing levels of TPCA-1 MYB expression also increased (Figure 3-15). This is contrary to the hypothesis that blocking NF-κB would reduce MYB expression. As the same trend was observed in the HaCaTs and primary cylindroma cultures this suggests that in keratinocytes alternate mechanisms are responsible for the expression of MYB.

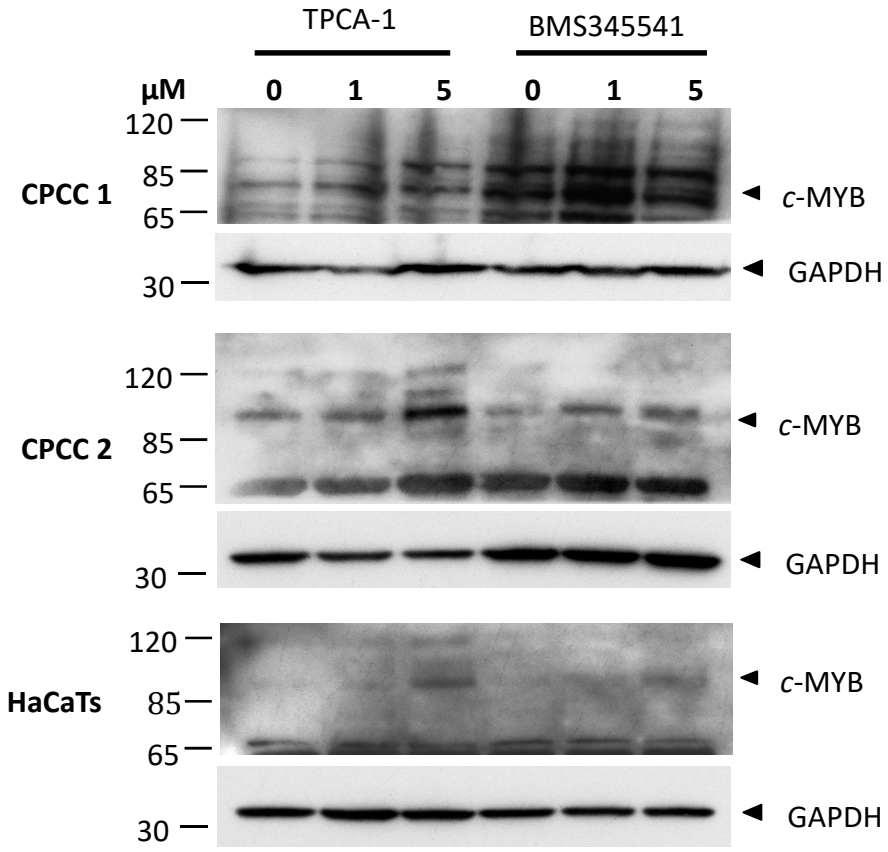

Figure 3-15: The effect of NF-κB inhibition in CPCCs and HaCaTs on MYB protein expression.

Cell cultures were treated with the NF-κB inhibitors TPCA-1 and BMS345541 at the concentrations indicated for 48 hours and MYB protein levels were analysed by Western blot. DMSO only was included as a control. The Western blots shown are from one experimental repeat on each cell culture sample. GAPDH was used as a loading control.

3.4 Discussion

MYB is a proto-oncogene that encodes for a transcription factor whose targets include genes associated with cell cycle progression and regulation of cell survival. As such, aberrant activation of MYB has been shown to be involved in many types of malignancies, including salivary gland cancers such as ACC (Ho *et al.*, 2013). In ACC the genomic rearrangement of *MYB* with *NFIB* leads to the expression of a fusion transcript that is considered a molecular hallmark of this tumour type (Stenman *et al.*, 2014). Due to the observation of the striking histological and morphological similarities between salivary gland tumours and cylindromas, this led others to hypothesise that the *MYB-NFIB* fusion may also be a recurrent gene fusion in cylindroma. Indeed in a cohort of sporadic cylindromas 55% of the tumours were found to be MYB-NFIB fusion positive, whilst some tumours that were lacking the fusion transcript still showed increased activation of MYB (Fehr *et al.*, 2011). These results suggesting that the activation of MYB is involved in the pathogenesis of sporadic tumours. However the status of MYB in inherited *CYLD*-defective tumours remained to be investigated and led to the hypothesis that *MYB* may be over-expressed or genomically rearranged in inherited tumours similar to their sporadic counterparts.

3.4.1 *MYB* activation but no *MYB-NFIB* fusion in inherited *CYLD*-defective tumours

The work in this chapter showed that in contrast to sporadic cylindromas, there was no expression of a *MYB-NFIB* fusion transcript in any of the 23 cylindromas taken from patients who have inherited germ-line mutations of *CYLD*. Two approaches were taken to identify if a fusion gene was present; firstly all tumour samples were negative for the amplification of a fusion product when using nested RT-PCR with primers designed for the most commonly found *MYB-NFIB* fusions (Figure 3-4). Secondly in support of this result FISH analysis indicated that the MYB locus was not rearranged or showed any gain/amplification, as the dual-colour red-green probe was shown to have not broken apart in the inherited tumour samples (n=10) (Figure 3-5). This also validated that other infrequent MYB fusions were not present, which may have been missed in the nested RT-PCR. Whilst no *MYB-NFIB* fusions were found, immunohistochemical analysis did show an increase in MYB expression, in the majority of inherited tumours when compared to perilesional skin (Figure 3-7), which is akin to a sub-set of *MYB-NFIB* fusion negative sporadic tumours (Fehr *et al.*, 2011). Furthermore it is evident from the immunohisotchemical staining that the nuclear localisation of MYB in the tumours,

compared to the cytoplasmic location in normal (*CYLD* wild-type) skin (Figure 3-6), is indicative of increased MYB activation, as MYB Is situated within the tumour cells in a position where it is available to carry out its function as a transcription factor.

The finding of MYB activation, whether it is by gene fusion or alternate mechanisms, in inherited and sporadic tumours suggests a link between the MYB and CYLD pathways. This result is intriguing as the formation of inherited cylindromas is largely restricted to the inheritance of a germ-line mutation of *CYLD* and LOH at the *CYLD* locus, in the majority (approximately 70%) of tumours (*n*=23) (Biggs *et al.*, 1996; Bignell *et al.*, 2000). Furthermore the discrepancy in the activation of MYB between the tumour types may be reflective of the timing of the acquirement of an activated MYB state, which could act synergistically with non-functional CYLD in promoting cylindroma development. Approximately 50% of sporadic tumours demonstrate LOH at the *CYLD* locus (*n*=14) (Biggs *et al.*, 1996), which correlates with 55% of tumours (*n*=12) having been shown to be MYB-NFIB fusion positive in a similar sized study (Fehr *et al.*, 2011). In contrast to the average age of onset at 16 years for inherited tumours (Rajan, Langtry*, et al.*, 2009) sporadic tumours typically present beyond the fifth decade of life (Rajan *et al.*, 2016; Sicinska *et al.*, 2007). It could therefore be speculated that the gain of MYB activation achieved through fusion transcripts could be due to increased genomic instability that comes with ageing (Vijg and Dolle, 2002; Vijg and Suh, 2013).

Alongside these findings it was also shown that the depletion of MYB expression using siRNA knockdown in CPCCs from three individual tumours led to a significant reduction in cellular proliferation (Figure 3-9) and in the expression of MYB target genes Bcl-2 and BIRC3 (data not shown-supplementary material from (Rajan *et al.*, 2016)). It was shown that in addition to Bcl-2 and BIRC3 a number of MYB target genes (*n*=48) were differentially expressed when comparing *CYLD*-defective tumours to perilesional skin controls (Table 3-4). Taken together these results reinforce the idea that MYB contributes to the promotion of these tumours, possibly through inhibition of apoptosis. Therefore it would be interesting to carry out further analysis with larger numbers of tumours to further explore the molecular heterogeneity of MYB activation and its targets between sporadic and inherited tumours types. Also to determine if genetic alterations of CYLD and increased MYB activation are mutually exclusive

molecular events to corroborate that together, changes to these two genes can promote tumourigenesis.

3.4.2 Mechanisms by which *MYB* expression may be altered in a *CYLD*-defective context

In light of the previous results confirming a link between MYB and CYLD, the association of aberrant MYB activation and the loss of functional CYLD, was explored further by assessing MYB expression in HEK293T cells overexpressing either wild-type *CYLD* or various *CYLD* mutants. An increase in MYB expression in the presence of mutant CYLD was not observed (Figure 3-11). This result could indicate that CYLD is not directly involved in the regulation of the expression of MYB. The lack of a response to catalytically inactive or truncated CYLD, with the exception of c.2290-94*del*, may also highlight the possible limitations of using the HEK293T cell line, cells of embryonic kidney origin, to model molecular mechanisms that occur in keratinocytes. HEK293T cells are a useful tool for over-expression studies for deducing protein function and mechanisms of action. However it may be that in this cellular context the protein partners involved in pathways that are perturbed by a loss of functional CYLD and are responsible for increased MYB expression in keratinocytes, may not be expressed in the HEK293T cells, as the cells are not dependent on them. Therefore exogenously over-expressing a non-functional form of CYLD has no effect. Certainly the expression and functions of MYB have been found to be cell-type specific, with differing protein interactions in differing cellular contexts regulating MYB activity (Ness, 2003; Zhou and Ness, 2011). Other possibilities are that off-target events as a consequence of the random integration of the lentiviral vector into the genome may negate an effect, however this is unlikely as these were polyclonal cultures and this would have had to occur across six separate transduction experiments.

The small reduction in MYB expression seen in cells over-expressing *CYLD* c.2290-94*del* could suggest that tumours from patients who have inherited this genotype may not have increased MYB expression; indeed 30% of tumours (*n*=16) in the immunohistochemical analysis did not show an increase in MYB expression. However care should be taken in the interpretation of this result as experimental factors such as the lower transfection efficiency for this CYLD mutant indicated by the lower level of overall CYLD expression may also account for this observation (Figure 3-11). Ideally

CYLD over-expression experiments would be repeated in HaCaT cells to assess the relationship between CYLD and MYB in a more biologically relevant context. The conflicting results from the silencing of CYLD with lentiviral shRNA constructs in the two cell lines would appear to support this strategy (Figure 3-10), as shCYL1 caused an opposing effect on MYB expression in the two cell lines; in HEK293T cells it was decreased whilst in HaCaTs it was increased. It is acknowledged that there are limitations to the data from the knockdown experiments as the result is not consistent between the two shRNA constructs. This may be a real result as the targeting of CYLD by the two individual constructs is different, or there could be differences in the achieved levels of knockdown that were not detectable on the Western blots. Therefore further experimental repeats perhaps with the inclusion of a third construct would give a more definitive result.

CYLD is a negative regulator of NF-κB signalling, with the deubiquitination of several targets including TRAF2, TRAF6, NEMO (Kovalenko *et al.*, 2003) and TAK1 (Reiley W. W. *et al.*, 2007) preventing IκB degradation and maintaining NF-κB in an inactive state. Consequently the loss of CYLD function in the tumours causes increased NF-κB signalling (Brummelkamp *et al.*, 2003). As mentioned previously MYB is a recognised target of NF-κB with the presence of NF-κB binding sites in the promoter of MYB (Lauder *et al.*, 2001), and an ability to overcome the transcriptional attenuation of MYB (Pereira *et al.*, 2015). It was therefore hypothesised that in a subset of tumours MYB may be activated due to aberrant activation of NF-κB caused by the loss of CYLD. In HaCaTs and two CPCCs treated with the NF-κB inhibitors TPCA-1 and BMS345541 it was found that there was no down-regulation of MYB following NF-κB inhibition (Figure 3-15). On the contrary MYB expression actually increased in response to both treatments particularly TPCA-1. Both TPCA-1 and BMS345541 indirectly target NF-κB, as they are potent selective inhibitors of IKK-β over IKK-α. Therefore NF-κB may not be fully inactivated, as IKK-α has been shown to be capable of activating NF-κB even in the absence of IKK-β, but the way the two kinases cooperate is dependent on the cell-type (Adli *et al.*, 2010). In the context of keratinocytes IKK-α is a key regulator of epidermal differentiation, although this is independent of NF-κB (Descargues *et al.*, 2008). The result may therefore demonstrate that inhibition by TPCA-1 of particular IKK components changes the activation of NF-κB and its downstream targets through

imbalances in the IKK-α: IKK-β ratio, leading to altered expression of MYB, that may be isoform specific, in an anti-differentiation response. The result could also suggest that alternative mechanisms are responsible for the activation of MYB within the tumours and that conversely inhibition of NF-κB could interfere with the negative regulation of MYB.

TPCA-1 is also an inhibitor of Stat3 (Signal transducer and activator of transcription 3) (Nan *et al.*, 2014) and it has been observed that Stat3 can repress MYB expression. For example In M1 leukaemia cells dominant-negative forms of Stat3 were shown to inhibit IL-6 induced repression of MYB and subsequent terminal differentiation (Nakajima *et al.*, 1996). Therefore the increase in MYB expression that was observed could potentially be due to Stat3 inhibition. Determination of the protein levels of Stat3 would be required to confirm this. Although the increased *p*-Stat3 expression in the tumours that was observed in Chapter 4, alongside increased MYB expression in the tumours is at odds with Stat3 having a negative regulatory role. On the other hand the tumours are a heterogeneous population of cells, which upon a genetic background of a loss of functional CYLD are committed to perturbed pathways of differentiation. Therefore dependent on the programming of the individual cells within the tumours, some cells may be driven by the activities of Stat3 whilst for others this may be MYB. Also of note is that these experiments were conducted in 2D cell cultures *in vitro,* which may have altered the signalling pathways within the cells. Therefore it may be useful in future to further explore the elusive mechanism of aberrant MYB expression in 3D cell cultures as discussed in Chapter 5.

As it appears that NF-κB may not be responsible for augmented MYB expression in CYLD-defective tumours, an alternative mechanism that requires further exploration is Wnt-1 signalling. This is a pathway of interest that is both dysregulated in the tumours (Rajan, Burn*, et al.*, 2011; Tauriello *et al.*, 2010) and is implicated in the regulation of MYB (Kanei-Ishii *et al.*, 2004). The Wnt-1 signal is transduced to MYB through TAK1 (TGF-β-activated kinase), HIPK2 (homeodomain-interacting protein kinase 2 and NLK, resulting in phosphorylation of MYB by NLK and leading to ubiquitination and subsequent degradation of MYB (Kanei-Ishii *et al.*, 2004). The E3 ubiquitin ligase responsible for ubiquitin attachment to MYB is Fbxw7 (F-box and WD40 domain

protein 7). Mutations of Fbxw7 have been reported in a number of malignancies (Welcker and Clurman, 2008) such as colorectal (Rajagopalan *et al.*, 2004), pancreatic (Calhoun *et al.*, 2003) and endometrial cancers (Spruck *et al.*, 2002), due to Fbxw7 inducing the degradation of a number of positive regulators of the cell cycle such as Cyclin E (Koepp *et al.*, 2001) or of proto-oncogenes such as c-MYC (Sato M. *et al.*, 2015) and c-Jun (Wei *et al.*, 2005). In addition Notch, another aberrantly active signalling pathway in the tumours (Rajan *et al.*, 2014), and NF-κB regulate the activity of miR223, which represses Fbxw7 (Kumar V. *et al.*, 2014). It would therefore be interesting to assess the expression of Fbxw7 or its mutational status, and expression of miR223 in the RNA-seq and microarray datasets. Validating these findings with qPCR and Western blotting to determine if alterations to Fbxw7 or its regulation were responsible for the up regulation of MYB.

A final hypothesis is that up-regulation of MYB may be due to epigenetic alterations such as chromatin remodelling of the *MYB* locus. Indeed recently activation of the *MYB* locus was demonstrated by epigenetic profiling of enhancer regions in *MYB-NFIB* fusion negative but translocation positive ACCs (Drier *et al.*, 2016). CYLD has been shown to negatively regulate the activity of the histone deacetylases, HDAC6 and 7 (Pannem *et al.*, 2014; Wickstrom *et al.*, 2010). Whilst interestingly in leukaemic cells treated with the pan-HDAC inhibitor Givinostat, MYB expression was strongly repressed (Amaru Calzada *et al.*, 2012). Taken together the results indicate that a loss of CYLD in the tumours could consequently alter the acetylation of histones associated with the promoter of MYB to drive its activation. A future approach could be to perform drug assays, treating CPCCs with HDAC inhibitors to see if the MYB result can be recapitulated or if cell viability is affected. Further to this the DNA-binding domain of MYB shares strong structural similarity to a SANT domain, a domain that is found in several chromatin remodelling enzymes (Boyer *et al.*, 2004). Through the SANT domain MYB has been found to be involved in chromatin organisation by directing Histone H3 acetylation and tail positioning (Mo *et al.*, 2005), indicating that MYB also has a role in the epigenetic regulation of target genes. Conversely the strategy of HDAC inhibition may then also prevent the acetylation and activation of MYB target genes by indirectly down regulating MYB expression.

3.4.3 MYB 9B isoform expression in inherited cylindromas

Splicing of the *MYB* gene is complex with 6 alternate exons and two exons that contain alternate splice donor sites a number of variants can be generated (Close *et al.*, 2004; O'Rourke and Ness, 2008; Zhou and Ness, 2011). The functional significance of each variant however is not fully understood. The data in this chapter showed that at the mRNA level not only was the expression of MYB higher in the *CYLD*-defective tumours (Figure 3-12) as indicated by the increased depth of the reads aligned to the *MYB* gene, but in parallel there was increased expression of alternatively spliced isoforms of MYB which were almost exclusive to the tumours compared to perilesional skin, as evidenced by the increased read depth at alternatively spliced exon junctions (Figure 3-13 and Table 3-5). In particular in the tumours exon 9B was the most frequently incorporated alternate exon, but others such as 8A, 9A and 10A were also used (see Appendix). Conflictingly at the protein level in the normal ($CYLD^{+/+}$) skin samples the MYB 9B isoform was detected (Figure 3-14) with the presence of a band that corresponded to MYB 9B at 89kDA on the Western blot membranes. This was also seen in the HaCaTs (Figure 3-8), suggesting that in keratinocytes this is the isoform that is usually expressed and required for normal maintenance of the cell. Although only one perilesional ($CYLD^{+/-}$) skin sample showed inclusion of exon 9B in the RNA-seq data and had very low read counts. In agreement with the previous results though is the finding that in the same tumour samples in which MYB 9B was found on the Western blot a band for wild-type MYB at 75kDA was also detected, demonstrating increased expression of MYB (Figure 3-14) and a possible change in the dependency of particular MYB isoforms in the tumours. Of all the alternate isoforms MYB 9B is the best characterised. It has shown enhanced transactivational activities (Kumar A. *et al.*, 2003) and is required for the proliferation and survival of BCR/ABL expressing leukaemic cells (Manzotti *et al.*, 2012). Meanwhile aberrant expression of MYB 9A was also found to promote T-cell leukaemia (Nakano *et al.*, 2016). This suggests that the isoforms are capable of promoting tumourigenesis but again reiterates that each MYB isoform may have a different role in different cellular contexts.

Speculative explanations for the discord between the mRNA and protein levels could be non-specific binding of the antibody on the Western blots, however the same band was also present in a proportion (3/6) of the tumours at increased levels consistent

with the RNA-seq data. Alternatively it is recognised that the control samples used in each experimental instance were derived from different genetic backgrounds of CYLD using normal skin (*CYLD*$^{+/+}$) for Western blotting and perilesional skin from *CYLD* mutated carriers (*CYLD*$^{+/-}$) for RNA-seq. So the expression of MYB protein in the perilesional samples is unknown and it may be that there are perturbations within these cells that can alter the splicing of MYB prior to a complete loss of CYLD. Another consideration is that the area of the body from which the control samples were taken may have had an affect. The exact sites are unknown, but the perilesional skin is likely to have come from a hairy area of skin such as the scalp, chest or pubic region, as this is where the tumours are frequently found. These samples may therefore have a dense concentration of hair follicles compared to normal skin taken from less hairy sites, and the expression of MYB isoforms may again be altered in different skin compartments.

Finally even though only detected in two tumours on the Western blot, strong TrkB.T1 expression was seen in the same tumour samples that were positive for MYB. This implies that there could be an association between the overexpression of TrkB and MYB in some tumours. This is of interest as it has been found that expression of another Trk family member TrkC, is increased in ACC (Ivanov *et al.*, 2013) and NGF/TrkA signalling may contribute to perineural invasion of ACC (Kobayashi *et al.*, 2015) As TrkB signalling has previously been shown to be dysregulated in *CYLD*-defective tumours (Rajan, Elliott*, et al.*, 2011), this link may be worth exploring in future studies.

The expression of these isoforms in *CYLD*-defective tumours clearly requires further clarification. Particularly as no evidence could be found in the literature of isoforms of MYB having been looked at in the skin so these are novel findings. The alternate isoforms identified in the RNA-seq data will need to be validated by RT-PCR and qPCR. At the protein level Western blots need to be repeated on an increased number of samples from different individuals as the positive results seen were from tumours taken from the same patient. Cellular fractionation of the lysates may also enhance the detection of individual isoforms, as MYB is active in the nucleus. Obtaining positive controls such as the MYB isoform vector constructs used by Nakano *et al.* (Nakano *et al.*, 2016) would be useful to validate the antibody and increase confidence in the

interpretation of the results. However the evidence here supports increased splicing of MYB in the tumours, and gaining further insight into the functions of the different isoforms and whether they differ in the genes they target would be useful, as it may point to a potential mechanism by which the Increased expression of MYB can promote tumour development.

3.4.4 MYB and disease severity in females

It has been reported that the severity of CYLD defective tumour syndromes such as BSS and FC is greater in women (Rajan, Langtry*, et al.*, 2009). In a cohort of 26 patients 5 women required complete scalp removal compared to only one man (Rajan, Langtry*, et al.*, 2009). Furthermore in the same familial study one woman reported an increase in the number of tumours during pregnancy and when hormone replacement therapy started (Rajan, Langtry*, et al.*, 2009). Interestingly it has been shown in breast cancer cells that the over-expression of MYB is dependent on the ER receptor as activation of the receptor can override the transcriptional attenuation region in the first intron of the MYB gene (Drabsch *et al.*, 2007). Furthermore there were genome-wide changes in MYB activity in human MCF7 breast cancer cells treated with beta-estradiol and consequently changes in gene expression (Quintana *et al.*, 2011). Therefore MYB is an interesting target to potentially explore in the context of differing disease severity between the genders, as increased exposure to oestrogen in the females may alter the activity of MYB and the expression of target genes in the inherited tumours.

3.4.5 Targeting MYB as a therapeutic option for *CYLD*-defective tumours

Small molecule inhibitors of MYB are being developed as MYB is recognised as an attractive therapeutic target for the treatment of leukaemia and other solid tumours such as ACC, that are driven by deregulation of MYB (Uttarkar *et al.*, 2017). A strategy for the inhibition of MYB is to target the MYB/p300 interaction (Uttarkar *et al.*, 2015), as this is an essential partner for the transcriptional activation of MYB (Dai P. *et al.*, 1996). A promising compound, the naphthoquinone Plumbagin has been identified, which binds to the p300 binding site of MYB and was found to selectively supress the proliferation of primary AML cells but not normal haematopoietic progenitors (Uttarkar *et al.*, 2016). Another favourable compound is the multi-kinase inhibitor Rigosertib, which has been shown to selectively induce cell death in diffuse large B cell lymphoma through suppression of MYB and TRAF6 (Dai Y. H. *et al.*, 2016). This

mechanism of action is interesting as TRAF6 is an adaptor protein involved that is involved in tumour development through its role in NF-κB signalling (Inoue *et al.*, 2007) and has been shown to be a target of CYLD (Sun S. C., 2010; Trompouki *et al.*, 2003). Therefore it would be interesting to carry out preclinical experiments to assess the effect of MYB inhibitors on the proliferation and survival of primary cylindroma cells.

3.4.6 Conclusions

In summary it has been shown that in a proportion of both sporadic and inherited *CYLD*-defective tumours there is increased activation of MYB, however in the sporadic tumours this is commonly caused by the expression of a *MYB-NFIB* fusion transcript. The expression of MYB changed in response to both CYLD silencing and overexpression experiments, and together the *ex vivo* and *in vitro* studies here strongly indicate an association between MYB and CYLD for the first time in inherited cylindromas. The molecular mechanisms behind overexpression of MYB in the cylindromas however remains to be determined, as the evidence from these results did not support dysregulated NF-κB signalling as the mechanism responsible for MYB activation. In the tumours increased expression of alternate isoforms of *MYB* particularly of *MYB 9B,* were also observed which may have implications for the activity of MYB within the cells. Overall the overexpression of MYB is intriguing, as it demonstrates an additional molecular event that has the potential to contribute to tumour formation. Whilst the role of MYB does require further exploration, the development of inhibitory MYB compounds makes it an attractive therapeutic target for the treatment of *CYLD*-defective tumours.

Chapter 4

Investigation of TrkB isoforms in *CYLD*-defective tumours

4 Chapter 4: Investigation of TrkB isoforms in *CYLD*-defective tumours

4.1 Introduction

4.1.1 Chapter aims

The over-expression of TrkB and neurotrophic ligands in *CYLD*-defective tumours, and the known functions of receptor activation in the skin and hair follicle compartments and their potential contributory roles to tumourigenesis, the overall objective of the work in this chapter was to investigate the implications of TrkB upregulation upon the underlying pathology of *CYLD*-defective tumours. The main aims were:

- Identify the expression of TrkB isoforms in *CYLD*-defective tumours
- Identify signalling pathways activated by TrkB isoforms in *CYLD*-defective tumours
- Assess if pharmacological inhibition of identified signalling cascades affects primary *CYLD*-defective tumour cell cultures

4.1.2 Neurotrophins and Trk receptors

The four mammalian neurotrophins (NT), nerve-growth factor (NGF), brain-derived neurotrophic factor (BDNF), neurotrophin-3 (NT-3) and neurotrophin-4/5 (NT-4/5), are a family of growth factors that are critical to the development and maintenance of the nervous system. Neurotrophins exert their trophic effects through activation of two different receptor classes, the tropomyosin-related kinase (Trk) family of receptor tyrosine kinases, TrkA, TrkB and TrkC, and the tumour necrosis factor superfamily member, p75 neurotrophin receptor ($p75^{NTR}$) (Patapoutian and Reichardt, 2001). Interestingly binding of neurotrophic ligands to the different receptor types can produce opposing cellular responses. Upon engagement of the neurotrophins with their cognate Trk receptors a number of signalling cascades can be initiated which promote cell proliferation, differentiation and survival. These include signalling pathways associated with phosphatidylinositol-3-kinase (PI3K), mitogen-activated protein kinase (MAPK) and phospholipase-C-gamma (PLC-γ) (Huang E. J. and Reichardt, 2001). Alternatively engagement of neurotrophins with $p75^{NTR}$ can induce cell death (Lu *et al.*, 2005).

Neurotrophins were the first to be discovered, due to a search for survival factors to affirm the neurotrophic factor hypothesis: that targets of neuronal innervation secrete limiting amounts of survival factors, which function to ensure a suitable ratio between the size of the target organ and the density of innervating neurons (Levi-Montalcini, 1987). Having initially been discovered as an oncogene, the Trk receptors then came to pre-eminence in the field of neurobiology after the ligand-binding domain of proto-Trk was recognised as the elusive receptor for the neuronal survival factor NGF (Kaplan *et al.*, 1991). Since their discovery neurotrophins and their receptors have been remarkably insightful to our understanding of key molecular mechanisms in cell biology. Experiments that led to their discovery revealed the significant role of cellular interactions in cell survival and differentiation (Jacobson *et al.*, 1997; Raff *et al.*, 1993). Alongside this the early discovery of NGF internalisation by receptor-dependent processes, the requirement of cytoskeletal and energy-dependent processes for transport along axons in membranous vesicles, and lysosomal ligand turnover, opened up research into mechanisms that are now recognised to be used by many if not all cells in controlling ligand-receptor cycling and function (Huang E. J. and Reichardt, 2001; Thoenen and Barde, 1980).

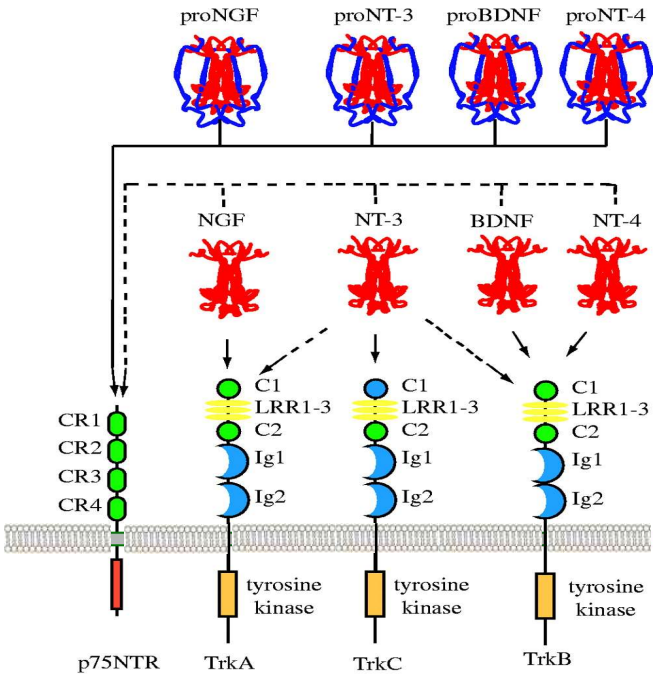

Figure 4-1: The protein structure of Trk and p75^{NTR} receptors and their binding ligands.

An illustration of the major interactions of the neurotrophins and the structural domains of the three Trk receptors: TrkA, TrkB and TrkC, and structurally unrelated p75NTR. All proneurotrophins can bind to p75NTR but not Trk receptors. Each of the mature neurotrophins can bind to their preferred Trk receptor or p75NTR. NT-3 is able to bind to each of the Trk receptors, as indicated by the dashed arrows, but it is dependent on the cellular context whether it does so. Binding of the pro or mature neurotrophins initiates activation of the intracellular tyrosine kinases of Trk receptors or death domain of p75NTR. C1/C2: cysteine repeats, LRR1-3: Leucine-rich repeats, Ig1/Ig2: Immunoglobulin domains. CR1-4: cysteine rich domain. Figure adapted from (Reichardt, 2006).

Each of the neurotrophic factors interacts with the three Trk receptors with selective affinity; NGF binds most specifically to TrkA, BDNF and NT-4/5 to TrkB and NT-3 to TrkC (Figure 4-1). However NT-3 can activate TrkA and TrkB, but with less efficiency in some cell types (Ip *et al.*, 1993; Reichardt, 2006). Mouse models with null mutations in each of the Trk receptors (Klein *et al.*, 1994; Klein *et al.*, 1993; Smeyne *et al.*, 1994), or global knockouts for each of the neurotrophins (Conover *et al.*, 1995; Ernfors, Lee, & Jaenisch, 1994; Ernfors, Lee, Kucera*, et al.*, 1994), were shown to have overlapping phenotypes when either a neurotrophin or its cognate receptor was deficient, supporting the *in vitro* work of these biochemical interactions and particularly the promiscuity of NT-3 (Farinas *et al.*, 1998). The importance of these factors and their receptors to the developing nervous system were shown in the mice, with losses of specific neuronal populations a particular receptor or neurotrophin was lacking and highlighted that differing neuron populations have specific neurotrophin dependencies. The loss of TrkB was the most severe with animals not surviving more than a day (Klein *et al.*, 1993), however the other models still only survived a few weeks. In particular sympathetic and sensory neurons of the peripheral nervous system are severely affected by the absence of Trk receptors or their neurotrophins. In keeping with the work of Levi-Montalcini *et al.* sympathetic neurons were almost completely lost in the absence of NGF or TrkA (Crowley *et al.*, 1994; Levi-Montalcini, 1987), alongside nociceptive neurons (Huang E. J. and Reichardt, 2001). Meanwhile specific sensory losses of proprioceptive neurons (awareness of limbs) were seen when TrkC was deficient (Ernfors, Lee, Kucera*, et al.*, 1994). Also Huang *et al.* demonstrated that in the developing sensory neuron ganglia of mice, expression of the Trk receptors occurs in two waves with initial generation of TrkB and TrkC expressing neurons followed by TrkA expressing neurons, and limited co-expression of Trk receptors in the later stages suggesting that Trk expression becomes more restrictive during development (Huang E. J. *et al.*, 1999). Within the central nervous system, TrkB and TrkC are more widely expressed but their patterns of expression are also restricted to specific areas of the brain (Huang E. J. and Reichardt, 2001).

However the neurotrophins and their receptors are not exclusive to the nervous system. Early immunohistochemical analyses showed cell-type specific, Trk receptor expression in many human tissues such as the colon, kidney and spleen (Shibayama

and Koizumi, 1996), warranting further investigation of the function of neurotrophic signalling in non-neuronal tissues. In particular neurotrophins and their receptors are expressed during cardiovascular development (as reviewed by (Caporali and Emanueli, 2009), with NGF shown to be an autocrine pro-survival factor to cardiomyocytes (Caporali *et al.*, 2008). Moreover studies using global knockout mouse models have revealed deficiencies in BDNF to cause reductions in endothelial cell-cell contact with severe consequences to heart function such as intraventricular wall haemorrhage and depressed cardiac contractility (Donovan *et al.*, 2000), and deficiencies in TrkB to cause a reduction in blood vessel density and an increase in the number of apoptotic endothelial cells in the developing heart (Wagner *et al.*, 2005). More recently BDNF has even been explored as a therapeutic option for heart failure (Okada *et al.*, 2012; Samal *et al.*, 2015). Meanwhile NT-3 and TrkC deficiencies cause cardiac malformations, with some defects appearing at embryonic day 9.5, which is before the onset of cardiac innervation in mice (Donovan *et al.*, 1996; Tessarollo *et al.*, 1997). Likewise broader functions for the neurotrophins in the immune system have been suggested (Vega *et al.*, 2003), with TrkA and TrkB functionally deficient mice indicating the importance of these receptors and ligands in the development of immune organs such as the thymus and the survival of thymocytes (Garcia-Suarez *et al.*, 2002; Garcia-Suarez *et al.*, 2000). Alongside the organs individual expression patterns of neurotrophins, Trk receptors and $p75^{NTR}$ are observed to have immunomodulatory roles in the different subsets of immunocompetent cells such as lymphocytes, affecting a range of functions from proliferation and survival to the induction of antibody synthesis (Brodie *et al.*, 1996).

Of particular interest to the work within this thesis is the function of the neurotrophins and their cognate receptors in the skin (discussed in more detail in section 4.1.9). These proteins are differentially distributed in distinct cell populations of the skin, and structures within the skin like the hair follicle are both a target and source of neurotrophins; the same structure from which *CYLD*-defective tumours are potentially derived from (Massoumi, Podda*, et al.*, 2006). Additionally Trk and $p75^{NTR}$ signalling have been shown to have contrasting effects on hair follicle morphogenesis and hair cycling (Botchkarev *et al.*, 2006). After having been shown to have an array of functions in and outside of the nervous system, it is not surprising that neurotrophin-

Trk signalling is implicated in neurodegenerative diseases such as Alzheimer's (Allen S. J. *et al.*, 2011), Parkinson's (Meldolesi, 2017; Murer *et al.*, 2001), and various cancers such as neuroblastoma (Evangelopoulos *et al.*, 2004) prostate (Montano and Djamgoz, 2004), lung (Ricci *et al.*, 2001; Sinkevicius *et al.*, 2014), breast (Tsai *et al.*, 2017; Vanhecke *et al.*, 2011) and melanoma (Pasini *et al.*, 2015; Truzzi *et al.*, 2008).

4.1.3 Neurotrophin processing and signalling

Similar to other secreted proteins, neurotrophins are processed from precursor molecules, proneurotrophins, which undergo proteolytic cleavage and post-translational modifications to produce their mature forms. Proneurotrophins have three ultimate fates: intracellular cleavage followed by secretion; secretion followed by extracellular cleavage; or secretion without subsequent cleavage (Lu *et al.*, 2005). Initial pre-proneurotrophin synthesis occurs in the endoplasmic reticulum, before the proneurotrophin translocates to the *trans*-Golgi network for cleavage by enzymes such as Furin or prohormone convertases, and sorting and processing into two secretory pathways: the constitutive or the regulated pathway. Within each of these pathways neurotrophins are packed into distinct secretory vesicles; in the constitutive pathway the vesicles are continuously released in a calcium-independent manner, meanwhile in the regulatory pathway exocytosis of the vesicles occurs in response to an extracellular stimulus that triggers the release of intracellular calcium stores, including ligand engagement of Trk receptors (Canossa *et al.*, 2001; Lessmann and Brigadski, 2009).

The key determinant of the efficiency with which neurotrophins are cleaved and sorted is the sequence information within the C-terminal region of the prodomain of the neurotrophin (Nomoto *et al.*, 2007), as studies have found that in neurons swapping of the prodomains between the different neurotrophins can alter the pathway of secretion for the neurotrophin (Brigadski *et al.*, 2005). In general BDNF and NT-3 are targeted more efficiently for regulatory secretion, meanwhile NGF and NT-4 are primarily secreted through the constitutive pathway (Lessmann and Brigadski, 2009). The importance of the propeptide sequence is also highlighted by the secretion of BDNF in neurons, a naturally occurring polymorphism can cause a Valine to Methionine exchange in the prodomain and consequently BDNF is no longer efficiently targeted to regulatory secretion vesicles and release of BDNF through this pathway is

hindered (Egan *et al.*, 2003). In addition this sequence information is also required for co-localisation of neurotrophins with the intracellular sortilin receptor; in the case of BDNF it is thought that this association promotes an appropriate configuration of proBDNF, which in conjunction with a sequence within the mature domain that promotes an interaction with carboxypeptidase E, allows for the sorting of BDNF into regulatory secretory vesicles (Lou *et al.*, 2005; Lu *et al.*, 2005). Other factors that regulate this process include the availability and localisation of proteases, as the enzymes are differentially expressed between cell-types and their pH-optimum dictates in which cellular compartment proteolysis can occur (Lessmann and Brigadski, 2009). Proneurotrophin cleavage may also occur extracellularly by plasmin or matrix-metalloproteinases if there are inefficiencies intracellularly (Bruno and Cuello, 2006).

In addition proneurotrophins can be secreted and left uncleaved. In this form proneurotrophins have been found to be biologically active signalling mediators within their own right, distinct from their mature counterparts (Lee R. *et al.*, 2001). Moreover the different neurotrophin forms are capable of inducing opposing biological responses, with proneurotrophins binding with high affinity to $p75^{NTR}$ receptors and inducing pro-apoptotic signalling responses (Feng *et al.*, 2010; Lee R. *et al.*, 2001), whilst in contrast mature neurotrophins preferentially bind to Trk receptors to promote survival signalling. Therefore the ratio of pro- to mature neurotrophins represents an additional mechanism that can direct the actions of neurotrophin signalling and determine a cells fate.

4.1.4 The protein structure of Trk receptors

The structural organisation of the Trk receptors (Figure 4-1), particularly of the extracellular domain, is important in the regulation of the specificity and strength of neurotrophin binding to each Trk family member (Huang E. J. and Reichardt, 2003). Heavily glycosylated, the extracellular domain consists of three leucine-rich repeats flanked by two cysteine repeats. These are followed by two C2-type immunoglobulin (Ig) domains, which are adjacent to a single transmembrane region (Deinhardt and Chao, 2014). Each receptor terminates with a cytoplasmic, tyrosine kinase domain containing several tyrosine-containing motifs, which serve as phosphorylation-dependent docking sites for adaptor proteins and enzymes to mediate signalling

cascades (Skaper, 2012)

The membrane-proximal (second) Ig domain was found to be the major interface for ligand binding (Urfer *et al.*, 1995), with further evidence suggesting that the Ig domains function to stabilise the receptors in their monomeric forms and prevent their dimerization in the absence of ligand (Arevalo *et al.*, 2000). Although several studies have found each of the extracellular subdomains of the Trk receptors can contribute to ligand binding (Arevalo *et al.*, 2001; Arevalo *et al.*, 2000; MacDonald and Meakin, 1996; Ninkina *et al.*, 1997). The intricate details of the specificity of the neurotrophin and Trk receptor interaction became clearer with the determination of the crystal structure of this domain in each of the Trk receptors (Ultsch *et al.*, 1999), together with the ligand bound forms of the domain of TrkA with NGF (Wiesmann *et al.*, 1999) and TrkB with NT-4/5 (Banfield *et al.*, 2001). Structure comparisons found two important interaction surfaces, a conserved patch of contacts, common throughout the Trk receptor family members, contributing to the affinity for neurotrophin binding. Alongside a second set of highly specific contacts, which stabilises the N-terminal structure of a neurotrophin when bound to its complementary receptor surface, determining the specificity of neurotrophin selection for a particular Trk receptor (Banfield *et al.*, 2001).

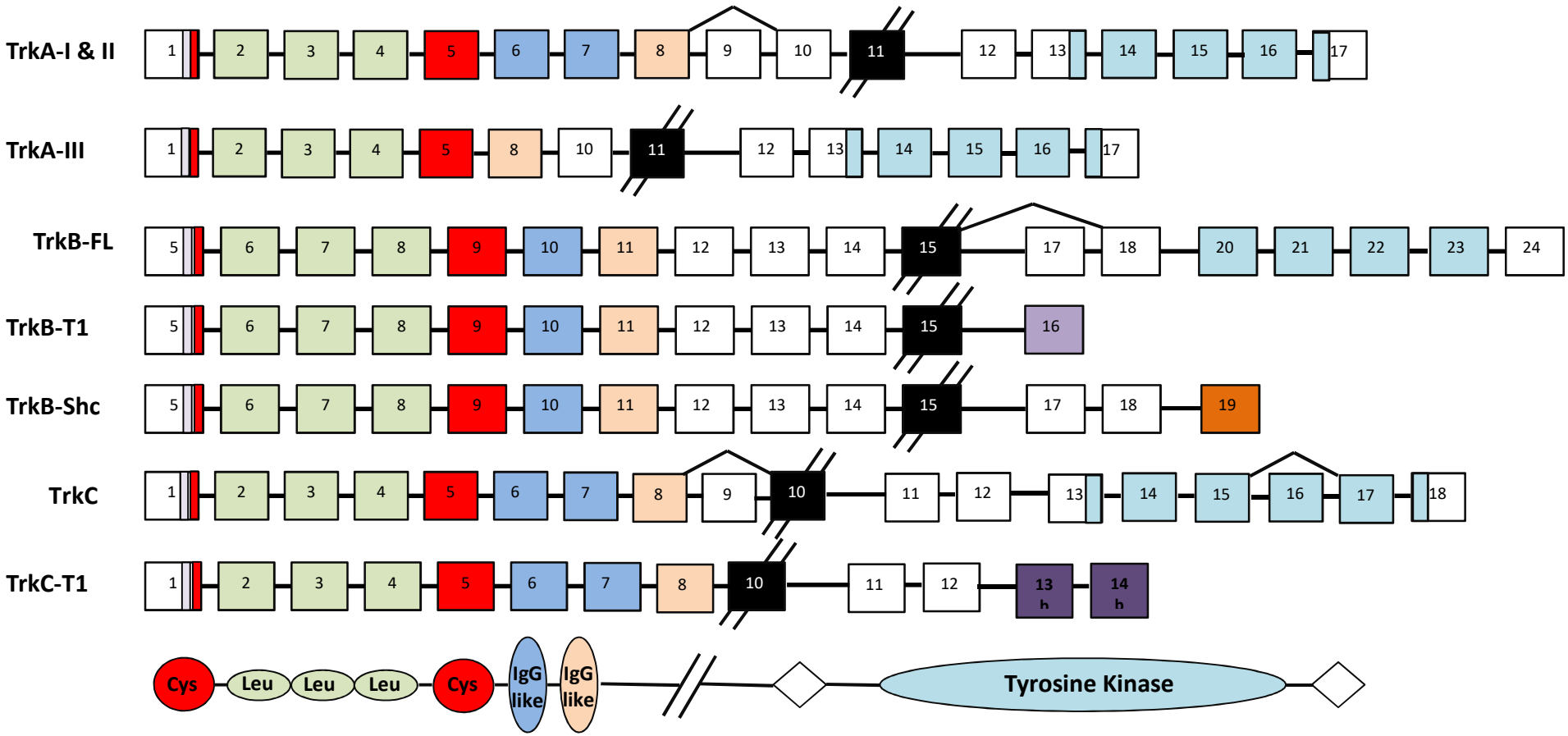

Figure 4-2: The transcripts and functional domains of Trk receptor isoforms.

The splicing pattern of each Trk receptor is shown with the colours corresponding to the schematic of functional domains, with the exception of unique alternate exons shaded purple and orange. Black boxes with lines represent the transmembrane region. Isoforms are drawn from information from (Ichaso *et al.*, 1998; Luberg *et al.*, 2015; Stoilov *et al.*, 2002).

4.1.5 Trk receptor isoforms

The three Trk receptors are each encoded for by a single gene *NTRK1* (TrkA)*, NTRK2* (TrkB)*,* or *NTRK3* (TrkC)*.* However alternative splicing of each of the genes can produce distinct isoforms that affect the function of the receptor (Figure 4-2), up until recently there were three known isoforms of TrkA in humans. TrkA-I, mainly expressed in non-neuronal cells, lacks exon 9, a six amino acid insert in the transmembrane region that is included in the full-length TrkA-II isoform, expressed mainly in neuronal cells (Barker *et al.*, 1993). Whilst in the thymus and undifferentiated neural progenitor cells a third isoform exists (Tacconelli *et al.*, 2007; Tacconelli *et al.*, 2004). TrkA-III splices out exons 6, 7 and 9, and therefore lacks the first Ig domain and several glycosylation sites. Consequently the receptor cannot bind NGF and is autophosphorylated and constitutively active (Luberg *et al.*, 2015). However Luberg *et al.* described numerous transcripts of human *TrkA*, due to the inclusion of multiple novel 5' terminal exons, which could encode for other protein isoforms (Luberg *et al.*, 2015). There are four TrkB isoforms in humans, two full-length receptors that differ due to the inclusion of exon 17, and two C-terminal truncated isoforms that lack the kinase domain. Although more recently Luberg *et al.* have described thirty-six novel isoforms of TrkB proteins with unique properties within neural cells, highlighting the need for further study of TrkB variants as the synthesis and regulation of the receptor is clearly a complex process (Luberg *et al.*, 2010). TrkB.T1 is more broadly expressed and the transcript includes the unique, alternative exon 16 (Stoilov *et al.*, 2002). Meanwhile TrkB-Shc is only found in the brain and spinal cord, the transcript includes the unique alternative exon 19, and retains the Shc binding domain in the cytoplasmic tail (Wong J. and Garner, 2012). TrkC also has truncated receptor isoforms with shortened cytoplasmic tails that are not catalytically active (Brahimi *et al.*, 2016; Menn *et al.*, 1998; Valenzuela *et al.*, 1993), in addition to isoforms that have insertions of variable sizes in the kinase domain that can reduce the kinase activity of the receptor (Tsoulfas *et al.*, 1993; Valenzuela *et al.*, 1993). It is the truncated isoforms that are predominantly expressed in non-neuronal tissues as well as being found in the mature nervous system. The roles of these truncated isoforms are still largely unknown, however original postulations that they act solely as dominant negative receptors are being undermined, as studies suggest that truncated receptors may have signalling capabilities of their own (Fenner, 2012; Renn *et al.*, 2009; Rose *et al.*, 2003).

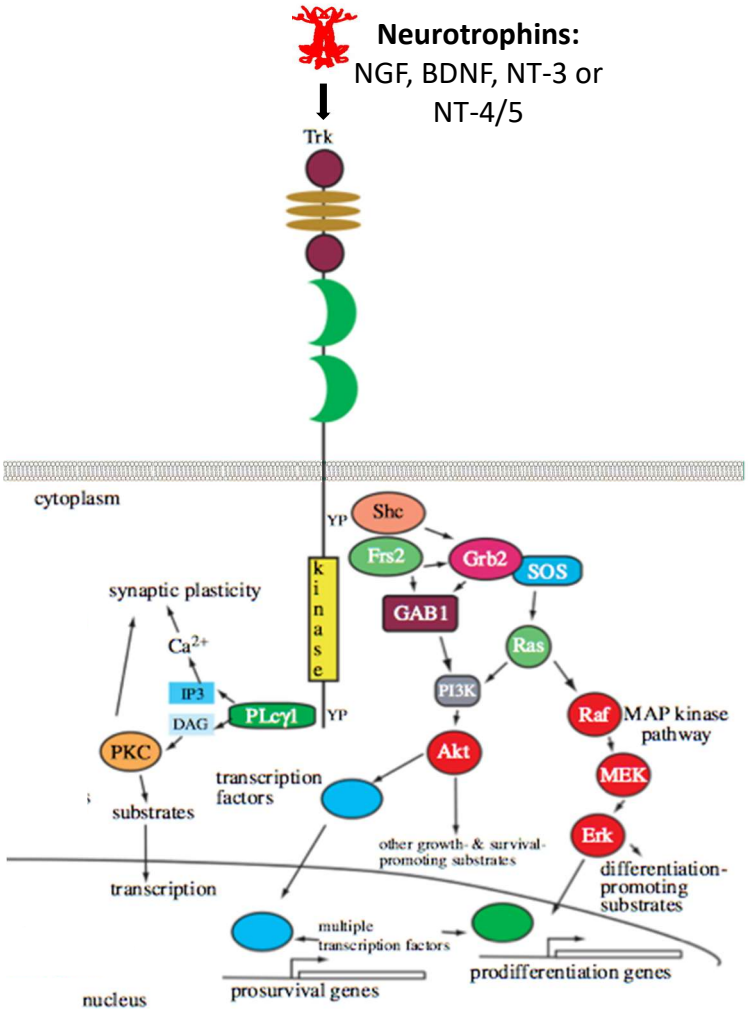

Figure 4-3: Neurotrophin-Trk signalling pathways.

A simplified schematic overview depicting the three main intracellular signalling pathways by which neurotrophins exert their cellular responses through Trk receptors: PI3K-Akt, Ras-MAPK-Erk and PLC-γ. Once the receptor is activated by a neurotrophin, it dimerises with another Trk receptor and initiates phosphorylation of the kinase domain. This in turn leads to the recruitment of an array of adaptor proteins (not all are depicted in the figure for simplicity). Signalling through the Trk receptors promotes cell survival through activation of PI3K via Ras and Gab1, whilst activation of Ras and MAPK promotes cell differentiation, either by interacting with proteins or by influencing the transcription of genes involved in each of the cellular processes, such as anti-apoptotic proteins. In addition activation of PLC-γ results in the release of intracellular calcium stores and activation of PKC regulated pathways, which in neurons promote synaptic plasticity. Figure adapted from (Reichardt, 2006).

4.1.6 Signalling via Trk receptors

The signalling pathways activated by neurotrophins through Trk receptors have been extensively studied and comprehensively reviewed by (Chao, 2003; Deinhardt and Chao, 2014; Huang E. J. and Reichardt, 2001, 2003; Kaplan and Miller, 2000; Reichardt, 2006). As shown in Figure 4-3 these pathways include the PI3K, MAPK and PLC-γ signalling pathways, which are discussed in more detail below. Neurotrophin-Trk signalling has been shown to influence many aspects of neural development, function and maintenance after injury including: precursor cell proliferation and commitment, cell survival and differentiation, synaptic formation and plasticity, axon and dendrite growth, growth cone motility, and cell death. Initially Trk signalling was mainly delineated in the rat adrenal pheochromocytoma (PC12) cell line, which expresses TrkA and $p75^{NTR}$ (Barker and Shooter, 1994), and later validated in normal primary neurons, as well as being studied in non-neuronal tissues and cell cultures. Ligand binding to Trk receptors by their corresponding mature neurotrophin induces receptor dimerization, and activation of the kinase domain through phosphorylation of several of ten conserved tyrosine (Y) residues present on the cytoplasmic tail of the receptor. Three of these tyrosines Y670, Y674, Y675 (numbering scheme based on human TrkA) are within the auto-regulatory loop of the tyrosine kinase domain, and when phosphorylated potentiate tyrosine kinase activity (Cunningham and Greene, 1998). Whilst also providing a mechanism for initiation of signalling pathways via recruitment of adaptor proteins such as FRS2 (fibroblast growth factor receptor substrate) and Shc (Src homology domain containing) (Meakin *et al.*, 1999), Grb2 (growth factor receptor-bound protein-2), SH2B and rAPS (Arevalo and Wu, 2006; Qian *et al.*, 1998). Outside of the kinase domain, the phosphorylation of the tyrosine residues Y490 and Y785 have been the most characterised, with these positions creating docking sites for adaptor proteins which trigger downstream signalling, phosphorylation of Y490 coupling the Trk receptors to pathways such as Ras-ERK and PI3K-Akt, and phosphorylation of Y785 to PLC-γ (Patapoutian and Reichardt, 2001). Although these tyrosine sites have been the main focus in unravelling Trk signalling, mutations to three of the five remaining tyrosines inhibited NGF-dependent neurite outgrowth, suggesting that they too contribute to Trk-mediated signalling (Inagaki *et al.*, 1995). Additionally others have indicated that the cytoplasmic tyrosine kianse c-Abl has a role in mediating a differentiation response via Trk receptors. Yet c-Abl interacts with the juxtamembrane

region of TrkA in PC12 cells regardless of the phosphorylation status of tyrosines in this region, thus indicating that not all Trk interactions are dependent on phosphorylation of tyrosines (Yano *et al.*, 2000).

In addition to the three main pathways discussed in more detail below neurotrophin-Trk signalling can activate members of the Rho (Ras homolog gene family, member A) family of GTPases, which control cytoskeleton organisation and cell motility, including Cdc42 and Rac (Reichardt, 2006). Furthermore in neuronal cell populations Trk receptors can also be activated through neurotrophin independent mechanisms, such as glucocorticoids (Jeanneteau *et al.*, 2008) and adenosine and G-protein coupled receptors (Lee F. S. and Chao, 2001).

4.1.6.1 PI3K-Akt signalling pathway

The initiation of PI3K signalling by Trk receptors has been shown to be a main mechanism by which Trk signalling promotes cell survival and is mediated by two distinct pathways (Vaillant *et al.*, 1999). The phosphorylation of tyrosine Y490, and the analogous phospho-tyrosine residues in TrkB and TrkC, leads to the recruitment of the adaptor protein Shc, which in complex with Grb2 and the Ras exchange factor SOS (son of Sevenless) stimulates activation of Ras and consequently PI3K (Patapoutian and Reichardt, 2001; Rodriguez-Viciana *et al.*, 1994). Alternatively phosphorylated Grb2 also provides a docking site for Gab-1 (Grb2 associated binding protein-1), which allows for subsequent binding and activation of PI3K independently of Ras (Holgado-Madruga *et al.*, 1997). Additionally in some neuronal subpopulations it has been shown that phosphorylation of IRS1 (insulin receptor substrate) by Trk receptor activation is also involved in the recruitment and activation of PI3K (Yamada *et al.*, 1997). The generation of P3-phosphorylated phosphoinositide lipids by PI3K, together with PDKs (phosphoinositide-dependent protein kinases), recruit and activate the protein kinase Akt, leading to the phosphorylation of several substrates that are important regulators of cell survival. For instance the phosphorylation of BAD (Bcl-2/Bcl-x-associated death promoter) and the transcription factor FKHRL1 (Forkhead) induces their association with 14-3-3 proteins. Thus suppressing apoptosis via preventing the pro-apoptotic binding of BAD to Bcl-xL (Datta *et al.*, 1997), and inhibiting the transcription of apoptosis promoting genes such as Bim and FasL by FKHRL1 (Brunet *et al.*, 1999; Brunet *et al.*, 2001). Moreover the inhibition of GSK3-β

(glycogen synthase kinase 3-β) through Akt-mediated phosphorylation is another mechanism by which signalling through this pathway promotes cell survival, as elevated levels of GSK3-β have been shown to promote apoptosis in cultured neurons (Hetman *et al.*, 2000). Whilst similarly targets of Akt also include the S6 kinases and liberation of NF-κB, which can both regulate the transcription and translation of subsets of mRNAs that contribute to cell survival (Hamanoue *et al.*, 1999; Moritz *et al.*, 2010). Likewise another potential target of PI3K capable of promoting cell survival is the IAP (inhibitor of apoptosis) family of caspase inhibitors, with suppression of XIAP (X-linked inhibitor of apoptosis) levels decreasing NGF-induced survival in chick neurons (Wiese *et al.*, 1999). Finally aside from cell survival mechanisms recruitment by P3-phosphorylated phosphoinositides of signalling molecules to the plasma membrane, including regulators of the cdc42, Rac, and Rho family of G proteins that organise the F-actin cytoskeleton, thus implicating PI3K mediated signalling in the promotion of axonal growth and neuronal differentiation (Yuan *et al.*, 2003).

4.1.6.2 MAPK signalling pathway

The activation of Ras through the adaptor proteins Shc-Grb2 and SOS can also initiate Raf-MEK-Erk and p38MAPK signalling. Through the activation of Akt and Erk, Trk signalling can promote cell survival via a two-pronged mechanism, suppressing apoptotic proteins and activating anti-apoptotic proteins, with the activation of ERK increasing the activity or expression of Bcl-2 (Liu Y. Z. *et al.*, 1999). Alternatively the activation of Ras also promotes cell differentiation, with transient or prolonged activation of ERK determining the outcome of neurotrophin binding (Meakin *et al.*, 1999). Prolonged expression of ERK signalling induces transcription factors, and at least in PC12 cells has its own distinct pathway that requires the recruitment of Frs2 (fibroblast growth factor receptor substrate 2) to phospho-Y490. This adaptor protein provides binding sites for additional signalling proteins such as Grb2 and Crk, Src, SH-PTP2 (Src homology protein tyrosine phosphatase-2) and the cyclin-dependent kinase substrate $p13^{suc1}$. The association with Crk activates the Rap1 exchange factor C3G, triggering Rap1-Raf dependent ERK signalling (Reichardt, 2006). Alternatively Crk can be recruited to the Trk receptor by binding to ARMS (ankyrin repeat-rich membrane spanning adaptor) (Arevalo *et al.*, 2004). Meanwhile the association of SH-PTP2 with Frs2 facilitates activation of the MAPK pathway, particularly in response to BDNF

(Easton *et al.*, 2006). The Src family of kinases work synergistically with MAPK to promote differentiation (Huang E. J. and Reichardt, 2003).

It is thought that the activation of p38MAPK is initiated through the sequential activation of Ras-RalGDS-Ral and Src (Ouwens *et al.*, 2002). In turn p38MAPK activates MAP kinase-activated protein kinase-2 and ERK5. The activation of ERK5 may also occur due to Ras activation of Wnk1, MEKK2 and MEK5. The complexities of Trk signalling and the diversity in signalling outcomes further illustrated by the fact that these cascades can have overlapping as well as distinct targets such as differing transcription factor targets, for example ERK5 specifically activates MEF2 (myocyte enhancer factor-2) while ERK1/2 specifically activates Elk1 (Reichardt, 2006). In contrast overlapping targets of the MAPK signalling cascades include CREB (cAMP response element binding protein), which activates the transcription of genes that regulate the normal differentiation and survival of neurons (Riccio *et al.*, 1999).

4.1.6.3 PLC-γ signalling pathway

The phosphorylation of Y785 on TrkA, and corresponding tyrosines in TrkB and TrkC, recruits PLC-γ to the receptor where it is then activated by Trk kinase. This triggers a cascade of events involving hydrolysis of phosphatidylinositides to generate DAG and IP_3, and consequently leading to the release and increase of intracellular Ca^{2+}(calcium) levels. This flux of calcium activates enzymes such as Ca^{2+}-calmodulin regulated protein kinases and PKC (protein kinase C) isoforms (Huang E. J. and Reichardt, 2003). Targets include ion channels such as TRPC (transient receptor potential channel) (Li H. S. *et al.*, 1999) and the voltage-dependent sodium channel PN1 (Choi *et al.*, 2001).

4.1.6.4 Specificity in Trk signalling

The complexities of Trk signalling are further revealed in the specificity of Trk signalling, highlighting that not only can the cell type influence the response depending on which signalling adaptors are present, but also the type of neurotrophin and which receptor signalling is initiated from. The work of Minichello *et al.* with mutant Y490 TrkB mice showed a loss of NT-4/5 dependent but not of BDNF-dependent neurons, possibly due to the reduced ability of NT-4/5 to activate MAPK signalling, indicating that signalling by two different neurotrophins through the same receptor could have different consequences (Minichiello *et al.*, 1998). Furthermore

Atwal et al. showed in primary sympathetic neurons that in contrast to TrkA being dependent on PI3K for survival, TrkB uses both PI3K and MAPK, indicating that each receptor may have distinct signalling properties and preferential interactions with certain signalling substrates (Atwal *et al.*, 2000).

4.1.7 Regulation of neurotrophin responsiveness by Trk

There are many complexities to neurotrophin and Trk receptor interactions which make it an over simplification to suggest that endogenous expression of a specific Trk receptor confers responsiveness to a particular neurotrophin. As stated in section 4.1.5, alternative splicing generates Trk receptor isoforms with differing extra- and intracellular domains, including isoforms that lack the catalytic intracellular domain, which can influence a ligands interaction with the Trk receptors and subsequent signalling. For example, studies have shown the inclusion of a short amino acid sequence into the juxtamembrane regions of each of the Trk receptors (Clary and Reichardt, 1994; Shelton *et al.*, 1995; Strohmaier *et al.*, 1996). In TrkA the inclusion of the exon strengthens its affinity for NT-3, in addition to NGF (Clary and Reichardt, 1994), similarly the insertion allows for activation of TrkB by NT-3 and NT-4/5, in addition to BDNF (Boeshore *et al.*, 1999; Strohmaier *et al.*, 1996). Meanwhile amino acid inserts in the tyrosine kinase domain of TrkC modifies the receptors ability to activate particular downstream substrates (Guiton *et al.*, 1995). Additionally the co-expression of the pan-neurotrophin $p75^{NTR}$ receptor can modulate the function of the Trk receptors and regulate neurotrophin responsiveness in a number of ways (see Section 4.1.8), one of which is to refine the specificity of the Trk receptor for its cognate ligand (Benedetti *et al.*, 1993). Likewise the processing and secretion of neurotrophins from pro-neurotrophins (see section 4.1.3) dictates the availability and levels of each type of neurotrophin, thus influencing the cells environment and the type of response (Lu *et al.*, 2005).

Other major determinants of the responsiveness of Trk receptors to neurotrophins are the kinetics of Trk receptor trafficking and localisation, which can dictate the biological response of a cell by bringing the activated receptors into proximity with different cellular compartments, especially in neurons where the axon terminals can be far from the cell body, and by making the receptor available to adaptor and intermediate signalling proteins in specific membrane compartments. Saragovi *et al.* who showed

that rapid internalisation of TrkA, induced by an NGF-mAb complex in PC12 cells (a rat pheochromocytoma cell line), prevented NGF-dependent phosphorylation of the adaptor protein FRS2 and normal differentiation. This suggested that activated receptors require sufficient time on the cell surface to interact with FRS2, as it may not be immediately accessible due to it being myristoylated and located in lipid rafts (Saragovi *et al.*, 1998). Furthermore Zhang *et al.* showed that disruption of receptor internalisation, via a thermo-sensitive mutant of dynamin in PC12 cells, altered the biological response of the cells to NGF. Activated receptors embedded in the plasma membrane elicited a survival response via PI3K, but endocytosis of the neurotrophin-receptor complex was necessary for differentiation of the cells by preferential activation of MAPK (Zhang Y. *et al.*, 2000). Alongside this it was shown in neuronal cells that the endocytosis of TrkA receptors was specifically required for sustained ERK activation by NGF and that this internalisation was facilitated by PI3K (York *et al.*, 2000). Taken together it is evident that membrane sorting influences the ability of Trk receptors to activate specific signalling pathways.

4.1.7.1 Endocytosis and transport of Trk receptors

As demonstrated by the examples above, upon binding the neurotrophin-Trk receptor complex is internalised into endosomal compartments that provide a vehicle for retrograde transport and allowing propagation of the signal to the effector site. However it is thought that activated Trk receptors are regulated by the sorting of the complex into distinct endosome populations that can affect the outcome of intracellular signalling. An example of this was shown in sensory neurons where local application of NGF to distal axons or cell bodies activated both ERK1/2 and ERK5 locally. But when NGF was applied to distal axons ERK5 only was activated in the cell body (Watson *et al.*, 2001). Two mechanisms have been proposed for internalisation of the activated receptors, clathrin-mediated endocytosis and a Trk selective process of macropinocytosis mediated by Pincher, with these endosomes differing in their signalling potential (Valdez *et al.*, 2005; Valdez *et al.*, 2007). Both of these pathways converge on peripheral early endosomes, however whilst this can lead to recycling of the components or maturation to late endosomes and lysosomal degradation, pincher-associated endosomes appear to be preferentially recruited for retrograde signalling as they are not readily degraded by lysosomes and are associated with EKR5 (Valdez *et*

al., 2005).

4.1.7.2 Ubiquitylation of Trk receptors

The post-translational modification of ubiquitylation is a relatively recent area that is being explored as a mechanism for regulating Trk receptor internalisation, recycling and degradation (reviewed by (Sanchez-Sanchez and Arevalo, 2017)). Other tyrosine kinases such as EGFR are rapidly degraded upon ligand activation due to ubiquitination (Yokouchi *et al.*, 1999). Indeed TrkA has been found to be ubiquitinated by the E3 ubiquitin ligase TRAF6, influenced by interactions with $p75^{NTR}$ and p62 (Geetha *et al.*, 2008; Jadhav *et al.*, 2008). This promotes lysine (K) 63-linked polyubiquitination and consequently internalisation of the receptor and downstream signalling events (Geetha *et al.*, 2005). However others have suggested $p75^{NTR}$ to negatively regulate ubiquitination of Trks to delay internalisation and degradation (Makkerh *et al.*, 2005). Likewise Nedd4-2, a ligase that specifically ubiquitylates TrkA due to a PPXY motif not present in the other Trks, has been shown to regulate TrkA degradation by modulating receptor trafficking and sorting of the receptor to the degradative pathway (Arevalo and Wu, 2006; Yu T. *et al.*, 2014; Yu *et al.*, 2011). Others have found that the ubiquitin ligase Cbl also induces lysosomal degradation of TrkA (Takahashi Y. *et al.*, 2011), and that SOCS2 (suppressor of cytokine signalling 2) may mediate the ubiquitination of TrkA to regulate its signalling (Uren and Turnley, 2014).

To date little is known about the ubiquitination of TrkB and TrkC. Although TRAF6/p62 and Cbl have been implicated in the ubiquitination of TrkB (Jadhav *et al.*, 2008; Pandya *et al.*, 2014). Mutations of specific lysine residues on TrkB (Lys811) impaired ubiquitination and the ability of p62 to interact with the receptor, disrupting downstream signalling through the PI3K pathway (Jadhav *et al.*, 2008). Meanwhile ligases for TrkC remain at the prediction stages based on bioinformatic information, so further characterisation is needed for both of theses receptors. Interesting observations have been made though about the TrkB receptors dependency on ubiquitination in inducing different responses to the different ligands BDNF and NT-4. Activation by BDNF induces ubiquitination efficiently and causes downregulation of the receptor, while NT-4 causes slower ubiquitination and internalisation of the receptor leading to the receptor being kept active and sustaining downstream signalling, suggestive of a further possible mechanism for regulating the specificity of Trk

signalling (Proenca *et al.*, 2016).

The reversal of ubiquitination by deubiquitinase enzymes is required for TrkA recycling and degradation (Geetha and Wooten, 2008). Furthermore CYLD, which as mentioned previously in the introduction is a deubiquitinase responsible for the removal of K63-linked polyubiquitin chains, has been suggested as an enzyme that mediates the deubiquitination of Trks after Geetha *et al.* showed polyubiquitination of TrkA to be increased when CYLD is depleted and that p62 facilitates this interaction. Although no direct interaction was found between TrkA and CYLD (Geetha *et al.*, 2005). Taken together these studies highlight ubiquitination as an important regulatory modification and suggest possible mechanisms by which CYLD could be involved in Trk homeostasis.

Through extensive research efforts the complexity of Trk receptor mediated signalling has become evident. Distinct biological processing pathways, the availability of different neurotrophins in the local environment, cellular co-expression of Trk receptor splice variants and other associated receptors, trafficking and cellular localisation of the Trk receptors, and the recruitment and availability of adaptor and intermediate signalling molecules, are all factors that have to integrate to evoke a signalling response, which can be specific to a Trk receptor or cell type.

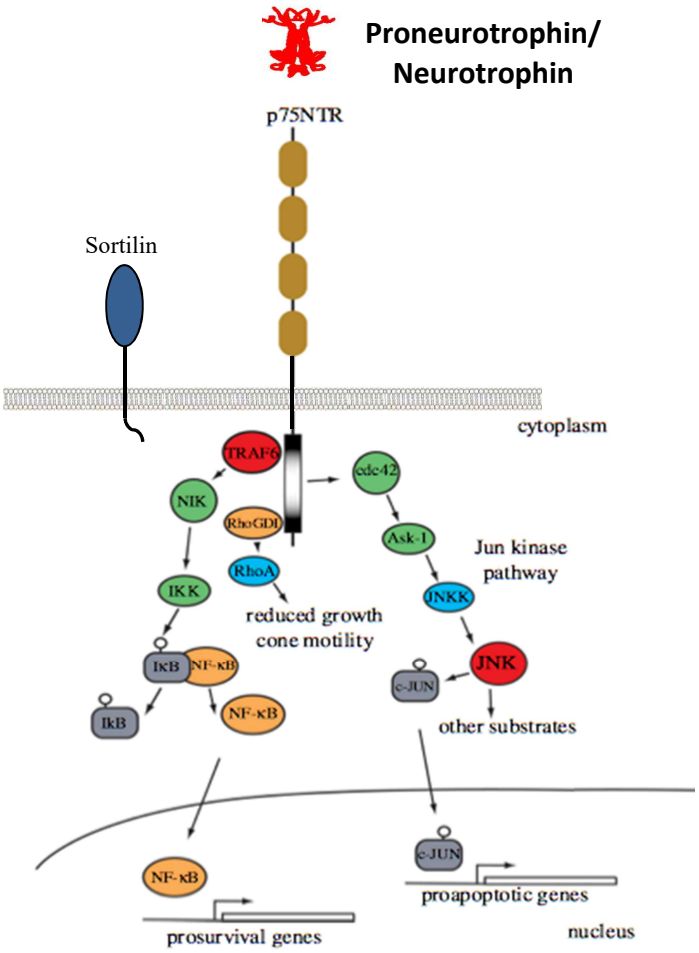

Figure 4-4: Neurotrophin-p75^{NTR} signalling pathways.

A simplified schematic overview depicting the main intracellular signalling pathways by which neurotrophins exert their cellular responses through p75^{NTR}: JNK and NF-κB. The p75^{NTR} receptor can be activated by either pro- or mature neurotrophins, however for proneurotrophin signalling activation requires the Sortilin receptor. The activation of signalling pathways by p75^{NTR} can initiate opposing cellular outcomes, with proneurotrophins usually activating an apoptotic response through the JNK pathway. Alternatively independently of neurotrophnis p75^{NTR} can also activate NF-κB signalling to promote cell survival. The p75^{NTR} receptor can also mediate Trk receptor specificity and facilitate Trk signalling. Figure adapted from (Reichardt, 2006).

4.1.8 The p75^{NTR} receptor

As mentioned previously, alongside Trk receptors neurotrophins also interact with the structurally unrelated p75^{NTR}. Initially thought of as just an accessory binding partner to modulate Trk receptor signalling (Chao and Hempstead, 1995), it subsequently became apparent that p75^{NTR} had a key role in sculpting the nervous system too. As both a Trk co-receptor and as an autonomous signalling unit, the receptor can mediate an array of cellular responses (Figure 4-4), from cell proliferation and survival, to myelination and ligand-dependent cell death (as reviewed by (Kraemer *et al.*, 2014; Lee F. S. *et al.*, 2001; Roux and Barker, 2002)).

In humans the receptor is encoded for by the *NGFR* gene, which contains six exons and spans 23kb of the chromosome region 17q12 -17q22, producing a 3.8kb mRNA with a single consensus polyadenylation signal included in the long (2000 nucleotides) 3'untranslated region (Huebner *et al.*, 1986; Johnson *et al.*, 1986). A Type 1 transmembrane protein, which is 427$\alpha\alpha$ (amino acid) in length (inclusive of it's 28 $\alpha\alpha$ signal peptide), p75^{NTR} has an extra cellular domain comprised of four repeated cysteine-rich motifs, with a single transmembrane domain which connects to a cytoplasmic region that includes a 'death' domain (Johnson *et al.*, 1986; Liepinsh *et al.*, 1997). A splice variant of the full-length form of p75^{NTR} that lacks exon III has been reported (von Schack *et al.*, 2001). Exon III is the coding region for the cysteine-rich domains 2, 3 and 4, which are required for neurotrophin binding. Therefore the receptor cannot bind neurotrophic factors but retention of the transmembrane and cytoplasmic domains means that it is still capable of interacting with Trk receptors (von Schack *et al.*, 2001). However the existence of s- p75^{NTR} remains controversial and its function is unknown (Kraemer *et al.*, 2014).

The p75^{NTR} receptor is capable of binding to each of the mature neurotrophins with similar affinity, however this is approximately 1000 fold lower than the receptors preferred pro-neurotrophin ligands (Reichardt, 2006). Crystallographic studies of the three-dimensional structure of NT-3, pro- and mature NGF each in complex with p75^{NTR} indicate that all four cysteine rich motifs are involved in binding neurotrophin dimers (Gong *et al.*, 2008; He and Garcia, 2004), and suggest that the binding stoichiometries of p75^{NTR} with the different pro and mature neurotrophins may

mediate distinct signalling activities due to conformational changes of p75, as pro-NGF dimers bind in a 2:2 complex whilst mature NGF- binds in a 2:1 complex with the receptor, through sets of contact residues that are conserved across the neurotrophin family (Feng *et al.*, 2010). Furthermore a disulphide link, which connects $p75^{NTR}$ monomers, in the transmembrane domain acts as a pivot point so that upon neurotrophin binding the intracellular domains can separate to facilitate the binding of signalling molecules (Vilar *et al.*, 2009).

The receptor is widely expressed during early development of the nervous system with a more restrictive expression pattern in adult cell populations, however $p75^{NTR}$ is re-expressed in response to neuronal injury (Ibanez and Simi, 2012). Many studies have highlighted the role of $p75^{NTR}$ in promoting programmed cell death in response to proneurotrophin binding in a number of different neuronal and non-neuronal cell types both *in vitro* and *in vivo;* such as oligodendrocytes (Casaccia-Bonnefil *et al.*, 1996), retinal neurons (Frade *et al.*, 1996), vascular smooth muscle cells (Wang S. *et al.*, 2000) and keratinocytes (Botchkarev *et al.*, 2006) The phenoptypes of $p75^{NTR\ -/-}$ mice (Lee K. F. *et al.*, 1992; von Schack *et al.*, 2001) showed an increase in the number of some neuronal populations (summarised by (Underwood and Coulson, 2008). This demonstrated that $p75^{NTR}$ is a key regulator of normal developmental neural apoptosis; providing a mechanism that promotes the elimination of neurons that aren't receiving sufficient neurotrophic support to refine target innervation (Kraemer *et al.*, 2014; Lee F. S. *et al.*, 2001; Nykjaer *et al.*, 2005).

In order for pro-neurotrophins to elicit an apoptotic response $p75^{NTR}$ is required to form a receptor complex with Sortilin, a Vps10p-domain containing receptor protein. The co-expression of these two receptors creates a high affinity receptor complex for pro-neurotrophins (Nykjaer *et al.*, 2004; Teng *et al.*, 2005), with pro-NGF interacting with Sortilin via its pro-domain and $p75^{NTR}$ by its mature domain (Nykjaer *et al.*, 2004). Furthermore the presence of Sortilin regulates the rate of $p75^{NTR}$ cleavage (Skeldal *et al.*, 2012). The cleavage of the intracellular domain (ICD) of $p75^{NTR}$ has been shown to potentiate cell death or survival in a cell-type specific manner in differing neuron types (Vicario *et al.*, 2015). The ectodomain is firstly liberated in an α-secretase TACE/ADAM17 (tumour necrosis factor-α converting enzyme/ a disintegrin and

metallopeptidase domain)-dependent, followed by γ-secretase mediated release of the ICD into the cytoplasm where it acts as a signalling entity (Kanning *et al.*, 2003; Weskamp *et al.*, 2004), and can interact with a number of cytoplasmic adaptor proteins such as TRAF6 (Khursigara *et al.*, 1999), NRIF (neurotrophin receptor interacting factor) (Kenchappa *et al.*, 2006), NRAGE (neurotrophin receptor p75 interacting MAGE (melanoma associated antigen) homologue) (Salehi *et al.*, 2000), RhoGDI (Rho GDP-dissociation inhibitor) (Yamashita and Tohyama, 2003) and NADE ($p75^{NTR}$-associated cell death executor) (Mukai *et al.*, 2000). These interactions then mediate mobilisation of the ICD to the nucleus, which depending on the cellular context can promote apoptosis or survival.

Neurotrophin binding to $p75^{NTR}$ results in the activation of different intracellular signalling pathways (Figure 4-4). Without an intracellular catalytic domain downstream signalling occurs through the interaction with cytoplasmic adaptor proteins, such as those mentioned previously, and frequently this induces an apoptotic response. A major pathway that is activated is the JNK (c-Jun N terminal kinase)-p53 signalling cascade leading to the up-regulation in transcription of genes for a number of pro-apoptotic proteins including Bax, Bim and Bad, accumulating in the release of cytochrome c and caspase-dependent apoptosis involving the mitochondria (Becker *et al.*, 2004; Bhakar *et al.*, 2003; Linggi *et al.*, 2005). TRAF6 has been shown to be an important adaptor protein in mediating $p75^{NTR}$ cell death (Khursigara *et al.*, 1999), with sympathetic neurons in *TRAF6* -/- mice failing to activate JNK in response to BDNF and thus do not undergo apoptosis (Yeiser *et al.*, 2004). Furthermore BDNF induced JNK activation was significantly attenuated in sympathetic neurons from *NRIF* -/- mice (Linggi *et al.*, 2005). Meanwhile the over expression of NRIF together with TRAF6 enhanced JNK activation (Gentry *et al.*, 2004), alongside TRAF6 mediated ubiquitination of NRIF having been shown to be required for its nuclear entry (Geetha *et al.*, 2005). Altogether the evidence suggesting that the interaction of NRIF and TRAF6 is essential for $p75^{NTR}$ mediated apoptosis. In addition $p75^{NTR}$ can stimulate ceramide production in certain circumstances to stimulate JNK activation (Brann *et al.*, 2002).

Conversely $p75^{NTR}$ is also capable of promoting cell survival, with indications of this role coming from the observation of a loss of sensory innervation of the limbs of $p75^{NTR\ -/-}$ mice (Lee K. F. *et al.*, 1992). The survival response is mediated by $p75^{NTR}$ in response to neurotrophins either via interacting with Trk receptors or activating NF-κB signalling independently of Trks, through the formation of TRAF6-IRAK-aPKC-p62 complexes (Hamanoue *et al.*, 1999; Khursigara *et al.*, 1999; Wooten *et al.*, 2001). The presence of the adaptor protein RIP2 (receptor-interacting protein 2) in Schwann cells was found to interact with the $p75^{NTR}$ ICD, and mediate NGF-dependent activation of NF-κB through TRAF6 and suppression of JNK activation; presenting a potential molecular switch to determine an apoptotic or survival outcome through TRAF6 signalling (Khursigara *et al.*, 2001).

Alternatively through cooperation with the Trk receptor family $p75^{NTR}$ can also regulate cell survival. A key mediator of regulating responsiveness to neurotrophins as mentioned previously in section 4.1.7, the influence of $p75^{NTR}$ on neurotrophin mediated cell survival is three fold. Firstly $p75^{NTR}$ expression can facilitate NGF binding to TrkA, co-expression of the two receptors creates a high-affinity receptor complex (Hempstead *et al.*, 1991) enhancing the nanomolar affinity of NGF for TrkA 100-fold (Esposito *et al.*, 2001). Secondly $p75^{NTR}$ expression refines the ligand specificity of Trk receptors to inhibit the activation of Trk receptors by non-preferred ligands, increasing the selectivity of TrkA for NGF over NT-3 (Benedetti *et al.*, 1993) and TrkB for BDNF over NT-3 and NT4/5 (Bibel *et al.*, 1999). Thirdly $p75^{NTR}$ expression can modulate the signalling pathways activated by Trks. Potential mechanisms include influencing the ubiquitylation and internalisation of Trk receptors, although reports are conflicting in how this positively affects Trk signalling (see section 4.1.7.2). In addition $p75^{NTR}$ was required for Akt activation and promotion of cell survival, as silencing of $p75^{NTR}$ in PC12 cells reduced neurotrophin-induced activation of Akt (Ceni *et al.*, 2010). In a reciprocal manner Trk activation was found to induce $p75^{NTR}$ cleavage, which was also required for activation of Akt (Ceni *et al.*, 2010; Kommaddi *et al.*, 2011). Furthermore to potentiate a survival response Trk activation also suppresses pro-apoptotic Jun kinase signalling mediated by $p75^{NTR}$, but does not affect the induction of survival promoting NF-κB signalling in the same way (Yoon *et al.*, 1998). Yet in conjunction with Sortilin, ProNGF binding to $p75^{NTR}$ upregulated PTEN (phosphatase and tensin homolog)

resulting in suppression of Akt signalling and apoptosis of basal forebrain neurons, even if TrkB was activated by BDNF suggesting that Akt activity is regulated by neurotrophin processing and co-receptor expression. Therefore Trk and $p75^{NTR}$ exist together in a paradoxical relationship, each capable of suppressing and enhancing the others actions.

Additional roles of the engagement of neurotrophins with $p75^{NTR}$ include regulation of RhoA signalling (Yamashita *et al.*, 1999), which can affect neurite outgrowth, and activation of acidic sphingomyelinase resulting in the generation of ceramide (Dobrowsky *et al.*, 1994), which can alter TrkA activity through phosphorylation of the receptor (MacPhee and Barker, 1999).

4.1.9 Neurotrophins and Trk receptors in the skin

The important role that neurotrophins and their receptors were found to play in the nervous system, regulating cell proliferation, apoptosis and differentiation have been replicated in non-neuronal tissues (Sariola, 2001). The ectodermal origin of both the nervous system and skin epithelium has prompted investigations into the possible role of neurotrophins in skin development and homeostasis, with differential expression patterns of the neurotrophins and their receptors found in distinct non-neuronal cell populations of the skin (Botchkarev *et al.*, 2006; Bothwell, 1997). Unsurprisingly neurotrophins have been found to influence innervation of the skin (Davis B. M. *et al.*, 1997; Harper and Davies, 1990), but have also been shown to have roles in hair follicle cycling and act as growth factors governing skin homeostasis (Botchkarev *et al.*, 2004). Further evidenced by neurotrophin expression in mice occurring early on in embryonic development at E9.5 and coinciding with the expression of the epidermal keratin markers K5 and K14 (Botchkarev *et al.*, 2006)

4.1.9.1 Keratinocytes

In human keratinocytes all four neurotrophin receptors, TrkA, TrkB and TrkC and $p75^{NTR}$ are expressed (Marconi *et al.*, 2003), alongside synthesis and secretion of their cognate ligands, NGF (Di Marco *et al.*, 1991), BDNF, NT-4/5 and NT-3 (Botchkarev *et al.*, 1999; Marconi *et al.*, 2003) (botchkarev, 1999, Marconi, 2003) respectively, although at low levels. Keratinocytes produce and secrete biologically active NGF at the highest levels compared to the other neurotrophic factors, with keratinocyte stem

cells expressing and secreting the most whilst in transit amplifying cells levels almost disappear (Marconi *et al.*, 2003). NGF is capable of inducing proliferation of human keratinocytes, supported by the establishment of an autocrine NGF loop, as NGF is released in increasing amounts by proliferating cells, whereas secretion ends in more differentiated keratinocytes (Di Marco *et al.*, 1991; Di Marco *et al.*, 1993; Pincelli *et al.*, 1994). Furthermore inhibition of TrkA phosphorylation with the natural alkaloid K252a, in the absence of exogenous NGF, led to a reduction in keratinocyte proliferation (Pincelli *et al.*, 1994).

Alongside this NT-3 also promotes keratinocyte proliferation, as shown by the inhibition of proliferation with increasing levels of anti-NT-3 neutralising antibody, in the absence of exogenous NT-3. Whilst NT-4/5 and BDNF appeared to have no effect on keratinocyte proliferation (Marconi *et al.*, 2003). Furthermore NT-3 and NGF up-regulate each other's secretion, although NGF does this to a greater extent (Marconi *et al.*, 2003). Expression of the cognate Trk A and TrkC receptors for NGF and NT-3 respectively, have been shown in keratinocytes and therefore mediate the proliferation response by the neurotrophins, particularly as overexpression of TrkA in keratinocytes was shown to increase their proliferative capacity compared to controls. However keratinocytes were found to express only the truncated TrkB isoform (TrkB.T1) (Marconi *et al.*, 2003), but as the function of this isoform isn't fully understood, the notion of NT4/5 or BDNF still being able to exert a response can't be totally disregarded.

In human keratinocytes neurotrophins have also been shown to influence the susceptibility of keratinocytes to apoptosis. *In vitro* NGF and TrkA expression is downregulated by ultraviolet-B (UVB) irradiation, whereas NGF over-expressing keratinocytes are protected from UVB-induced apoptosis via expression of anti-apoptotic Bcl-2 family members (Marconi *et al.*, 2003; Marconi *et al.*, 1999). Also UVB augments secretion of NT-3 and NT-4/5, suggesting that they may have a role in promoting apoptosis in certain circumstances, as they could interact with $p75^{NTR}$. Indeed $p75^{NTR}$ is almost exclusively expressed in transit-amplifying keratinocytes and treatment with either BDNF or NT-4/5 of normal keratinocyte cultures significantly induced apoptosis, with BDNF shown to induce proapoptotic JNK phosphorylation and reduce the DNA-binding activity of NF-κB (Truzzi *et al.*, 2011).

4.1.9.2 Fibroblasts

Fibroblasts are the main cellular component of the dermis, the layer of the skin that underlies the epidermis, and are important for wound healing and the production of ECM proteins such as collagens (Sorrell and Caplan, 2004). Similar to keratinocytes, fibroblasts express all neurotrophins and their corresponding receptors (Palazzo *et al.*, 2012). Neurotrophins were shown to have a number of effects on fibroblasts, supporting their survival through both Trk and $p75^{NTR}$ receptors, stimulating their migration, promoting their differentiation into myofibroblasts, and finally NGF and BDNF stimulated their contraction in a 3D collagen gel. The more differentiated myofibroblasts releasing higher amounts of neurotrophins, mostly NGF and NT-3, and expressing TrkB and $p75^{NTR}$ at higher levels (Palazzo *et al.*, 2012). These results together showing that a neutrophin network extends across the layers of the skin and at the level of the dermis is responsible for regulation of it biomechanical functions.

4.1.9.3 Melanocytes

Another cell population of the skin, melanocytes reside in the basal layer and hair follicles to produce pigmentation in the skin and hairs. Neurotrophins have been found to be important for melanocyte migration and viability (Pincelli and Yaar, 1997) and also for melanogenesis (Marconi *et al.*, 2006). Melanocytes express all neurotrophins at low levels and appear to release only NT-3 and NT-4/5 under physiological culture conditions, yet treatment with the differentiation inducer TPA increases expression of TrkA, TrkB and p75ntr but not TrkC, suggesting that melanocytes are stimulated by neurotrophins in a paracrine manner (Marconi *et al.*, 2006; Yaar *et al.*, 1994). In addition NGF expression is thought to be a protective mechanism for melanocytes to sun-exposure, as in response to UV irradiation NGF secretion increases and enhances cell survival through promoting Bcl-2 expression to prevent apoptosis (Stefanato *et al.*, 2003). In response to UVB irradiation NT-3 levels were also increased, suggesting that this factor too may support survival of the cells (Marconi *et al.*, 2006).

4.1.10 Neurotrophins and Trk receptors in the hair follicle

The hair follicle is considered a mini organ within the skin (see Introduction chapter) and neurotrophins have been found to be involved in the control of both hair follicle development and cycling (Botchkarev *et al.*, 2006). Indeed in transgenic mouse models overexpressing NGF, BDNF or NT-3, NGF and NT-3 were shown to increase hair follicle

morphogenesis, whilst the same effect was not seen in BDNF mice (Botchkarev *et al.*, 1998; Botchkareva *et al.*, 2000). In contrast accelerated hair morphogenesis was seen in $p75^{NTR}$ knockout mice, and results indicated an inhibitory role for $p75^{NTR}$ in hair follicle development mediated by an effect of $p75^{NTR}$ upon FGF7 (fibroblast growth factor) signalling (Botchkareva *et al.*, 1999). Furthermore there were restrictive expression patterns of the Trk receptors and their ligands to certain areas of the hair follicle during development, which during the final stages showed TrkA and NGF expression to be restricted to the ORS, TrkB and BDNF to the ORS and also the dermal papilla, and finally TrkC appearing in these regions also, but NT-3 only appearing at the late stages of development (Botchkarev *et al.*, 1998; Botchkareva *et al.*, 2000). Meanwhile there are fluctuations in neurotrophin levels throughout the hair cycle. NGF levels increase during the hair growth stage of anagen, whilst BDNF and NT-4/5 increase prior to the onset of the hair regression phase of catagen, during which NT-3 levels are also upregulated. Further evidenced in BDNF over-expressing mice, who displayed shortened hair lengths when compared to wild-type animals (Botchkarev *et al.*, 2004). In cultured late anagen, human scalp hair follicles, BDNF-TrkB signalling was found to inhibit hair shaft elongation and induce catagen through upregulation of TGFβ2 (Peters *et al.*, 2005), with BDNF secreted from both the dermal papilla and TrkB expressing keratinocytes in the inner and outer root sheaths. Together this data suggests mesenchymal-epithelial cross-talk occurs to promote catagen, with BDNF functioning as a terminal differentiation promoter in this skin compartment (Peters *et al.*, 2005), with further support from $p75^{NTR}$ expression (Peters *et al.*, 2006).

4.1.11 Neurotrophins and Trk receptors in *CYLD*-defective tumours

As the hair follicle is a primary source and target of functional neurotrophin signalling in the skin and this is the same compartment from which *CYLD*-defective tumours are thought to originate, it is intriguing that Rajan *et al.* using a gene expression microarray, found that Trk receptors and neurotrophin expression was altered in *CYLD*-defective tumours. TrkB and TrkC in particular were overexpressed as well as each of the neurotrophin ligands NT-3, NT-4/5, BDNF and NGF, whilst in contrast TrkA expression was down regulated (Rajan, Elliott*, et al.*, 2011). *In vitro* experiments on primary tumour cells showed that silencing of TrkB and TrkC reduced cell viability and 3D primary cell cultures were sensitive to pan-Trk inhibitor treatment, together

indicating that the tumours were dependent on Trk signalling for their survival (Rajan, Elliott*, et al.*, 2011).

Indeed CYLD was previously found to be involved in the deubiquitination of TrkA, which could consequently disrupt Trk homeostasis and internalisation (Geetha *et al.*, 2005), and with others having shown ubiquitination of TrkB by the same E3 ligases, TRAF6 and p62, as TrkA (Jadhav *et al.*, 2008), it is not inconceivable that CYLD may also be capable of deubiquitination of the TrkB receptor, in which case a loss of CYLD may disrupt Trk regulatory mechanisms and alter receptor homeostasis which may lead to tumourigenesis.

Furthermore previous work identified TrkB.T1 as the predominantly expressed TrkB isoform in cultured, normal human keratinocytes (Marconi *et al.*, 2003). Therefore an aim of this chapter was to determine if this was the case in *CYLD*-defective tumours, as it is only in the nervous system that this isoform has been more extensively explored. Evidence suggests that far from being solely a dominant negative inhibitor of TrkB.FL via sequestration of neurotrophic ligands and inhibition of Trk autophosphorylation (Eide *et al.*, 1996), it is an independent receptor, which even without a catalytic domain can induce intracellular signalling cascades (Fenner, 2012). For example in astrocytes TrkB.T1 has been shown to mediate calcium signalling, through BDNF stimulation of TrkB.T1 inducing activation of G-protein dependent PLC activation leading to calcium release and entry (Rose *et al.*, 2003). In glial cells TrkB.T1 was shown to be capable of mediating ligand dependent RhoGDI1 (Rho GDP dissociation inhibitor) signalling leading to inhibition of Rho GTPases and cytoskeletal rearrangement (Ohira *et al.*, 2005). In addition it can also affect cellular metabolism (Baxter *et al.*, 1997) and regulate TrkB.FL surface expression (Haapasalo *et al.*, 2002) and neuronal differentiation (Fenner, 2012; Yacoubian and Lo, 2000). Therefore as the truncated isoform has not been characterised in keratinocytes and TrkB expression is upregulated in *CYLD*-defective tumours, this warranted further investigation.

4.1.12 Neurotrophins and the TrkB receptor in cancer

The control of cell fate that Trk signalling can have, alongside the range of signalling networks that are responsive to Trk activation, are now recognised mechanisms that

can contribute to the pathogenesis of a variety of cancers. Indeed whilst neurotrophin-Trk signalling came to pre-eminence in the field of neurobiology, *NTRK* was initially identified as a proto-oncogene (Martin-Zanca *et al.*, 1986). The 5' region of *TPM3* (non-muscle tropomyosin) fused with a tyrosine kinase domain characteristic of a cell surface receptor, that was capable of transforming NIH3T3 cells (Martin-Zanca *et al.*, 1986; Martin-Zanca *et al.*, 1989). Mutations and genetic rearrangements of the Trk receptors, which create oncogenic fusion genes, can occur in multiple types of malignancies such as colon, lung and thyroid, although these tend to be sporadic incidences (Amatu *et al.*, 2016; Geiger *et al.*, 2011). In recent years pan-Trk inhibitors have been developed, prompted by the significance of the receptors role in carcinogenesis. Although in early phase clinical trials the inhibitors are showing promising anti-tumour effects (Lange and Lo*,* 2016).

The expression of TrkB is often associated with poor prognosis and increased metastatic potential in numerous cancers, including neuroblastoma (Nakagawara *et al.*, 1994), head and neck carcinoma (Kupferman *et al.*, 2010), lung (Sinkevicius *et al.*, 2014), breast (Vanhecke *et al.*, 2011), colon (Tanaka K. *et al.*, 2014) and pancreatic (Sclabas *et al.*, 2005). Furthermore in neuroblastoma expression of TrkA and TrkC is predictor of a good prognosis highlighting that the receptors can be differentially regulated in tumour cells and the activated transciptomes have different functional effects (Thiele *et al.*, 2009). Some of the tumour promoting functions that the BDNF-TrkB signalling axis has been found to be responsible for include increased resistance of neuroblastoma cells to cytotoxic drugs (Scala *et al.*, 1996) and survival under limited growth factor conditions (Kim C. J. *et al.*, 1999), in addition to induction of angigogenesis via increased VEGF (vascular endothelial growth factor) through TrkB induction of HIF-1α (Nakamura *et al.*, 2006). Similarly TrkB signalling was found to mediate the acquirement of metastatic ability in breast cancer, via c-Src dependent PI3K-Akt and IL6-JAK2-Stat3 activation. Signalling via these pathways led to upregulation of target genes such as Twist 1 and 2, which contributed to cancer stem cell renewal and epithelial-mesenchymal transition (EMT), traits of cells with metastatic potential (Kim M. S. *et al.*, 2015). Furthermore Yin *et al.* showed that a subpopulation of TrkB positive cancer stem cells in triple negative breast cancer (TNBC) were responsible for tumour recurrence. Differentiated TNBC cells upregulate

BDNF secretion during paclitaxel chemotherapy treatment, which acts in a paracrine manner to promote cell self renewal of the TrkB positive cancer stem cell subpopulation through induction of KL4 expression (Yin *et al.*, 2015). However the role that alternate TrkB isoforms may have has not been extensively studied in cancer cells. Yet a recent study showed that in breast tumours, autocrine BDNF and NT4/5 stimulation had an anti-apoptotic effect that was mediated by TrkB.T1 in cooperation with $p75^{NTR}$, contributing to tumour cell survival. Alongside this there was limited expression of TrkB.FL (Vanhecke *et al.*, 2011). Altogether these studies exemplifying the many ways in which TrkB expression has a pathological role in a multitude of cell contexts.

4.2 Chapter specific material and methods

4.2.1 Polymerase chain reaction (PCR) for TrkB (*NTRK2*) isoforms

The cDNA from tumour samples and the SHSY-5Y cell-line treated with retinoic acid were used for PCR for detection of *NTRK2* isoforms. Primers were designed around exons 15-18 for the full-length isoform (TRKB.FL) and 15-16 for the truncated isoform (TRKB.T1), and were based on sequences obtained from Ensembl (www.ensembl.org) (Table 4-1). Each of the *NTRK2* transcripts was amplified using MyTaq™ HS Mix polymerase (Bioline) in a total reaction volume of 25µl (reaction mix shown in Table 4-2). Primers and reactions were run in a thermal cycler following the conditions in Table 4-3. All reactions were repeated at least three times.

Primer	Forward/Reverse	Sequence	Amplicon Size
NTRK2 Exon 15	Forward	5'-TGGGATTTTGCCTTTTGGTA-3'	-
NTRK2.FL Exon 18	Reverse	5'-CTGGCTTGAGCTGACTGTTG-3'	300bp
NTRK2.T1 Exon 16	Reverse	5'-ATCAACCAACAAGCACCACA-3'	158bp

Table 4-1:Primers used for amplification of *NTRK2* isoforms

Reaction Components	Volume
2xMyTaq™ HS Mix	12.5µl
Primer F	1µl
Primer R	1µl
ddH_2O	5.5µl
Template (100ng) or from PCR1	5µl

Table 4-2: Reaction mixture composition for *NTRK2* isoforms

Step/Cycles	Temperature	Time
Polymerase activation	95°C	2 minutes
Denaturation	95°C	30 seconds
Annealing	60°C	30 seconds
Extension	72°C	30 seconds
(Repeat for x40 cycles)		
	4°C	Hold

Table 4-3: Thermocycler PCR program for *NTRK2* isoforms

4.2.2 Pathscan® antibody array

To give an overview of receptor tyrosine kinases that could be active in cell models of cylindroma, a PathScan® RTK Signalling Antibody Array (#7982, Cell Signaling Technologies, USA) was carried out according to the manufacturer's protocol. The kit incorporates glass slides with panels that have been spotted with antibodies, which allows for the simultaneous detection of 28 receptor tyrosine kinases and 11 signalling nodes when phosphorylated at specified residues (Table of Antibody layout in Appendix). The principle of the assay is the binding of added sample lysate to primary antibody on the slide, and detection via amplifying the binding signal with horseradish peroxidase, which is then detected via chemiluminescence and the signal captured onto film.

4.2.2.1 Preparing cell lysates

1X Cell Lysis Buffer- 1ml of 10X Cell Lysis Buffer diluted in 9mls dH_2O with PMSF (1mM final concentration)

Cells were grown until confluent in 25cm^2 flasks, media was removed and the cells were initially washed with 1ml of ice cold PBS (Invitrogen), before adding 600µl of ice cold 1X cell lysis buffer and incubating the flask on ice for 5 minutes. Cells were dislodged with a cell scraper and the lysed cells were transferred to a 1.5ml eppendorf tube on ice. The samples were centrifuged at 14000rpm for 10 minutes at 4°C to remove cell debris. The concentration of each sample was determined using the Qubit Protein Assay (see Section 2.4.3), and the samples diluted to 0.5mg/ml in Array Diluent Buffer.

4.2.2.2 Preparing tissue lysates

Frozen tissue from CYLD defective tumours and normal skin was cut using a cryostat and the curls collected into Precellys® 2ml bead tubes to which 100µl of cell lysis buffer was added. To lyse the tissue the samples underwent a 30 second shake cycle program at 6000 rpm in a Precellys Evolution machine. The samples were then centrifuged at 14000rpm and the supernatant transferred to a 1.5ml eppendorf. The concentration of each sample was determined using the Qubit Protein Assay (see Section 2.4.3), and the samples diluted to 0.5mg/ml in Array Diluent Buffer.

4.2.2.3 Antibody array

1X Array Wash Buffer- 1ml of 20X Array Wash Buffer diluted in 19mls dH_2O

1X Detection Antibody Cocktail- 150µl of 10X Detection Antibody Cocktail diluted in 1350µl Array Diluent Buffer

1X HRP-linked Streptavidin- 150µl of 10X HRP-linked Streptavidin diluted in 1350µl Array Diluent Buffer

The antibody array slide was fitted with an 8-well gasket and 150µl of Array Blocking Buffer was added to each well and left to incubate on a rocker at room temperature for 15 minutes. All further incubation and wash steps were also carried out at room temperature with agitation on a rocker. After removal of the Blocking Buffer, 150µl of the diluted cell lysates were added to each well and incubated for 2 hours. Subsequently each well was washed for 5 minutes in Array Wash Buffer and repeated three more times. The wells then had 150µl of Detection Antibody Cocktail added and left to incubate for 1 hour before the same washing procedure as before. Finally 150µl HRP-linked Streptavidin was added to each well and left to incubate for 30 minutes before the usual washing steps followed by a brief wash of the slide after removal of the well gasket. To visualize antibody binding via a chemiluminescent readout, LumiGlo and peroxide reagents were diluted and the slide submerged in the solution. The slide was transferred into a plastic protector and exposed to photographic film to develop an image.

4.2.2.4 Analysis of array

Array images were analysed using ImageJ software (v 1.48) and duplicate spot intensities for each antibody were quantified. Following correction for background, the pixel intensity for each antibody was plotted using GraphPad Prism software v6.0.

4.3 Results

4.3.1 Trk related genes distinguish the majority of CYLD-defective tumours from controls

Prior to this study a dataset was derived from microarray gene expression studies carried out by Dr. Neil Rajan, monitoring the gene expression of 24,526 transcripts in a pool of 32 CYLD defective tumours, including cylindromas, spiradenomas and trichoepitheliomas, and a pool of 10 perilesional skin controls (Rajan et al, Oncogene, 2011). Using this independent dataset the expression of *NTRK2* (TrkB) transcripts and associated receptors and cognate ligands were analysed. Differentially expressed genes in *CYLD*-defective tumours compared to controls were determined with a threshold for statistical significance of $p < 0.05$ after correction for multiple hypothesis testing. To visualise the expression of each of the genes (n=16) at an individual sample level, normalised signal values were plotted on a heat map, following logarithmic transformation (Figure 4-5). Clustering by Euclidean distance separated the majority of tumours from control skin with the exception of a trichoepithelioma (tumours 1) and two control samples (Control 3 and 7). Indeed in tumour samples the expression levels of *NTRK2* (Figure 4-5) transcripts were increased in the tumour samples as indicated by the red colour of the heat map. The same was also seen for certain transcripts of TrkB neurotrophic ligands BDNF and NT-4/5.

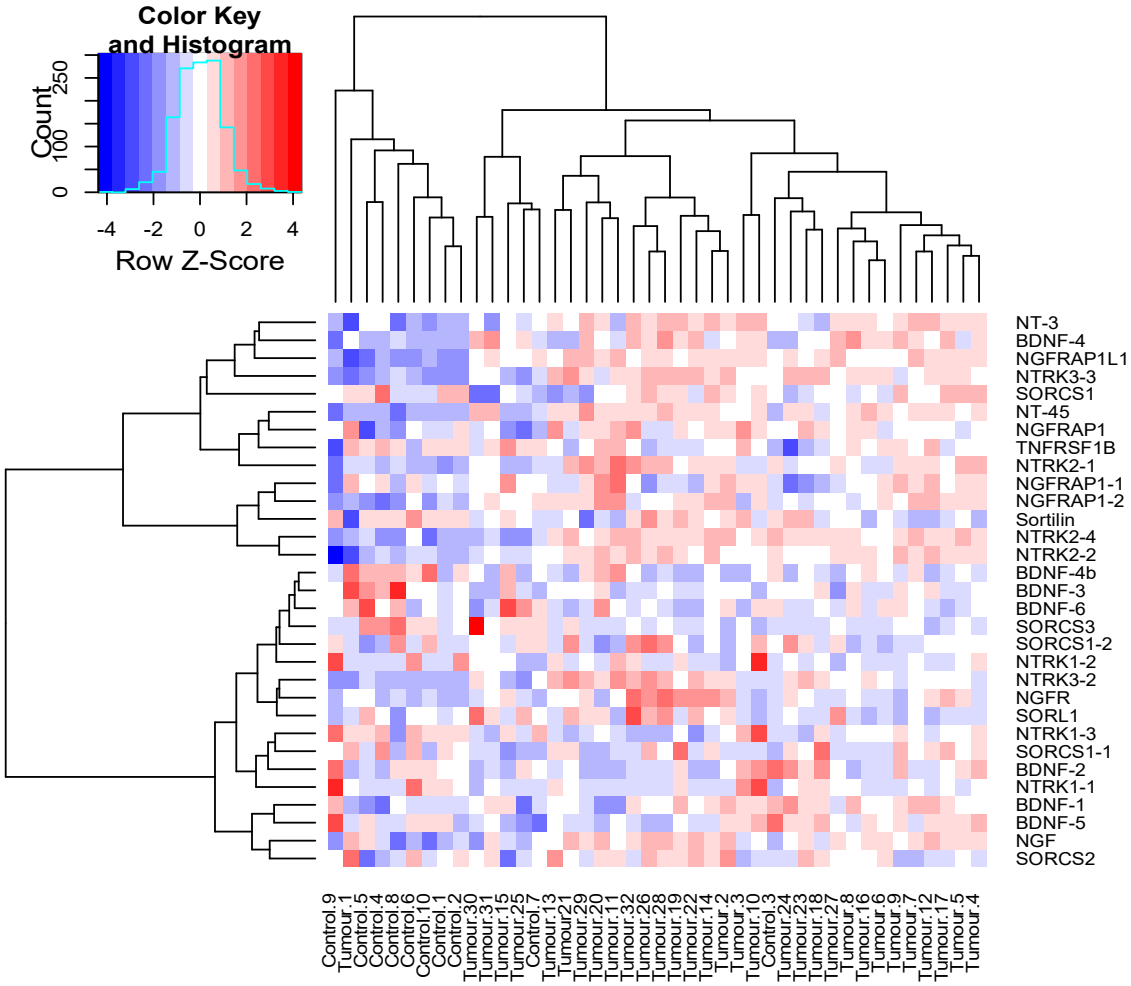

Figure 4-5: The expression of Trk related genes in *CYLD*-defective tumours and perilesional skin.

A heat map plot illustrating the expression levels of *NTRK2* and associated receptors and ligands in 32 *CYLD*-defective tumours and 10 controls (samples indicated at the bottom of the heat map). Differentially expressed genes were determined (p <0.05) between tumours and controls, and transcript expression levels at a single sample level are displayed on the heat map; red, over-expressed transcripts; blue, under-expressed transcripts; gene names indicated on the right-hand side of the figure; where data from multiple transcripts for a single gene were available are indicated with a numerical suffix (n = 7*).* Clustering by similarity is shown, determined by Euclidean distance. BDNF = brain derived neurotrophic factor, NGF = nerve growth factor, NT-3 & 45 = neurotrophins 3 and 4/5, NGFR = $p75^{NTR}$ receptor, NGFRAP1 = $p75^{NTR}$ associated protein 1 (Bex3), NGFRAP1L1 = $p75^{NTR}$ associated protein 1 like (Bex5), NTRK1, 2 & 3 = Trk receptors A, B and C, SORCS1, 2 & 3 = sortilin related Vps10 domain containing receptor 1,2 and 3, SORL- sortilin-related receptor, TNFRSF1B = tumour necrosis factor receptor superfamily member 1B.

4.3.2 TrkB.T1 is the predominantly expressed TrkB isoform in *CYLD*-defective tumours

Having previously found that TrkB is over-expressed in *CYLD*-defective tumours (Rajan, Elliott*, et al.*, 2011), and that TrkB.T1 is the predominant isoform expressed in keratinocytes (Marconi, 2003), alongside the differential expression of the different *NTRK2* transcripts shown in the previous data-set (Section 4.3.1), the splicing of *NTRK2* was investigated further to identify which of the full-length (FL) and truncated (T1) isoforms of TrkB were present in *CYLD*-defective tumours. RNA-seq analysis of a pool of 16 *CYLD*-defective tumours and 4 perilesional skin controls (from mutated *CYLD* carriers) was performed and the sorted reads visualized using the UCSC genome browser. Expression of the truncated *NTRK2* (TrkB.T1) isoform was increased in tumours compared to the controls (Figure 4-6), as indicated by the scale of the Y-axis and the difference in height of the read-depth peaks.

To validate the RNA-seq data, RT-PCR was carried out on cDNA generated from a panel of male and female cylindroma tumours. The neuroblastoma cell line SH-SY5Y (treated with 1μM retinoic acid - section 4.2.1) was used as a positive control, as this cell line has been shown to express both TrkB isoforms when treated (Kaplan et al., 1993). For the isoform *NTRK2.FL,* two products were detected in all samples that were of the expected sizes of 300bp and 252bp. A single product was detected in all samples for the isoform *NTRK2.T1,* which was of the expected size of 158bp (Figure 4-7). The two full-length products are due to splicing of exon 17, which is 48bp in length and corresponds with the size of the two PCR products seen.

Following this the levels of expression of each of the *NTRK2* isoforms in cylindromas were semi-quantitatively measured using qPCR. Two control groups were also included; normal control skin from patients with no *CYLD* mutation, and perilesional skin from a *CYLD*-defective patient taken from hair-bearing (HB) (scalp) and non-hair bearing (non-HB) sites. All tumours showed an increase in *NTRK2.FL* and *NTRK2.T1* expression when compared to normal skin (Figure 4-8).

The increase at transcript level translated to an increase in TrkB.T1 protein (90kDA) in *CYLD*-defective tumours compared to normal skin controls (Figure 4-9). The TrkB.FL protein (140kDA) was not detected in any of the samples, suggestive of *TrkB.FL* not

being translated into protein in either sample type despite the increases seen at the mRNA level in the tumours. The membranes were also probed for CYLD (108kDA), which showed a lack of full-length protein in the tumour samples.

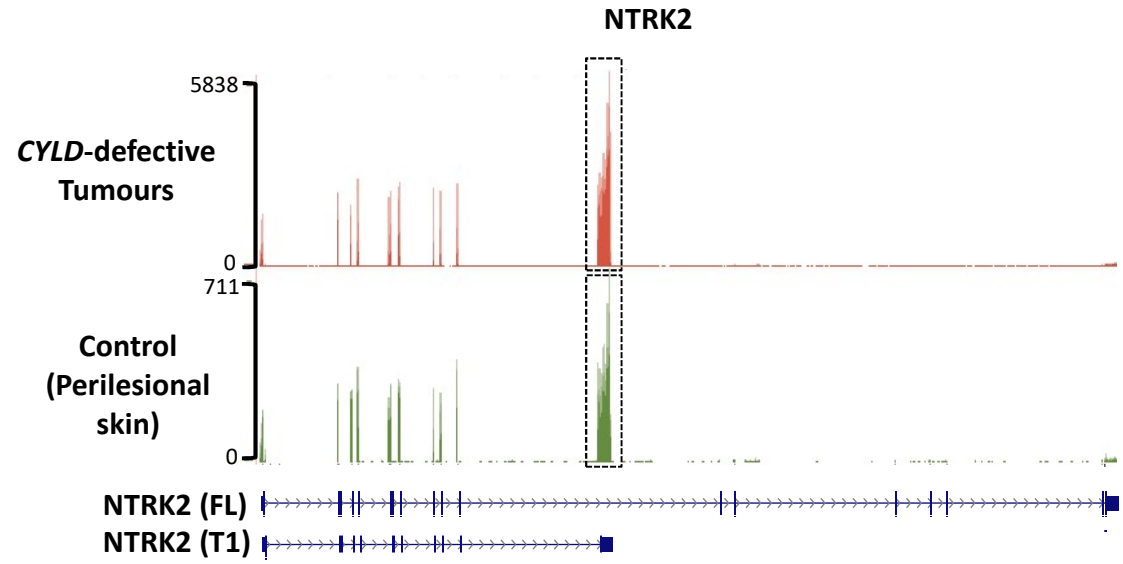

Figure 4-6: *NTRK2* transcripts in *CYLD*-defective tumours.
UCSC genome browser view of the *NTRK2* gene showing aligned RNA-seq reads from a panel of *CYLD*-defective tumours (red track) and perilesional skin controls (green track). The height of the peaks illustrating the number of reads which align to the exons of the NTRK2 gene, with a scale given on the Y-axis (note the scales are different on each axis to reflect the difference between *CYLD*-defective tumours and perilesional skin controls). The black dashed line rectangles highlight the increased inclusion of the alternate exon 16 in the samples, indicative of the TrkB.T1 isoform.

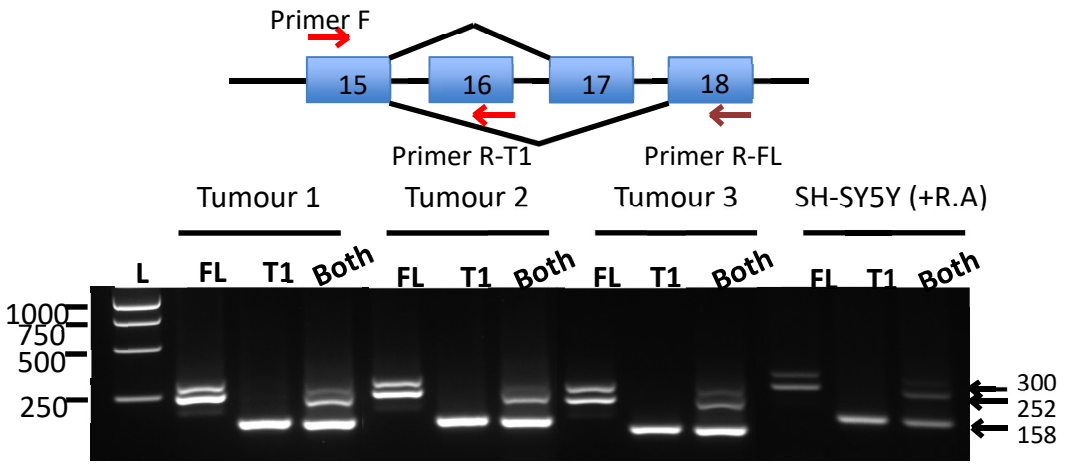

Figure 4-7: TrkB.FL and TrkB.T1 mRNA is expressed in *CYLD*-defective tumours.
PCR products were generated from cylindroma cDNA for each of the TrkB isoforms, with primer pairs designed around exons 15-18 for *TrkB.FL* and exons 15-16 for *TrkB.T1*, as exon 16 is exclusive to the *TrkB.T1* isoform. cDNA from SH-SY5Y cells treated with 1μM retinoic acid was used as a positive control. A representative agarose gel image is shown (*n*=6).

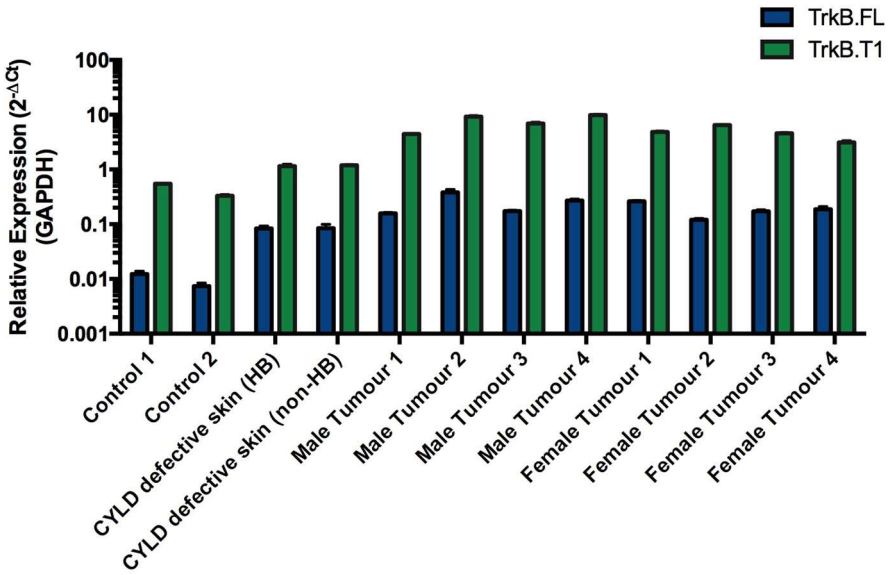

Figure 4-8: TrkB.FL and TrkB.T1 mRNA is over-expressed in *CYLD*-defective tumours compared to normal skin.
Primers were designed around exon regions exclusive to each of the TrkB isoforms (*TrkB.FL:* exons 23-24; *TrkB.T1:* exon 16) and their expression quantified by qPCR analysis in normal skin, perilesional *CYLD*-defective skin and *CYLD*-defective tumours, using the SYBR green method. mRNA expression for each isoform was normalised and expressed relative to the housekeeping gene GAPDH. Data are the mean and error bars represent the SEM of *n*=3 experiments.

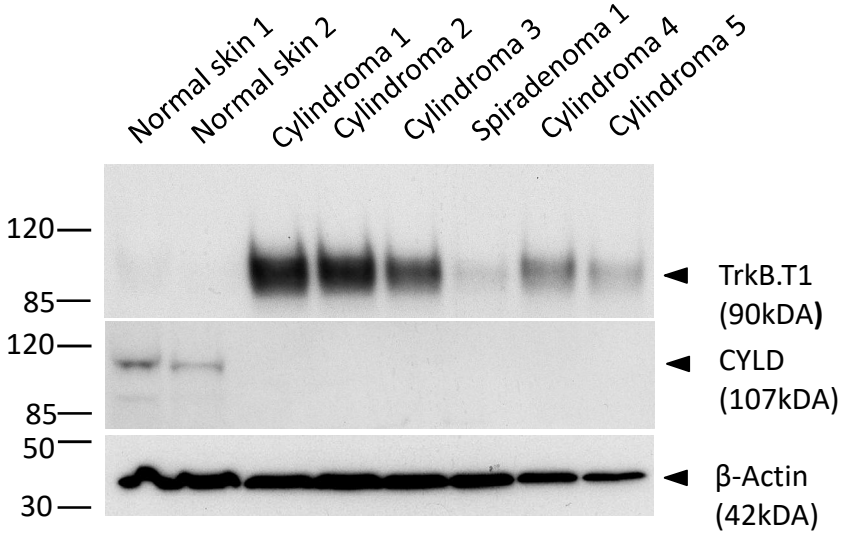

Figure 4-9: TrkB.T1 protein is increased in *CYLD*-defective tumours compared to normal skin.

Tissue lysates collected from *CYLD*-defective tumours and normal skin were subjected to immunoblotting with antibodies raised against TrkB and CYLD to determine the levels of protein expression, with β-actin used as a loading control. Western blot shown is representative of *n*=2 experimental repeats.

4.3.3 Exogenous overexpression of TrkB.T1 in the keratinocyte cell line, HaCaT, does not induce a proliferative advantage

Having shown that TrkB.T1 is the predominantly expressed isoform in *CYLD*-defective tumours, particularly in cylindromas, the isoform was explored further *in vitro* to characterise the role of TrkB.T1 in keratinocytes. The human keratinocyte cell line, HaCaT was transfected with the lentiviral vector p*LEX*-TrkB.T1 and empty p*LEX*-MCS expression vector as a control (Figure 4-10A). Unfortunately repeated attempts to transfect HaCaT cells with p*LEX*-TrkB.FL were unsuccessful, so comparative experiments between the isoforms in a more biologically relevant keratinocyte cell model were not possible in this project.

To see if TrkB.T1 conferred a growth advantage to the cells, a cell viability assay was performed 72 hours after plating into 96 well plates. The assay detected ATP levels to determine metabolically active or 'live' cells via a luminescent read out. Cell viability was increased in HaCaTs over expressing TrkB.T1 compared to empty vector control but did not reach a level of significance (Figure 4-10B). The TrkB.T1 ligand BDNF (100ng/ml) was added to the culture media for 72 hours before assaying as above, to assess if activation of the receptor by the ligand would influence cell survival or growth. The addition of BDNF consistently reduced cell viability in HEK293T cells over expressing TrkB.FL, nearly reaching significance (paired t-test; $p = 0.06$) (Figure 4-11A). However in both cell lines no such reduction was seen in cells over expressing TrkB.T1 (Figure 4-11A & B).

Colony forming assays were also carried out, in HaCaTs only, to see if TrkB.T1 over expression induced proliferation of the cells. Cells were seeded into a 6 well plate and left to grow for 8 days before being fixed and stained. Plates were scanned and particles analysed using ImageJ software. Cell over expressing TrkB.T1 did not show a significant difference in colony size or number compared to empty vector controls (Figure 4-12) This was further supported when the number of cells/colony, with a threshold of >10 cells/colony, were counted by eye on a microscope within a defined region of the same size in T75cm^2 cell culture flasks. This result showed that there was no difference in the average colony size between control and TrkB.T1 over expressing cells, with a similar total number of colonies counted for each sample within the

designated area which met the threshold; Empty vector: 103 TrkB.T1: 108. Taken together these results suggest that TrkB.T1 may confer a survival advantage but does not necessarily promote cell proliferation in keratinocytes.

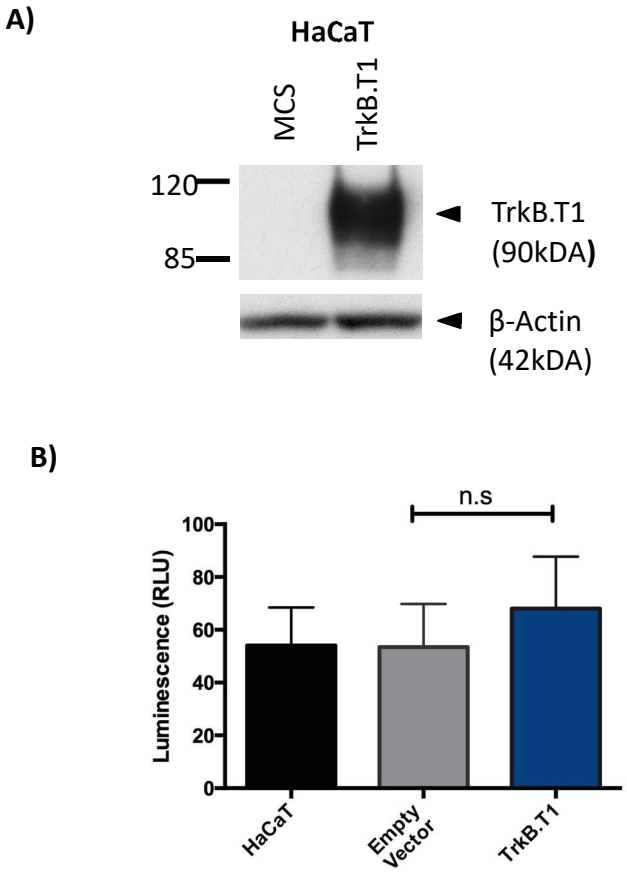

Figure 4-10: Over-expression of TrkB.T1 in HaCaT cells does not significantly increase cell viability.

A) HaCaT cells were transfected with *pLEX* TrkB.T1 vector to over-express TrkB.T1, or *pLEX* MCS vector (empty vector control), and successfully transfected cells selected for with puromycin. Protein lysates were collected and Western blotting carried out to ensure successful transfection. B) HaCaT cells transfected with either empty vector or p*LEX* TrkB.T1 vector were seeded in a 96 well plate at a density of 10000 cells/well and left for 72hours before being analysed. Non-transfected HaCaTs were used as a control. Data are the mean and error bars represent the SEM of *n*= 3 independent experiments. (Statistical analysis unpaired t-test).

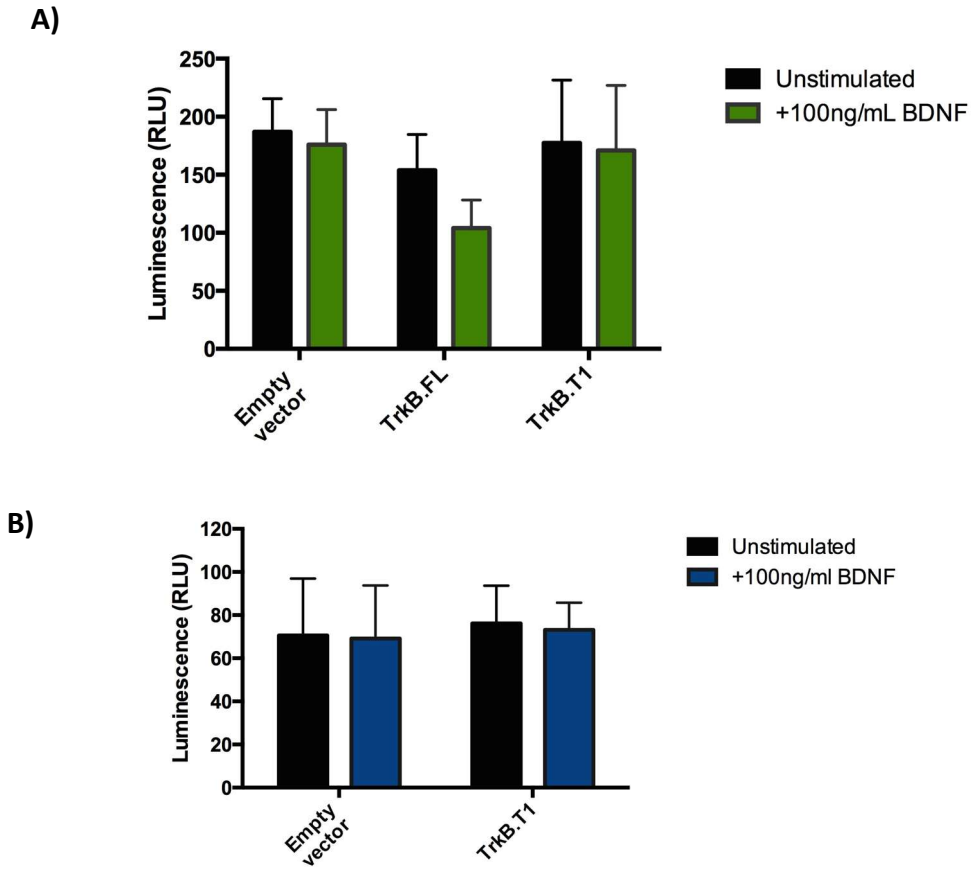

Figure 4-11: Exogenous BDNF stimulation does not increase cell viability in TrkB.T1 over-expressing cells.

A) HEK293T cells transfected with either empty vector, p*LEX* TrkB.FL or p*LEX* TrkB.T1 vector were seeded in a 96 well plate at a density of 10000 cells/well, treated with 100ng/ml BDNF and left for 72 hours before being analysed. B) HaCaT cells transfected with either empty vector or p*LEX* TrkB.T1 were treated the same as the cells in (A). In both figures data are the mean and error bars represent the SEM of *n*= 3 independent experiments.

A)

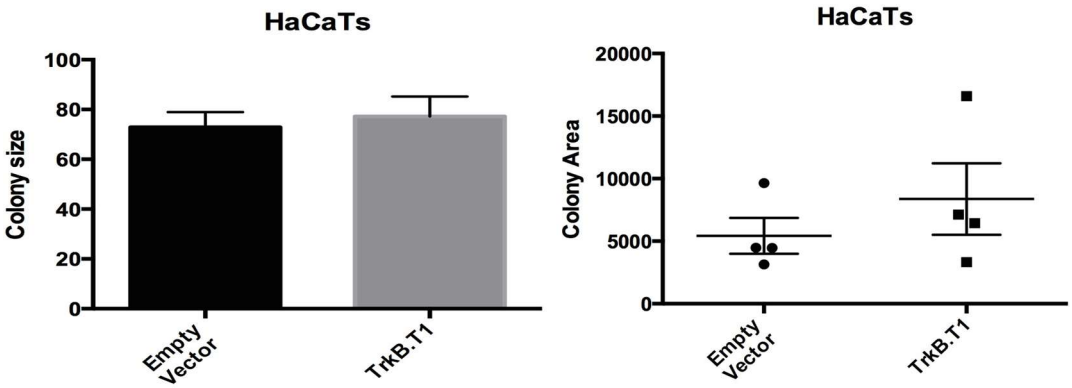

B)

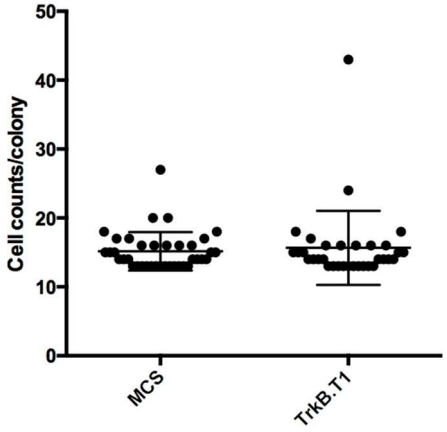

Figure 4-12: TrkB.T1 does not increase colony formation in TrkB.T1 over-expressing HaCaT cells.

A) Cells were plated at a density of 2000 cells/well in triplicate into 6 well plates and left to grow for 8 days before being fixed in 4% PFA and stained with Sulphorhodamine B. Plates were scanned and images were analysed using ImageJ software. The size of the colonies and the area of the plate that the colonies covered were measured. The experiment was repeated 4 times. Data are the mean and error bars represent the SEM of *n*=4. B) Colonies within a defined area of a75cm^2 flask were counted on a microscope with a threshold of >10 cells/colony and each colony size value plotted. The experiment was repeated on 3 flasks for each sample. Data are the mean and error bars represent SEM of colony size.

4.3.4 Identification of potential targets of TrkB isoform signalling using an antibody array

TrkB is a member of one of a variety of receptor tyrosine kinase families that are able to transduce signals through a variety of signalling pathways. To give an overview of the effect of TrkB overexpression on the phosphorylation of other tyrosine kinases and downstream signalling nodes and to identify which pathways could be activated, the Pathscan® RTK signalling antibody array was used (Section 4.2.2). The resulting film image was analysed using ImageJ to quantify signal intensity. The array was performed on a number of cell types, firstly HEK293T cells transfected with *pLEX-TrkB*.FL. p*LEX-TrkB*.T1 or empty vector as a control (Figure 4-13A). In cells overexpressing TrkB.T1 there were increases in the phosphorylation of *p*-Akt (Ser473) and *p*-Src (pan Tyrosine) compared to cells overexpressing TrkB.FL or empty vector (Figure 4-13 B, C & D). These are known downstream targets of neurotrophin-TrkB signalling that are involved in promoting cell survival and differentiation. The TrkB signal on the array acted as an internal control in these cells, however it was noted that there was only an intense signal from the TrkB.FL over-expressing cells and not TrkB.T1. It is assumed this is because TrkB.T1 does not contain the tyrosine kinase domain where phosphorylation occurs and therefore the antibody cannot recognise the phosphorylated residues and bind to create a signal. Secondly the array was performed using HEK293T cells transfected with *pLEX-CYLD* or a *CYLD* gene that harboured one of four different patient mutations, which encoded for truncated or catalytically inactive CYLD protein. This showed that over-expression of CYLD caused a reduction in Stat3 (Tyr705) phosphorylation (Figure 4-14). Lastly *CYLD*-defective tumour lysates were used on the array alongside normal skin controls. In the previously identified targets from the over-expression cell lines, *p*-Akt (Ser473), *p*-Src (pan Tyrosine) and *p*-Stat3 (Tyr705), phosphorylation of these targets was increased but there was variation in phosphorylation levels across the tumour samples, representing the heterogeneity of the samples. However one of the tumour samples (Tumour-5) consistently had lower readings compared to the other samples suggesting a loading or technical error (Figure 4-15).

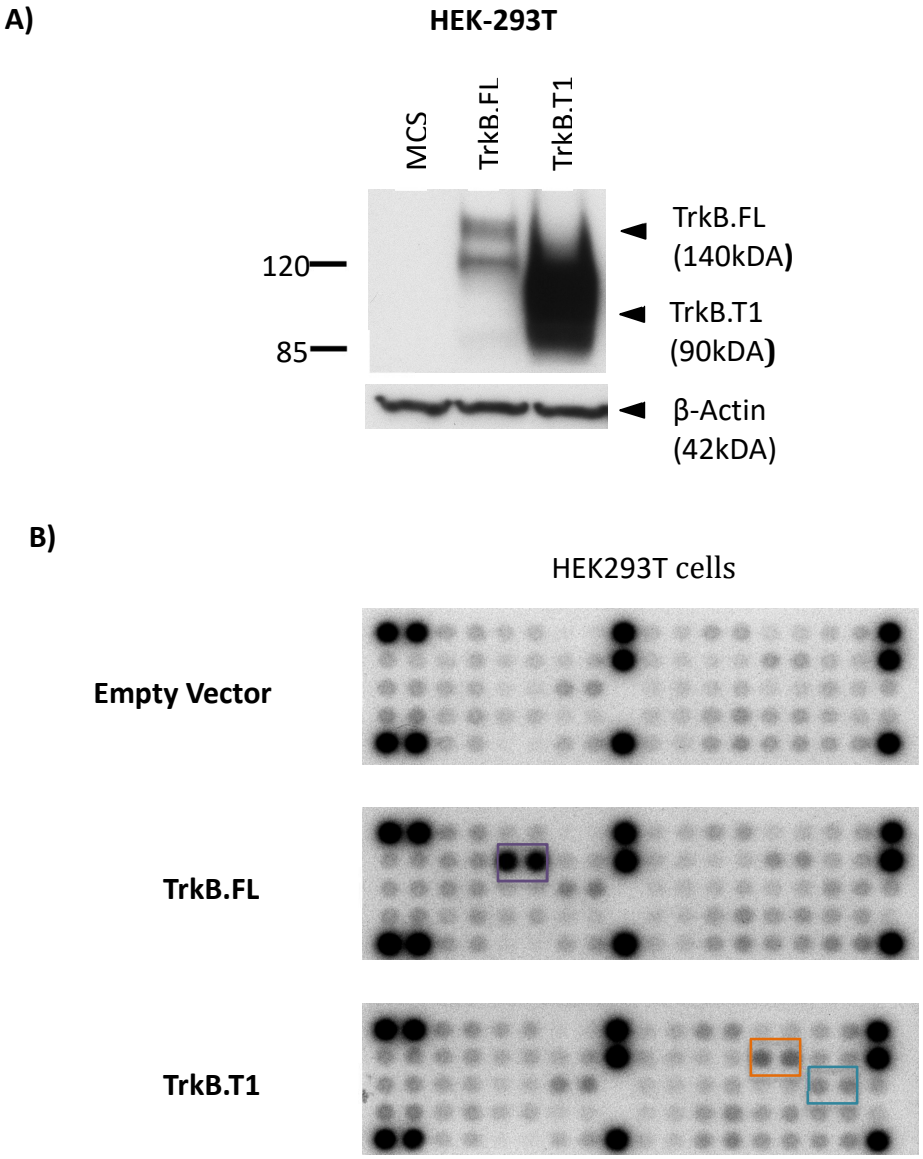

Figure 4-13: Identification of targetable kinases and their downstream targets in HEK293T cells over-expressing TrkB isoforms using an antibody array.

A) HEK293T cells were transfected either with empty, *pLEX* TrkB.FL or *pLEX* TrkB.T1 expression vectors and selected for with puromycin. Protein lysates were collected and Western blotting carried out to ensure successful transfection. β-Actin was used as a loading control B) Protein lysates were prepared and quantified with 0.5mg/ml of each sample was used for the array. Pathscan Array panel captured onto film to show the expression of the proteins. Antibody dots are paired; purple box = TrkB, orange box = *p*-Akt (Ser473), turquoise box = Src. C&D) Protein expression was quantified using densitometry (see next two pages). The experiment was only carried out once with each sample and the duplicate readings for each antibody were plotted. Data are the mean and error bars represent the SEM of *n*=2.

C)

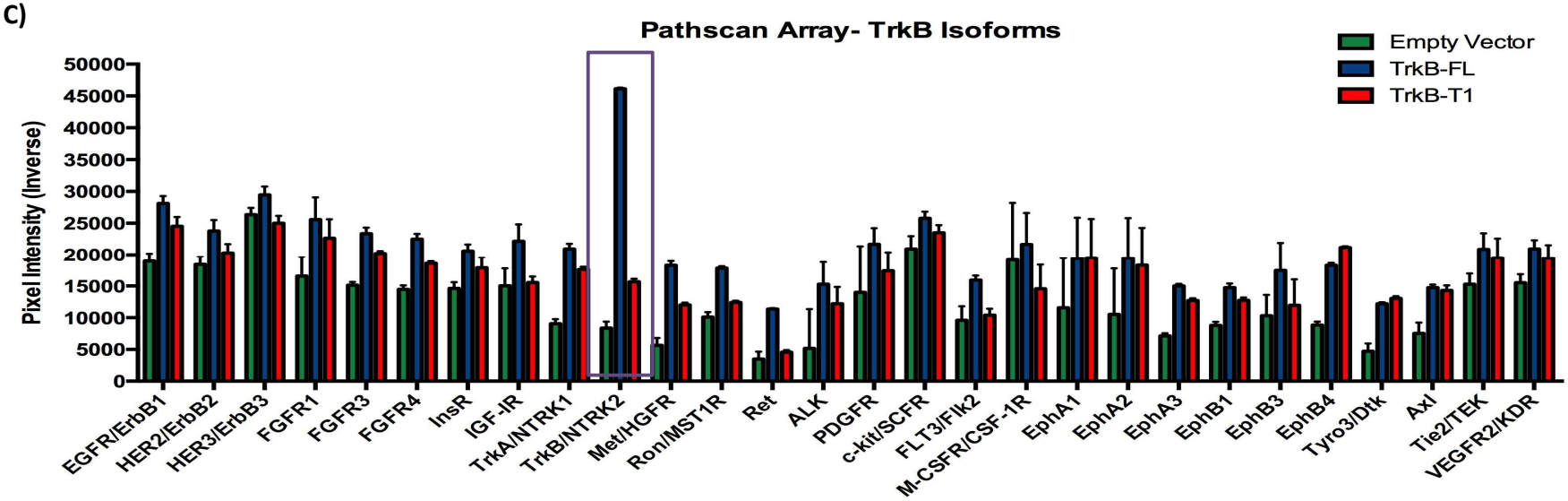
Pathscan Array- TrkB Isoforms
Empty Vector
TrkB-FL
TrkB-T1
Pixel Intensity (Inverse)
50000
45000
40000
35000
30000
25000
20000
15000
10000
5000
0
EGFR/ErbB1
HER2/ErbB2
HER3/ErbB3
FGFR1
FGFR3
FGFR4
InsR
IGF-IR
TrkA/NTRK1
TrkB/NTRK2
Met/HGFR
Ron/MST1R
Ret
ALK
PDGFR
c-kit/SCFR
FLT3/Flk2
M-CSFR/CSF-1R
EphA1
EphA2
EphA3
EphB1
EphB3
EphB4
Tyro3/Dtk
Axl
Tie2/TEK
VEGFR2/KDR

D)

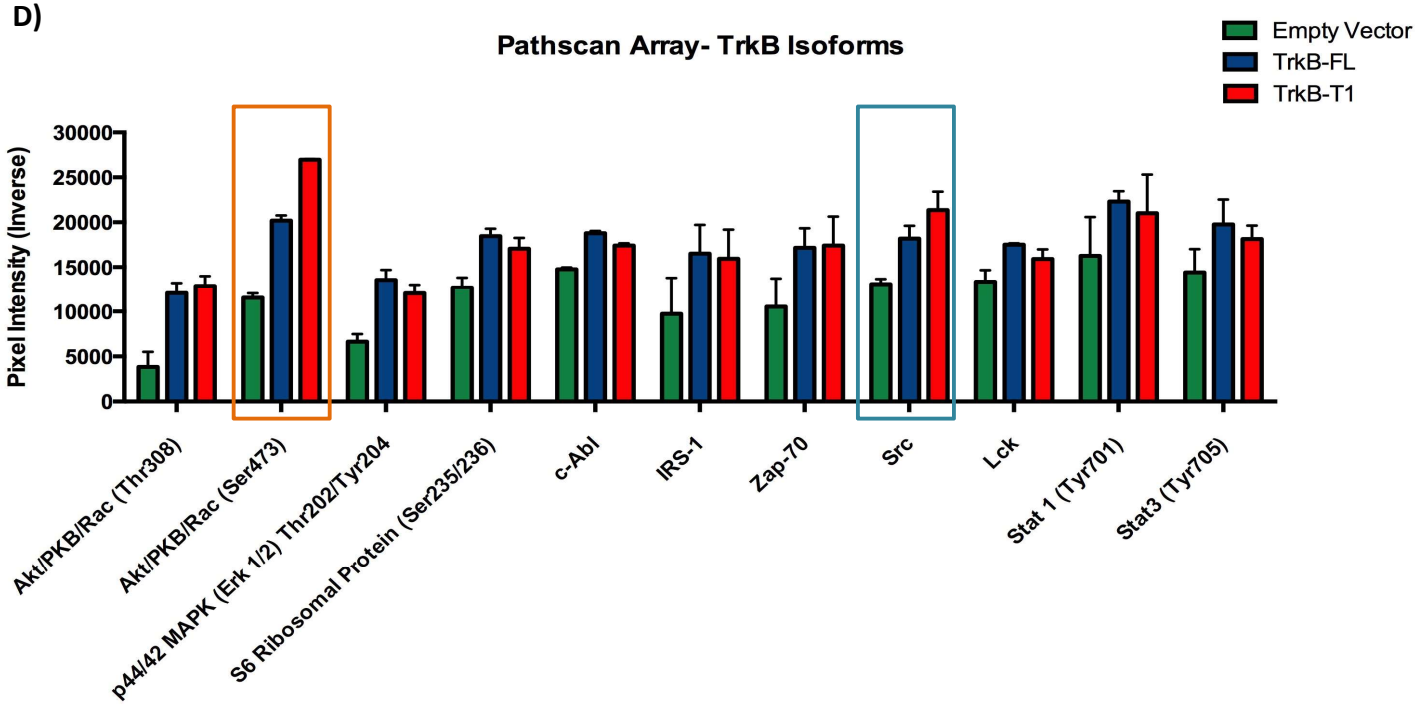
Pathscan Array- TrkB Isoforms
Empty Vector
TrkB-FL
TrkB-T1
Pixel Intensity (Inverse)
30000
25000
20000
15000
10000
5000
0
Akt/PKB/Rac (Thr308)
Akt/PKB/Rac (Ser473)
p44/42 MAPK (Erk 1/2) Thr202/Tyr204
S6 Ribosomal Protein (Ser235/236)
c-Abl
IRS-1
Zap-70
Src
Lck
Stat 1 (Tyr701)
Stat3 (Tyr705)

A)

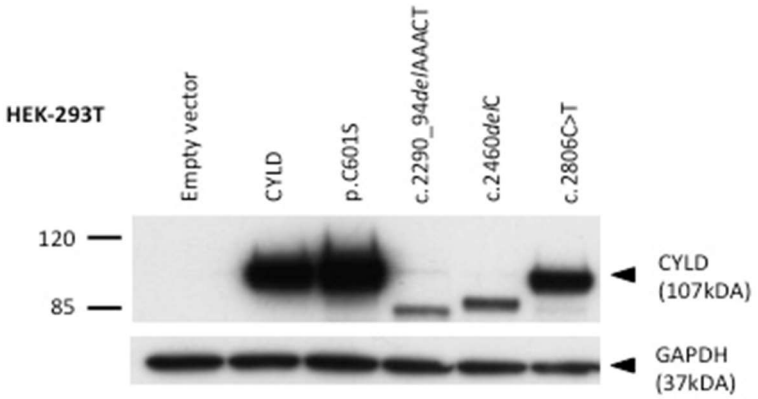

B)

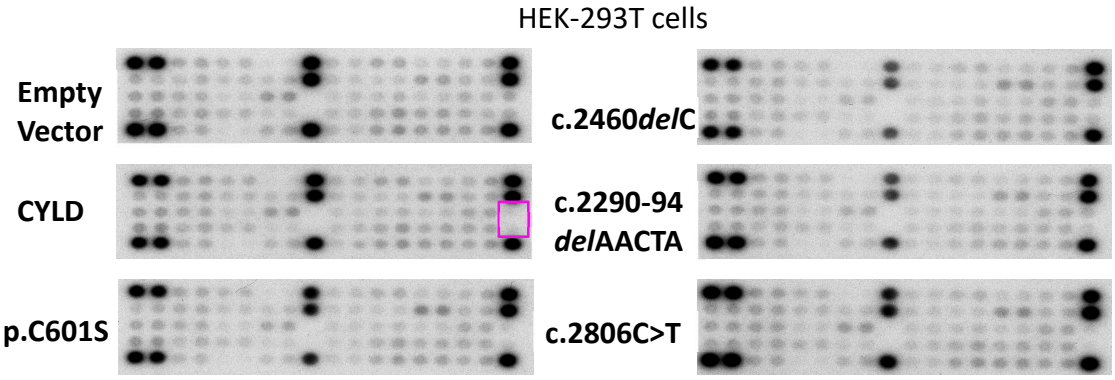

Figure 4-14: Identification of targetable kinases and their downstream targets in HEK293T cells over-expressing mutant *CYLD* using an antibody array.

A) HEK293T cells were transfected with empty vector or vectors with the specified CYLD mutations that are reflective of the mutations found in patients and selected for with puromycin. Protein lysates were collected and Western blotting carried out to ensure successful transfection. GAPDH was used as a loading control. B) Protein lysates were prepared and quantified with 0.5mg/ml of each sample was used for the array. Pathscan Array panel captured onto film to show the expression of the proteins. Antibody dots are paired; pink box = *p*-Stat3 (Tyr705). C) Protein expression was quantified using densitometry. The experiment was only carried out once with each sample and the duplicate readings for each antibody were plotted. Data are the mean and error bars represent the SEM of *n*=2.

C)

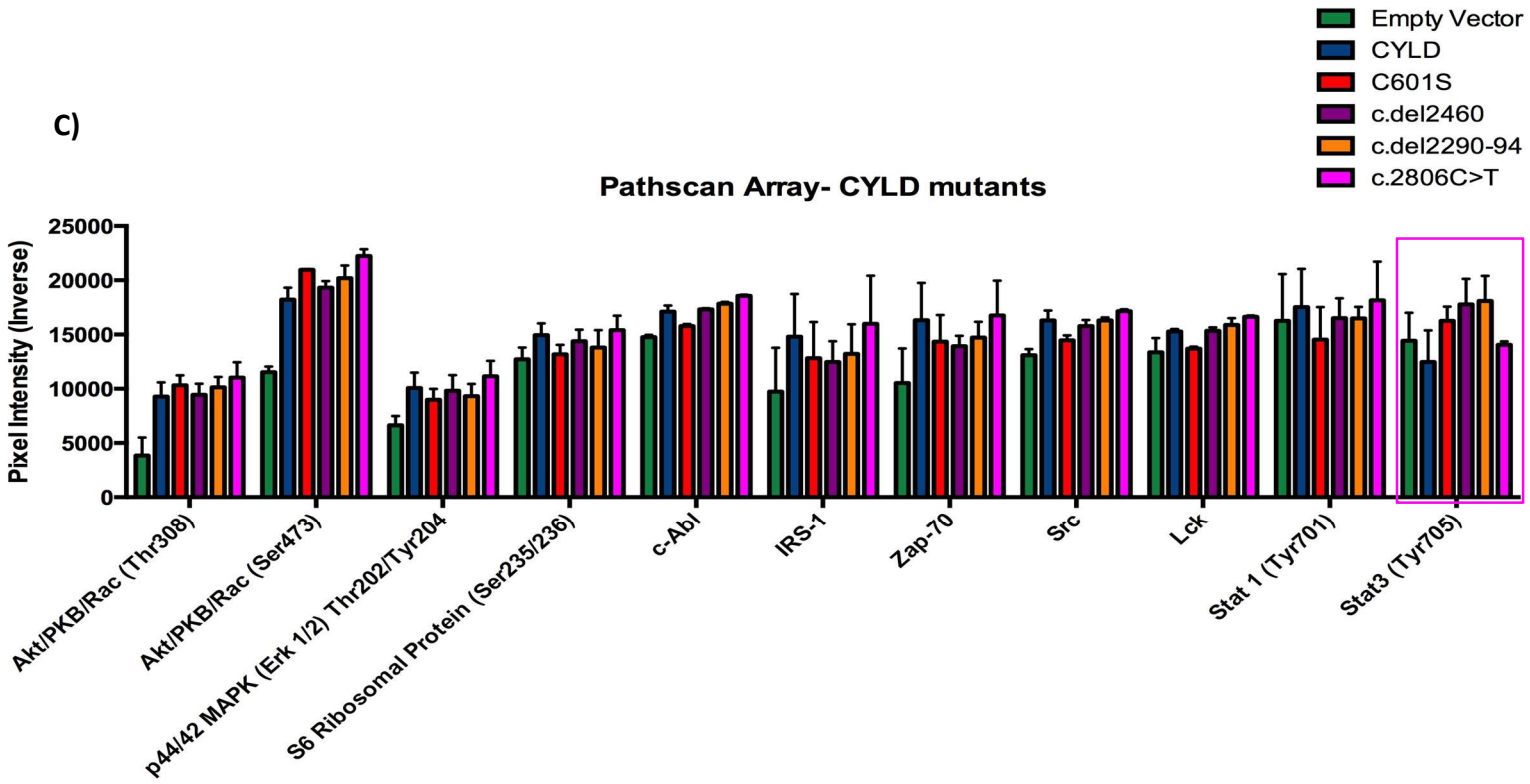
Empty Vector
CYLD
C601S
c.del2460
c.del2290-94
c.2806C>T
Pathscan Array- CYLD mutants
Pixel Intensity (Inverse)
25000
20000
15000
10000
5000
0
Akt/PKB/Rac (Thr308)
Akt/PKB/Rac (Ser473)
p44/42 MAPK (Erk 1/2) Thr202/Tyr204
S6 Ribosomal Protein (Ser235/236)
c-Abl
IRS-1
Zap-70
Src
Lck
Stat 1 (Tyr701)
Stat3 (Tyr705)

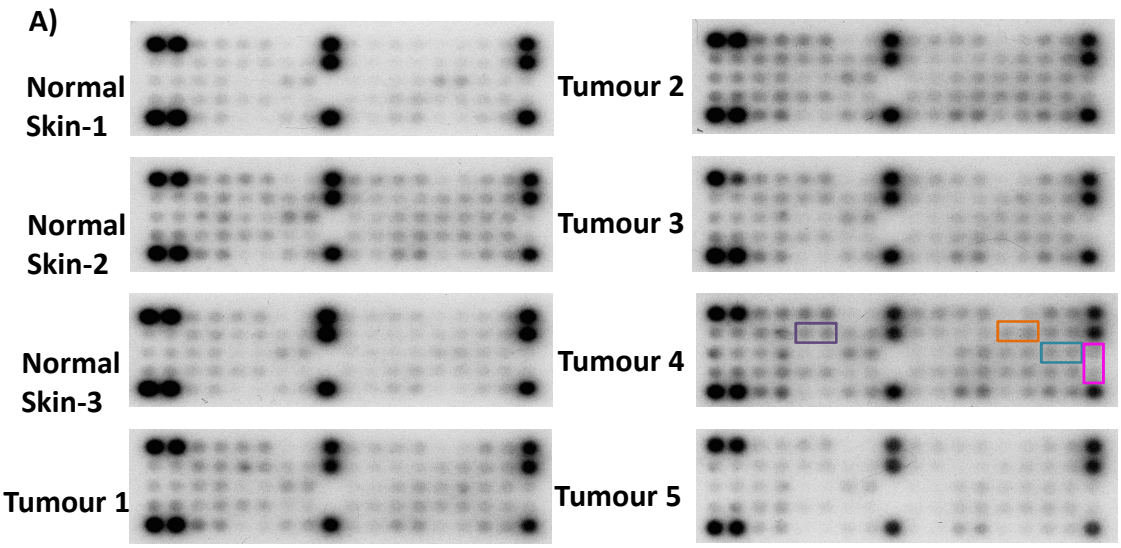

Figure 4-15: Identification of targetable kinases and their downstream targets in *CYLD*-defective tumours using an antibody array.

A) Protein lysates were collected from *CYLD*-defective tumours and normal skin samples as control. The amount of protein was quantified and 0.5mg/ml of each sample used in the array. The Pathscan Array panel was captured onto film to show the expression of the proteins. Antibody dots are paired; purple box = TrkB, orange box = *p*-Akt (Ser473), turquoise box = Src and pink box = *p*-Stat3 (Tyr705). B,C) Protein expression was quantified using densitometry. The experiment was only carried out once with each sample and the duplicate readings for each antibody were plotted. Data are the mean and error bars represent the SEM of *n*=2.

B)

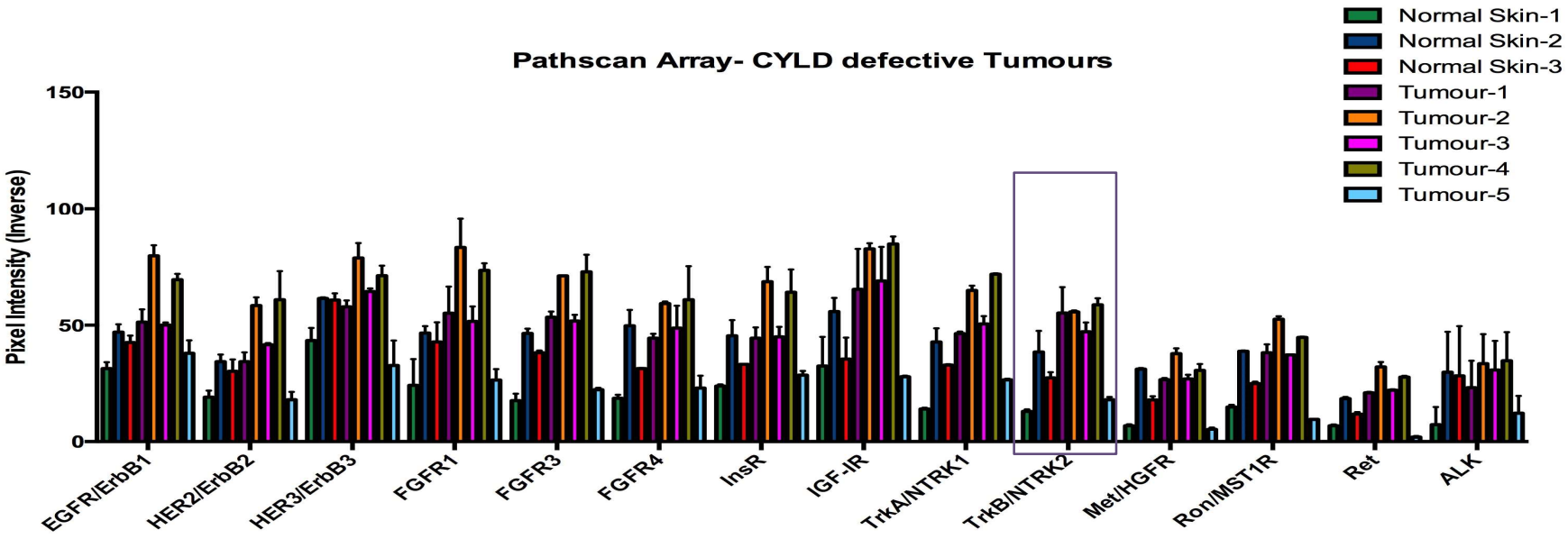
Pathscan Array- CYLD defective Tumours
Normal Skin-1
Normal Skin-2
Normal Skin-3
Tumour-1
Tumour-2
Tumour-3
Tumour-4
Tumour-5
Pixel Intensity (Inverse)
150
100
50
0
EGFR/ErbB1
HER2/ErbB2
HER3/ErbB3
FGFR1
FGFR3
FGFR4
InsR
IGF-IR
TrkA/NTRK1
TrkB/NTRK2
Met/HGFR
Ron/MST1R
Ret
ALK

C)

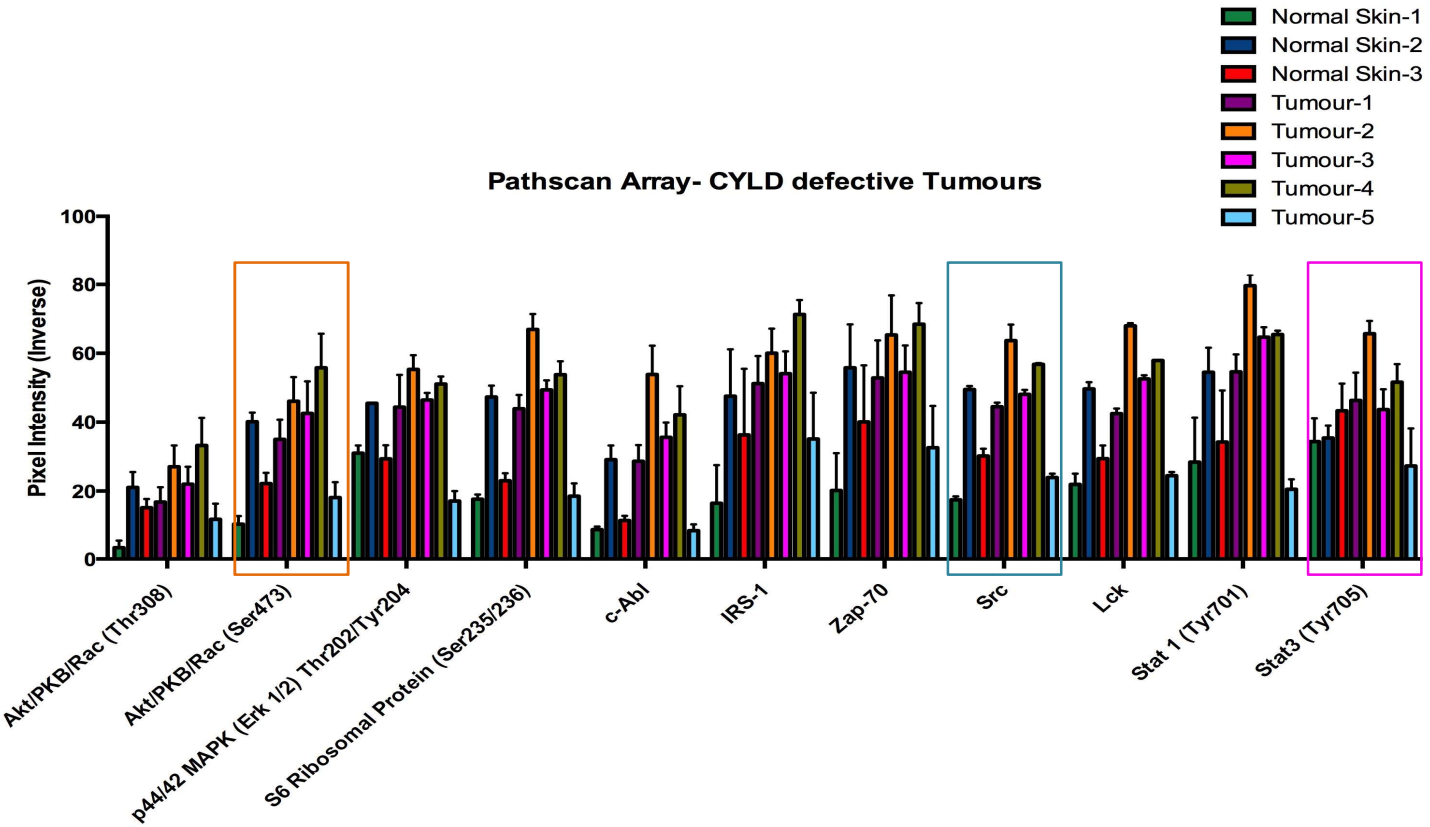
Pathscan Array- CYLD defective Tumours
Normal Skin-1
Normal Skin-2
Normal Skin-3
Tumour-1
Tumour-2
Tumour-3
Tumour-4
Tumour-5
Pixel Intensity (Inverse)
100
80
60
40
20
0
Akt/PKB/Rac (Thr308)
Akt/PKB/Rac (Ser473)
p44/42 MAPK (Erk 1/2) Thr202/Tyr204
S6 Ribosomal Protein (Ser235/236)
c-Abl
IRS-1
Zap-70
Src
Lck
Stat 1 (Tyr701)
Stat3 (Tyr705)

4.3.5 Validation of identified targets Akt, Src and Stat3 in TrkB.T1 over-expressing HaCaTs

From the findings of the Pathscan® RTK signalling antibody array, the identified targets Akt, Src and Stat3 were validated in BDNF (100ng/ml) stimulated TrkB.T1 over-expressing HaCaTs and compared to empty vector as a control. A time course indicated that phosphorylation of Akt (Ser 473) did not occur until after four hours of exposure to BDNF (Figure 4-16A) in TrkB.T1 over-expressing cells, indicating a delayed response in Akt phosphorylation. Whist no difference in Akt phosphorylation was observed between control and TrkB.T1 over-expressing cells, with both showing the same level of *p*-Akt (Ser473) expression, which did not change upon BDNF stimulation (Figure 4-16B). However the cells were only stimulated with BDNF for 15 minutes due to experimental constraints of using the lysates to look at different targets, therefore it may be that sustained stimulation of TrkB.T1 is required to initiate Akt signalling.

The experiment was repeated in 2D cylindroma primary cell cultures, comparing cells from three separate cylindromas. The result replicated what had been shown in the over-expressing cell line, with *p*-Akt (Ser 473) remaining unchanged in cells exposed to BDNF, and that Akt was already phosphorylated in untreated cells (Figure 4-16C). Similarly the levels of Src phosphorylation did not change when TrkB.T1 over-expressing cells were stimulated with BDNF or over a prolonged period as indicated (Figure 4-17A & B). With no apparent changes these targets were not explored further.

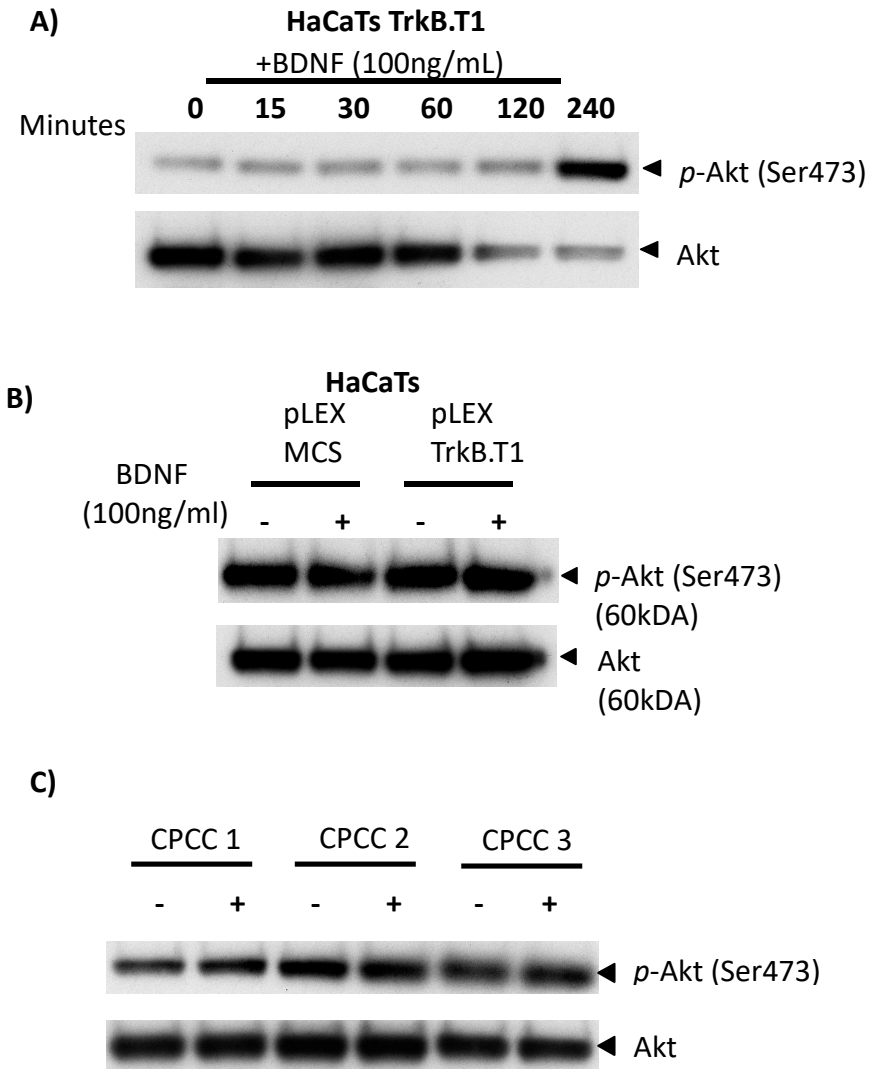

Figure 4-16: Phosphorylation of Akt (Ser473) remains unchanged following BDNF stimulation in HaCaTs over-expressing TrkB.T1 and 2D primary cylindroma cells.

A) HaCaT cells over-expressing TrkB.T1 were treated with BDNF (100ng/ml) for the time points stated. Lysates were collected for Western blot and membranes were probed with *p*-Akt (Ser 473), and Akt antibodies. Western blot shown is representative of *n*=1 experimental repeat B) HaCaT cells over-expressing TrkB.T1 and empty vector as a control were treated with BDNF (100ng/ml) for 15 minutes and lysates were probed with the same antibodies as (A). Western blot shown is representative of *n* = 3 experimental repeats. C) Primary cylindroma cells were treated with BDNF and membranes probed under the same experimental conditions. Western blot shown is representative of *n=1* experimental repeat.

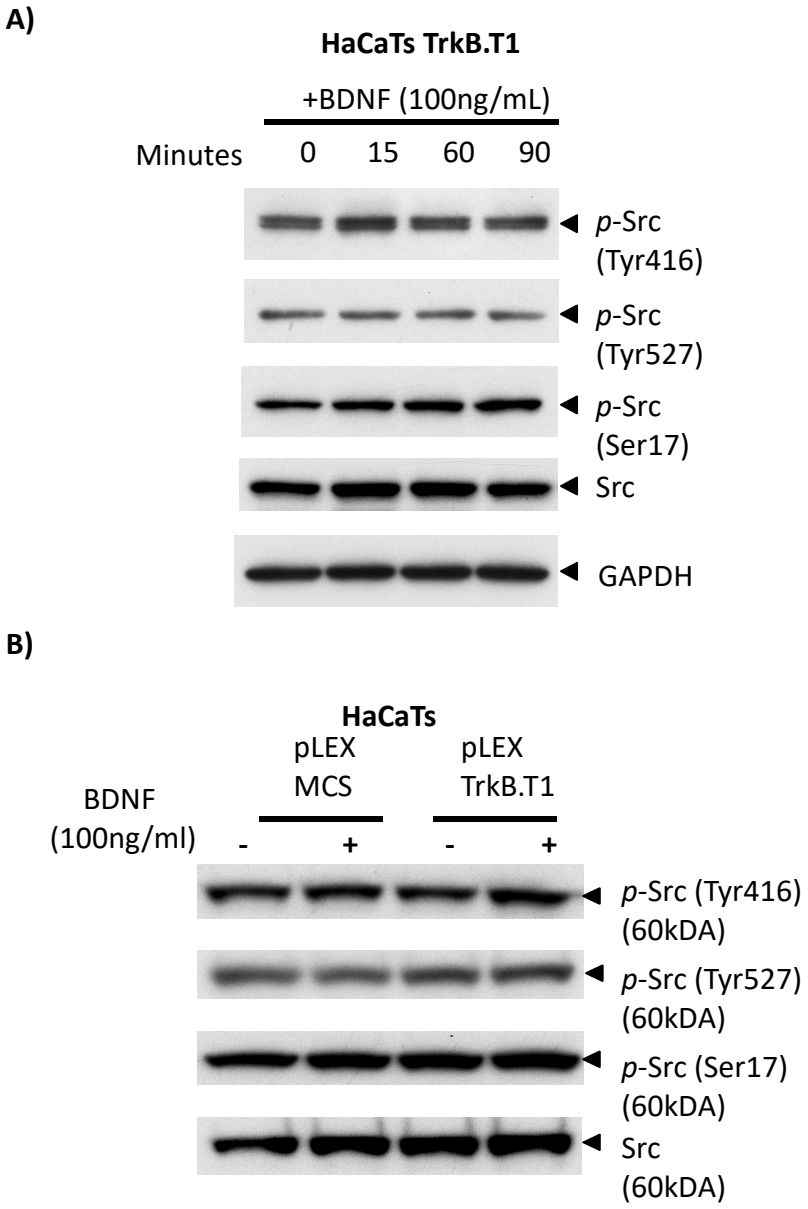

Figure 4-17: Phosphorylation of Src remains unchanged following BDNF stimulation in HaCaTs over-expressing TrkB.T1.

A) HaCaT cells over-expressing TrkB.T1 were treated with BDNF (100ng/ml) for the time points stated. Lysates were collected for Western blot and membranes were probed with *p*-Src (Tyr 416), *p*-Src (Tyr 527), *p*-Src (Ser 17), and Src antibodies. GAPDH was used as a loading control. Western blot shown is representative of *n*=3 experimental repeat B) HaCaT cells over-expressing TrkB.T1 and empty vector as a control were treated with BDNF (100ng/ml) for 15 minutes and lysates were probed with the same antibodies as (A). Western blot shown is representative of *n* = 1 experimental repeat.

4.3.6 Exogenous over-expression of TrkB.T1 leads to an increase in *p*-Stat3 (Tyr705) expression *in vitro*

From the Pathscan® RTK signalling antibody array it was interesting that in the presence of CYLD *p*-Stat3 (Tyr705) expression was reduced, and conversely in cells over-expressing mutant CYLD expression was increased. The increase in *p*-Stat3, particularly at the Tyrosine 705 residue, was a trend also observed in HEK293T cells over-expressing the two TrkB isoforms and in *CYLD*-defective tumour lysates. Furthermore Stat3 has been shown to be a downstream target of neurotrophin signalling (Ng *et al.*, 2006), and phosphorylation of Stat3 at Tyr 705 leads to homo-dimerisation and activation of Stat3 molecules, consequently *p*-Stat3 relocates to the nucleus and can initiate gene transcription. Therefore Stat3 was explored in HaCaTs over-expressing TrkB.T1. A time course of BDNF (100ng/ml) treatment of TrkB.T1 HaCaTs, to see the effect on Stat3 phosphorylation levels at the stated time points, showed that *p*-Stat3 (Tyr705) peaked at 15 minutes after which the levels dropped off, meanwhile *p*-Stat3 (Ser727) was increased between 5 and 15 minutes and this level was sustained for the following time points (Figure 4-18A). Compared to the empty vector control, cells over-expressing TrkB.T1 had a higher basal level of phosphorylated Stat3 at Tyr705, with exposure to BDNF (100ng/ml) causing a significant increase (p = 0.0169) in Stat3 phosphorylation that was not duplicated in BDNF treated empty vector control HaCaTs (Figure 4-18B & C). This increase was also observed in the primary cylindroma cells (Figure 4-19). The phosphorylation of Stat3 at Ser727 remained unchanged upon BDNF treatment in both empty vector and TrkB.T1 cells (Figure 4-18B). The expression levels are conflicting for untreated TrkB.T1 cells and the zero time point, however all cells were exposed to BDNF in the time course, with BDNF removed straight away at the zero time point. Meanwhile cells were not treated with BDNF in the comparative study therefore it may be that BDNF has an immediate biological effect on phosphorylation of Stat3 at this site.

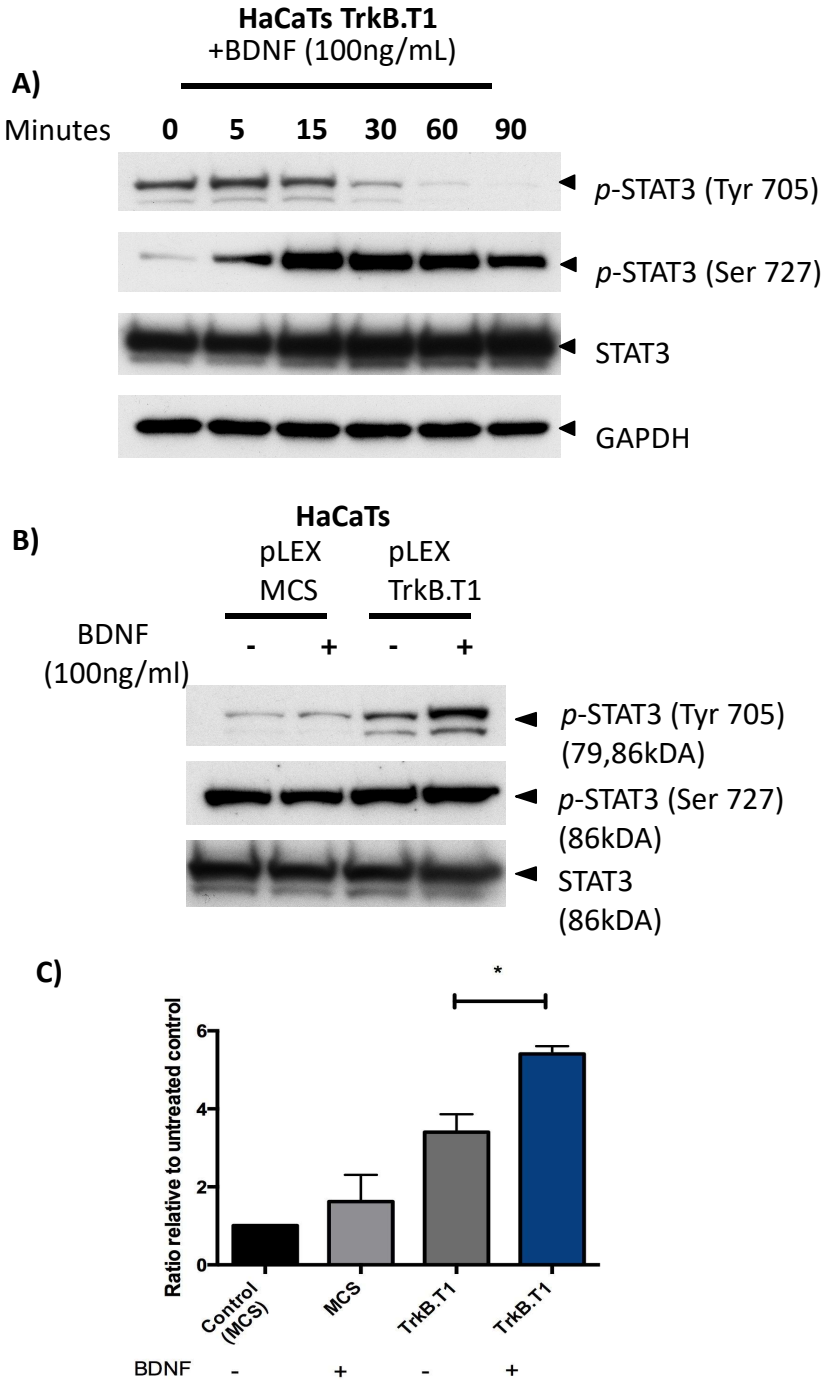

Figure 4-18: Phosphorylation of Stat3 (Tyr705) is increased following BDNF stimulation in HaCaTs over-expressing TrkB.T1.

A) HaCaT cells over-expressing TrkB.T1 were treated with BDNF (100ng/ml) for the time points stated. Lysates were collected for Western blot and membranes were probed with *p*-Stat3 (Tyr705), *p*-Stat3 (Ser727) and Stat3 antibodies. GAPDH was used as a loading control. Western blot shown is representative on *n*=3 experimental repeats. B) HaCaT cells over-expressing TrkB.T1 and empty vector as a control were treated with BDNF (100ng/ml) for 15 minutes. Lysates were collected for Western blot and membranes were probed with *p*-STAT3 (Tyr705), *p*-STAT3 (Ser727) and STAT3 antibodies. Western blot shown is representative on *n*=3 experimental repeats. C) Densitometry analysis of Western blots in (B). The samples were normalised to Stat3 and expressed relative to untreated empty vector control. Data are the mean and error bars represent the SEM of *n*=3 (* $p < 0.05$, paired t-test).

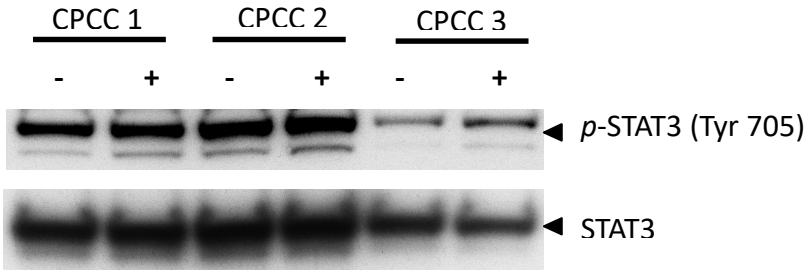

Figure 4-19: *p*-Stat3 (Tyr705) is increased following BDNF stimulation in 2D primary cylindroma cells.

Primary cylindroma cells were treated with BDNF (100ng/ml) for 15 minutes. Lysates were collected for Western blot and membranes were probed with *p*-STAT3 (Tyr705) and STAT3 antibodies. Western blot shown is representative of *n=1* experimental repeat.

4.3.7 Stat3 expression is increased in *CYLD*-defective tumours

Having found that *p*-Stat3 expression is increased upon BDNF stimulation of TrkB.T1 over-expressing cells, *p*-Stat3 expression was assessed in *CYLD*-defective tumours, as they also over-express TrkB.T1, by using immunohistochemistry. Tissue sections from 17 tumours including both cylindromas and spiradenomas, were probed with *p*-Stat3 (Tyr705) and total Stat3 antibodies, visualised with DAB and quantified (*p*-Stat3 samples only). Samples were considered *p*-Stat3 (Tyr705) positive if >15% of cells demonstrated *p*-Stat3 expression. In both cylindromas and spiradenomas *p*-Stat3 (Tyr705) expression was shown to have a nuclear localisation, which varied in intensity throughout the tissue sections, with some areas of the tumour showing no immunoreactivity. In control perilesional skin (CYLD +/-), some cells of the basal layer of the epidermis demonstrated nuclear *p*-Stat3 (Tyr705) and Stat3 expression (Figure 4-20 A & B). In both tumour types there was a scattered pattern of *p*-Stat3 (Tyr705) expression, however in the cylindroma cells expression was more restricted to the basal cells of the tumour cell islands (Figure 4-20C and black arrow in inset), in contrast to the immuno-positive cells that were seen throughout the spiradenoma (Figure 4-20E). In comparison Stat3 expression had cytoplasmic and nuclear localisation in both tumour types (Figure 4-20D & F), and did not show the same restrictive expression pattern as was seen in the cylindroma for the phosphorylated form. Semi-quantitative analysis of the immunostaining intensity using ImageJ software showed that out of the 17 tumours analysed, 11 tumours (65%) were considered *p*-Stat3 (Tyr705)-positive (Figure 4-21A). Furthermore there was a significant increase in *p*-Stat3 (Tyr705) expression in the *CYLD*-defective tumours when compared to adjacent normal epidermis (CYLD +/-) ($p = 0.0017$) (Figure 4-21B). Within the different structures of the skin, the eccrine glands showed a scattered pattern of *p*-Stat3 expression and the inner layers of the hair follicle were positive for *p*-Stat3 (Figure 4-20G-J).

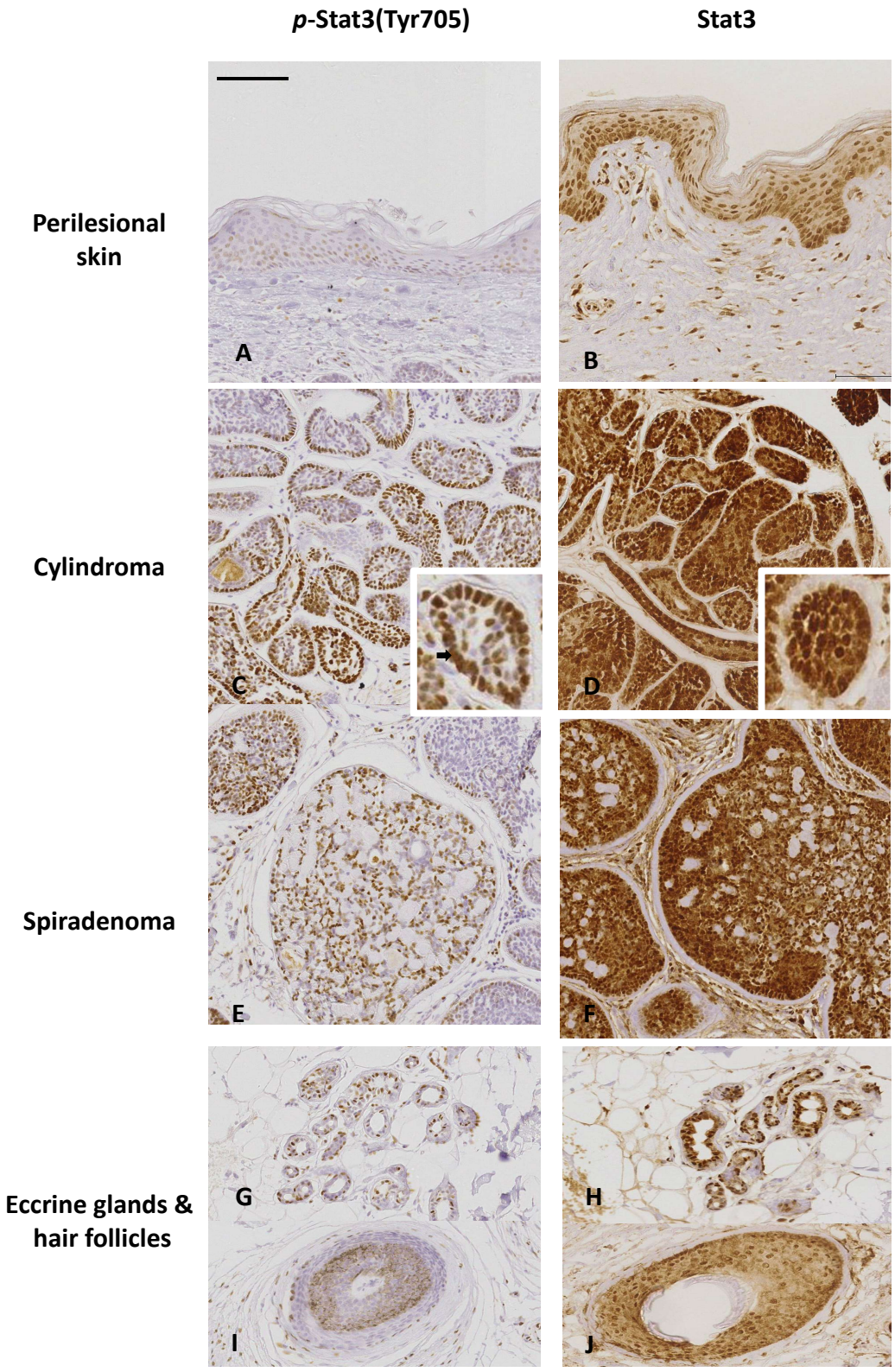

Figure 4-20: Stat3 expression is increased in CYLD-defective tumours as assessed by immunohistochemistry.

Sections of *CYLD*-defective tumours underwent antigen retrieval and were probed with *p*-stat3 (Tyr 705) and Stat3 antibodies. A & B) *p*-Stat3 (Tyr 705) and Stat3 expression in control perilesional skin from a *CYLD* mutation carrier, (C & D) cylindroma (E & F) spiradenoma and (G, H, I & J) structures of the skin such as the eccrine gland and hair follicles. In cylindroma *p*-stat3 expression was demonstrated to have nuclear localisation in the peripheral cells of the cylindroma tumour islands (black arrow, inset (C)). Scale bar represents 100μm.

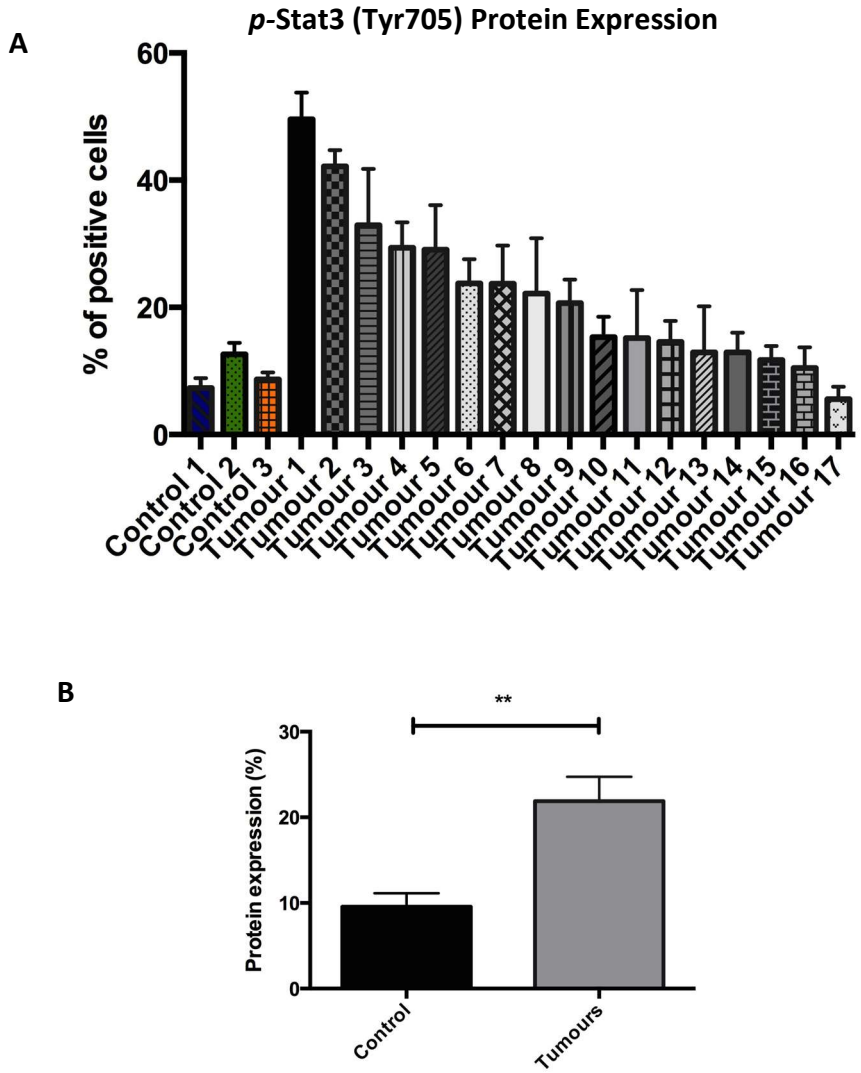

Figure 4-21: Quantification of *p*-Stat3 (Tyr705) protein expression in *CYLD*-defective tumours.

A) Semi-quantitative analysis of the immunostaining intensity of *p*-Stat3 (Tyr705) was carried out using ImageJ. A ratio of positive DAB staining was determined and the data represent the mean of the ratios taken from across 5 images per sample B) The protein expression of *p*-Stat3 (Tyr705) was compared between *CYLD*-defective tumours and control perilesional skin. Data are the mean and error bars represent the SEM of *n*= 3 control and *n* = 17 tumours (**$p < 0.01$,unpaired t-test).

Furthermore the increased expression was replicated in tumour lysates from cylindromas when run on a Western blot and probed with *p*-Stat3 (Tyr705) and compared to normal skin samples. This showed a variation in the levels of *p*-Stat3 protein expression but in 3 out of the 4 tumour samples it was increased. It was also observed that for 2 out of the 4 tumour samples this corresponded with increased TrkB.T1 protein expression (Figure 4-22).

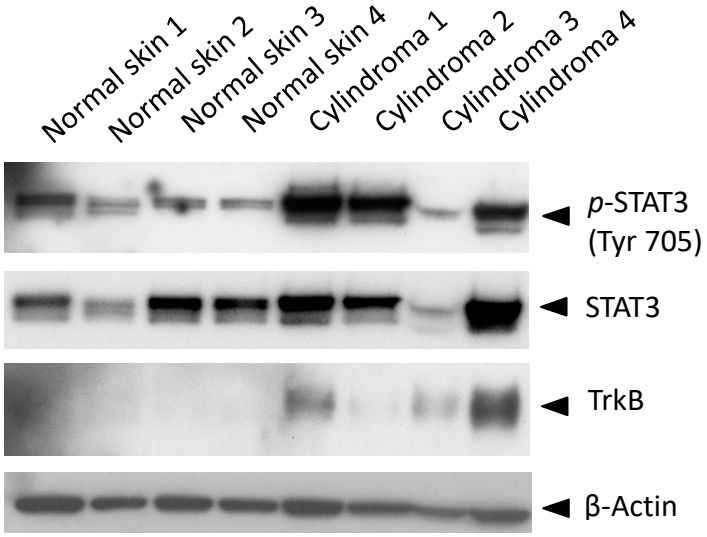

Figure 4-22: Stat3 protein expression is increased in CYLD-defective tumours.
Lysates from tumours and normal skin controls were collected and Western blot membranes were probed with *p*-Stat3 (Tyr705), Stat3 and TrkB antibodies. β-Actin was used as a loading control. Western blot shown is representative of *n*= 2 experiments.

4.3.8 BDNF expression is upregulated at the mRNA level in *CYLD*-defective tumours

As an activating ligand of TrkB and with TrkB expression upregulated in the tumours, experiments were performed to try and determine if the tumour cells themselves were a source of BDNF, which may be driving TrkB.T1 activation and downstream signalling. The heat map in Figure 4-5 showed that there was increased expression of some transcripts of BDNF in the *CYLD*-defective tumours from that data set. In support of this, qPCR analysis of BDNF expression in a panel of cylindroma tumours showed that at the mRNA level BDNF expression was significantly increased (p = 0.0015) in all the tumours compared to perilesional control skin, although there was variation in the level of BDNF over-expression between tumour samples (Figure 4-23 A & B). To see if increased BDNF mRNA expression translated into protein and whether this was then secreted in an autocrine manner by the tumour cells, attempts were made to determine protein levels by utilising both Western blotting and ELISA (enzyme-linked immunosorbent assay) methods. BDNF was detected in the majority of the tumour lysates on Western blot membranes, with levels also detected in the normal skin (Figure 4-24). Unfortunately the ELISA experiments were unsuccessful with no detectable concentrations of BDNF protein detected in either tumour lysates, cultured primary cylindroma cell lysates, or in media harvested from the same cell cultures. This may be indicative of problems with the experimental procedure such as interference of inhibitory enzymes in the lysis buffer preventing the reactions in the ELISA and the media samples not being concentrated. Alternatively biological reasons such as the tumour cells secreting very low concentrations of the protein may account for the negative results and requires further investigation.

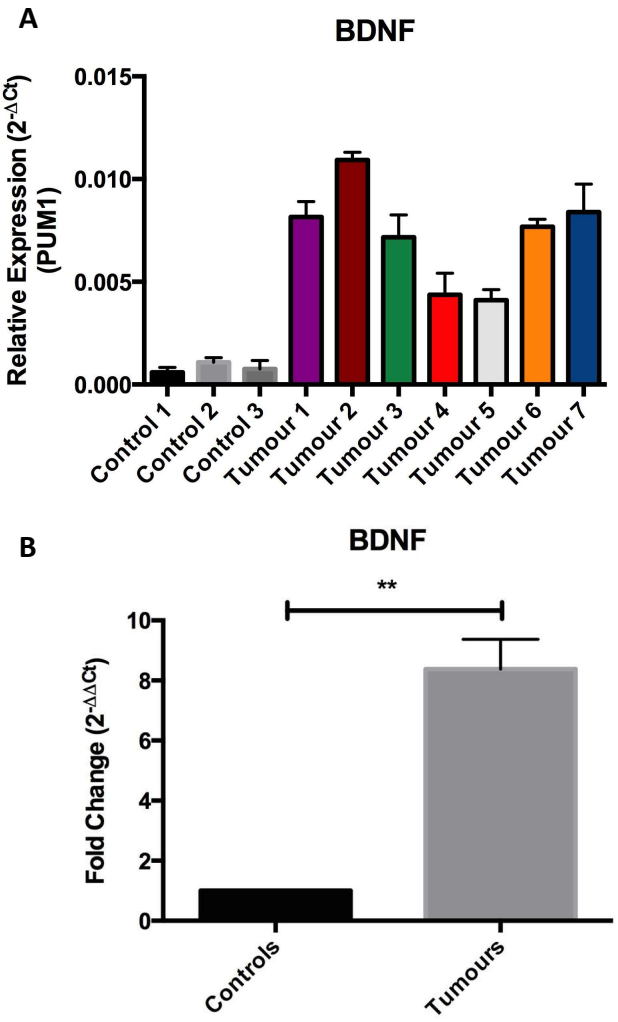

Figure 4-23: BDNF mRNA expression is increased in *CYLD*-defective tumours.
A) The expression of BDNF was determined by qPCR using Taqman probes, with the levels of expression normalised and expressed relative to the housekeeping gene PUM1. Data are the mean and error bars represent the SEM of *n*=3 experiments B) Data are the mean and error bars represent the SEM of *n*=3 perilesional skin control and *n*=7 tumour samples (** $p < 0.01$, unpaired t-test).

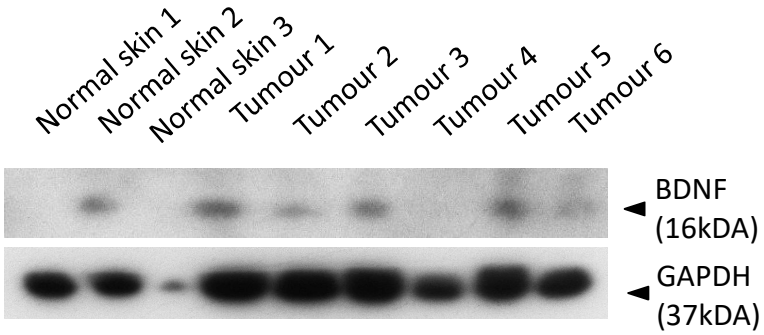

Figure 4-24: BDNF protein expression is increased in a panel of *CYLD*-defective tumours.

Lysates from tumours and normal skin controls were collected and Western blot membranes were probed with BDNF antibody. GAPDH was used as a loading control. Western blot shown is representative of *n*= 3 experimentsal repeats.

4.3.9 Stat3 relocates to the nucleus upon BDNF stimulation in primary cylindroma cell cultures

From the results of the over-expression studies in HaCaTs and the expression of BDNF in tumour cells, this led to looking at the effect of BDNF stimulation on tumour cells *in vitro.* Primary cylindroma cells were plated onto transwell cell culture slides and left for 5 days before adding either BDNF (100ng/ml) or IL-6 (25ng/ml) to the culture medium for 30 minutes. Cells were fixed following stimulation and the expression of Stat3 and CK17 assessed using immunofluorescence. Cells were treated with IL-6 as a positive control, as this is a known activator of Stat3 signalling (Zhong *et al.*, 1994), and CK17 was used as a marker for keratinocytes. In cylindroma primary cell cultures addition of BDNF induced translocation of Stat3 to the nucleus (Figure 4-25), matching the response seen from IL-6 stimulation of the cells (see Appendix). This relocation of Stat3 suggests it is activated and able to promote the transcription of target genes in response to BDNF. Further to this the expression of TrkB and Stat3 in cylindroma tissue sections was also assessed using IF and IHC. There was an overlap in TrkB and Stat3 expression observed, particularly in cells at the periphery of the tumour islands (Figure 4-26 & 27).

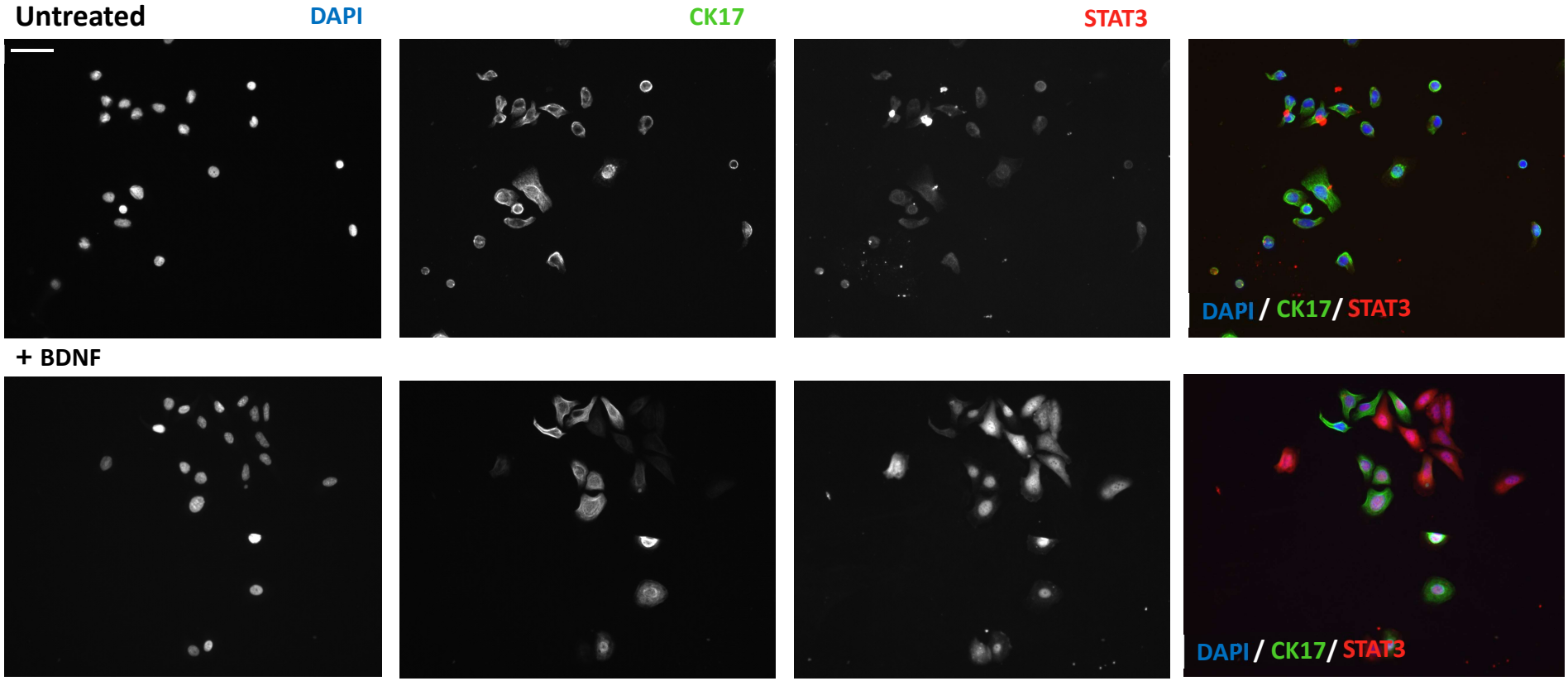

Figure 4-25: Stat3 nuclear localisation is seen in response to BDNF stimulation.
Primary cylindroma cells were treated with BDNF (100ng/ml) for 30 minutes, before being fixed and undergoing immunofluorescence using CK17 and Stat3 antibodies. Representative images are shown with experiments set up in duplicate and repeated on primary cells derived from three separate tumours. Scale bars represent 50μm.

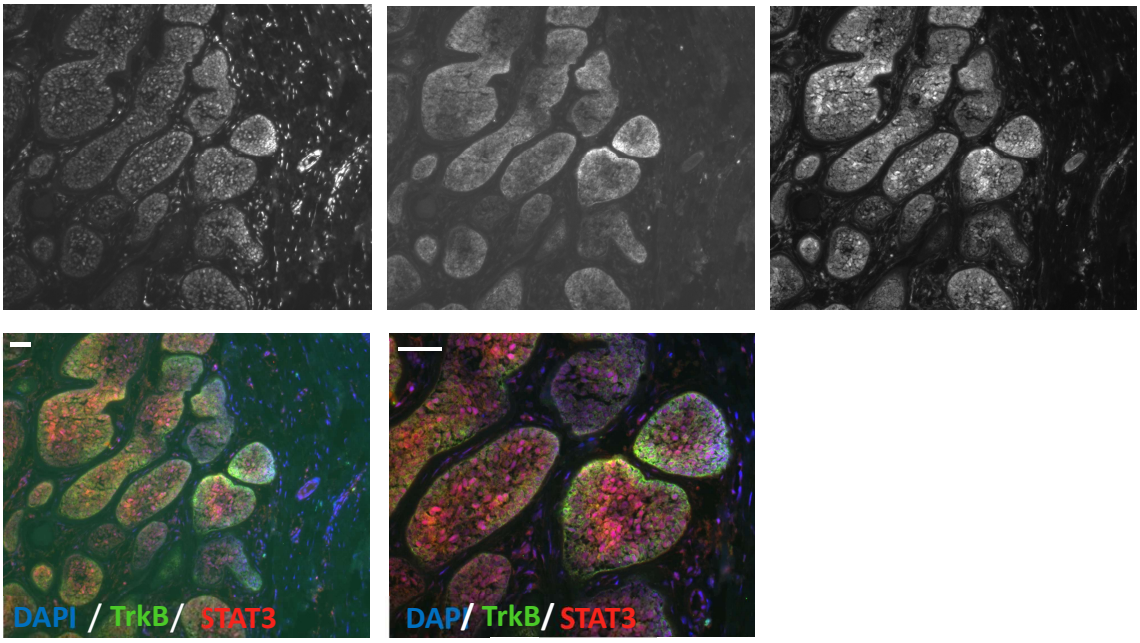

Figure 4-26: Stat3 and TrkB are expressed together *in vivo.*
Cylindroma tissue sections underwent antigen retrieval and indirect double stain immunofluorescence using antibodies against TrkB and Stat3. DAPI was used as a nuclear stain. Scale bars represent 50μm.

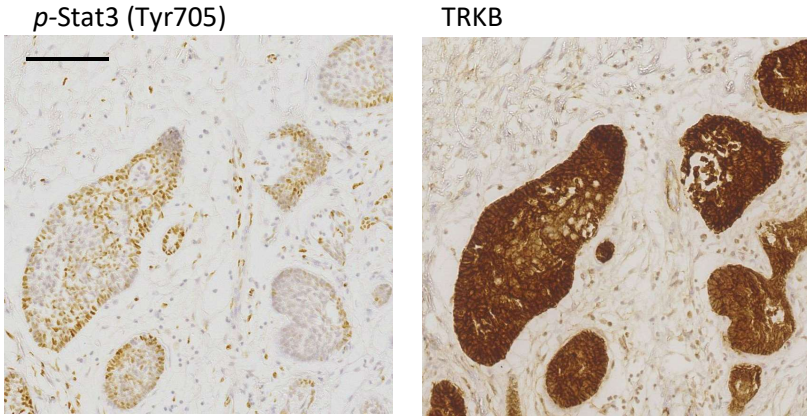

Figure 4-27: Stat3 and TrkB are expressed together *in vivo.*
Cylindroma tissue sections underwent antigen retrieval and immunohistochemical staining using DAB and antibodies against TrkB and *p*- Stat3. Scale bars represent 50μm.

4.3.10 Stat3 target gene expression is altered in *CYLD*-defective tumours.

As stated in Section 3.3.1, microarray gene expression studies in a pool of *CYLD*-defective tumours (*n*=32) and perilesional skin controls (*n*=10) had previously been performed by Dr. Neil Rajan (Rajan, Elliott*, et al.*, 2011). Using this dataset the expression of selected Stat3 target genes from the published literature were analysed. Differentially expressed Stat3 target genes in *CYLD*-defective tumours compared to controls were determined with a threshold for statistical significance of $p < 0.05$ after correction for multiple hypothesis testing. To visualise the expression of each of the genes (*n*=18) at an individual sample level, normalised signal values were plotted on a heat map, following logarithmic transformation. Clustering by Euclidean distance separated the majority of tumours, including all cylindromas and spiradenomas, from control skin with the exception of two trichoepitheliomas (tumours 1 and 30) (Figure 4-28). In this independent dataset, gene targets that were found to be upregulated in *CYLD*-defective tumours included the anti-apoptotic protein Bcl-2 (fold-change increase = x 2.34), and well-documented oncogenes such as Myc (fold-change increase = x 1.36), and Jun (fold-change increase = x 1.33) (Table 4-4). In addition at the protein level other targets including Bcl-xL and CyclinD1 were also increased in the cylindromas (Figure 4-29), suggesting possible mechanisms in which increased Stat3 activity may promote tumourigenesis.

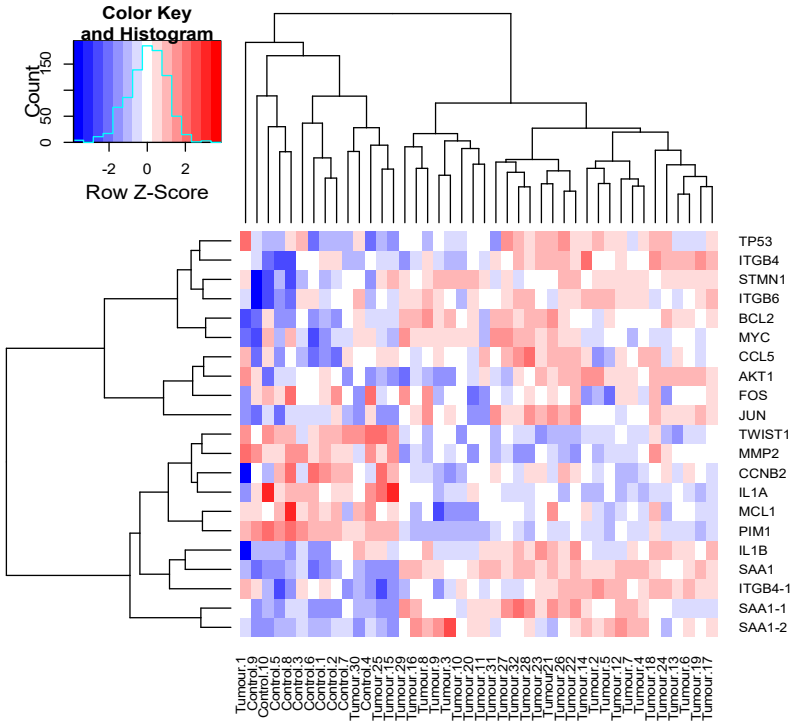

Figure 4-28: The expression of Stat3 target genes in *CYLD*-defective tumours and perilesional skin.

A heat map plot illustrating the expression levels of known Stat3 target genes in 32 *CYLD*-defective tumours and 10 controls (samples indicated at the bottom of the heat map). Differentially expressed genes were determined (p <0.05) between tumours and controls, and transcript expression levels at a single sample level are displayed on the heat map; red, over-expressed transcripts; blue, under-expressed transcripts; gene names indicated on the right-hand side of the figure; where data from multiple transcripts for a single gene were available are indicated with a numerical suffix (n = 2*).* Clustering by similarity is shown, determined by Euclidean distance.

Transcript	ILMN probe	Fold change	Unigene
SAA1	ILMN_23045	5.13	serum amyloid A1
SAA1	ILMN_18087	2.74	serum amyloid A1
SAA1	ILMN_17010	2.71	serum amyloid A1
BCL2	ILMN_22469	2.34	B-cell CLL/lymphoma 2
STMN1	ILMN_16577	2.27	stathmin 1
IL1B	ILMN_17755	2.19	interleukin 1, beta
ITGB6	ILMN_17898	2.01	integrin, beta 6
ITGB4	ILMN_23175	1.85	integrin, beta 4
ITGB4	ILMN_23342	1.66	integrin, beta 4
CCL5	ILMN_20981	1.63	chemokine (C-C motif) ligand 5
TP53	ILMN_17793	1.51	tumor protein p53
AKT1	ILMN_24109	1.36	v-akt murine thymoma viral oncogene homolog 1
MYC	ILMN_21109	1.36	v-myc avian myelocytomatosis viral oncogene homolog
JUN	ILMN_18060	1.33	jun proto-oncogene
MCL1	ILMN_17568	0.65	myeloid cell leukemia 1
FOS	ILMN_16695	0.64	FBJ murine osteosarcoma viral oncogene homolog
CCNB2	ILMN_18019	0.64	cyclin B2
IL1A	ILMN_16584	0.50	interleukin 1, alpha
MMP2	ILMN_17621	0.50	matrix metallopeptidase 2
TWIST1	ILMN_16729	0.47	twist family bHLH transcription factor 1
PIM1	ILMN_18150	0.27	Pim-1 proto-oncogene, serine/threonine kinase

Table 4-4: Differentially expressed Stat3 target genes in *CYLD*-defective tumours compared to perilesional control skin.

The fold changes (FC) of transcripts are included for differentially expressed genes with a threshold of p < 0.05. Red indicates genes that are overexpressed and blue indicates genes that have reduced expression in *CYLD*-defective tumours compared to control.

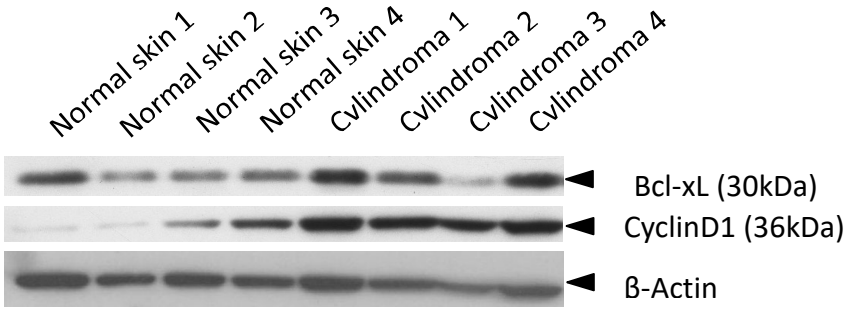

Figure 4-29: Stat3 target genes in tumour lysates

Lysates from tumours and normal skin controls were collected and Western blot membranes were probed with Bcl-xL and CyclinD1 antibody. β-Actin was used as a loading control. Western blot shown is representative of *n*= 2 experimentsal repeats.

4.3.11 Three dimensional (3D) primary cylindroma cell cultures are sensitive to Stat3 inhibition

Having identified that Stat3 is overexpressed and phosphorylation is increased in *CYLD*-defective tumours, this warranted determining if the tumours were dependent on the expression and activity of Stat3 for their survival. Primary cylindroma cell cultures, and HaCaTs were grown on 3D scaffolds in the presence of Stat3 inhibitors. The four different Stat3 inhibitors that were used were Cryptotanshinone, Niclosamide, NSC74859 and Stattic (Figure 4-30). The primary cylindroma cells were more susceptible to Stat3 inhibition compared to HaCats, with the exception of Cryptotanshinone. The CPCC demonstrated sensitivity to Stat3 inihbition at micromolar concentrations in the presence of NSC74859 and nanomolar cocentrations of Stattic, which was not seen in the HaCaTs (Figure 4-31).

Stattic

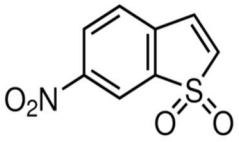

NSC74859

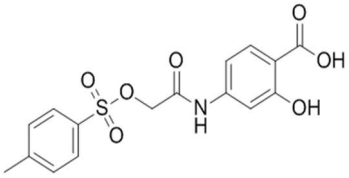

Niclosamide

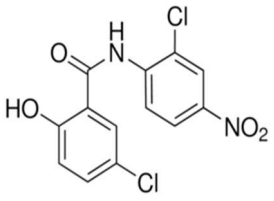

Cryptotanshinone

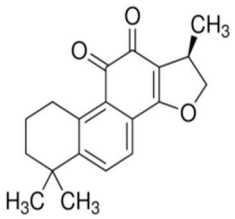

Stat3 Inhibitor (Tocris Bioscience)	Mechanism of Action	Reference
Stattic	Target the SH2 domain of Stat3 to inhibit Stat3 activation, dimerisation and nuclear translocation. (Although Niclosamide may act independently of the SH2 domain).	(Schust *et al.*, 2006)
NSC 74859		(Siddiquee *et al.*, 2007)
Niclosamide		(Ren *et al.*, 2010)
Cryptotanshinone		(Shin *et al.*, 2009)

Figure 4-30: Chemical structures of Stat3 inhibitors and their mechanism of action.

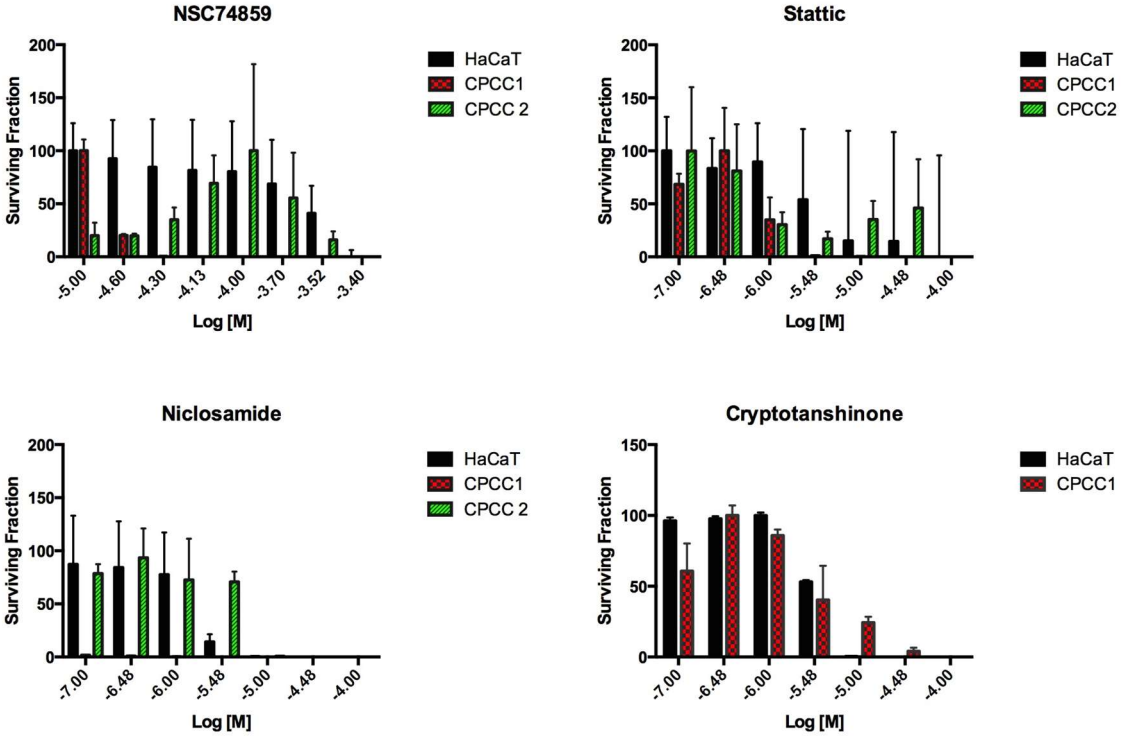

Figure 4-31: Primary cylindroma cells are sensitive to Stat3 inhibition.

Primary cylindroma cells and HaCaTS were cultured on 3D culture scaffolds for 4 weeks before being plated out in triplicate in 96 well plates and grown in the presence of NSC74859, Stattic, Niclosamide and Cryptotanshinone for 2 weeks. Cells were derived from two individual tumours from two patients. Cell viability was then assessed using a luminescent assay. Data are displayed as the mean of triplicate readings and error bars represent the SEM.

4.4 Discussion

TrkB is a receptor tyrosine kinase that once activated by its cognate neurotrophic ligands BDNF or NT-4/5, is capable of inducing a myriad of signalling responses including promotion of cell proliferation and survival (as reviewed by (Reichardt, 2006)). In this chapter it was shown that a BDNF-TrkB.T1-Stat3 signalling axis is active and targetable in cylindromas. Trk receptor homeostasis had previously been shown to be dysregulated in *CYLD*-defective tumours, with increased expression of both TrkB and TrkC (Rajan, Elliott*, et al.*, 2011). Further to this primary cylindroma cells grown on 3D cell culture scaffolds were sensitive to pan-Trk inhibition, suggesting a dependency on the Trk signalling pathway for survival. Yet normal keratinocytes were previously shown to express the TrkB.T1 isoform of the receptor (Marconi *et al.*, 2003). This isoform lacks a kinase domain and its function is not completely understood nor has it been thoroughly investigated in keratinocytes. Therefore this warranted further investigation of the TrkB receptor in *CYLD*-defective tumour cells.

4.4.1 *CYLD*-defective tumours express the truncated TrkB.T1 isoform

Within this study TrkB isoform expression was characterised in *CYLD*-defective tumours, as it was shown that the expression of TrkB was increased both at a transcriptomic and protein level (Figure 4-8 & 4-9), alongside altered expression of other associated receptors and ligands as indicated by the microarray data set (Figure 4-5). The TrkB receptor is known to have three major protein isoforms that are expressed in humans, which differ in their inclusion of the tyrosine kinase domain (Stoilov *et al.*, 2002). When the isoforms of TrkB were looked at in more detail in the *CYLD*-defective tumours, the RNA-seq data showed that for TrkB (*NTRK2*) an increased number of reads aligned to the alternate exon, exon 16 (Figure 4-6). Using RT-PCR it was found that cylindroma tumours expressed both full-length and truncated transcripts. Further corroboration at the transcript level using qPCR found that expression levels of both isoform transcripts were increased in the cylindromas. Whilst at the protein level only the truncated TrkB.T1 isoform could be detected (Figure 4-9). This result is in keeping with previous *in vitro* studies of keratinocytes, in which TrkB.T1 transcripts were the predominantly expressed isoform in epidermal keratinocytes ((Marconi *et al.*, 2003)). Yet in contrast to the report in which no full-length expression was found with RT-PCR, low levels of expression were seen in the normal skin samples used for qPCR in this study. This could possibly be due to the samples used by Marconi

et al. being from cultured keratinocytes compared to the tissue lysates used here.

To determine a role for TrkB.T1 in the cells, HaCaT and HEK293T cells were transduced with overexpression vectors for the TrkB isoforms. HaCaT cells overexpressing TrkB.T1 showed an increase in cell viability compared to controls, although this didn't reach a level of significance. Also in colony forming assays no significant difference was seen in the number and size of colonies between control and TrkB.T1 overexpressing cells (Figure 4-12), suggesting TrkB.T1 expression does not confer a proliferative advantage. Furthermore when compared to the overexpression of TrkB.FL in HEK293 cells, TrkB.T1 overexpressing cells showed sustained cell viability when exposed to BDNF, in contrast to a reduction in cell viability in TrkB.FL expressing cells (Figure 4-11). Taken together the results suggest that expression of TrkB.T1 may be protective to the cells and could indicate a survival role, which is also favourable for tumour cells. Unfortunately the TrkB.FL vector could not be characterised in the keratinocytes due to repeated unsuccessful transduction of the cell line, therefore no direct comparisons could be made between the isoforms in the keratinocytes in this study. In contrast a study by Rossler *et al.* in which HaCaT cells expressed the full length TrkB receptor, BDNF induced proliferation of the cells was dependent on Erk activation (Rossler and Thiel, 2004). Yet no difference in Erk phosphorylation was found in TrkB.T1 overexpressing cells (data not shown) but with the change in Stat3 phosphorylation (discussed in more detail in section 4.4.2) it may represent the different functional roles of the TrkB isoforms in this cell context. In further support of a cell survival role, within normal hair follicles BDNF-TrkB signalling is thought to prevent hair follicle keratinocyte proliferation via upregulation of TGF-β2 causing initiation of the regression stage of hair follicle cycling (Peters *et al.*, 2005). Together this suggests that increased expression of the TrkB.T1 receptor isoform in tumours of hair follicle origin such as cylindroma, could cause perturbed differentiation and promote a benign tumour that is recognised to be slow growing.

The isoforms of TrkB are due to alternative splicing, in TrkB.T1 the inclusion of exon 16, which contains a stop codon, leads to the translation of a protein without a tyrosine kinase domain (Stoilov *et al.*, 2002) (Figure 4-2). It was previously thought that without a tyrosine kinase domain the TrkB.T1 isoform functioned only as a dominant negative receptor, capable of binding ligands and forming receptor dimers with full-length

receptors but unable to instigate intracellular signalling. However more recent studies have started to support that TrkB.T1 may be a signalling entity, although many of these studies are limited to a neural cell context. As mentioned previously, Rose et al showed that in astrocytes TrkB.T1 was responsible for mediating calcium signalling, through BDNF stimulation of TrkB.T1 inducing activation of G-protein dependent PLC activation leading to calcium release and entry (Rose *et al.*, 2003). In glial cells TrkB.T1 was shown to be capable of mediating ligand dependent RhoGDI1 (Rho GDP dissociation inhibitor) signalling leading to inhibition of Rho GTPases and cytoskeletal rearrangement (Ohira *et al.*, 2005). In addition, a protein called TTIP (truncated TrkB interacting protein) was found by immunoprecipitation experiments in 15N neuroblastoma cells, showing specific binding to TrkB.T1. However to date very little is known about this protein but this demonstrates potential cytoplasmic adaptors capable of transducing signals (Kryl and Barker, 2000). In support of these findings, in this study TrkB.T1 was characterised in a keratinocyte cell line and was found to increase phosphorylation of Stat3 in response to BDNF activation.

A possible consequence of TrkB.T1 expression in regards to translational relevance is that therapeutic interventions targeting Trk receptor signalling may not be completely effective in these tumours. Many receptor tyrosine kinase antagonists, including Trk inhibitors, inhibit phosphorylation of the receptor to inactivate downstream signalling. This may have implications for treatment, as inhibitory Trk kinase compounds such as K252a, to which primary cylindroma cells were susceptible (Rajan, Elliott*, et al.*, 2011), tend to inhibit the phosphorylation of the receptor to inactivate signalling. Whilst these treatments may kill off some of the tumour cells as shown *in vitro*, in those cells that may be dependent on TrkB.T1 signalling it may leave residual tumour cells capable of future tumour growth. As reported in this chapter the predominant isoform expressed in these tumours lacks a catalytic domain and was shown to be capable of inducing Stat3 signalling, therefore it could be assumed that this treatment option may not be successful as a stand-alone therapy, as signalling could still occur and the receptor could still be activated by BDNF. Therefore either a synergistic therapeutic approach, targeting other downstream targets alongside Trks or those that target the binding pocket for the neurotrophic ligands with the receptor may be more beneficial.

4.4.2 Stat3 as a downstream target of TrkB signalling

A novel finding of this chapter was that TrkB.T1 overexpression in keratinocytes could induce Stat3 Tyr705 phosphorylation in the presence of BDNF. A receptor tyrosine kinase array was first utilised, to give an overview of expression and phosphorylation of downstream signalling nodes that may be influenced by overexpression of the TrkB isoforms, having found that expression of TrkB.T1 was capable of promoting cell survival and emerging evidence suggesting it was involved in cellular signalling. For comparison two HEK293 models were used; depicting TrkB isoform overexpression or expression of mutated forms of CYLD causing truncation and catalytic inactivation of CYLD, matching the mutations found in patients. Also *CYLD*-defective tumour lysates were also applied to compare *in vitro* to *in vivo*. In cells overexpressing the different TrkB isoforms, Akt and Src were the most influenced by TrkB.T1 overexpression, yet *p*-Stat3 (Tyr705) was also increased compared to control. Stat3 was deemed a target of interest after it was shown that overexpression of CYLD caused a decrease in *p*-stat3 levels and levels were increased in the *CYLD*-defective tumours. When TrkB.T1 was further investigated *in vitro*, it was demonstrated in both HaCaTs and primary cylindroma cells, that TrkB.T1 could induce activation of Stat3 as stimulation by the cognate ligand, BDNF, led to increased phosphorylation of Stat3 Tyr705 (Figure 4-18 & 4-19), in addition to an alteration in the location of Stat3 from the cytoplasm to the nucleus indicative of Stat3 activation (Figure 4-25), which can only be mediated by the TrkB.T1 receptor as the tumour cells were found to only express this isoform at the protein level.

Stat3 is a transcription factor that was initially discovered to regulate gene transcription in response to cytokine signals (Darnell *et al.*, 1994), and subsequently downstream of growth factor tyrosine kinases such as epidermal growth factor (Shao *et al.*, 2003). The canonical Stat 3 activation pathway involving activation of a receptor by its corresponding ligand and inducing phosphorylation of tyrosine residues on JAKs (Janus kinases). Subsequently the JAKs serve as docking sites that are capable of phosphorylating Stat3 at the Tyr 705 residue, which leads to activation and dimerization of Stat3 followed by translocation of the homodimers to the nucleus and binding to promoters of various target genes to initiate their transcription (Darnell, 1997). Many target genes of Stat3 are involved in promoting cellular proliferation and

resistance to apoptosis, therefore constitutive activation of Stat3 has also been recognised in many solid and haematological malignancies (as reviewed by (Yu H. *et al.*, 2014). Furthermore constitutive Stat3 expression has been reported to alter the behavior of keratinocyte stem/progenitor cells within the hair follicle (Rao *et al.*, 2015) and when a constitutively active form of Stat3 was expressed in keratinocytes of transgenic mice, it led to an increased susceptibility to skin tumourigenesis by both chemical and UV carcinogenesis (Chan *et al.*, 2008; Kim D. J. *et al.*, 2009).

Indeed Stat3 has previously been recognised as a downstream target of Trk signalling, although this is mainly delineated in neural cells in which full-length receptor isoforms are expressed. The originality of this study is that the particular isoforms of TrkB have been investigated and have shown for the first time that TrkB.T1 overexpression can mediate phosphorylation of Stat3 at the Tyr705 residue. The work of Ng *et al.* was the first report to demonstrate the ability of Trk receptors to influence Stat3 phosphorylation, but in contrast to the work in this chapter it was NGF stimulation of TrkA in PC12 cells that resulted in phosphorylation of residue Ser727 on Stat3 (Ng *et al.*, 2006). Also within the same study in cultured hippocampal neurons silencing of Stat3 expression abrogated BDNF induced neurite extension (Ng *et al.*, 2006). Furthermore it was shown that BDNF could induce neural stem cell survival and differentiation through activation of Stat3, in addition to Akt and Erk, although the phosphorylation site was not specified. The presence of BDNF also enhanced neural stem cell proliferation in the presence of EGF (epidermal growth factor) (Islam *et al.*, 2009). In keeping with the work included in this thesis, it was acknowledged in the study by Islam et al that phosphorylation of Akt, Erk and Stat3 in response to BDNF may be mediated by TrkB.T1, as the neural stem cells were shown to predominantly express this isoform (Islam et al., 2009).

Trk-Stat3 signalling has also been explored in cancer, for example in non-small-cell lung cancer BDNF-TrkB signalling triggers Stat3 activation due to phosphorylation of Tyr705, which can then stimulate BDNF synthesis in an autocrine feedback loop, contributing to cell proliferation through TrkB-Stat3 dependent Akt activation (Chen B. *et al.*, 2016). In contrast in *in vitro* transformation of NIH3T3 cells expressing constitutively active Trk oncogenes, with intact kinase domains, reduced Stat3 levels are associated with morphological transformation but transcriptional Stat3 activity is required for cell

growth (Miranda *et al.*, 2010).

Traditionally phosphorylation of Stat3 at the Tyrosine 705 residue is a prerequisite for activation and homodimerisation of Stat3 molecules (Kaptein *et al.*, 1996). Meanwhile the role of Ser727 phosphorylation of Stat3 is more ambiguous. It has been suggested that Ser727 phosphorylation is required for maximal transcriptional activity of Stat3 (Wen *et al.*, 1995), in contrast others have demonstrated an inhibitory effect on Tyr705 phosphorylation of Stat3 (Wakahara *et al.*, 2012). Furthermore Ser727 phosphorylation of Stat3 has also been reported to mediate transcriptional activation of Stat3 independently of Tyr705 phosphorylation. This was shown in PC12 cells where NGF stimulation induced CyclinD1 expression and increased association of Stat3 with the transcriptional regulator p300, demonstrating the importance of Ser727 Stat3 activation, as phosphorylation at the Tyr705 site was not observed in the neuronal cells (Ng *et al.*, 2006). In this thesis it was shown that in the HaCaT cells overexpression of TrkB.T1 did not alter phosphorylation of Stat3 at the serine residue (Figure 4-18) and was therefore not extensively looked at, but yet the presence of phosphorylation at this site may indicate that Stat3 could also have Tyr705 independent functions in the tumours.

Stat3 (Tyr705) phosphorylation was significantly increased by BDNF stimulation in TrkB.T1 overexpressing HaCaTs, which was reproduced in 2D primary cylindroma cultures treated with BDNF (Figure 4-18 & 4-19), even when expression of TrkB is lower in 2D primary cell cultures (see chapter 5). In addition immunohistochemical analysis showed a significant increase in *p*-Stat3 (Tyr705) in the tumours compared to perilesional controls (Figure 4-20 & 40-21). There was an irregular pattern of expression of *p*-Stat3 that was found in the tumour sections, which may be due to a possible transient nature of Stat3 phosphorylation as levels started to reduce after 15 minutes of stimulation with exogenous BDNF in TrkB.T1 overexpressing HaCaTs. Although this is within an artificial system and it is not to say that *in vivo* BDNF expression and therefore activation is not sustained. Positive p-stat3 (Tyr705) expression also corresponded with TrkB expression in some cells (Figure 4-26 & 27). All these results support that in the keratinocyte cell context in response to BDNF stimulus Stat3 Tyr705 phosphorylation is triggered, although the precise kinase mechanism needs to be further investigated. In different cell contexts, the availability

of kinases, the cellular stimuli and the levels of receptor expression could affect Stat3 phosphorylation (Miranda *et al.*, 2010). Indeed in other overexpression studies, such as PC12 cells overexpressing TrkA and stimulated with NGF, showed Tyr705 phosphorylation when this isn't usually seen in PC12 cells, with the authors hypothesising that overexpression my lead to perturbation of an intrinsic dephosphorylation mechanism (Miranda *et al.*, 2010; Ng *et al.*, 2006). In this scenario it is possible that in the tumour cells as a consequence of TrkB.T1 expression levels increasing, alterations to the phosphorylation equilibrium of Stat3 leading to aberrant activation of Stat3 and driving expression of target genes that promote tumour growth or survival.

To improve our understanding of TrkB.T1 and Stat3 in this cell context, future experiments would assess if a direct interaction or molecular mechanism has not been established in the *CYLD*-defective cells for TrkB.T1 and Stat3 activation. Therefore in future experiments, preferably in 3D cultures particularly as primary cylindroma cell spheroid cultures have been generated (see Chapter 5), it would be useful to treat these with a neutralizing TrkB antibody or use TrkB shRNA, followed by BDNF stimulation and assess if the levels of p-Stat3 Tyr 705 were affected. Although as the primary cells are sensitive to Trk inhibition this may lead to cell death so may not be a viable option. In addition to repeating the BDNF stimulation of primary cells in 3D cultures, to see if phosphorylation occurs as this is more reflective of the *in vivo,* tumour environment. Without a kinase domain, immunoprecipitation assays may also be utilised to identify novel interacting partners of TrkB.T1, to elucidate how TrkB.T1 is capable of initiating phosphorylation of Stat3. Alternatively calcium signalling could be another area for further research as TrkB.T1 was found to be capable of evoking calcium signalling (Rose *et al.*, 2003) and the TRPM7 calcium channel can regulate Stat3 phosphorylation in breast cancer cells (Davis F. M. *et al.*, 2014).

4.4.3 Stat3 inhibition in *CYLD*-defective tumours

To determine if primary cylindroma cultures were dependent on Stat3 for their survival, 3D scaffold cultures were treated with small molecule Stat3 inhibitors (mechanisms of action described in Figure 4-30). The cylindroma cells were shown to be susceptible to Stat3 inhibition in comparison to the HaCaTs, demonstrating a dependency of the tumour cells on this pathway. NSC74859 and Stattic in particular

caused a reduction in cell viability at micromolar concentrations (Figure 4-31), demonstrating that this could be a potential treatment strategy. As would be expected there was variability in the response between the different tumour cultures reflective of the inherent heterogeneity of the tumours, but also the error bars may be reflective of irregular cell growth across the scaffold (as will be discussed in chapter 5).

Inhibition of Stat3 has been an area of intense investigation in cancer therapy research in recent years as it is a target that is constitutively active in a variety of malignancies and Stat3 activation has been recognised as a mechanism of resistance to primary tyrosine kinase inhibitor treatment such as those targeting BCR-Abl and EGFR (Bewry *et al.*, 2008; Ishiguro *et al.*, 2013). Conversely disruption of the Stat3 feedback mechanism restored sensitivity to inhibitors of the oncogenic pathway to which the tumours were addicted (Lee H. J. *et al.*, 2014). However moving from *in vitro* to clinical trials with small molecule inhibitors of Stat3 compounds has proven challenging, with concerns of unpredictable pharmacokinetic profiles and potential toxicity (Wong A. L. *et al.*, 2015; Wong A. L. A. *et al.*, 2017). An advantage of the skin is the accessibility of lesions for topical treatment options, which can reduce some of the systemic side effects and drug toxicity. A topical ointment containing the Stat3 inhibitory compound STA-21 has been used in a trial for psoriatic lesions, which demonstrates a possibility of topical Stat3 compounds that could potentially be repurposed and trialled in patients with CYLD cutaneous syndrome (Miyoshi *et al.*, 2011).

Stat3 is also a convergence point for other signalling pathways, such as NF-κB. The two transcription factors have been shown to cooperate in a number of ways including modifying their transcriptionl activity through direct interactions between NF-κB family member RelA and Stat3 (Lee H. *et al.*, 2009). In addition both factors can collaboratively bind at target gene promoters to induce their expression (Hagihara *et al.*, 2005). Therefore as NF-κB is a pathway that is well documented to be dysregulated due to a loss of CYLD (Brummelkamp *et al.*, 2003), targeting of Stat3 is attractive as this could demonstrate an opportunity in cylindroma cells to use a multi-pronged approach and be a wider reaching intervention, treating cells even if they aren't dependent on Trk signalling. Indeed it is acknowledged that Stat3 is a convergence point for different signalling pathways and the changes in expression of Stat3 target genes demonstrated in the heat map (Figure 4-28), might not all be mediated by TrkB.T1 activation of Stat3.

Therefore further research is required to investigate other moderators of Stat3 in these tumours as further understanding of the mechanisms could inform of synergistic treatment strategies to gain maximum therapeutic benefit.

4.4.4 The source of BDNF and establishment of an autocrine loop

In this study it was found that the expression of BDNF was shown to be increased in the tumour cells compared to perilesional controls at the transcriptomic level, which was replicated at the protein level (Figure 4-23 & 24). This leads one to propose that the cells are capable of producing and secreting BDNF, and may function in an autocrine manner, as has been demonstrated in lung tumour cells where an autocrine loop of BDNF-TrkB-Stat3 signalling is established to induce BDNF expression and drive Stat3 activity (Chen B. *et al.*, 2016). In this study the ELISA method employed to try and quantitate the amount of BDNF secreted was unsuccessful. Technical reasons for this could have been inhibitory enzymes such as phosphatases may have stopped the reaction working or the samples were too dilute. For the media samples in particular it would be useful to concentrate the media in future to increase the chances of detection. Alternatively BDNF may also be produced in a paracrine manner from surrounding stromal fibroblasts or even possible infiltrating immune cells. The prevalent expression of *p*-Stat3 in the outer palisading cells of the tumour islands could be an indicator of a paracrine source as these are the cells in contact with the stroma and infiltrating immune cells. Immunohistochemical analysis of BDNF expression in tumour sections would also be useful to look at.

4.4.5 Conclusions

Overall the increased expression of the truncated Trk receptor isoform, TrkB.T1, has been identified to have potential intracellular signalling capabilities. In keratinocytes in response to its cognate ligand BDNF, there was increased phosphorylation of Stat3 at the Tyr705 residue leading to activation and relocation to the nucleus. This indicates that increased TrkB.T1 expression has the potential to drive the transcription of target genes, which may be capable of supporting tumour formation in *CYLD*-defective cells. Indeed in primary cultures the sensitivity of cells to inhibition of Stat3 supports that targeting of Stat3 may be a potential therapeutic strategy for CYLD cutaneous syndrome.

Chapter 5

Development of three dimensional (3D) primary cylindroma spheroid cultures

5 Chapter 5: Development of three dimensional (3D) primary cylindroma spheroid cultures

5.1 Introduction

5.1.1 Chapter aims

Taking in to account that cells cultured in 3D are more representative of their *in vivo* counterparts, and the drawbacks of an established scaffold culture method for CPCC: the laborious nature, long time scales and difficulty in monitoring cell growth, the overall objective of the work in this chapter was to establish a reproducible and more amenable 3D cylindroma primary cell culture model that could be utilised in a variety of downstream applications. The main aims were:

- To develop a protocol for the generation of cylindroma primary cell spheroid cultures
- To perform functional analyses on cylindroma primary cell spheroids to validate transcriptomic and experimental data using immunofluorescence staining
- To evaluate the efficacy of compounds against potential therapeutic targets

5.1.2 An overview of cell culture

Since its conception and development over the past century, cell culture is now a routine technique that allows for the maintenance of cells outside of the body from a variety of animal and human tissues, using growth medium supplemented with nutrients to support their growth and survival (Antoni *et al.*, 2015). It is a method that has contributed vastly and is invaluable to all fields of contemporary biology; not only advancing our understanding of basic cell biology, but also to allowing the modelling of disease systems, following through to compound screening as part of the drug discovery process, and leading to translational outputs from the knowledge gained. However the routine culturing of cells as two dimensional (2D) monolayers isn't without disadvantages, a key limitation being the lack of the three dimensional (3D) microenvironment in which cells reside *in vivo*; surrounded by other cells and an extracellular matrix (ECM) (Edmondson *et al.*, 2014). To this end a significant advancement in the technique has been the development of 3D cell culture methods,

which take into account the spatial organisation and interactions of the cells to provide more physiologically relevant knowledge of cell behaviour, and aid in bridging the gap between *in vitro* and *in vivo* (Haycock, 2011).

5.1.2.1 Keratinocyte cell culture

Serial cultivation of primary human epidermal keratinocytes was first established in 1975 by Rheinwald and Green (Rheinwald and Green, 1975). The formation of keratinocyte colonies was initiated in the presence of an irradiated NIH3T3 embryonic mouse fibroblast feeder layer, which supported keratinocyte growth through secretion of soluble growth factors into the culture medium and propagation of extracellular matrix deposition. More modern, commercially available animal derivative-free, defined culture mediums have been developed (Rasmussen *et al.*, 2013). Most of these being variations of the serum free, low calcium supplemented MCDB153 medium, which supports the clonal expansion of keratinocytes independently of fibroblast feeder layers (Boyce and Ham, 1983; Tsao *et al.*, 1982). Keratinocytes in culture have the ability to form three distinguishable clonal types: holoclones, paraclones and meroclones, classified by the frequency with which they give rise to terminal progeny (Barrandon and Green, 1987). Holoclones are composed of proliferative cells with the greatest growth potential, whilst paraclones have a limited replicative lifespan. Meroclones are considered a transitional stage containing a mixture of cells with different growth potentials.

The original culture method still remains widely used to date, however it has also inspired *in vitro* advances, taking keratinocyte cultures from 2D to 3D with the generation of living skin equivalents (LSE). These 3D multi-layered organtoypic models are formed when keratinocytes are seeded onto a collagen lattice containing dermal fibroblasts, which are then grown at the liquid-air interface. This allows for epidermal stratification of the cells that recapitulates a number of features of the human epidermis including the morphology and spatiotemporal expression of both proliferative/terminal differentiation markers and re-epithelialisation markers (Mertsching *et al.*, 2008; O'Leary *et al.*, 2002). Whilst as skin equivalents, like with all *in vitro* models, they cannot completely simulate the complexity of human skin, these models do offer a tool with which to study cutaneous biology experimentally that is more physiologically relevant than 2D cell monolayers.

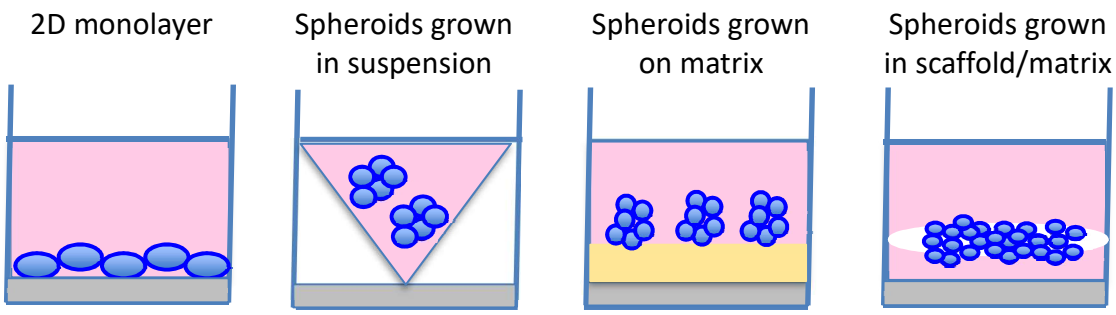

Figure 5-1: A diagram of different 3D cell culture models.
In typical 2D cell culture, cells adhere to plastic culture vessels and grow in monolayers. 3D cell cultures can be achieved with a variety of methods. Cells can be seeded into specialised culture vessels treated with a non-adherent coating to promote cell aggregation leading to the formation of spheroid cultures in suspension. Spheroids may also be generated by coating culture plastic-ware with protein mixtures such as Matrigel® or ECM proteins such as collagen hydrogels, to mimic the cellular microenvironment and encourage cell-ECM interactions to support the growth of spheroids either within the mixture or on top. Alternatively support may be provided in the form of a synthetic or natural material 3D membrane such as a porous scaffold, on to which cells can be seeded to encourage cellular interaction and growth in 3D. (Image adapted from (Edmondson *et al.*, 2014).

5.1.3 Methods for 3D cell cultures

A number of methods have been developed for 3D cell cultures which fall into two main categories: (i) scaffold/matrix-based and (ii) non-scaffold based, as shown in Figure 5-1 and reviewed by (Breslin and O'Driscoll, 2013). The generation of 3D cell aggregates, also known as spheroids, in suspension can be achieved using either of the hanging drop method, forced floating method, or agitation-based approaches such as rotational culture systems or spinner flask bioreactors. In each case the main principle of the method design is to promote cell-cell interactions, leading the cells to adhere to each other rather than the surface of the culture vessel. This is achieved either by rotary movement or by coating the surface of the culture vessels with substances such as agarose or poly-2-hydroxyethyl methacrylate (poly-HEMA), and having round or conical shaped well bottoms. The benefits, particularly when using the forced floating and hanging drop methods, are that these are generally low cost procedures and allow for the production of a large number of spheroids in reproducible conditions, which is particularly useful for drug cytotoxicity assays (Breslin and O'Driscoll, 2013).

Alternatively cells that are difficult to aggregate can be cultured on artificial substrates to generate 3D spheroid cultures. One method is to culture cells on or within a matrix that contains components of the ECM, such as agar or Matrigel® (BD Biosciences),

which is an extract of Engelbreth-Holm-Swarm (EHS) mouse sarcoma proteins. These substances encourage cell-ECM interactions in 3D to promote cell aggregation and organisation of the cells, which can then grow into structures that mimic those found *in vivo* (Kleinman and Martin, 2005; Zegers *et al.*, 2003), such as the LSE organotypic model mentioned above. Another method is to use scaffolds made from either synthetic materials such as polystyrene, like the ones used in this thesis from Alvetex®, or biodegradable materials such as collagen or alginate as hydrogels. The scaffold inserts are porous to allow for the exchange of oxygen and nutrients, with cells seeded onto the scaffolds left to grow in the interstitial space within the structure, maintaining their 3D morphology. Finally other more complex 3D culturing systems use microfluidics and coated microcarrier beads (Kim J. B., 2005).

5.1.4 Comparison of 2D vs 3D cell cultures

The requirement for 3D cultures has been recognised for a number of decades, with the conception of one of the first 3D cultures in agar in the 1970's (Hamburger and Salmon, 1977) The disparity between 2D and 3D cultures was highlighted by Bissell and colleagues, who discovered that human breast epithelial cells in monolayer cultures displayed characteristics of tumour cells *in vivo,* but when grown in 3D culture reverted back to their usual growth behaviour (Petersen *et al.*, 1992). To this end the limitations of 2D cultures have been reviewed by many (Breslin and O'Driscoll, 2013; Edmondson *et al.*, 2014; Kim J. B., 2005; Kimlin *et al.*, 2013; Ravi *et al.*, 2015; Rimann and Graf-Hausner, 2012) (summarised in Table 5-1 below), and it is evident that it is not just the genome, but the interpretation of cues from the extracellular environment of a cell that dictates its phenotype; cues that need to be taken into account when examining cellular biology (Tibbitt and Anseth, 2009).

The superiority of 3D to 2D cell cultures is evident in many aspects of cell biology, which has made their use particularly attractive for exploring tumour biology. Firstly the growth of cells as a monolayer on a flat rigid surface flattens and stretches the cells, compared to 3D where the morphology is more representative of that seen *in vivo* (Edmondson et al., 2014). The morphological alteration can influence many processes such as cell proliferation, differentiation, apoptosis and gene expression (Birgersdotter *et al.*, 2005; Chen C. S. *et al.*, 1997), which have been highlighted in a number of comparison experiments. For example a number of cell lines have shown a

reduced proliferation rate in 3D cultures, including those from endometrial (Chitcholtan *et al.*, 2012) and colorectal cancers (Luca *et al.*, 2013), as well as non-cancerous kidney HEK293 (Kim E. and Jeon, 2013) and mammary epithelial MCF10A cell lines (Wang X. *et al.*, 2010). Meanwhile JIMT1 breast cancer cells have shown an increased and decreased rate, dependent on the 3D model used (Hongisto *et al.*, 2013). Furthermore MCF-7 cells when grown on a chitosan-based scaffold, provided a model that simulated both tumour-like metabolic activity, as the cells produced more lactate compared to cells grown on plastic, and drug efficacy with increased Tamoxifen resistance in the scaffold cultures (Dhiman *et al.*, 2005).

These changes in behaviour are governed by altered gene and protein expression, with gene expression patterns of 3D cultures being comparable to those observed in solid tumours *in vivo* (Costa et al., 2016). Indeed it is approximated that 30% of genes are differentially expressed in cell lines compared to their corresponding tissues (Sandberg R. and Ernberg, 2005; Virtanen *et al.*, 2002). For instance in melanoma NA8 cells, genes that have been shown to have a role in melanoma progression and metastasis, such as IL-8 and CXCL1, were over-expressed when cultured as spheroids as opposed to monolayers (Ghosh *et al.*, 2005). Likewise in colorectal cancer cell lines that were cultured in a laminin-rich-ECM and compared to 2D cultures, alongside differential gene expression, which included genes involved in the MAPK pathway, there was also a reduction in the protein expression of epidermal growth factor receptor (EGFR), a therapeutic target for advanced colorectal cancer, and whose reduction may be associated with acquisition of therapy resistance during cancer progression (Luca *et al.*, 2013). These studies again demonstrate the importance of the cell and ECM interactions when modelling these cell types for molecular studies. Furthermore modifications to the ECM structure can be instrumental in tumour progression and migration (van Dijk *et al.*, 2013), but genes for cell adhesion and cell-ECM signalling proteins are commonly repressed in cell lines. However it was shown that the expression of these gene types was restored when immortalised cell lines were transplanted back into mice (Birgersdotter *et al.*, 2005; Creighton *et al.*, 2003).

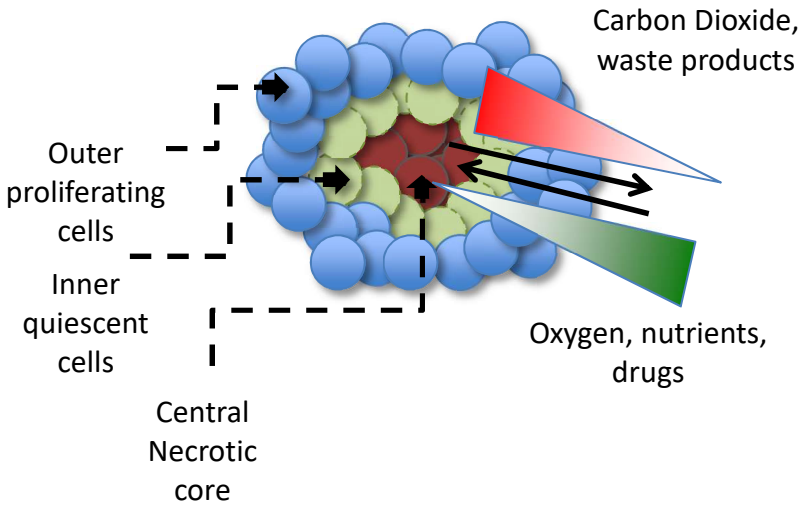

Figure 5-2: The structure of spheroid cell cultures.
Spheroids are organised into three layers with the outer layer (represented by the blue circles) containing proliferating cells, whilst an inner layer (represented by the green circles) contains quiescent live cells. In spheroids reaching certain sizes (>500μm diameter) the core of the spheroid will contain necrotic or hypoxic cells (represented by the red circles), which mimic the biology of the tumour, as this is reflective of the cell microenvironments found in tumours. Nutrient and oxygen gradients (represented by the green triangle) and the reciprocal waste gas and products gradient (represented by the red triangle) are established between the different cell layers. For drug assays these gradients can mirror the pharmacokinetics of drug delivery within *in vivo* tumours. Image adapted from (Edmondson *et al.*, 2014).

The structural formation of spheroid cultures is another aspect of 3D cell culture in which these cell models are more representative of the *in vivo* environment. Spheroid cultures are comprised of a heterogeneous population of proliferative, quiescent and hypoxic cells organised by the differential distribution of oxygen, nutrients and carbon dioxide along diffusion gradients (as shown in Figure 5-2). These closely resemble the multiple phenotypes found in solid tumours (Kim J. B., 2005). This is in stark contrast to the cellular homogeneity of 2D cultures, where all the aforementioned requirements of the cell are equally accessible and waste products are removed during routine culturing. Additionally it has been found that 3D cultures are more resistant to anticancer therapeutics (Breslin and O'Driscoll, 2013), the differences in drug sensitivity and response between the two culture environments attributed to a number of factors, which again mimic the behaviour of tumours in response to therapy *in vivo*. Firstly hypoxic regions within the core of a spheroid, generated from the build up of waste products, create a low pH environment. This can reduce drug uptake by the cells (Swietach *et al.*, 2012) and also alter the gene expression profile of the cell (Wilson W. R. and Hay, 2011). This occurs in tumour cells where low pH induces the

expression of members of the hypoxia inducible factor-1 family (HIF-1), which in turn enhances the survival of malignant cells (Eales *et al.*, 2016). The size of the spheroid also affects the pharmacokinetics of the drug and the rate at which it can diffuse into the spheroid, meaning cells receive variable concentrations of the drug much like the drug gradients that can be created in tumours *in vivo* (Thurber and Wittrup, 2008). Moreover cellular interactions, alterations to signal transduction and gene expression in 3D cultures can all influence the spatial organisation and localisation of cell surface receptors, alongside the availability of proteins involved in the pharmacodynamics of a drug, including the targets to which a drug maybe designed for, thus leading to differences in the effectiveness of the treatment (Edmondson *et al.*, 2014). Equally some drugs are effective at specific cell stages, such as 5-fluorouracil and Paclitaxel which target proliferating cells, so have poorer therapeutic efficacy in the quiescent interior cells of spheroids and tumours alike (Edmondson *et al.*, 2014; Mitchison, 2012). Overall these features contribute to producing a model that resembles the *in vivo* tumour and the acquirement of drug resistance, thus making spheroid cultures a useful drug-screening tool.

Cell characteristic	2D	3D
Morphology	Cells grow in a monolayer, adhering to a plastic or glass surface	Cells grow in their natural shape forming a spheroid/aggregate structure
Cell cycle stage	All cells tend to be at a similar proliferative stage as necrotic cells detach and are removed during medium changes	Cells are at different cell cycle stages with outer proliferating cells, inner quiescent but viable cells, and a core of necrotic or hypoxic cells (dependent on the spheroid size)
Cellular barriers	Cells have limited interaction with each other as monolayers	Cell interaction is increased and promotion of deposition of ECM proteins and cellular adhesion
Gene/protein expression	Cells have altered gene and protein expression levels to those seen *in vivo* due to a lack of cellular interaction in monolayers	Cells have gene and protein expression profiles that are comparable to those found in the tissue of origin
Drug exposure	All cells are exposed equally to drug treatments in the media and the distribution of the drug within all the cells is therefore equal	Drugs may not be able to penetrate into all cells of the spheroids, particularly those within the core
Drug sensitivity	Cells are often more sensitive, and drugs appear very effective	Cells are more resistant to drug treatments, and therefore better predictors of the *in vivo* response

Table 5-1: A summary of the cellular characteristics that differ between 2D and 3D cell cultures (adapted from (Edmondson *et al.*, 2014)

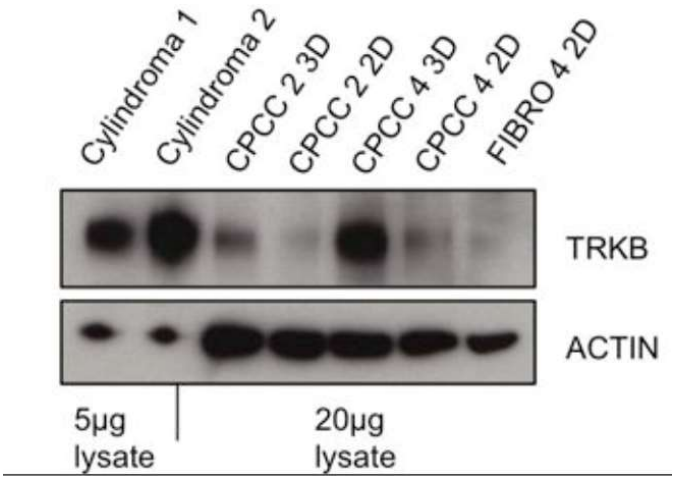

Figure 5-3: A Western blotting image of CPCC grown in 2D and 3D.
Membranes were probed with TrkB antibody to show the difference in expression of TrkB between cells grown in 2D cell culture and cells that had been seeded onto a 3D scaffold and left to grow for 4 weeks. As a control lysates from fresh tumours were also included for comparison. Image taken from (Rajan, Elliott*, et al.*, 2011).

5.1.5 3D spheroid cell cultures to model *CYLD* defective tumours

Cylindroma primary cell cultures (CPCC) have previously been described (Bruckner-Tuderman *et al.*, 1991; Weber L. *et al.*, 1984), with a methodology of enzymatic digestion of the tissue with trypsin and collagenase and culture of the cells in serum-free keratinocyte medium. This protocol was further developed and optimised by Dr. Rajan (Rajan, Elliott*, et al.*, 2011) and again in this thesis, to successfully produce primary cultures (Material and Methods section 2.6). The cylindroma cells displayed two morphologies: typical small keratinocytes and occasional larger flat cells with an increased nuclear size, whilst the colonies formed were predominantly holoclones and meroclones. These primary cell cultures derived from *CYLD* defective tumours are important *in vitro* models, as at present CYLD deficient mouse models do not spontaneously develop tumours (Massoumi, Chmielarska*, et al.*, 2006), impeding functional analyses in relevant models *in vivo*. Therefore primary cell cultures provide a tool for functional studies of perturbed gene expression profiles and signalling pathways identified by transcriptomic analyses, in a *CYLD* defective context. The lack of an *in vivo* model reinforcing the need to make the *in vitro* primary cell culture models as representative of the tumours as possible.

Indeed with the establishment of primary cultures from CYLD defective tumours, Rajan *et al.* have previously investigated culturing the cells in 3D by seeding the primary cells

onto polystyrene scaffolds (Rajan, Elliott*, et al.*, 2011). As highlighted above cells in a 3D cell culture environment differ in their gene and protein expression profiles from 2D cultured cells (Edmondson *et al.*, 2014). To recapitulate the point, the work by Rajan *et al.* found that cylindroma primary cells cultured on scaffolds in 3D showed an increase in expression of both TrkB and TrkC, compared to matched cells grown in 2D culture (Figure 5-3). This was influential to the identification of Trk receptors as potential therapeutic targets in subsequent downstream *in vitro* assays (Rajan, Elliott*, et al.*, 2011). The generation of these 3D scaffold cultures however takes 28 days, and as is the nature of long-term cultures this is therefore a costly and labour-intensive process. Though having demonstrated that 3D primary cell cultures provide a more biologically relevant cylindroma culture model, this warranted development of the methodology to generate an alternative 3D cell culture system such as spheroids, which has not previously been attempted in this cell model.

5.2 Chapter specific materials and methods

The protocol for generating spheroids was adapted from an established protocol for 3D culture of murine keratinocyte stem cells provided by Dr. Julia Reichelt (Wallace and Reichelt, 2013).

Solutions for 3D cell culture:

102mM $CaCl_2$: 102µl of a 1M $CaCl_2$ stock solution was diluted per 1ml of distilled H_2O

1.2mM $CaCl_2$ in KSFM: 1.2µl of a 1M $CaCl_2$ stock solution was diluted per 1ml of KSFM cell culture medium

1.2% alginate: 0.6g of alginate salt (Sigma-Aldrich) was added to 100mls of distilled H_2O, and left to dissolve on a heated magnetic stirrer ensuring that half of the solution was evaporated off to reach the desired concentration.

5.2.1 Obtaining primary cells

Primary cylindroma cells, derived from fresh tumour samples taken from patients undergoing surgery and processed into a single cell suspension, were defrosted and plated out initially into cell culture flasks coated with collagen I. Cells were left to grow until 70-90% confluent before being trypsinised for seeding for 3D cell cultures (according to Materials and Methods section 2.6).

5.2.2 Cell seeding for spheroid formation

For the generation of spheroids in large numbers AggreWell™400 Ex plates (STEMCELL technologies) were used. These are 6 well plates with each well containing an insert composed of 4,700 microwells, with a repellent surface that prevents the adhesion of cells. Plates were first prepared by washing each well with 2ml of AggreWell™Rinsing solution (a surfactant solution to lower the surface tension of the plate to aid the removal of bubbles), and centrifuged at 300 x g for 10 minutes to remove bubbles. Wells were then rinsed with 1ml of KSFM (keratinocyte-serum free medium) before adding 2ml of KSFM containing 1.2mM calcium chloride ($CaCl_2$). Trypsinised cells were counted and the required number of cells added to a volume of KSFM w/ $CaCl_2$, to give a total volume of 3mls that was then added to each 6 well (final volume in the well 5mls). Between 2.26 x 10^5 and 6.78 x 10^5 cells were seeded per well equating to 50-

150 cells per microwell The cell suspension in each 6 well was gently resuspended to ensure even distribution of the cells between the microwells, before a final centrifugation at 200 x g for 3 minutes. Cells were left for at least 24 hours at 37°C/5% CO_2 to allow for spheroid formation, and left in culture for 5-7 days, with 3ml media exchanges every 48 hours.

5.2.3 Cell seeding for spheroid formation for assays in a 96 well format

For the generation of spheroids per well for proliferation and drug assays primary cells and HaCaTs were seeded into the inner 60 wells of ultra-low attachment surface 96 well microplates (Corning). Trypsinised cells were counted, and the volume of cells calculated to obtain the required number of cells per well. The cell suspension was then centrifuged and the cell pellet resuspended in the same volume of KSFM w/ $CaCl_2$. The cells were seeded at a density of 2.5 x 10^4 cells per well. All wells were then topped up to a final volume of 280µl with KSFM w/ $CaCl_2$ before plates were centrifuged at 100xg for 3 minutes. Cells were left for 24 hours at 37°C/5% CO_2 to allow for spheroid formation, before a 1:1 media change (140µl removed and 140µl fresh media). Cells were then left for another 72 hours before being treated.

5.2.3.1 Drug Assay of CPCC spheroids

Once spheroids had formed and had been in culture for 72 hours, they were then treated with the following inhibitors, diluted in DMSO, with a final concentration of DMSO at 0.1%; NSC74859, Stattic (both TOCRIS) or K252a (Sigma Aldrich). Each drug was prepared as a 10X stock solution at a range of concentrations in KSFM media containing 1.2mM $CaCl_2$. Then 28µl of drug added per well to the spheroid culture plate in triplicate for each concentration of each compound (Figure 6-4). Spheroids were treated for a further 72 hours before being assayed using CellTiter-Glo® (Materials and Methods section 2.6.10).

5.2.3.2 Proliferation Assay of CPCC spheroids

Cells were also seeded at a range of densities from 1.25 x10^3 to 8 x10^4 in triplicate, with a final well volume of 280µl. The spheroids were then maintained for four days before being assayed using CellTiter-Glo® (Materials and Methods section 2.6.9).

5.2.4 Harvesting of CPCC spheroids

For use in downstream applications, medium was carefully removed until 1ml remained. Spheroids were then fixed in 5mls of 4% PFA for 20 minutes, before being replaced (again leaving 1ml) with 5mls of PBS and left for an hour. PBS was then removed and the remaining 1ml was pipetted over the bottom of the well to dislodge the spheroids. The spheroids were then transferred into a FACS plastic tube and left to sit for 5 minutes to settle down to the bottom. PBS was removed until 500μl remained, before the spheroids were resuspended and transferred to a 1.5ml eppendorf and centrifuged at 5000rpm for 1 minute. The spheroids could then be stored at 4°C until needed.

5.2.5 Cryosectioning of CPCC spheroids

For immunofluorescence analysis, spheroids were frozen down in OCT for cryosectioning. Harvested spheroids had as much of the storage PBS removed without disturbing the spheroids, leaving 20-30μl. To this 40μl of 1.2% alginate was added and the spheroids resuspended. The spheroid-alginate solution was then dripped from a pipette into a petri dish containing 102mM $CaCl_2$ solution and left for 10 minutes to solidify and form a ball. The spheroid-alginate drops were then removed with tweezers and placed on to blue roll before being placed into OCT on parafilm, which had been stained with 10μl of 1% Neutral Red solution to help distinguish the spheroid-alginate drops. The OCT containing the spheroid-alginate drops was left to set on dry ice before being transferred into a pot to store at -80°C. The OCT drop was then mounted onto a corkboard and the spheroids sectioned at a thickness of 7μm and mounted onto slides.

5.2.6 IF on CPCC spheroids

Sections underwent immunoflourescence as described in section 2.5.4. Additional antibodies that had not been used in any of the previous experiments and were used for spheroid characterisation are included below.

Protein	Antibody type	Clone	Isotype	Dilution	Supplier	Cat no.
Primary Antibodies						
Ki67	Monoclonal	8D5	Mouse IgG1	1:400	Cell Signalling	#9449
CK14	Monoclonal	LL002	Mouse IgG3	1:200	Abcam	Ab7800
CK17	Monoclonal	Ks17.E3	Mouse IgG2b	1:200	Abcam	Ab19067
β-actin	Monoclonal	D6A8	Rabbit IgG	1:200	Cell Signalling	#8457
β-catenin	Monoclonal	-	Mouse IgG1	1:50	BD Biosciences	610153

Table 5-2: Primary and antibodies used for immunofluorescent staining of spheroid cultures

5.3 Results

5.3.1 Spheroid culture of cylindroma primary cells is a novel *in vitro* model

As mentioned in the methods a protocol had been developed by the Reichelt Lab to generate spheroid cultures from murine keratinocyte stem cells. This was adapted and optimised for the generation of cylindroma primary cell culture spheroids. The protocol included growing the cells in a physiological calcium concentration of 1.2mM, which is higher than the low calcium (0.05mM) conditions the cells are usually grown in in 2D cultures. Primary cylindroma cells that were 70-90% confluent were trypsinised in the usual manner and counted, before being seeded at the correct density in to the appropriate plate and centrifuged to encourage aggregate formation. Figure 5-4 depicts the process of culturing and seeding the primary cylindroma cells, through to the successful generation of spheroids in both the Aggrewell™ and 96 well plate formats (A-D). The following images show the processing of the spheroids into OCT blocks so that functional analyses could be carried out such as H & E staining and immunofluorescence (E-F). To gain insight into the number of cells that made up the spheroids and the proportions from the numbers plated, the nuclei of 50 spheroids,which had been stained with DAPI, were counted with an average of 24.6 ($\pm$13.78 SD) cells per spheroid. Overall this protocol was a much quicker process compared to the 4 week culturing of the cells on scaffolds, with successful generation of spheroid cultures in 24 to 48 hours.

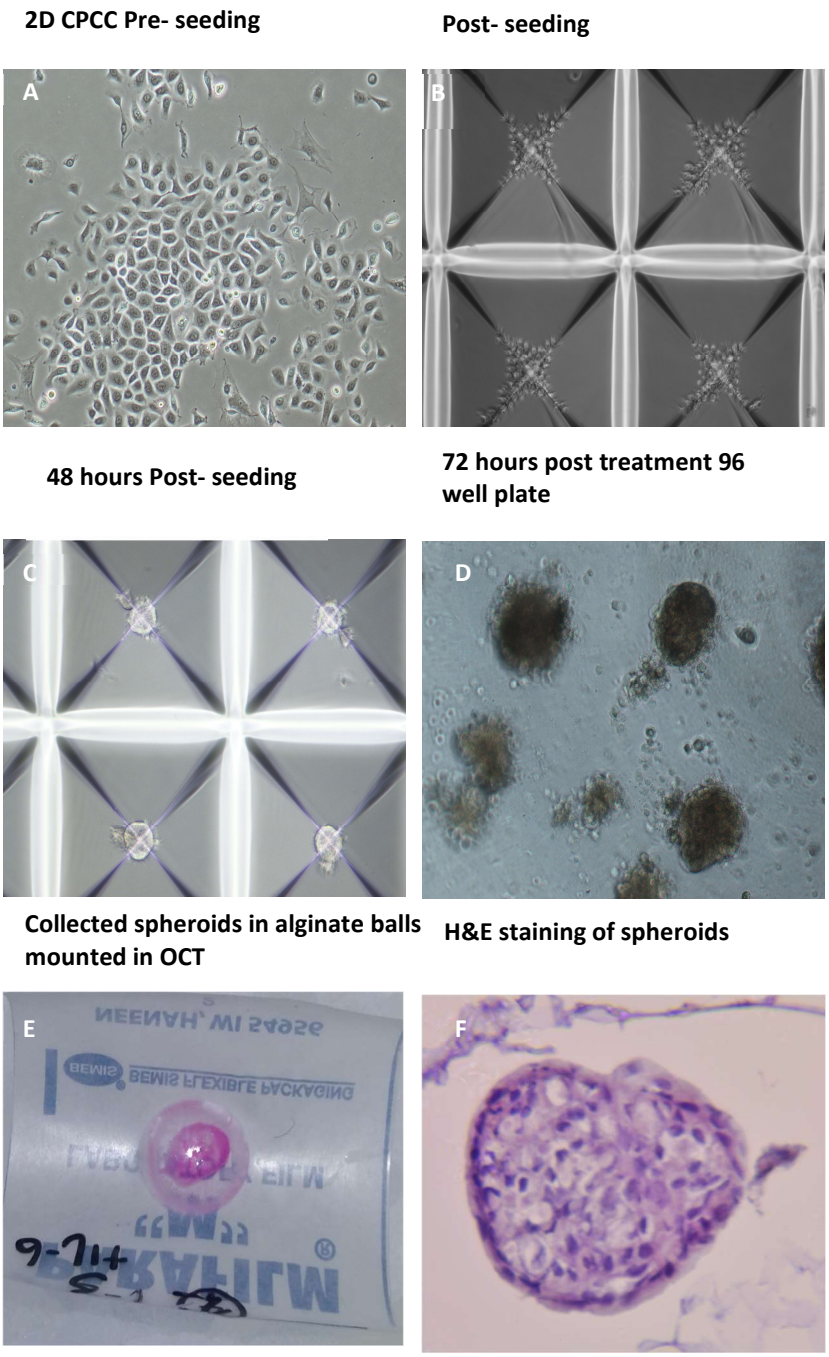

Figure 5-4: The generation and processing of CPCC spheroids.
A) Brightfield image of primary cylindroma cells in 2D. B) Primary cells were trypsinised and seeded into Aggrewell plates. C) Cells that had been in Aggrewell plates for 48 hours and had formed spheroids. D) Spheroids that had formed in 96 well plates and had been treated with an inhibitor. E) Spheroids that had been fixed were suspended in alginate, which solidified in calcium chloride. Theses alginate balls were then mounted in OCT with neutral red included for visualisation. F) H&E staining of spheroid sections.

5.3.2 CPCC spheroids have a protein signature that recapitulates human cylindroma tumours

The primary cells once they had formed CPCC spheroids were characterised, to determine a) if as a model of cylindroma they replicated the expression pattern of proteins that have previously been shown in *CYLD*-defective tumours, such as cytokeratins (CKs), TrkB, MYB and Stat3, and b) to gain insight into the 3D structure and behaviour of the spheroids, looking at the expression of cytoskeletal proteins such as β-actin and β-catenin alongside the proliferation marker Ki-67. Spheroid sections underwent antigen retrieval followed by indirect immunofluorescence staining with antibodies raised against the range of proteins mentioned above, that are expressed *in vivo*. No primary antibody controls were included for each antibody, examples of which are shown in Figure 5-5. The spheroid sections used for this analysis were generated from cells from one cylindroma tumour from one patient. A proportion of cells within the spheroids were shown to be proliferating, as a number of the cells were positive for Ki-67 expression (Figure 5-6A). The spheroids were found to express both CK14 and CK17, markers of keratinocytes and keratinocytes of the hair follicle respectively (Figure 5-6B & C). There was also cytoplasmic staining of the cytoskeletal protein β-actin, with a thicker border surrounding the spheroid and mainly cytoplasmic staining of the cell adhesion protein β-catenin observed in the spheroids (Figure 5-6D & E).

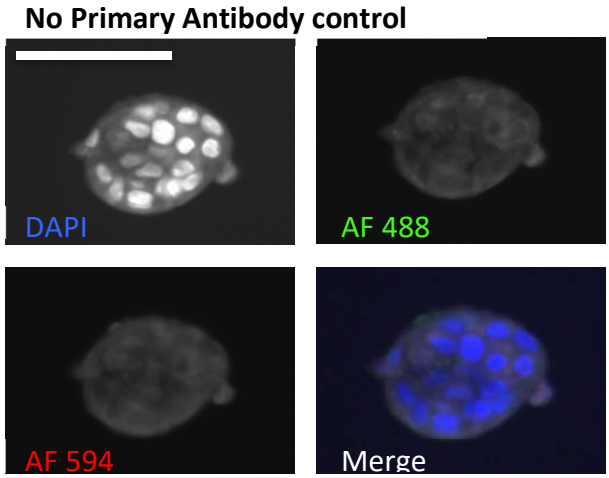

Figure 5-5: Representative images of no primary antibody controls for immunofluorescence staining of CPCC spheroid sections.
DAPI was used as a nuclear counterstain. All images 20x magnification. Scale bar represents 50μm.

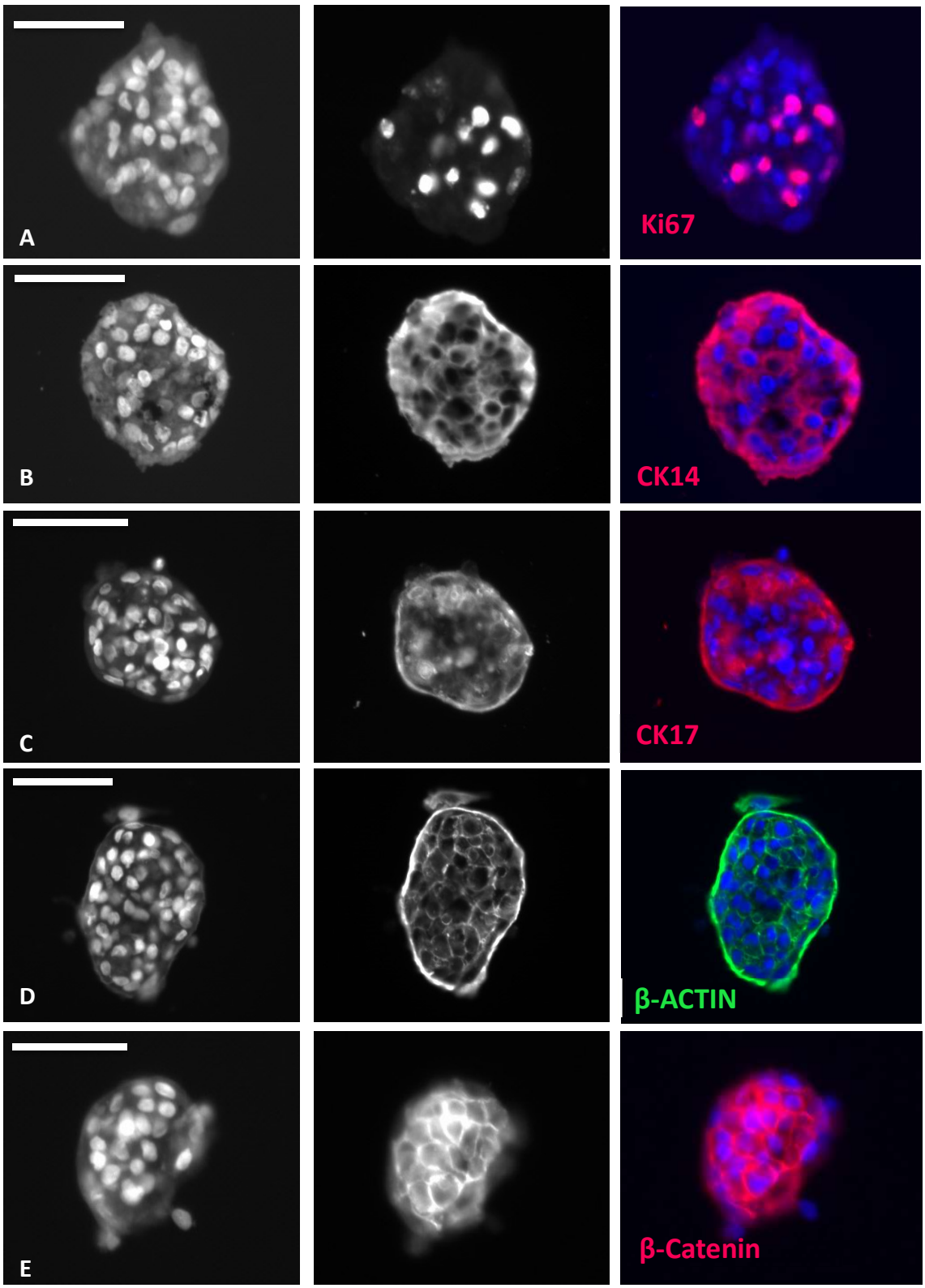

Figure 5-6: Characterisation of CPCC spheroids using immunofluorescence.
CPCC spheroid sections were probed with a panel of antibodies. A) The proliferation marker Ki-67, B & C) the keratinocyte marker CK14 and hair follicle keratinocyte marker CK17, D) the cytoskeletal protein β-Actin and E) the cell adhesion protein β-Catenin. DAPI was used as a nuclear counterstain.. DAPI images on the left, protein probed for middle images and merged images on the right. All images 20x magnification. Scale bar represents 50μm.

Further to this Stat3 was previously found to be over-expressed in *CYLD*-defective tumours (Chapter 4), and *p*-Stat3 (Tyr705) levels were increased in TrkB.T1 over-expressing HaCaT cells following stimulation with BDNF. Therefore the expression of TrkB, *p*-Stat3 (Tyr705) and Stat3 proteins was looked at in the spheroids, to corroborate these 3D cultures as models that replicate cylindroma tumours. Many of the spheroid cells were positive for TrkB, with some cells showing stronger cytoplasmic staining of TrkB (Figure 5-7A). The spheroids were also shown to express Stat3, with some cells displaying nuclear expression indicated by the pink-purple colour tone of the nuclei indicating active Stat3 (Figure 5-7B).

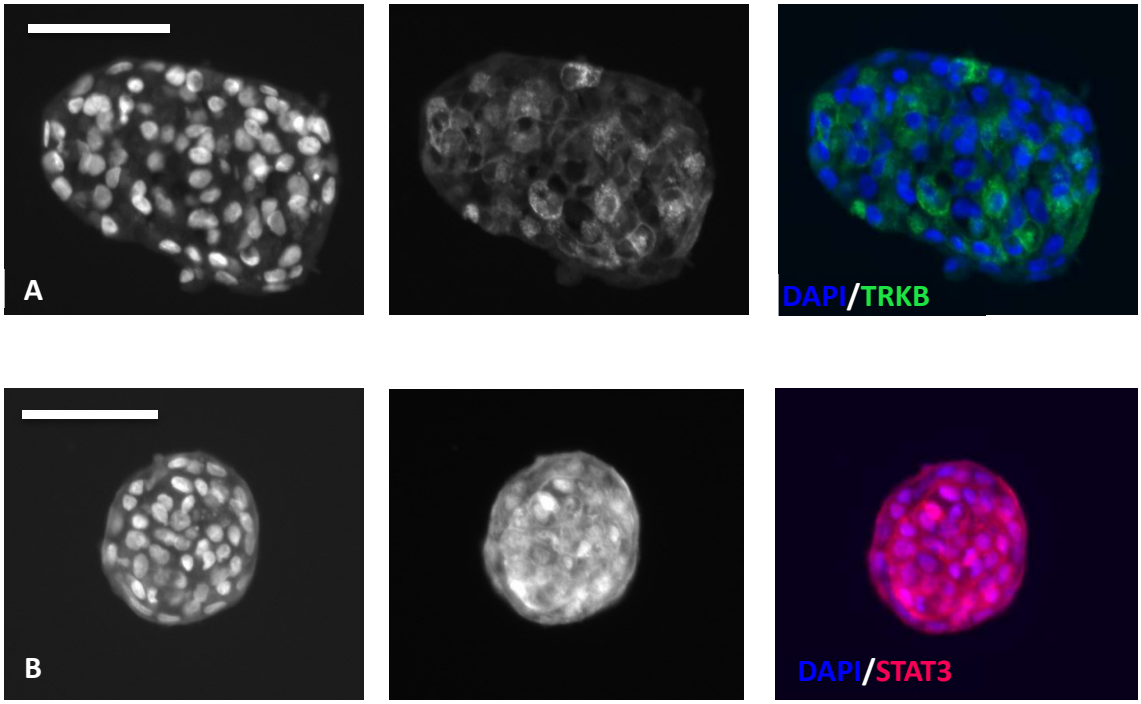

Figure 5-7: Expression of TrkB and Stat3 in CPCC spheroids.
CPCC spheroid sections were probed with antibodies for proteins that had previously been shown to be over-expressed in cylindromas A) TrkB and B) Stat3. DAPI was used as a nuclear counterstain. The images shown are representative of at least 3 different CPCC spheroids. DAPI images on the left, protein probed for middle images and merged images on the right. All images 20x magnification. Scale bar represents 50μm.

Some of the spheroid sections were also analysed using confocal microscopy. The enhanced detail again showed that TrkB wasn't expressed in all the cells. In those cells that were positive for TrkB, alongside membranous staining there was also a punctate/pigmented pattern of staining in the cytoplasm (Figure 5-8). This could suggest localisation of the TrkB receptor to certain organelle structures such as the mitochondria. Alternatively it could also represent the vesicular endocytosis and

transport of the receptor within the cell. Overall the results here show that the enhanced cell-cell contact that is promoted in CPCC spheroids leads to the maintenance of a protein expression profile that is similar to that seen *in vivo.*

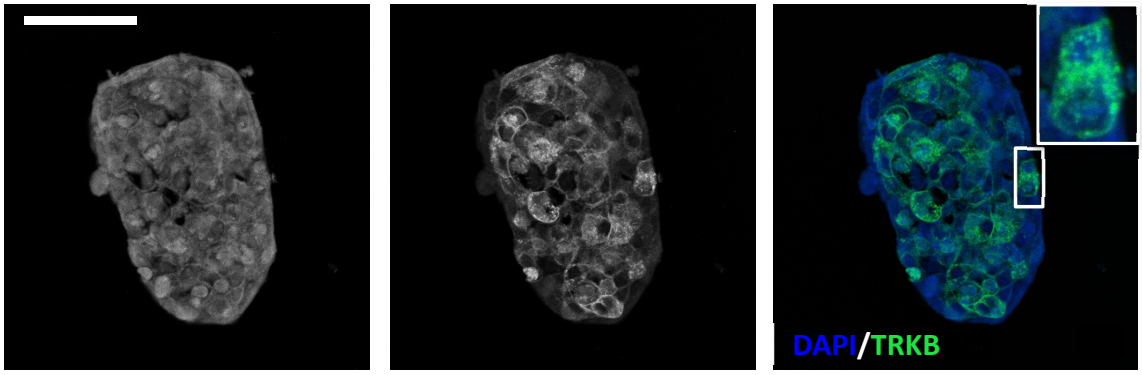

Figure 5-8: TrkB expression in CPCC spheroids visualised by confocal microscopy.
Spheroid sections were probed with a TrkB antibody. Confocal microscopy images are shown, with one image from a series of 19. White box indicates zoomed in section to show the punctate pattern of TrkB staining. DAPI was used as a nuclear counterstain. DAPI image on the left, TrkB centre image and merged image on the right. All images 20x magnification. Scale bar represents 50μm.

5.3.3 Stat3 signal transduction is modulated by BDNF and IL-6 in CPCC spheroids

To investigate the effect of BDNF on TrkB and Stat3, as was shown in the 2D cultures in Chapter 4, spheroid cultures were treated with 100ng/mL BDNF or 25ng/mL IL-6 for 30 minutes prior to being fixed, harvested and sectioned. Untreated spheroids were included as a negative control, whilst IL-6 was included as a positive control for Stat3 activation. Indirect immunofluorescence double staining was attempted on sections of the treated spheroids to see if TrkB and Stat3 were active within the same cells in response to BDNF. As expected it was shown that TrkB and Stat3 were both expressed in all spheroids regardless of treatment (Figure 5-9A&B). There was however no noticeable difference in the localisation of Stat3 between spheroids exposed to BDNF and untreated spheroids, with nuclear expression seen in both conditions, suggesting that Stat3 is active regardless of whether exogenous BDNF is present or not in contrast to the result in 2D. Meanwhile in IL-6 treated spheroids Stat3 expression was exclusively nuclear, showing that the positive control had worked (see Appendix). It was noted that the spheroids used for these experiments appeared a lot smaller than the previous samples. Thus with the quality of the images it could not be deduced whether cells in which Stat3 was deemed to be active were also the same cells that displayed strong TrkB expression.

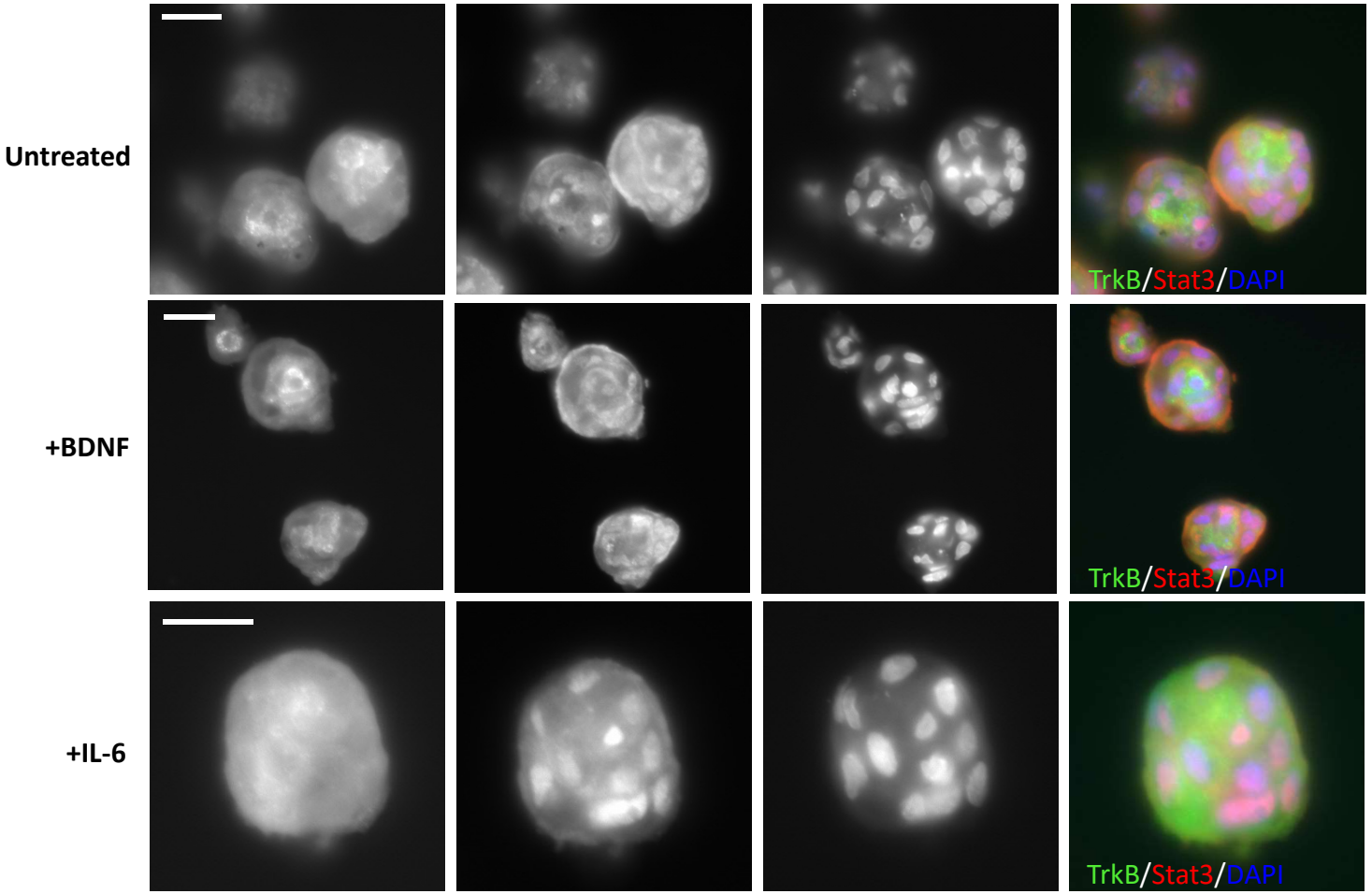

Figure 5-9: The effect of BDNF treatment on TrkB and Stat3 expression in CPCC spheroids. CPCC spheroids were initially treated with BDNF or IL-6 ligands for 30 minutes. Spheroids were then processed and sectioned. Sections of treated spheroids were double stained with TrkB and Stat3 antibodies. DAPI was used as a nuclear counterstain. Far left images TrkB, inner left Stat3, inner right DAPI and far right merged images. All images 40x magnification. Scale bar represents 20μm. (Data representative of *n* = 1 experiment).

5.3.4 CPCC spheroids are sensitive to Stat3 and Trk inhibition

As spheroid cultures are regarded as more biologically relevant models for testing compounds for drug development, the CPCC spheroids were assessed as models for drug assays, and whether as a model they were comparable to the 3D scaffold cultures (as seen in Chapter 4) in their response. The density at which to seed the cells into assay plates was initially determined by a viability assay which showed a linear trend with an increase in the number of cells correlating with an increase in the luminescence read out (Figure 5-10). 25,000 cells/well were therefore plated due to the level of luminescence and the number of available cells.

CPCC spheroids were established in 96 well ULA plates and treated for 72 hours with the Stat3 inhibitors NSC74859 and Stattic at the specified concentrations, with DMSO as a drug free control. These inhibitors were selected due to the scaffold cultures in Chapter 4 being more susceptible to these treatments compared to HaCaTs, out of the four compounds initially tested. The pan Trk inhibitor K252a was used as a positive control, as cylindroma cells grown on scaffolds had previously been shown to be sensitive to this treatment (surviving fraction (SF_{50}) 366nM) (Rajan, Elliott*, et al.*, 2011). Indeed the CPCC spheroids demonstrated increased sensitivity to the K252a inhibitor compared to the keratinocyte cell line HaCaT, at nanomolar concentrations (Figure 5-11). The CPCC spheroids were more sensitive than the HaCaTs in response to both NSC74859 and Stattic compounds, but with variability in the response between the individual cylindroma samples (Figure 5-12 & 13). It was also shown that the CPCC spheroids were more sensitive to Stattic than NSC74859, with a significant reduction in cell viability seen at nanomolar concentrations with Stattic compared to the high micromolar concentrations with NSC74859. This is in accordance with the scaffold data from Chapter 4.

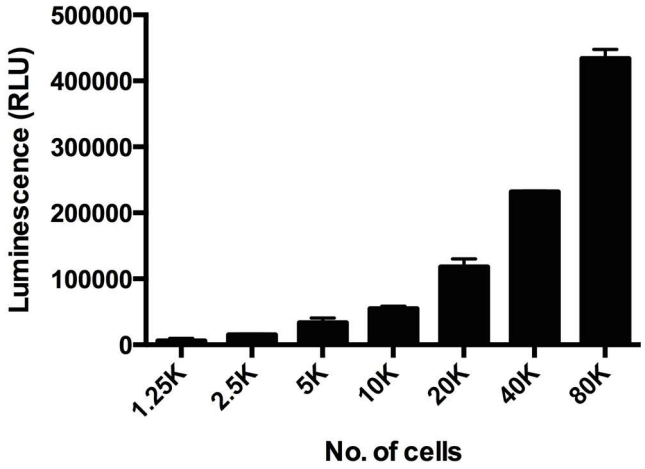

Figure 5-10: Cell viability assay to determine the number of cells to plate for CPCC spheroids.
Cells were plated into 96 well ULA plates at the specified numbers in triplicate and left for 72 hours for spheroid formation and cell viability assessed. Data are the mean of triplicate readings and error bars represent the SEM.

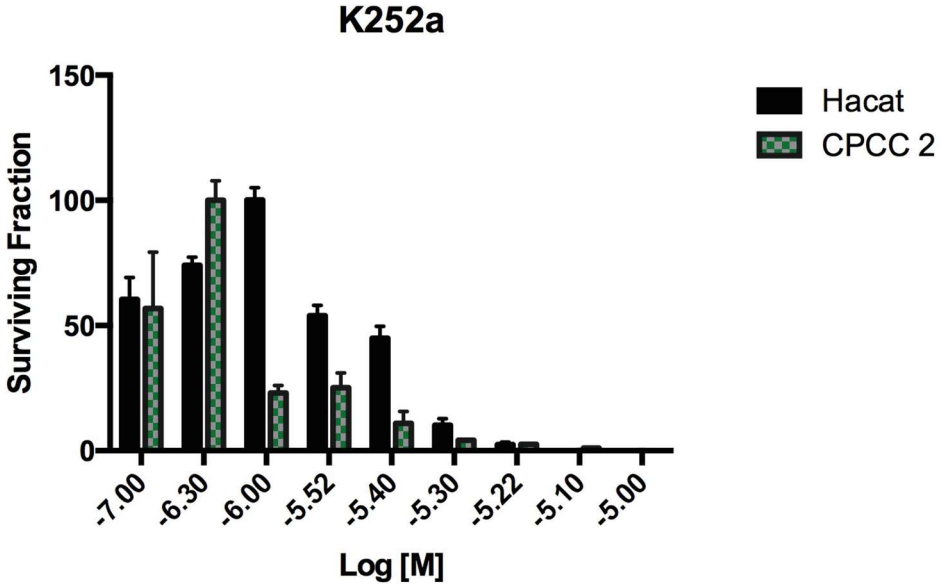

Figure 5-11: Trk inhibition of CPCC spheroids with K252a
Primary cylindroma and HaCaT cells were plated into 96 well ULA plates and left for 72 hours to allow for spheroid formation. Cells were then treated with K252a at a range of concentrations for 72 hours before cell viability was assessed using a luminescent assay. Data are the mean of triplicate readings and error bars represent the SEM.

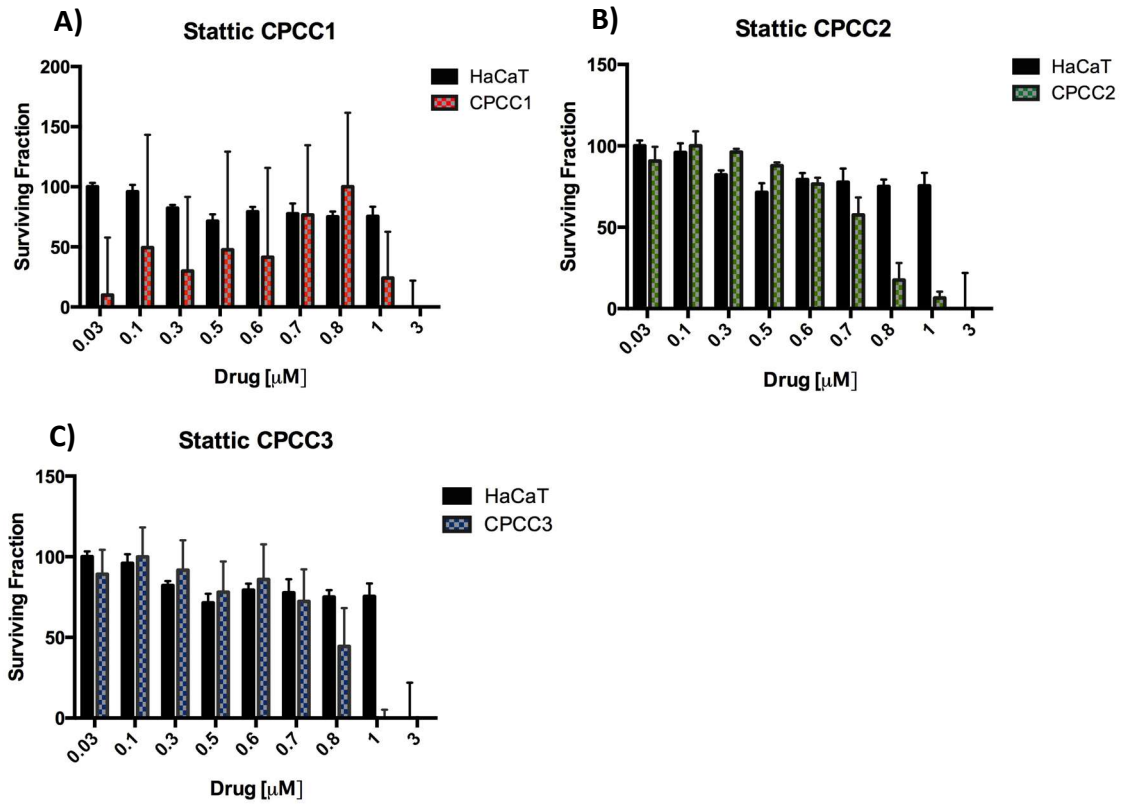

Figure 5-12: CPCC spheroids are susceptible to Stat3 inhibition by Stattic.
Primary cylindroma and HaCaT cells were plated into 96 well ULA plates and left for 72 hours to allow for spheroid formation. Cells were then treated with Stattic at a range of concentrations for 72 hours before cell viability was assessed using a luminescent assay. Each graph represents cells derived from an individual tumour from the same patient. Data shown are normalised and error bars represent the SEM of triplicate readings.

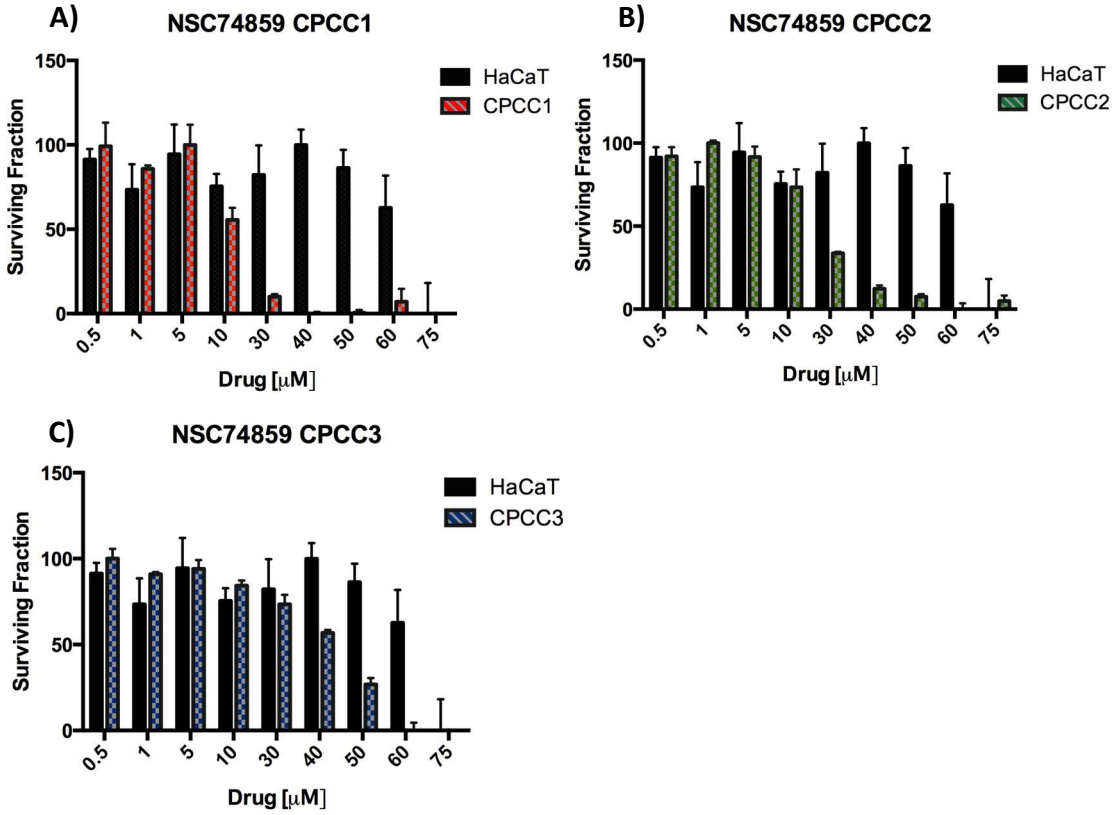

Figure 5-13: CPCC spheroids are susceptible to Stat3 inhibition by NSC74859.
Primary cylindroma and HaCaT cells were plated into 96 well ULA plates and left for 72 hours to allow for spheroid formation. Cells were then treated with NSC74859 at a range of concentrations for 72 hours before cell viability was assessed using a luminescent assay. Each graph represents cells derived from an individual tumour from the same patient. Data shown are normalised and error bars represent the SEM of triplicate readings.

5.4 Discussion

Although 2D cell culture has proven to be a valuable method for cell-based studies, as a technique it is cost-effective, reproducible, easy to handle, and enables the growth of a myriad of cell types, the limitations have increasingly become recognised. A key inadequacy being that it does not take into account the natural 3D environment of the cells; the forced monolayer morphology of cells grown on a flat surface in 2D cultures is at odds with the *in vivo* environment, in which almost all cells are surrounded by other cells and extracellular matrix (Antoni *et al.*, 2015; Breslin and O'Driscoll, 2013; Edmondson *et al.*, 2014; Rimann and Graf-Hausner, 2012). As a result, 2D cell culture experiments sometimes provide misleading and non-predictive data for *in vivo* responses (Hongisto *et al.*, 2013). This can waste valuable time and resources when looking for promising treatment options, as compounds are permitted to enter clinical trials which subsequently show little efficacy or unacceptable toxicity, or potential candidate targets and compounds are over-looked, making the 2D cell cultures inefficient models for drug development (Fang and Eglen, 2017). To this end advances have been made over the last decade in the generation of 3D spheroid cultures as a tool for biological discovery and drug-screening platforms, particularly in the field of cancer research (Kim J. B., 2005; Kimlin *et al.*, 2013). These 3D culture systems are born out of the natural tendency of some cell types to aggregate, allowing for cell-cell and cell-matrix interactions, which can both influence the cells behaviour due to alterations in cell signalling and gene expression (Birgersdotter *et al.*, 2005; Luca *et al.*, 2013). As such 3D cultured cells are considered to be more representative of their *in vivo* counterparts, making the 3D cultures more suitable model systems.

5.4.1 The development of novel CPCC 3D cultures-from scaffold to spheroid

The work included in this chapter showed the successful establishment of 3D spheroid cultures from cylindroma primary cell cultures for the first time (Figure 5-4). The CPCC spheroids were comparable, both in their expression of proteins and in their responses to the different drug treatments, to the scaffold cultures (Chapter4). This illustrated the viability of the CPCC spheroids as an alternative 3D culture model that can overcome some of the limitations of the scaffold cultures. The protocol was more amenable for primary cell cultures and downstream assays, not least because of the reduction in time from 4 weeks to 24-48 hours to establish the 3D cultures. This would allow for an increased throughput of cell samples from a larger cohort of tumours for

future study, with the additional benefits of reducing the infection risk and the acquirement of additional genomic mutations that come with long-term cultures. This leads to the primary cells maintaining a similar genomic profile to the tumour *in vivo.* The protocol also increased the robustness and reproducibility of the 3D cultures as there was assurance that the same number of cells could be seeded per well to produce spheroids that had a degree of homogeneity in their size. This is in contrast to the scaffolds where attempts are made to seed the same number of cells onto each scaffold, however there is no way of knowing how many cells have adhered to the scaffold. Furthermore due to using primary cylindroma cells from different patients there is variability in cell growth between the different CPCC samples, which can't be easily monitored under a microscope throughout the culture period due to the opaque nature of the scaffolds. This means that 2mm punches from different areas of the scaffold taken periodically for viability assays are required to monitor cell growth, which reduces the amount of working sample; an important consideration when cells are limited in supply due to their rarity. Overall this leads to an inefficient use of time and reagents and increases costs, which the spheroid cultures can overcome.

5.4.2 CPCC spheroids maintain stem cell like characteristics when grown in high calcium conditions

Within the skin, it is hypothesised that the loss of functional CYLD within the keratinocyte stem cell (KSC) niche of the hair follicle perturbs the normal proliferation and differentiation of the stem cells or their progeny to give rise to adnexal tumours such as cylindroma (Rajan and Ashworth, 2015; Verhoeft *et al.*, 2016). The ability of cells derived from primary cylindromas to form spheroids demonstrates that these cells maintain stem cell like characteristics when cultured in this 3D format, as the capacity to form cell aggregates in suspension is a hallmark of stem cells (Vollmers *et al.*, 2012), which is exemplified by the aggregate formation of mesenchymal stem cells (Cesarz and Tamama, 2016; Frith *et al.*, 2010). This is further evidenced by the fact primary murine keratinocyte cultures and cell cultures not enriched for KSCs are unable to form spheroids (Vollmers *et al.*, 2012).

In skin biology a widely accepted view is that calcium gradients control the differentiation of keratinocytes, with the calcium concentration increasing as immature keratinocytes in the basal cell layer of the epidermis proliferate, then

terminally differentiate and migrate through the spinal and granular layers to the outermost layer of the skin to replace fully differentiated keratinocytes (as reviewed by (Bikle *et al.*, 2012). Although a conflicting report found that the calcium concentration within the epidermal basal layer, of which the hair follicle is an extension of and is where epidermal stem cells reside, is as high as that found in the granular layer (Leinonen *et al.*, 2009). Indeed the aggregation and growth of CPCC spheroid cultures was achieved in the presence of a high calcium concentration in the medium. Whilst keratinocytes are usually propagated in a low calcium environment in 2D cell cultures to prevent differentiation of the cells, it does not induce the differentiation of keratinocyte stem cells in 3D culture (Vollmers *et al.*, 2012). Instead extracellular calcium is required for the formation of cell-cell contacts, allowing the formation of calcium-dependent cell junctions and inducing changes to overall cytoskeletal organisation (Watt *et al.*, 1984; Zamansky *et al.*, 1991). This was in accordance with the positive expression of the cytoskeletal protein β-actin and cell-adhesion protein β-catenin in the spheroids (Figure 5-6). In addition β-catenin is also a signal transducer in the Wnt signalling pathway (Valenta *et al.*, 2012), and as a pathway that has been shown to be dysregulated in *CYLD*-defective tumours (Rajan, Burn*, et al.*, 2011), the positive expression further supports that the model is representative of the tumours. However the predominantly cytoplasmic staining suggests the function of β-catenin is to promote cell-adhesion in these 3D cell cultures. The cytoplasmic location corresponds with interactions with the cell adhesion glycoprotein E-cadherin complexes, located at the cell membrane, as opposed to a nuclear location in a downstream response to active Wnt signalling (Gottardi and Gumbiner, 2004). Furthermore in previous studies nuclear β-catenin was found in a minority of cylindroma cells, and at the periphery of tumour islands (Rajan, Burn*, et al.*, 2011). This suggests that the tumour stroma may be necessary for activated Wnt/β-catenin signalling within the cells, and as this is lacking in cell culture it may be that this pathway is not active.

The positive Ki-67 expression that was shown in a proportion of the cells within the spheroids (Figure 5-6) indicates that these cells can maintain a proliferative phenotype in 3D spheroid culture. Indeed cylindromas have been shown to have increased expression of α2β1 integrins (Tunggal *et al.*, 2002), which are part of a family of cell

surface receptors that mediate cell adhesion. Interestingly up-regulated expression of these integrins is associated with keratinocytes with the highest proliferative potential, the keratinocyte stem cells (Jones and Watt, 1993; Levy *et al.*, 2000). This evidence is concurrent with the argument that enhanced cell adhesion promoted by the high calcium environment maintains stem cell like properties of the primary cells, with proliferation an indicative marker of stem cells or undifferentiated progenitors. Altogether these findings strongly suggest that cylindroma primary cells cultured in a higher calcium 3D environment behave like their *in vivo* counterparts, and makes this culture system a representative *in vitro* model in which to explore cylindroma biology.

Calcium signalling could be a potential area of interest to take forward into future studies of *CYLD*-defective tumours with these models. Despite the well-established role of calcium in the differentiation of keratinocytes (Bikle *et al.*, 2012), a direct role for calcium in hair follicle cycling is unclear. As normal keratinocyte differentiation is clearly perturbed in *CYLD*-defective tumours it is not unreasonable to hypothesise that calcium homeostasis may also be altered. The TRP (transient receptor potential) channel family are cation channels that are permeable to calcium and can modulate intracellular calcium signalling through their activation (Gees *et al.*, 2010). The TRP family of receptors are recognised to have a contributory role to many physiological processes within the skin ranging from sensation to skin homeostasis (Caterina and Pang, 2016). The TRPA1 (transient receptor potential ankyrin 1) family member has been shown to be a target of CYLD, with deubiquitination of TRPA1 increasing the cellular pool of the receptor (Stokes *et al.*, 2006). This is interesting as the structurally similar family member TRPV1 (transient receptor potential vanilloid 1) is expressed within the hair follicle and is involved in negatively regulating human hair growth by inhibiting proliferation and down-regulating known hair growth promoters (Bodo *et al.*, 2005). Of note was the finding that in outer root sheath keratinocytes the cellular actions of TRPV1 were shown to be calcium dependent, but activation of TRPV1, at least by capsaicin, did not affect their terminal differentiation. This indicates that calcium has alternate biological functions in these cells that are independent of the promotion of differentiation (Bodo *et al.*, 2005). Furthermore in breast cancer cells activation of TRPV1 also caused inhibition of cell growth (Weber L. V. *et al.*, 2016). It is therefore speculated that as a member of the same TRP family it too could be a target

of CYLD, whose expression levels are possibly altered due to ubiquitination of the receptor, and subsequent changes in calcium signalling within the cell may promote cell growth. Alternatively in response to BDNF, TrkB.T1 elicits the release of calcium from intracellular stores in glia cells (Rose *et al.*, 2003). As TrkB.T1 is over-expressed in *CYLD*-defective tumours, this could represent another mechanism that leads to alterations in calcium signalling within the tumour cells and promote tumour formation.

5.4.3 The CPCC spheroids protein expression profile reflects that of the *in vivo* tumour

Spheroid cultures were characterised using indirect immunofluorescence. The spheroids were found to express keratinocyte markers, such as CK14 and CK17 (Figure 5-6), which are expressed in 2D and 3D scaffold CPCC cultures, but more importantly by the tumours *in vivo* (Meybehm and Fischer, 1997; Rajan, Elliott*, et al.*, 2011). CK14 is normally expressed in the proliferative basal layer of keratinocytes of stratified epithelia, which along with its partner CK5 decreases in expression as the cells differentiate (Alam *et al.*, 2011; Coulombe *et al.*, 1989). It is also expressed in the hair follicle (Coulombe *et al.*, 1989). Likewise CK17 is recognised as a marker for keratinocytes within the outer root sheath of the hair follicle, as it is a regulator for hair follicle cycling (Tong and Coulombe, 2006; Troyanovsky *et al.*, 1989). Recently CK17 expression was identified as a marker of another cutaneous lesion of the hair follicle, keratoacanthoma (Leblebici *et al.*, 2017). Expression of both CK14 and CK17 reflects that the CPCC spheroids model tumour biology by maintaining the expression of these keratinocyte markers, and is in keeping with the current consensus that the hair follicle is the site of origin for cylindromas (Massoumi, Podda*, et al.*, 2006; Sellheyer, 2015). Additionally their expression also indicates that the majority of the CPCC cells that form the spheroids are keratinocytes. As these are primary samples, a heterogeneous population of cell types can be found, indeed in 2D CPCC occasional fibroblasts are seen. Specific markers of fibroblasts would have to be applied to determine if these cell types were incorporated in the spheroids, but having a mixture of cells would again recapitulate the *in vivo* environment more so as the cells would be surrounded by those with which they live within the tumour. This is akin to alternative 3D skin models such as LSEs, where keratinocytes are grown atop of a support/lattice populated with fibroblasts (O'Leary *et al.*, 2002). The expression of TrkB further

supported CPCC spheroids as a tumour model. Whilst the majority of the cells had membranous staining of TrkB, aligning with its expression as a receptor protein, there was variation in the cytoplasmic expression, possibly indicating the cells in which TrkB signalling is active (Figure 5-7 & 8). The punctate pattern of staining was also of interest, suggesting the localisation of TrkB to certain cellular structures such as the mitochondria, the membranes of which TrkB has previously been shown to localise (Wiedemann *et al.*, 2006), or even endocytic vesicles for the recycling of the receptors (Chen Z. Y. *et al.*, 2005; Huang S. H. *et al.*, 2009) This could be determined with the use of a mitochondrial marker to see if the signal for both TrkB and mitochondria co-localised within the cells.

Finally due to the finding of Stat3 activation downstream of TrkB.T1 signalling in Chapter 4, TrkB/Stat3 immunofluorescence double staining was carried out on spheroids that had been treated with the TrkB ligand BDNF. Unfortunately the imaging of the spheroids was not clear enough, possibly due to the spheroids being too small, to conclusively state if activated TrkB signalling occurred in the same cells as active Stat3. However it was shown that there was no visible difference in the localisation of Stat3 between the treated and untreated spheroids (Figure 5-9). Within some untreated cells, Stat3 was shown to localise in the nucleus, indicating that it was active even in the absence of exogenous BDNF. This was in direct contrast to the 2D CPCC cultures where there was a clear alteration in the localisation of Stat3 with the addition of BDNF from the cytoplasm to the nucleus. Whilst on one hand this could demonstrate that Stat3 activity is not dependent on the activation of TrkB signalling. It may also illustrate that as a 3D spheroid culture, the cells may instead be producing their own supply of BDNF stimulated by either an unknown mechanism, Stat3 itself or even an increase in Trk expression, as it was previously shown that Trk expression is increased in 3D CPCCs compared to 2D CPCCs (Rajan, Elliott*, et al.*, 2011). This could therefore be activating Trk and driving Stat3 activation in an autocrine feedback loop, much like the one that was demonstrated by Chen *et al.* in lung cancer cells (Chen B. *et al.*, 2016). Again this highlights the suitability of 3D cultures as *in vitro* models, as the cells display signalling behaviours that are reminiscent of the *in vivo* tumours, even though a source of BDNF is still to be determined. In the future it would be interesting to carry out ELISA assays on the spheroids and the growth medium, to see if the

spheroid cultures produced BDNF, or other secreted ligands, to create signalling feedback loops. The previous attempts in 2D culture were not successful, which could be due to the lower levels of expression in the 2D CPCCs as discussed in Chapter 4. In addition this experiment was only carried out once due to difficulties with obtaining spheroid sections on slides again due to the small size. The spheroids therefore could be cultured for longer or a larger numbers of cells plated in future to allow for larger spheroids to form, and also to improve the clarity of the immunofluorescence staining.

5.4.4 CPCC spheroids are targetable with Stat3 inhibitors

In Chapter 4 Stat3 had previously been identified as a downstream target of interest of TrkB.T1 signalling, that was over-expressed in cylindromas and thus led to an *in vitro* treatment assay to determine if the cells would respond to Stat3 inhibition. These experiments were repeated on the CPCC spheroids to evaluate the sensitivity of this 3D culture method in comparison to the CPCC scaffolds. Cells grown in 3D are more resistant to treatment (Edmondson 2014) and HepG2 liver cells grown on these scaffolds had been shown to be less susceptible to lower concentrations of methotrexate compared to 2D cultures (Bokhari *et al.*, 2007). CPCC spheroids were sensitive to Stat3 inhibition, showing a reduction in cell viability, indicating that the loss of catalytically active CYLD increases the dependency of the cylindroma cells on Stat3 for their survival (Figure 5-12 & 13). There was a slight variation in response from the different CPCC cultures, which could be due to the heterogeneity of the cells within the samples. Also these results replicated the response seen in the scaffold cultures (Chapter4), with responses seen at micromolar and nanomolar concentrations for NSC74859 and Stattic respectively. This finding demonstrates that as a 3D cell culture model CPCC spheroids are comparable to CPCC scaffolds, and aspects of the cell biology are maintained between the two 3D methods. However in addition to the constraints of scaffold cultures mentioned above, the use of the scaffolds in drug assays exposes further limitations of the method. The potential for inconsistency in cell growth across the scaffold could give a bias to the results, as there is uncertainty of whether the result from a 2mm punch is reflective of the effect of the drug or that there were fewer cells in the first place. Setting up in triplicate does aim to minimise this but it can lead to large standard error. On the other hand the CPCC spheroids allows for control over the number of cells plated and assumption that the same

number of cells are being treated in each well meaning that experiments are easier to replicate.

The CPCC spheroids do have their own weaknesses with regards to reproducibility however. The potential morphological heterogeneity of the spheroids formed with regards to size and shape, are two areas of variability that could introduce a bias to drug assay results; the extent to which this heterogeneity contributes to data variability within spheroid cultures was recently explored by Zanoni *et al*. (Zanoni *et al.*, 2016). Larger spheroids (>500μm diameter) are structured into zones of cells at different proliferative stages (Figure 5-2) alongside developing chemical gradients. Having spheroids of different sizes may affect how effectively the drug can penetrate all of the cells causing discrepancy in the cells level of exposure, and the way in which the cells respond due to varying proportions of cells at different cell cycle stages. Whilst this may be a feature that is more reflective of the *in vivo* environment, a lack of vasculature in this model system means that some of the pharmacological complexities cannot be mimicked and in an experimental set-up control is needed over such variables. Equally irregular, non-spherical shaped spheroids were found to have alterations to the dimensions of the inner core and thickness of the exterior cell layer, alongside more frequent budding of secondary spheroids. Together this led to a significant increase in viability compared to spherical spheroids of the same volume, which again could impact the response of the cells to treatment (Zanoni *et al.*, 2016). To reduce data variability they suggested pre-selection criteria for spheroids that are homogenous in shape and size prior to treatment, using open source software for monitoring and selection (Piccinini, 2015; Piccinini *et al.*, 2015).

Indeed the parameters of size and shape were not specifically investigated or accounted for in the therapeutic screening of the CPCC spheroids included in this thesis. However in the monitoring of the generation of spheroid cultures it was observed that multiple spheroids formed in each of the 96 wells, but no measurements were taken as to the number or size of the CPCC spheroids formed in each well. The lack of formation of a single spheroid may be due to the fact that these are heterogeneous populations of primary cells, that may not all have the capability to aggregate and form a spheroid. In light of the limitations mentioned above though it

would indicate that the protocol needs optimising for future experiments to increase the robustness of the methodology. Possible ways in which to address these issues include more precision in the monitoring of the spheroids, using available resources such as AnaSP (Piccinini, 2015), or consider the generation of the spheroids in another vessel, from which homogenously sized spherical spheroids can be pre-selected and transferred to the 96 well ULA plate to ensure one spheroid per well. Whilst also taking into consideration the handling time for this protocol and not substantially adding to the workload.

The reagents used for the cytotoxicity assays of the spheroids are a final consideration, to ensure they can reliably penetrate the cells. In this instance the CellTiter-Glo® viability assay (Promega) was used, which showed an increasing linear trend when tested on increasing cell numbers (Figure 5-10) indicating that it can still penetrate the spheroids and give a reliable readout. Also the spheroid cultures were only left for 4 days prior to treatment and although not assessed experimentally, it is assumed that they would not have grown to 500μm in diameter in this time, so would still be small enough for the reagent to penetrate the spheroids. However it may be beneficial in the future to adopt the CellTiter-Glo® 3D viability assay. This works on the same principle as the 2D assay in detecting ATP levels as a marker of metabolically active cells, but has increased lytic capacity to allow for permeation through larger spheroids and shows superiority as spheroids reach 350μm in diameter, as shown in a technical resource from Promega (Valley *et al.*, 2014).

5.4.5 Conclusions

Primary cell cultures can be utilised to explore disease biology and to assess the efficacy of targeting identified dysregualted pathways with therapeutic agents. However when grown in 2D they do not best represent the *in vivo* sitatuion they are trying to model. In this chapter it has been demonstrated in this chapter that 3D spheroid cultures derived from primary cylindroma cells can be achieved, and that the increased cell-cell contact of the spheroids promotes an expression profile that models the *in vivo* tumour. Whilst having established 3D cultures on scaffolds previously, the spheroids represent a more amenable approach, which can be taken forward into

downstream applications. Yet they do hold their own limitations in size and reproducibility, which will require further optimisation.

Chapter 6

Concluding remarks and future directions

6 Chapter 6: Concluding remarks and future directions

CYLD cutaneous syndrome is a rare inherited condition in which painful and disfiguring tumours, namely cylindroma, spiradenoma and trichoepithelioma occur (Rajan, Langtry*, et al.*, 2009), yet at present there are no curative treatments. The only option for patients at present is repetitive surgery throughout a patient's lifetime to control tumour burden (Rajan, Trainer*, et al.*, 2009).

The MYB-NFIB fusion gene was one such target of interest that had previously been found in sporadic cylindromas (Fehr *et al.*, 2011) and considered an oncogenic hallmark in salivary gland tumours (Persson *et al.*, 2009). Genetic drivers of cylindromas beyond CYLD are poorly characterised, and hence an aim of this thesis was to see if this fusion transcript was also expressed in inherited cylindromas. Using RT-PCR and FISH analysis it was found that the inherited cylindromas were negative for the fusion transcript but instead were found to overexpress MYB, as shown by immunohistochemical analysis, which is also seen in the sporadic tumours in the absence of the fusion gene (Fehr *et al.*, 2011). A significant difference in expression was observed between the tumours and perilesional controls. Furthermore knockdown of MYB in primary cylindroma cells caused a reduction in cell viability, demonstrating that the cells were dependent on the expression of MYB for their survival. MYB is a transcription factor that has roles in regulating the proliferation and differentiation of stem cell niches (Lieu and Reddy, 2009; Malaterre *et al.*, 2007). As tumours of hair follicle origin it is interesting that within the mouse hair follicle, specific MYB expression was found in a population of cells just below the bulge region in which the stem cell niche is found, suggesting that MYB may be involved in regulating the activation of quiescent stem cells and commitment to differentiation of the cells (Vesela *et al.*, 2014). Therefore perturbed expression of MYB in human hair follicle stem cells expressing catalytically defunct CYLD could have a role in promoting hair follicle tumour formation.

To investigate the promotion of MYB overexpression in cylindromas both overexpression of mutated forms of *CYLD* and silencing of *CYLD* were utilised. This showed that truncating mutations of CYLD did not have any obvious effect on MYB

expression when compared to controls, suggesting that mechanisms independent of CYLD account for the increased expression in tumours. This was in contrast to the knockdown studies in which an increase in MYB expression was observed in the HaCaT, keratinocyte cell line. But as this was not a consistent result between the two shRNAs it requires further investigation with additional shRNAs to ensure the result is not accountable to off target effects. Alternatively MYB expression is regulated by a transcriptional attenuator sequence in the first intron, which can be overcome by NFκB (Pereira *et al.*, 2015), alongside the presence of NFκB binding sites in the *c-MYB* promoter (Lauder *et al.*, 2001). As the role of CYLD remained inconclusive it was hypothesised that dysregulated NFκB signalling in the tumour cells, due to a lack of functional CYLD (Brummelkamp *et al.*, 2003), may be causing increased MYB expression instead. To investigate, primary cylindroma cells were treated with NFκB inhibitors, however this caused a surprising increase in MYB expression as opposed to the expected decrease, suggesting that the NFκB pathway may act in a suppressive manner and alternate mechanisms are responsible for driving MYB expression in the tumours. Yet the same trend was seen in the HaCaT cells, which may also imply that inhibition may alter the ratio of certain MYB isoforms. This requires further clarification in future studies, with inhibition of NFκB in a larger cohort of primary samples.

Indeed a novel finding of this work was that in HaCaTs and primary cylindroma cells an 89kDA alternate isoform was observed at the protein level, which corresponds to MYB 9B (O'Rourke and Ness, 2008). Analysis of exon junctions from the RNA-seq data showed that the frequency of transcripts including these alternate exons was increased in the tumours, with MYB 9B the most predominant alternate form after c-MYB (75kDA), corresponding with the protein expression levels shown by Western blot. At present knowledge about the function of alternate isoforms of MYB is limited, especially in a keratinocyte cell context, although studies have demonstrated that the different splice variants can activate unique sets of target genes (Zhou and Ness, 2011). Therefore an alteration in the splicing of MYB and the ratio of alternate isoform expression may demonstrate an additional molecular event that has the potential to contribute to tumour formation. These isoforms will need further characterisation, in the *CYLD*-defective tumours using overexpression studies similar to the ones used in

this study for TrkB. The implications of MYB overexpression makes MYB an attractive therapeutic target to follow up and characterise further in *CYLD*-defective tumours in future work. In addition with the development of inhibitory MYB compounds (Dai Y. H. *et al.*, 2016; Uttarkar *et al.*, 2016) a natural progression based on the findings of this thesis is to perform preclinical experiments on 3D primary cell cultures and explore the translational potential of MYB as a treatment in the clinic.

Another target of interest that was explored in this thesis was the receptor tyrosine kinase TrkB, having previously found that TrkB was differentially expressed on a microarray comparing *CYLD*-defective tumours to perilesional control skin (Rajan, Elliott*, et al.*, 2011). Using RT-PCR and qPCR it was shown that in cylindromas the truncated TrkB.T1 isoform was the predominantly expressed isoform in the tumours, which was confirmed at the protein level by Western blot. This was in keeping with previous *in vitro* work in keratinocytes (Marconi *et al.*, 2003), however in cylindromas, this isoform was increased in tumours compared to normal skin. In addition expression of the TrkB receptors cognate ligand, BDNF was also increased in the tumours, suggesting that a stimulatory autocrine, signalling loop may exist in cylindromas.

To investigate the role of the TrkB.T1 isoform in the tumours overexpression of TrkB.T1 was achieved in the biologically relevant HaCaT cell line and HEK293T cells. TrkB.T1 was shown not to promote proliferation but possibly cell survival, by using cell viability and colony forming assays. As has been found with MYB, alternate isoforms can have their own distinct functions, and with TrkB.T1 not having a kinase domain it is only recently that its signalling capabilities have started to be realised (Ohira *et al.*, 2005; Rose *et al.*, 2003). A key novel finding of this work was that when cells overexpressing TrkB.T1 were exposed to BDNF this caused an increase in phosphorylation of Stat3 at the Tyrosine 705 residue that was replicated in primary cylindroma cell cultures. The phosphorylation of Stat3 at Tyr705 causing activation of Stat3, where it can then enter the nucleus and induce expression of target genes such as those involved in cell proliferation and cell cycling (Yu H. *et al.*, 2014), which are beneficial to aberrant growth of the tumour cells. The altered localisation of Stat3 was shown using immunofluorescence, in primary cylindroma cell cultures exposed to

BDNF treatment and coincided with altered expression of Stat3 target genes observed in the tumour microarray data.

Having identified Stat3 as a potential downstream target of TrkB, it was determined whether this was a mechanism by which the overexpression of TrkB.T1 could promote cell survival. Treatment of primary cylindroma cells grown on 3D scaffolds with Stat3 inhibitors in particular NSC74859 and Stattic caused a reduction in cell viability at micromolar and nanomolar levels respectively, demonstrating a dependency of the cells on Stat3 and validating Stat3 as a potential therapeutic target. To improve our understanding further future experiments would include identifying a direct link between TrkB.T1 and Stat3 in the cylindroma cells which could be achieved using knockdown studies to see if silencing of TrkB leads to a reduction in Stat3 phosphorylation in response to BDNF stimulation. In addition immunoprecipitation studies could be utilised to identify other potential interacting partners of TrkB.T1, which may have a pathogenic role in this highly disfiguring disease and may also be targetable.

For exploring targets in CYLD cutaneous syndrome, the need for robust experimental tools is reinforced by the lack of *in vivo* mouse models that can replicate the human phenotype, meaning that translation of experimental findings into the clinic is reliant on primary cell cultures at present. Although with access to patient tumour samples and a cutaneous tumour type, development of patient-derived xenograft (PDX) models could be considered for future studies. Either *CYLD*-defective tumour cell suspension or parts of the tumour tissue could be engrafted onto immunodeficient mice, creating models that could bridge the gap between the culture dish and clinical applications, providing a useful tool for validating *in vitro* findings and evaluating preclinical investigations (Lai *et al.,* 2017).

As further insights into tumour biology are gained in the era of transcriptomics and sequencing, leading to identification of potential targets such as MYB and Stat3 for therapeutic intervention, *in vitro* models are invaluable tools for validation of experimental findings. 3D cell culture is considered a more representative model and is increasingly evolving as a technique for drug screening platforms for disease

treatments, especially in cancer research (Kimlin *et al.*, 2013). Therefore in this thesis for the first time cylindroma spheroid cultures were generated, as previous scaffold methods were time consuming and difficult to monitor. Using immunofluorescence the 3D spheroid cultures recapitulated the expression profile of the tumours, and would be a valuable tool to develop further and take forward for future screening of candidate compounds as more knowledge is gathered at the molecular level. Indeed Stat3 inhibition reduced cell viability of cylindroma spheroids.

In conclusion both MYB and Stat3 have been identified as potential therapeutic targets for *CYLD* cutaneous syndrome, and warrant further preclinical investigation. Concurrently the establishment of primary cylindroma spheroid cultures, that are more biologically representative of the *in vivo* tumours, allows for enhanced translational relevance of such investigations and will aid with bringing potential non-surgical treatment strategies for this highly disfiguring disease into the clinic.

7 Appendices

Appendix A

Sample	Sex	Tumour type
1*	F	Cylindroma
2**	F	Spiradenoma
3***	F	Cylindroma
4	M	Spiradenoma
5**	F	Spiradenoma
6**	F	Spiradenoma
7****	M	n/a
8****	M	Spiradenocylindroma
9*	F	Spiradenocylindroma
10***	F	n/a
11***	F	Spiradenocylindroma
12***	F	Cylindroma
13*	F	Spiradenoma
14**	F	Spiradenoma
15	F	Cylindroma
16	F	Spiradenoma

Table 7-1: *CYLD*-defective tumour samples used for RNA-seq.

Appendix B

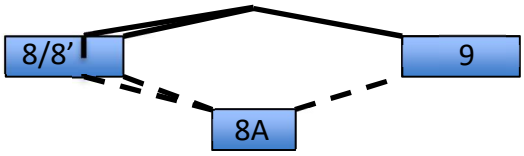

Sample	Exon 8/9	8/8A	8'/9	8'/8A	8A/9	8/10	8'/10
Control (1)****	6	-	15	-	-	-	-
Control (2)*	22	-	-	-	-	-	-
Control (3)***	-	-	19	-	-	-	-
Control (4)	1	-	39	-	-	-	-
1*	28	-	193	-	-	-	4
2**	84	-	460	2	32	-	-
3***	82	6	526	-	36	-	-
4	29	1	162	1	19	-	-
5**	39	5	282	6	8	-	-
6**	49	-	254	2	8	-	-
7****	94	-	678	7	24	-	-
8****	114	2	621	14	31	-	8
9*	76	-	269	-	-	-	-
10***	84	-	510	7	22	-	-
11***	75	-	510	-	-	-	-
12***	71	12	363	-	9	-	5
13*	88	-	465	2	21	-	-
14**	30	-	204	5	5	-	-
15	97	2	692	8	44	-	8
16	41	4	243	4	12	-	-

Table 7-2: RNA-seq exon junction read depth counts for MYB exon 8 and alternate exons 8' and 8A from a panel of *CYLD*-defective tumours and perilesional skin controls.

Appendix B (continued)

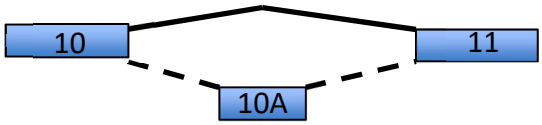

Sample	Exon 10/11	10/10A	10A/11	9/11
Control (1)****	29	-	-	-
Control (2)*	29	-	-	-
Control (3)***	33	1	1	-
Control (4)	47	-	-	-
1*	435	40	40	-
2**	878	29	50	-
3***	987	6	22	-
4	158	9	8	-
5**	741	-	-	-
6**	301	-	-	-
7****	1109	19	71	-
8****	1271	10	34	-
9*	590	8	37	-
10***	791	14	44	-
11***	954	2	30	-
12***	538	-	-	-
13*	827	14	24	-
14**	347	10	21	-
15	1089	9	57	-
16	513	2	15	-

Table 7-3: RNA-seq exon junction read depth counts for MYB exon 10 and alternate exons 10A from a panel of *CYLD*-defective tumours and perilesional skin controls.

Appendix C

Receptor Tyrosine Kinases

	Target	Phosphorylation Site	Family
1	EGFR/ErbB1	pan-Tyr	EGFR
2	HER2/ErbB2	pan-Tyr	EGFR
3	HER3/ErbB3	pan-Tyr	EGFR
4	FGFR1	pan-Tyr	FGFR
5	FGFR3	pan-Tyr	FGFR
6	FGFR4	pan-Tyr	FGFR
7	InsR	pan-Tyr	Insulin R
8	IGF-IR	pan-Tyr	Insulin R
9	TrkA/NTRK1	pan-Tyr	NGFR
10	TrkB/NTRK2	pan-Tyr	NGFR
11	Met/HGFR	pan-Tyr	HGFR
12	Ron/MST1R	pan-Tyr	HGFR
13	Ret	pan-Tyr	Ret
14	ALK	pan-Tyr	LTK
15	PDGFR	pan-Tyr	PDGFR
16	c-Kit/SCFR	pan-Tyr	PDGFR
17	FLT3/Flk2	pan-Tyr	PDGFR
18	M-CSFR/CSF-1R	pan-Tyr	PDGFR
19	EphA1	pan-Tyr	EphR
20	EphA2	pan-Tyr	EphR
21	EphA3	pan-Tyr	EphR
22	EphB1	pan-Tyr	EphR
23	EphB3	pan-Tyr	EphR
24	EphB4	pan-Tyr	EphR
25	Tyro3/Dtk	pan-Tyr	Axl
26	Axl	pan-Tyr	Axl
27	Tie2/TEK	pan-Tyr	Tie
28	VEGFR2/KDR	pan-Tyr	VEGFR

Signaling Nodes

	Target	Phosphorylation Site	Family
29	Akt/PKB/Rac	Thr308	Akt
30	Akt/PKB/Rac	Ser473	Akt
31	p44/42 MAPK (ERK1/2)	Thr202/Tyr204	MAPK
32	S6 Ribosomal Protein	Ser235/236	RSK
33	c-Abl	pan-Tyr	Abl
34	IRS-1	pan-Tyr	IRS
35	Zap-70	pan-Tyr	Zap-70
36	Src	pan-Tyr	Src
37	Lck	pan-Tyr	Src
38	Stat1	Tyr701	Stat
39	Stat3	Tyr705	Stat

Table 7-4: Receptor Tyrosine Kinase Antibody array layout.

Appendix D

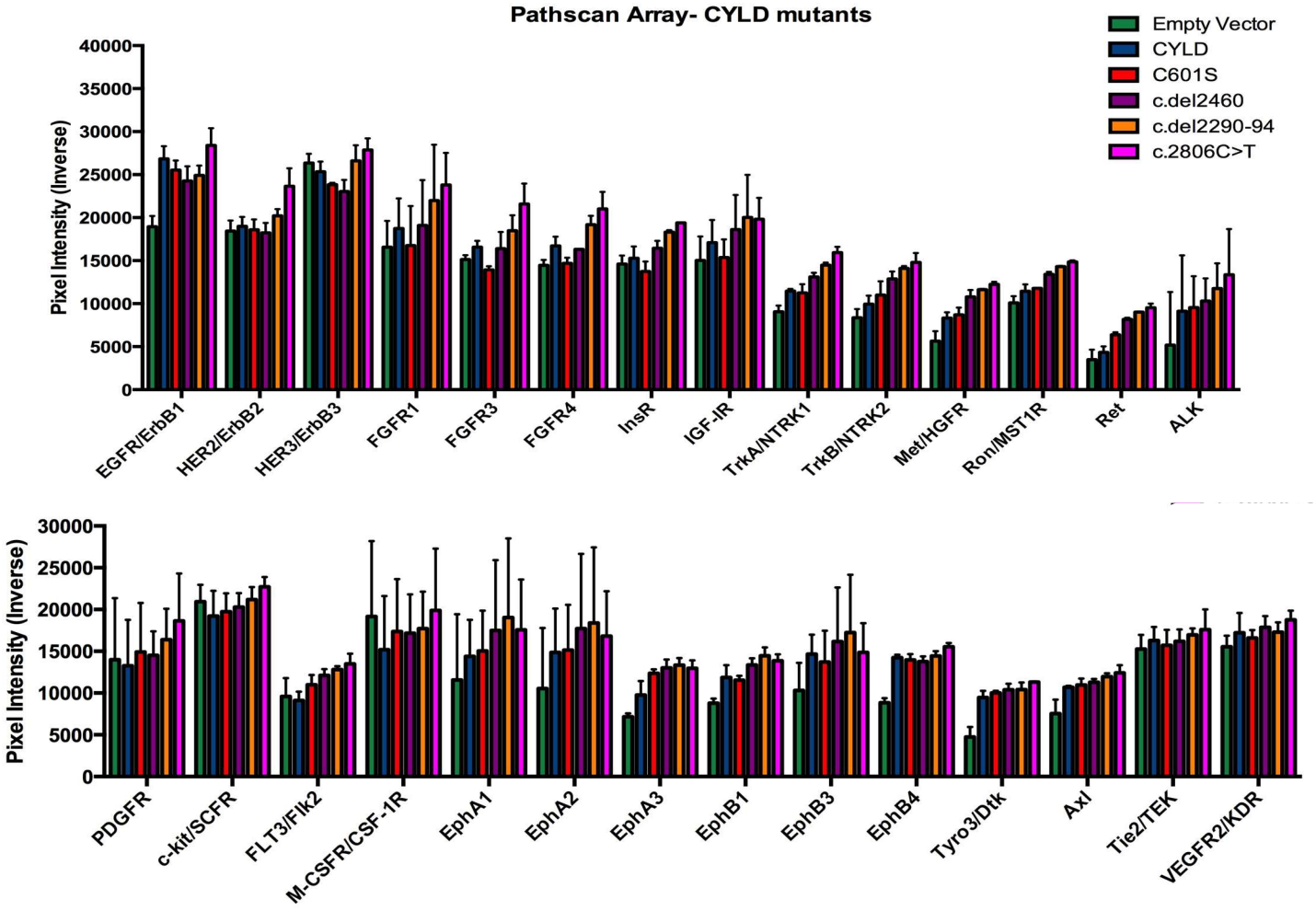
Pathscan Array- CYLD mutants
Empty Vector
CYLD
C601S
c.del2460
c.del2290-94
c.2806C>T
Pixel Intensity (Inverse)
40000
35000
30000
25000
20000
15000
10000
5000
0
EGFR/ErbB1
HER2/ErbB2
HER3/ErbB3
FGFR1
FGFR3
FGFR4
InsR
IGF-IR
TrkA/NTRK1
TrkB/NTRK2
Met/HGFR
Ron/MST1R
Ret
ALK
Pixel Intensity (Inverse)
30000
25000
20000
15000
10000
5000
0
PDGFR
c-kit/SCFR
FLT3/Flk2
M-CSFR/CSF-1R
EphA1
EphA2
EphA3
EphB1
EphB3
EphB4
Tyro3/Dtk
Axl
Tie2/TEK
VEGFR2/KDR

Appendix D (continued)

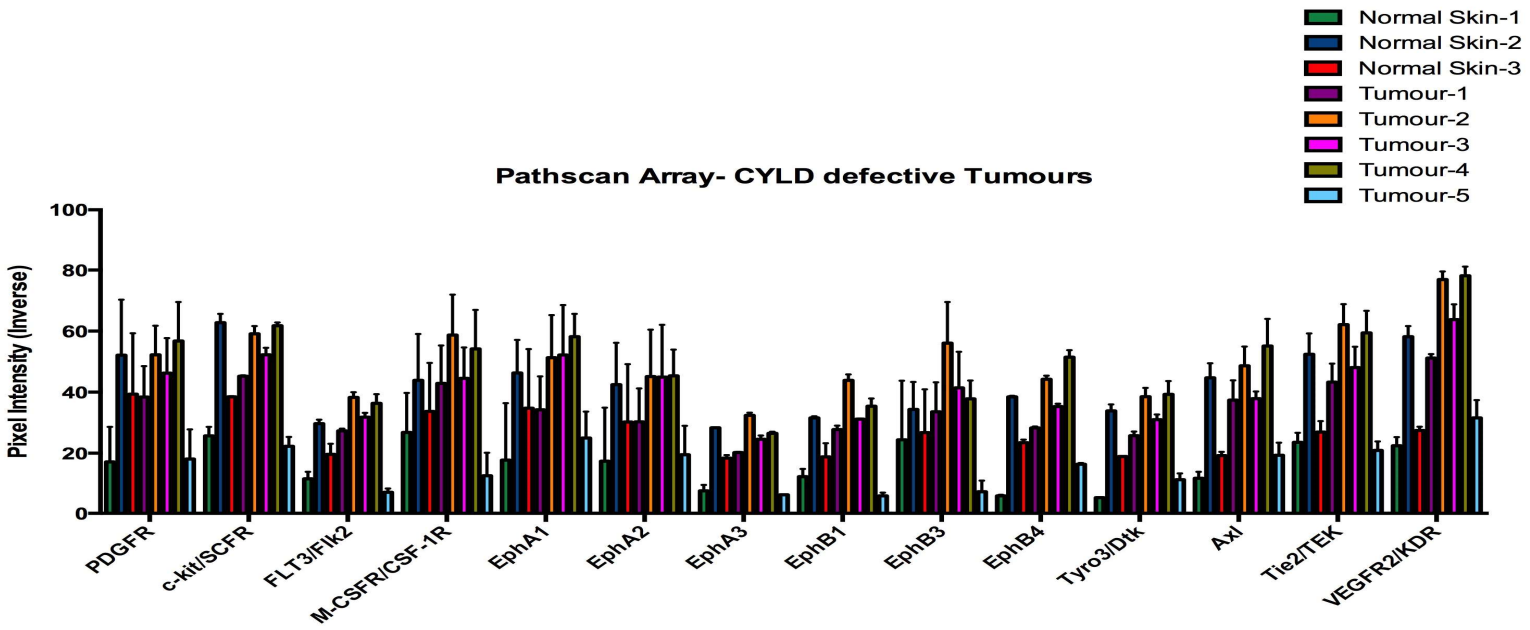

Figure 7-1: Densitometric quantification of the receptor tyrosine kinase antibody array (additional graphs).

Appendix E

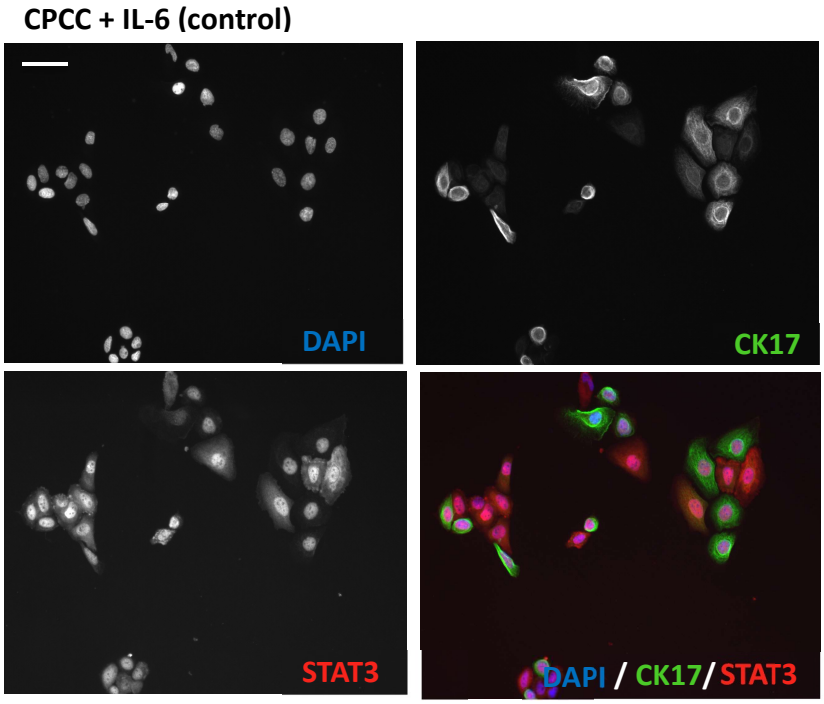

Figure 7-2: The effect of IL-6 (control) treatment on TrkB and Stat3 expression in 2D primary cylindroma cells.

Appendix F

Primer	Sequence
pLEX MCS	5’-CACCAAAATCAACGGGACTT-3’
CYLD #2	5’-CTCCAAATAGACGTGGGC-3’
CYLD #3	5’-GAGTGTGACGCAGGAAAGG-3’
CYLD #4	5’-GGCTGAAGTTAAGGAGAACC-3’
CYLD #5	5’-AGGCTGCATCAGGATTTACC-3’
CYLD #6	5’- CAGTGTCACTTCCCAAAGAC-3’

Primer	Sequence
M13 (pSC-B-amp/kan)	5’-TGTAAAACGACGGCCAGT-3’
NTRK2 #2	5’-TCCAGACACTCAGGATTTGTACTG-3’
NTRK2 #3	5’-TTACCAATCACACGGAGTACCAC-3’
NTRK2 #4	5’-AGTAACACTCCATCTTCTTCGG-3’
NTRK2 #5	5’-GGACGTGTACAGCACTGACTAC-3’

Table 7-5: Sequencing primers for cloning vectors.

Appendix G

Publications:

- Rajan N, Andersson MK, **Sinclair N**, Fehr A, Hodgson K, Lord CJ, Kazakov DV, Vanecek T, Ashworth A, & Stenman G. Overexpression of MYB drives proliferation of CYLD-defective cylindroma cells. *Journal of Pathology.* 2016 Jun; 239(2): 197-205.
- Rajan N, **Sinclair N**, Nakai H, Shimomura Y, Natarajan S. A tale of two sisters: identical IL36RN mutations and discordant phenotypes. *British Journal of Dermatology.* 2016 Feb; 174(2): 417-420.
- Rajan N, Elliott RJ, Smith A, **Sinclair N**, Swift S, Lord CJ, Ashworth A. The cylindromatosis gene product, CYLD, interacts with MIB2 to regulate notch signalling. *Oncotarget.* 2014 Dec; 5(23): 12126-12140.

8 References

Adelstein, D. J., Koyfman, S. A., El-Naggar, A. K., & Hanna, E. Y. (2012). Biology and management of salivary gland cancers. *Semin Radiat Oncol, 22*(3), 245-253. doi:10.1016/j.semradonc.2012.03.009

Adli, M., Merkhofer, E., Cogswell, P., & Baldwin, A. S. (2010). IKKalpha and IKKbeta each function to regulate NF-kappaB activation in the TNF-induced/canonical pathway. *PLoS One, 5*(2), e9428. doi:10.1371/journal.pone.0009428

Ahmed, N., Zeng, M., Sinha, I., Polin, L., Wei, W. Z., Rathinam, C., Flavell, R., Massoumi, R., & Venuprasad, K. (2011). The E3 ligase Itch and deubiquitinase Cyld act together to regulate Tak1 and inflammation. *Nat Immunol, 12*(12), 1176-1183. doi:10.1038/ni.2157

Alam, H., Sehgal, L., Kundu, S. T., Dalal, S. N., & Vaidya, M. M. (2011). Novel function of keratins 5 and 14 in proliferation and differentiation of stratified epithelial cells. *Mol Biol Cell, 22*(21), 4068-4078. doi:10.1091/mbc.E10-08-0703

Albores-Saavedra, J., Heard, S. C., McLaren, B., Kamino, H., & Witkiewicz, A. K. (2005). Cylindroma (dermal analog tumor) of the breast: a comparison with cylindroma of the skin and adenoid cystic carcinoma of the breast. *Am J Clin Pathol, 123*(6), 866-873. doi:10.1309/crwu-a3k0-mpqh-qc4w

Allen, R. D., 3rd, Bender, T. P., & Siu, G. (1999). c-Myb is essential for early T cell development. *Genes Dev, 13*(9), 1073-1078. doi:10.1101/gad.13.9.1073

Allen, S. J., Watson, J. J., & Dawbarn, D. (2011). The neurotrophins and their role in Alzheimer's disease. *Curr Neuropharmacol, 9*(4), 559-573. doi:10.2174/157015911798376190

Almeida, S., Maillard, C., Itin, P., Hohl, D., & Huber, M. (2008). Five new CYLD mutations in skin appendage tumors and evidence that aspartic acid 681 in CYLD is essential for deubiquitinase activity. *J Invest Dermatol, 128*(3), 587-593. doi:10.1038/sj.jid.5701045

Alsaad, K. O., Obaidat, N. A., & Ghazarian, D. (2007). Skin adnexal neoplasms--part 1: an approach to tumours of the pilosebaceous unit. *J Clin Pathol, 60*(2), 129-144. doi:10.1136/jcp.2006.040337

Amaru Calzada, A., Todoerti, K., Donadoni, L., Pellicioli, A., Tuana, G., Gatta, R., Neri, A., Finazzi, G., Mantovani, R., Rambaldi, A., Introna, M., Lombardi, L., & Golay, J. (2012). The HDAC inhibitor Givinostat modulates the hematopoietic transcription factors NFE2 and C-MYB in JAK2(V617F) myeloproliferative neoplasm cells. *Exp Hematol, 40*(8), 634-645.e610. doi:10.1016/j.exphem.2012.04.007

Amatu, A., Sartore-Bianchi, A., & Siena, S. (2016). NTRK gene fusions as novel targets of cancer therapy across multiple tumour types. *ESMO Open, 1*(2), e000023. doi:10.1136/esmoopen-2015-000023

An, J., Mo, D., Liu, H., Veena, M. S., Srivatsan, E. S., Massoumi, R., & Rettig, M. B. (2008). Inactivation of the CYLD deubiquitinase by HPV E6 mediates hypoxia-induced NF-kappaB activation. *Cancer Cell, 14*(5), 394-407. doi:10.1016/j.ccr.2008.10.007

Ancell, H. (1842). History of a remarkable case of tumours, developed on the head and face; accompanied with a similar disease in the abdomen. *Med Chir Trans, 25*, 227-306.211.

Antoni, D., Burckel, H., Josset, E., & Noel, G. (2015). Three-dimensional cell culture: a breakthrough in vivo. *Int J Mol Sci, 16*(3), 5517-5527. doi:10.3390/ijms16035517

Arevalo, J. C., Conde, B., Hempstead, B. I., Chao, M. V., Martin-Zanca, D., & Perez, P. (2001). A novel mutation within the extracellular domain of TrkA causes constitutive receptor activation. *Oncogene, 20*(10), 1229-1234. doi:10.1038/sj.onc.1204215

Arevalo, J. C., Conde, B., Hempstead, B. L., Chao, M. V., Martin-Zanca, D., & Perez, P. (2000). TrkA immunoglobulin-like ligand binding domains inhibit spontaneous activation of the receptor. *Mol Cell Biol, 20*(16), 5908-5916. doi 10.1128/mcb.20.16.5908-5916.2000

Arevalo, J. C., & Wu, S. H. (2006). Neurotrophin signaling: many exciting surprises! *Cell Mol Life Sci, 63*(13), 1523-1537. doi:10.1007/s00018-006-6010-1

Arevalo, J. C., Yano, H., Teng, K. K., & Chao, M. V. (2004). A unique pathway for sustained neurotrophin signaling through an ankyrin-rich membrane-spanning protein. *EMBO J, 23*(12), 2358-2368. doi:10.1038/sj.emboj.7600253

Arwert, E. N., Hoste, E., & Watt, F. M. (2012). Epithelial stem cells, wound healing and cancer. *Nat Rev Cancer, 12*(3), 170-180. doi:10.1038/nrc3217

Atwal, J. K., Massie, B., Miller, F. D., & Kaplan, D. R. (2000). The TrkB-Shc site signals neuronal survival and local axon growth via MEK and P13-kinase. *Neuron, 27*(2), 265-277.doi:10.1016/s0896-6273(00)00035-0

Baker, S. J., Kumar, A., & Reddy, E. P. (2010). p89c-Myb is not required for fetal or adult hematopoiesis. *Genesis, 48*(5), 309-316. doi:10.1002/dvg.20619

Banfield, M. J., Naylor, R. L., Robertson, A. G., Allen, S. J., Dawbarn, D., & Brady, R. L. (2001). Specificity in Trk receptor:neurotrophin interactions: the crystal structure of TrkB-d5 in complex with neurotrophin-4/5. *Structure, 9*(12), 1191-1199. doi:10.1016/S0969-2126(01)00681-5

Bansal, C., Batra, M., Lal, N., & Srivastava, A. N. (2012). Solitary cylindroma with malignant transformation. *Indian J Dermatol, 57*(2), 141-143. doi:10.4103/0019-5154.94289

Barker, P. A., Lomen-Hoerth, C., Gensch, E. M., Meakin, S. O., Glass, D. J., & Shooter, E. M. (1993). Tissue-specific alternative splicing generates two isoforms of the trkA receptor. *J Biol Chem, 268*(20), 15150-15157.

Barker, P. A., & Shooter, E. M. (1994). Disruption of NGF binding to the low affinity neurotrophin receptor p75LNTR reduces NGF binding to TrkA on PC12 cells. *Neuron, 13*(1), 203-215.

Barrandon, Y., & Green, H. (1987). Three clonal types of keratinocyte with different capacities for multiplication. *Proc Natl Acad Sci U S A, 84*(8), 2302-2306.

Baxter, G. T., Radeke, M. J., Kuo, R. C., Makrides, V., Hinkle, B., Hoang, R., Medina-Selby, A., Coit, D., Valenzuela, P., & Feinstein, S. C. (1997). Signal transduction mediated by the truncated trkB receptor isoforms, trkB.T1 and trkB.T2. *J Neurosci, 17*(8), 2683-2690.

Becker, E. B., Howell, J., Kodama, Y., Barker, P. A., & Bonni, A. (2004). Characterization of the c-Jun N-terminal kinase-BimEL signaling pathway in neuronal apoptosis. *J Neurosci, 24*(40), 8762-8770. doi:10.1523/jneurosci.2953-04.2004

Bell, D., Bell, A. H., Bondaruk, J., Hanna, E. Y., & Weber, R. S. (2016). In-depth characterization of the salivary adenoid cystic carcinoma transcriptome with emphasis on dominant cell type. *Cancer, 122*(10), 1513-1522. doi:10.1002/cncr.29959

Bender, T. P., Thompson, C. B., & Kuehl, W. M. (1987). Differential expression of c-myb mRNA in murine B lymphomas by a block to transcription elongation. *Science, 237*(4821), 1473-1476.

Benedetti, M., Levi, A., & Chao, M. V. (1993). Differential expression of nerve growth factor receptors leads to altered binding affinity and neurotrophin responsiveness. *Proc Natl Acad Sci U S A, 90*(16), 7859-7863.

Bengtsen, M., Klepper, K., Gundersen, S., Cuervo, I., Drablos, F., Hovig, E., Sandve, G. K., Gabrielsen, O. S., & Eskeland, R. (2015). c-Myb Binding Sites in Haematopoietic Chromatin Landscapes. *PLoS One, 10*(7), e0133280. doi:10.1371/journal.pone.0133280

Bergholtz, S., Andersen, T. O., Andersson, K. B., Borrebaek, J., Luscher, B., & Gabrielsen, O. S. (2001). The highly conserved DNA-binding domains of A-, B- and c-Myb differ with respect to DNA-binding, phosphorylation and redox properties. *Nucleic Acids Res, 29*(17), 3546-3556.

Beug, H., Blundell, P. A., & Graf, T. (1987). Reversibility of differentiation and proliferative capacity in avian myelomonocytic cells transformed by tsE26 leukemia virus. *Genes Dev, 1*(3), 277-286.

Beug, H., von Kirchbach, A., Doderlein, G., Conscience, J. F., & Graf, T. (1979). Chicken hematopoietic cells transformed by seven strains of defective avian leukemia viruses display three distinct phenotypes of differentiation. *Cell, 18*(2), 375-390.

Bewry, N. N., Nair, R. R., Emmons, M. F., Boulware, D., Pinilla-Ibarz, J., & Hazlehurst, L. A. (2008). Stat3 contributes to resistance toward BCR-ABL inhibitors in a bone marrow microenvironment model of drug resistance. *Mol Cancer Ther, 7*(10), 3169-3175. doi:10.1158/1535-7163.mct-08-0314

Bhakar, A. L., Howell, J. L., Paul, C. E., Salehi, A. H., Becker, E. B., Said, F., Bonni, A., & Barker, P. A. (2003). Apoptosis induced by p75NTR overexpression requires Jun kinase-dependent phosphorylation of Bad. *J Neurosci, 23*(36), 11373-11381.

Bibel, M., Hoppe, E., & Barde, Y. A. (1999). Biochemical and functional interactions between the neurotrophin receptors trk and p75NTR. *EMBO J, 18*(3), 616-622. doi:10.1093/emboj/18.3.616

Bies, J., Markus, J., & Wolff, L. (2002). Covalent attachment of the SUMO-1 protein to the negative regulatory domain of the c-Myb transcription factor modifies its stability and transactivation capacity. *J Biol Chem, 277*(11), 8999-9009. doi:10.1074/jbc.M110453200

Bies, J., & Wolff, L. (1997). Oncogenic activation of c-Myb by carboxyl-terminal truncation leads to decreased proteolysis by the ubiquitin-26S proteasome pathway. *Oncogene, 14*(2), 203-212. doi:10.1038/sj.onc.1200828

Biggs, P. J., Chapman, P., Lakhani, S. R., Burn, J., & Stratton, M. R. (1996). The cylindromatosis gene (cyld1) on chromosome 16q may be the only tumour suppressor gene involved in the development of cylindromas. *Oncogene, 12*(6), 1375-1377.

Bignell, G. R., Warren, W., Seal, S., Takahashi, M., Rapley, E., Barfoot, R., Green, H., Brown, C., Biggs, P. J., Lakhani, S. R., Jones, C., Hansen, J., Blair, E., Hofmann, B., Siebert, R., Turner, G., Evans, D. G., Schrander-Stumpel, C., Beemer, F. A., van Den Ouweland, A., Halley, D., Delpech, B., Cleveland, M. G., Leigh, I., Leisti, J., & Rasmussen, S. (2000). Identification of the familial cylindromatosis tumour-suppressor gene. *Nat Genet, 25*(2), 160-165. doi:10.1038/76006

Bikle, D. D., Xie, Z., & Tu, C. L. (2012). Calcium regulation of keratinocyte differentiation. *Expert Rev Endocrinol Metab, 7*(4), 461-472. doi:10.1586/eem.12.34

Birgersdotter, A., Sandberg, R., & Ernberg, I. (2005). Gene expression perturbation in vitro--a growing case for three-dimensional (3D) culture systems. *Semin Cancer Biol, 15*(5), 405-412. doi:10.1016/j.semcancer.2005.06.009

Blake, P. W., & Toro, J. R. (2009). Update of cylindromatosis gene (CYLD) mutations in Brooke-Spiegler syndrome: novel insights into the role of deubiquitination in cell signaling. *Hum Mutat, 30*(7), 1025-1036. doi:10.1002/humu.21024

Blanpain, C., & Fuchs, E. (2006). Epidermal stem cells of the skin. *Annu Rev Cell Dev Biol, 22*, 339-373. doi:10.1146/annurev.cellbio.22.010305.104357

Bodo, E., Biro, T., Telek, A., Czifra, G., Griger, Z., Toth, B. I., Mescalchin, A., Ito, T., Bettermann, A., Kovacs, L., & Paus, R. (2005). A hot new twist to hair biology: involvement of vanilloid receptor-1 (VR1/TRPV1) signaling in human hair growth control. *Am J Pathol, 166*(4), 985-998. doi:10.1016/s0002-9440(10)62320-6

Boeshore, K. L., Luckey, C. N., Zigmond, R. E., & Large, T. H. (1999). TrkB isoforms with distinct neurotrophin specificities are expressed in predominantly nonoverlapping populations of avian dorsal root ganglion neurons. *Journal of Neuroscience, 19*(12), 4739-4747.

Bokhari, M., Carnachan, R. J., Cameron, N. R., & Przyborski, S. A. (2007). Culture of HepG2 liver cells on three dimensional polystyrene scaffolds enhances cell structure and function during toxicological challenge. *J Anat, 211*(4), 567-576. doi:10.1111/j.1469-7580.2007.00778.x

Bonilla, X., Parmentier, L., King, B., Bezrukov, F., Kaya, G., Zoete, V., Seplyarskiy, V. B., Sharpe, H. J., McKee, T., Letourneau, A., Ribaux, P. G., Popadin, K., Basset-Seguin, N., Ben Chaabene, R., Santoni, F. A., Andrianova, M. A., Guipponi, M., Garieri, M., Verdan, C., Grosdemange, K., Sumara, O., Eilers, M., Aifantis, I., Michielin, O., de Sauvage, F. J., Antonarakis, S. E., & Nikolaev, S. I. (2016). Genomic analysis identifies new drivers and progression pathways in skin basal cell carcinoma. *Nat Genet, 48*(4), 398-406. doi:10.1038/ng.3525

Borik, L., Heller, P., Shrivastava, M., & Kazlouskaya, V. (2015). Malignant cylindroma in a patient with Brooke-Spiegler syndrome. *Dermatol Pract Concept, 5*(2), 61-65. doi:10.5826/dpc.0502a09

Botchkarev, V. A., Botchkarev, N. V., Albers, K. M., van der Veen, C., Lewin, G. R., & Paus, R. (1998). Neurotrophin-3 involvement in the regulation of hair follicle morphogenesis. *J Invest Dermatol, 111*(2), 279-285. doi:10.1046/j.1523-1747.1998.00277.x

Botchkarev, V. A., Botchkareva, N. V., Peters, E. M., & Paus, R. (2004). Epithelial growth control by neurotrophins: leads and lessons from the hair follicle. *Prog Brain Res, 146*, 493-513. doi:10.1016/s0079-6123(03)46031-7

Botchkarev, V. A., Metz, M., Botchkareva, N. V., Welker, P., Lommatzsch, M., Renz, H., & Paus, R. (1999). Brain-derived neurotrophic factor, neurotrophin-3, and neurotrophin-4 act as "epitheliotrophins" in murine skin. *Lab Invest, 79*(5), 557-572.

Botchkarev, V. A., Yaar, M., Peters, E. M. J., Raychaudhuri, S. P., Botchkareva, N. V., Marconi, A., Raychaudhuri, S. K., Paus, R., & Pincelli, C. (2006). Neurotrophins in skin biology and pathology. *Journal of Investigative Dermatology, 126*(8), 1719-1727.

Botchkareva, N. V., Botchkarev, V. A., Albers, K. M., Metz, M., & Paus, R. (2000). Distinct roles for nerve growth factor and brain-derived neurotrophic factor in controlling the rate of hair follicle morphogenesis. *J Invest Dermatol, 114*(2), 314-320. doi:10.1046/j.1523-1747.2000.00864.x

Botchkareva, N. V., Botchkarev, V. A., Chen, L. H., Lindner, G., & Paus, R. (1999). A role for p75 neurotrophin receptor in the control of hair follicle morphogenesis. *Dev Biol, 216*(1), 135-153. doi:10.1006/dbio.1999.9464

Bothwell, M. (1997). Neurotrophin function in skin. *J Investig Dermatol Symp Proc, 2*(1), 27-30.

Boukamp, P., Petrussevska, R. T., Breitkreutz, D., Hornung, J., Markham, A., & Fusenig, N. E. (1988). Normal keratinization in a spontaneously immortalized aneuploid human keratinocyte cell line. *J Cell Biol, 106*(3), 761-771.

Boyce, S. T., & Ham, R. G. (1983). Calcium-regulated differentiation of normal human epidermal keratinocytes in chemically defined clonal culture and serum-free serial culture. *J Invest Dermatol, 81*(1 Suppl), 33s-40s.

Boyer, L. A., Latek, R. R., & Peterson, C. L. (2004). The SANT domain: a unique histone-tail-binding module? *Nat Rev Mol Cell Biol, 5*(2), 158-163. doi:10.1038/nrm1314

Brabender, J., Lord, R. V., Danenberg, K. D., Metzger, R., Schneider, P. M., Park, J. M., Salonga, D., Groshen, S., Tsao-Wei, D. D., DeMeester, T. R., Holscher, A. H., & Danenberg, P. V. (2001). Increased c-myb mRNA expression in Barrett's esophagus and Barrett's-associated adenocarcinoma. *J Surg Res, 99*(2), 301-306. doi:10.1006/jsre.2001.6186

Brahimi, F., Maira, M., Barcelona, P. F., Galan, A., Aboulkassim, T., Teske, K., Rogers, M. L., Bertram, L., Wang, J., Yousefi, M., Rush, R., Fabian, M., Cashman, N., & Saragovi, H. U. (2016). The Paradoxical Signals of Two TrkC Receptor Isoforms Supports a Rationale for Novel Therapeutic Strategies in ALS. *PLoS One, 11*(10), e0162307. doi:10.1371/journal.pone.0162307

Brann, A. B., Tcherpakov, M., Williams, I. M., Futerman, A. H., & Fainzilber, M. (2002). Nerve growth factor-induced p75-mediated death of cultured hippocampal neurons is age-dependent and transduced through ceramide generated by neutral sphingomyelinase. *J Biol Chem, 277*(12), 9812-9818. doi:10.1074/jbc.M109862200

Brayer, K. J., Frerich, C. A., Kang, H., & Ness, S. A. (2016). Recurrent Fusions in MYB and MYBL1 Define a Common, Transcription Factor-Driven Oncogenic Pathway in Salivary Gland Adenoid Cystic Carcinoma. *Cancer Discov, 6*(2), 176-187. doi:10.1158/2159-8290.cd-15-0859

Breslin, S., & O'Driscoll, L. (2013). Three-dimensional cell culture: the missing link in drug discovery. *Drug Discov Today, 18*(5-6), 240-249. doi:10.1016/j.drudis.2012.10.003

Brigadski, T., Hartmann, M., & Lessmann, V. (2005). Differential vesicular targeting and time course of synaptic secretion of the mammalian neurotrophins. *J Neurosci, 25*(33), 7601-7614. doi:10.1523/jneurosci.1776-05.2005

Brodie, C., Oshiba, A., Renz, H., Bradley, K., & Gelfand, E. W. (1996). Nerve growth-factor and anti-CD40 provide opposite signals for the production of IgE in interleukin-4-treated lymphocytes. *Eur J Immunol, 26*(1), 171-178. doi:10.1002/eji.1830260127

Bruckner-Tuderman, L., Pfaltz, M., & Schnyder, U. W. (1991). Cylindroma overexpresses collagen VII, the major anchoring fibril protein. *J Invest Dermatol, 96*(5), 729-734.

Brummelkamp, T. R., Nijman, S. M., Dirac, A. M., & Bernards, R. (2003). Loss of the cylindromatosis tumour suppressor inhibits apoptosis by activating NF-kappaB. *Nature, 424*(6950), 797-801. doi:10.1038/nature01811

Brunet, A., Bonni, A., Zigmond, M. J., Lin, M. Z., Juo, P., Hu, L. S., Anderson, M. J., Arden, K. C., Blenis, J., & Greenberg, M. E. (1999). Akt promotes cell survival by phosphorylating and inhibiting a Forkhead transcription factor. *Cell, 96*(6), 857-868.

Brunet, A., Datta, S. R., & Greenberg, M. E. (2001). Transcription-dependent and -independent control of neuronal survival by the PI3K-Akt signaling pathway. *Curr Opin Neurobiol, 11*(3), 297-305.

Bruno, M. A., & Cuello, A. C. (2006). Activity-dependent release of precursor nerve growth factor, conversion to mature nerve growth factor, and its degradation by a protease cascade. *Proc Natl Acad Sci U S A, 103*(17), 6735-6740. doi:10.1073/pnas.0510645103

Bubici, C., & Papa, S. (2014). JNK signalling in cancer: in need of new, smarter therapeutic targets. *Br J Pharmacol, 171*(1), 24-37. doi:10.1111/bph.12432

Calhoun, E. S., Jones, J. B., Ashfaq, R., Adsay, V., Baker, S. J., Valentine, V., Hempen, P. M., Hilgers, W., Yeo, C. J., Hruban, R. H., & Kern, S. E. (2003). BRAF and FBXW7 (CDC4, FBW7, AGO, SEL10) mutations in distinct subsets of pancreatic cancer: potential therapeutic targets. *Am J Pathol, 163*(4), 1255-1260. doi:10.1016/s0002-9440(10)63485-2

Canossa, M., Gartner, A., Campana, G., Inagaki, N., & Thoenen, H. (2001). Regulated secretion of neurotrophins by metabotropic glutamate group I (mGluRI) and Trk receptor activation is mediated via phospholipase C signalling pathways. *EMBO J, 20*(7), 1640-1650. doi:10.1093/emboj/20.7.1640

Caporali, A., & Emanueli, C. (2009). Cardiovascular actions of neurotrophins. *Physiol Rev, 89*(1), 279-308. doi:10.1152/physrev.00007.2008

Caporali, A., Sala-Newby, G. B., Meloni, M., Graiani, G., Pani, E., Cristofaro, B., Newby, A. C., Madeddu, P., & Emanueli, C. (2008). Identification of the prosurvival activity of nerve growth factor on cardiac myocytes. *Cell Death Differ, 15*(2), 299-311. doi:10.1038/sj.cdd.4402263

Casaccia-Bonnefil, P., Carter, B. D., Dobrowsky, R. T., & Chao, M. V. (1996). Death of oligodendrocytes mediated by the interaction of nerve growth factor with its receptor p75. *Nature, 383*(6602), 716-719. doi:10.1038/383716a0

Castresana, J. S. (2015). Cancer as a Ciliopathy: The Primary Cilium as a New Therapeutic Target. *Carcinogenesis and Mutagenesis, 6*. doi:10.4172/2517-2518.1000e119

Caterina, M. J., & Pang, Z. (2016). TRP Channels in Skin Biology and Pathophysiology. *Pharmaceuticals (Basel), 9*(4). doi:10.3390/ph9040077

Ceni, C., Kommaddi, R. P., Thomas, R., Vereker, E., Liu, X., McPherson, P. S., Ritter, B., & Barker, P. A. (2010). The p75NTR intracellular domain generated by neurotrophin-induced receptor cleavage potentiates Trk signaling. *J Cell Sci, 123*(Pt 13), 2299-2307. doi:10.1242/jcs.062612

Cesarz, Z., & Tamama, K. (2016). Spheroid Culture of Mesenchymal Stem Cells. *Stem Cells Int, 2016*, 9176357. doi:10.1155/2016/9176357

Chan, K. S., Sano, S., Kataoka, K., Abel, E., Carbajal, S., Beltran, L., Clifford, J., Peavey, M., Shen, J., & Digiovanni, J. (2008). Forced expression of a constitutively active form of Stat3 in mouse epidermis enhances malignant progression of skin

tumors induced by two-stage carcinogenesis. *Oncogene, 27*(8), 1087-1094. doi:10.1038/sj.onc.1210726

Chao, M. V. (2003). Neurotrophins and their receptors: a convergence point for many signalling pathways. *Nat Rev Neurosci, 4*(4), 299-309. doi:10.1038/nrn1078

Chao, M. V., & Hempstead, B. L. (1995). p75 and Trk: a two-receptor system. *Trends Neurosci, 18*(7), 321-326.

Cheasley, D., Pereira, L., Lightowler, S., Vincan, E., Malaterre, J., & Ramsay, R. G. (2011). Myb controls intestinal stem cell genes and self-renewal. *Stem Cells, 29*(12), 2042-2050. doi:10.1002/stem.761

Chen, B., Liang, Y., He, Z., An, Y., Zhao, W., & Wu, J. (2016). Autocrine activity of BDNF induced by the STAT3 signaling pathway causes prolonged TrkB activation and promotes human non-small-cell lung cancer proliferation. *Sci Rep, 6*, 30404. doi:10.1038/srep30404

Chen, C. S., Mrksich, M., Huang, S., Whitesides, G. M., & Ingber, D. E. (1997). Geometric control of cell life and death. *Science, 276*(5317), 1425-1428.

Chen, S., Wang, Z., Dai, X., Pan, J., Ge, J., Han, X., Wu, Z., Zhou, X., & Zhao, T. (2013). Re-expression of microRNA-150 induces EBV-positive Burkitt lymphoma differentiation by modulating c-Myb in vitro. *Cancer Sci, 104*(7), 826-834. doi:10.1111/cas.12156

Chen, Z. Y., Ieraci, A., Tanowitz, M., & Lee, F. S. (2005). A novel endocytic recycling signal distinguishes biological responses of Trk neurotrophin receptors. *Mol Biol Cell, 16*(12), 5761-5772. doi:10.1091/mbc.E05-07-0651

Chitcholtan, K., Sykes, P. H., & Evans, J. J. (2012). The resistance of intracellular mediators to doxorubicin and cisplatin are distinct in 3D and 2D endometrial cancer. *J Transl Med, 10*, 38. doi:10.1186/1479-5876-10-38

Choi, D. Y., Toledo-Aral, J. J., Segal, R., & Halegoua, S. (2001). Sustained signaling by phospholipase C-gamma mediates nerve growth factor-triggered gene expression. *Mol Cell Biol, 21*(8), 2695-2705. doi:10.1128/mcb.21.8.2695-2705.2001

Clague, M. J., & Urbe, S. (2010). Ubiquitin: same molecule, different degradation pathways. *Cell, 143*(5), 682-685. doi:10.1016/j.cell.2010.11.012

Clappier, E., Cuccuini, W., Kalota, A., Crinquette, A., Cayuela, J. M., Dik, W. A., Langerak, A. W., Montpellier, B., Nadel, B., Walrafen, P., Delattre, O., Aurias, A., Leblanc, T., Dombret, H., Gewirtz, A. M., Baruchel, A., Sigaux, F., & Soulier, J. (2007). The C-MYB locus is involved in chromosomal translocation and genomic duplications in human T-cell acute leukemia (T-ALL), the translocation defining a new T-ALL subtype in very young children. *Blood, 110*(4), 1251-1261. doi:10.1182/blood-2006-12-064683

Clary, D. O., & Reichardt, L. F. (1994). An alternatively spliced form of the nerve growth factor receptor TrkA confers an enhanced response to neurotrophin 3. *Proc Natl Acad Sci U S A, 91*(23), 11133-11137.

Clement, C. A., Ajbro, K. D., Koefoed, K., Vestergaard, M. L., Veland, I. R., Henriques de Jesus, M. P., Pedersen, L. B., Benmerah, A., Andersen, C. Y., Larsen, L. A., & Christensen, S. T. (2013). TGF-beta signaling is associated with endocytosis at the pocket region of the primary cilium. *Cell Rep, 3*(6), 1806-1814. doi:10.1016/j.celrep.2013.05.020

Close, J., Game, L., Clark, B., Bergounioux, J., Gerovassili, A., & Thein, S. L. (2004). Genome annotation of a 1.5 Mb region of human chromosome 6q23

encompassing a quantitative trait locus for fetal hemoglobin expression in adults. *BMC Genomics, 5*(1), 33. doi:10.1186/1471-2164-5-33

Cogswell, P. C., Guttridge, D. C., Funkhouser, W. K., & Baldwin, A. S., Jr. (2000). Selective activation of NF-kappa B subunits in human breast cancer: potential roles for NF-kappa B2/p52 and for Bcl-3. *Oncogene, 19*(9), 1123-1131. doi:10.1038/sj.onc.1203412

Conover, J. C., Erickson, J. T., Katz, D. M., Bianchi, L. M., Poueymirou, W. T., McClain, J., Pan, L., Helgren, M., Ip, N. Y., Boland, P., & et al. (1995). Neuronal deficits, not involving motor neurons, in mice lacking BDNF and/or NT4. *Nature, 375*(6528), 235-238. doi:10.1038/375235a0

Costa, E. C., Moreira, A. F., de Melo-Diogo, D., Gaspar, V. M., Carvalho, M. P., & Correia, I. J. (2016). 3D tumor spheroids: an overview on the tools and techniques used for their analysis. *Biotechnol Adv, 34*(8), 1427-1441. doi:10.1016/j.biotechadv.2016.11.002

Cotton, D. W., & Braye, S. G. (1984). Dermal cylindromas originate from the eccrine sweat gland. *Br J Dermatol, 111*(1), 53-61.

Coulombe, P. A., Kopan, R., & Fuchs, E. (1989). Expression of keratin K14 in the epidermis and hair follicle: insights into complex programs of differentiation. *J Cell Biol, 109*(5), 2295-2312.

Crain, R. C., & Helwig, E. B. (1961). Dermal cylindroma (dermal eccrine cylindroma). *Am J Clin Pathol, 35*, 504-515.

Creighton, C., Kuick, R., Misek, D. E., Rickman, D. S., Brichory, F. M., Rouillard, J. M., Omenn, G. S., & Hanash, S. (2003). Profiling of pathway-specific changes in gene expression following growth of human cancer cell lines transplanted into mice. *Genome Biol, 4*(7), R46. doi:10.1186/gb-2003-4-7-r46

Crowley, C., Spencer, S. D., Nishimura, M. C., Chen, K. S., Pitts-Meek, S., Armanini, M. P., Ling, L. H., McMahon, S. B., Shelton, D. L., Levinson, A. D., & et al. (1994). Mice lacking nerve growth factor display perinatal loss of sensory and sympathetic neurons yet develop basal forebrain cholinergic neurons. *Cell, 76*(6), 1001-1011.

Cunningham, M. E., & Greene, L. A. (1998). A function-structure model for NGF-activated TRK. *EMBO J, 17*(24), 7282-7293. doi:10.1093/emboj/17.24.7282

Cures, A., House, C., Kanei-Ishii, C., Kemp, B., & Ramsay, R. G. (2001). Constitutive c-Myb amino-terminal phosphorylation and DNA binding activity uncoupled during entry and passage through the cell cycle. *Oncogene, 20*(14), 1784-1792. doi:10.1038/sj.onc.1204345

Daa, T., Nakamura, I., Yada, N., Arakane, S., Nishida, H., Kashima, K., Suzuki, M., & Yokoyama, S. (2013). PLAG1 and CYLD do not play a role in the tumorigenesis of adenoid cystic carcinoma. *Mol Med Rep, 7*(4), 1086-1090. doi:10.3892/mmr.2013.1311

Dai, P., Akimaru, H., Tanaka, Y., Hou, D. X., Yasukawa, T., Kanei-Ishii, C., Takahashi, T., & Ishii, S. (1996). CBP as a transcriptional coactivator of c-Myb. *Genes Dev, 10*(5), 528-540.

Dai, Y. H., Hung, L. Y., Chen, R. Y., Lai, C. H., & Chang, K. C. (2016). ON 01910.Na inhibits growth of diffuse large B-cell lymphoma by cytoplasmic sequestration of sumoylated C-MYB/TRAF6 complex. *Transl Res, 175*, 129-143.e113. doi:10.1016/j.trsl.2016.04.001

Darnell, J. E., Jr. (1997). STATs and gene regulation. *Science, 277*(5332), 1630-1635.

Darnell, J. E., Jr., Kerr, I. M., & Stark, G. R. (1994). Jak-STAT pathways and transcriptional activation in response to IFNs and other extracellular signaling proteins. *Science, 264*(5164), 1415-1421.

Dash, A. B., Orrico, F. C., & Ness, S. A. (1996). The EVES motif mediates both intermolecular and intramolecular regulation of c-Myb. *Genes Dev, 10*(15), 1858-1869.

Datta, S. R., Dudek, H., Tao, X., Masters, S., Fu, H., Gotoh, Y., & Greenberg, M. E. (1997). Akt phosphorylation of BAD couples survival signals to the cell-intrinsic death machinery. *Cell, 91*(2), 231-241.

Davis, B. M., Fundin, B. T., Albers, K. M., Goodness, T. P., Cronk, K. M., & Rice, F. L. (1997). Overexpression of nerve growth factor in skin causes preferential increases among innervation to specific sensory targets. *J Comp Neurol, 387*(4), 489-506.

Davis, F. M., Azimi, I., Faville, R. A., Peters, A. A., Jalink, K., Putney, J. W., Jr., Goodhill, G. J., Thompson, E. W., Roberts-Thomson, S. J., & Monteith, G. R. (2014). Induction of epithelial-mesenchymal transition (EMT) in breast cancer cells is calcium signal dependent. *Oncogene, 33*(18), 2307-2316. doi:10.1038/onc.2013.187

Davis, R. J. (2000). Signal transduction by the JNK group of MAP kinases. *Cell, 103*(2), 239-252.

Deinhardt, K., & Chao, M. V. (2014). Trk receptors. *Handb Exp Pharmacol, 220*, 103-119. doi:10.1007/978-3-642-45106-5_5

Descargues, P., Sil, A. K., & Karin, M. (2008). IKKalpha, a critical regulator of epidermal differentiation and a suppressor of skin cancer. *EMBO J, 27*(20), 2639-2647. doi:10.1038/emboj.2008.196

Dhiman, H. K., Ray, A. R., & Panda, A. K. (2005). Three-dimensional chitosan scaffold-based MCF-7 cell culture for the determination of the cytotoxicity of tamoxifen. *Biomaterials, 26*(9), 979-986. doi:10.1016/j.biomaterials.2004.04.012

Di Marco, E., Marchisio, P. C., Bondanza, S., Franzi, A. T., Cancedda, R., & De Luca, M. (1991). Growth-regulated synthesis and secretion of biologically active nerve growth factor by human keratinocytes. *Journal of Biological Chemistry, 266*(32), 21718-21722.

Di Marco, E., Mathort, M., Bondanza, S., Cutuli, N., Marchisio, P. C., Cancedda, R., & De Luca, M. (1993). Nerve growth factor binds to normal human keratinocytes through high and low affinity receptors and stimulates their growth by a novel autocrine loop. *Journal of Biological Chemistry, 268*(30), 22838-22846.

Dobrowsky, R. T., Werner, M. H., Castellino, A. M., Chao, M. V., & Hannun, Y. A. (1994). Activation of the sphingomyelin cycle through the low-affinity neurotrophin receptor. *Science, 265*(5178), 1596-1599.

Donovan, M. J., Hahn, R., Tessarollo, L., & Hempstead, B. L. (1996). Identification of an essential nonneuronal function of neurotrophin 3 in mammalian cardiac development. *Nat Genet, 14*(2), 210-213. doi:10.1038/ng1096-210

Donovan, M. J., Lin, M. I., Wiegn, P., Ringstedt, T., Kraemer, R., Hahn, R., Wang, S., Ibanez, C. F., Rafii, S., & Hempstead, B. L. (2000). Brain derived neurotrophic factor is an endothelial cell survival factor required for intramyocardial vessel stabilization. *Development, 127*(21), 4531-4540.

Drabsch, Y., Hugo, H., Zhang, R., Dowhan, D. H., Miao, Y. R., Gewirtz, A. M., Barry, S. C., Ramsay, R. G., & Gonda, T. J. (2007). Mechanism of and requirement for estrogen-regulated MYB expression in estrogen-receptor-positive breast cancer

cells. *Proc Natl Acad Sci U S A, 104*(34), 13762-13767. doi:10.1073/pnas.0700104104

Drier, Y., Cotton, M. J., Williamson, K. E., Gillespie, S. M., Ryan, R. J., Kluk, M. J., Carey, C. D., Rodig, S. J., Sholl, L. M., Afrogheh, A. H., Faquin, W. C., Queimado, L., Qi, J., Wick, M. J., El-Naggar, A. K., Bradner, J. E., Moskaluk, C. A., Aster, J. C., Knoechel, B., & Bernstein, B. E. (2016). An oncogenic MYB feedback loop drives alternate cell fates in adenoid cystic carcinoma. *Nat Genet, 48*(3), 265-272. doi:10.1038/ng.3502

Dubois, A., Hodgson, K., & Rajan, N. (2017). Understanding Inherited Cylindromas: Clinical Implications of Gene Discovery. *Dermatol Clin, 35*(1), 61-71. doi:10.1016/j.det.2016.08.002

DuBridge, R. B., Tang, P., Hsia, H. C., Leong, P. M., Miller, J. H., & Calos, M. P. (1987). Analysis of mutation in human cells by using an Epstein-Barr virus shuttle system. *Mol Cell Biol, 7*(1), 379-387.

Durani, B. K., Kurzen, H., Jaeckel, A., Kuner, N., Naeher, H., & Hartschuh, W. (2001). Malignant transformation of multiple dermal cylindromas. *Br J Dermatol, 145*(4), 653-656.

Dwane, L., Gallagher, W. M., Ni Chonghaile, T., & O'Connor, D. P. (2017). The Emerging Role of Non-traditional Ubiquitination in Oncogenic Pathways. *J Biol Chem, 292*(9), 3543-3551. doi:10.1074/jbc.R116.755694

Eales, K. L., Hollinshead, K. E., & Tennant, D. A. (2016). Hypoxia and metabolic adaptation of cancer cells. *Oncogenesis, 5*, e190. doi:10.1038/oncsis.2015.50

Easton, J. B., Royer, A. R., & Middlemas, D. S. (2006). The protein tyrosine phosphatase, Shp2, is required for the complete activation of the RAS/MAPK pathway by brain-derived neurotrophic factor. *J Neurochem, 97*(3), 834-845. doi:10.1111/j.1471-4159.2006.03789.x

Edmondson, R., Broglie, J. J., Adcock, A. F., & Yang, L. (2014). Three-dimensional cell culture systems and their applications in drug discovery and cell-based biosensors. *Assay Drug Dev Technol, 12*(4), 207-218. doi:10.1089/adt.2014.573

Egan, M. F., Kojima, M., Callicott, J. H., Goldberg, T. E., Kolachana, B. S., Bertolino, A., Zaitsev, E., Gold, B., Goldman, D., Dean, M., Lu, B., & Weinberger, D. R. (2003). The BDNF val66met polymorphism affects activity-dependent secretion of BDNF and human memory and hippocampal function. *Cell, 112*(2), 257-269.

Eguether, T., Ermolaeva, M. A., Zhao, Y., Bonnet, M. C., Jain, A., Pasparakis, M., Courtois, G., & Tassin, A. M. (2014). The deubiquitinating enzyme CYLD controls apical docking of basal bodies in ciliated epithelial cells. *Nat Commun, 5*, 4585. doi:10.1038/ncomms5585

Eide, F. F., Vining, E. R., Eide, B. L., Zang, K., Wang, X. Y., & Reichardt, L. F. (1996). Naturally occurring truncated trkB receptors have dominant inhibitory effects on brain-derived neurotrophic factor signaling. *J Neurosci, 16*(10), 3123-3129.

Emambokus, N., Vegiopoulos, A., Harman, B., Jenkinson, E., Anderson, G., & Frampton, J. (2003). Progression through key stages of haemopoiesis is dependent on distinct threshold levels of c-Myb. *EMBO J, 22*(17), 4478-4488. doi:10.1093/emboj/cdg434

Ernfors, P., Lee, K. F., & Jaenisch, R. (1994). Mice lacking brain-derived neurotrophic factor develop with sensory deficits. *Nature, 368*(6467), 147-150. doi:10.1038/368147a0

Ernfors, P., Lee, K. F., Kucera, J., & Jaenisch, R. (1994). Lack of neurotrophin-3 leads to deficiencies in the peripheral nervous system and loss of limb proprioceptive afferents. *Cell, 77*(4), 503-512.

Espinosa, L., Cathelin, S., D'Altri, T., Trimarchi, T., Statnikov, A., Guiu, J., Rodilla, V., Ingles-Esteve, J., Nomdedeu, J., Bellosillo, B., Besses, C., Abdel-Wahab, O., Kucine, N., Sun, S. C., Song, G., Mullighan, C. C., Levine, R. L., Rajewsky, K., Aifantis, I., & Bigas, A. (2010). The Notch/Hes1 pathway sustains NF-kappaB activation through CYLD repression in T cell leukemia. *Cancer Cell, 18*(3), 268-281. doi:10.1016/j.ccr.2010.08.006

Esposito, D., Patel, P., Stephens, R. M., Perez, P., Chao, M. V., Kaplan, D. R., & Hempstead, B. L. (2001). The cytoplasmic and transmembrane domains of the p75 and Trk A receptors regulate high affinity binding to nerve growth factor. *J Biol Chem, 276*(35), 32687-32695. doi:10.1074/jbc.M011674200

Evangelopoulos, M. E., Weis, J., & Kruttgen, A. (2004). Neurotrophin effects on neuroblastoma cells: correlation with trk and p75NTR expression and influence of Trk receptor bodies. *J Neurooncol, 66*(1-2), 101-110.

Evans, C. D. (1954). Turban tumour. *Br J Dermatol, 66*(12), 434-443.

Ezratty, E. J., Stokes, N., Chai, S., Shah, A. S., Williams, S. E., & Fuchs, E. (2011). A role for the primary cilium in Notch signaling and epidermal differentiation during skin development. *Cell, 145*(7), 1129-1141. doi:10.1016/j.cell.2011.05.030

Fang, Y., & Eglen, R. M. (2017). Three-Dimensional Cell Cultures in Drug Discovery and Development. *SLAS Discov, 22*(5), 456-472. doi:10.1177/1087057117696795

Farinas, I., Wilkinson, G. A., Backus, C., Reichardt, L. F., & Patapoutian, A. (1998). Characterization of neurotrophin and Trk receptor functions in developing sensory ganglia: direct NT-3 activation of TrkB neurons in vivo. *Neuron, 21*(2), 325-334.

Favier, D., & Gonda, T. J. (1994). Detection of proteins that bind to the leucine zipper motif of c-Myb. *Oncogene, 9*(1), 305-311.

Fehr, A., Kovacs, A., Loning, T., Frierson, H., Jr., van den Oord, J., & Stenman, G. (2011). The MYB-NFIB gene fusion-a novel genetic link between adenoid cystic carcinoma and dermal cylindroma. *J Pathol, 224*(3), 322-327. doi:10.1002/path.2909

Feng, D., Kim, T., Ozkan, E., Light, M., Torkin, R., Teng, K. K., Hempstead, B. L., & Garcia, K. C. (2010). Molecular and structural insight into proNGF engagement of p75NTR and sortilin. *J Mol Biol, 396*(4), 967-984. doi:10.1016/j.jmb.2009.12.030

Fenner, B. M. (2012). Truncated TrkB: beyond a dominant negative receptor. *Cytokine Growth Factor Rev, 23*(1-2), 15-24. doi:10.1016/j.cytogfr.2012.01.002

Fisher, G. H., & Geronemus, R. G. (2006). Treatment of multiple familial trichoepitheliomas with a combination of aspirin and a neutralizing antibody to tumor necrosis factor alpha: A case report and hypothesis of mechanism. *Arch Dermatol, 142*(6), 782-783. doi:10.1001/archderm.142.6.782

Foos, G., Natour, S., & Klempnauer, K. H. (1993). TATA-box dependent trans-activation of the human HSP70 promoter by Myb proteins. *Oncogene, 8*(7), 1775-1782.

Frade, J. M., Rodriguez-Tebar, A., & Barde, Y. A. (1996). Induction of cell death by endogenous nerve growth factor through its p75 receptor. *Nature, 383*(6596), 166-168. doi:10.1038/383166a0

Frasor, J., Danes, J. M., Komm, B., Chang, K. C., Lyttle, C. R., & Katzenellenbogen, B. S. (2003). Profiling of estrogen up- and down-regulated gene expression in human breast cancer cells: insights into gene networks and pathways underlying

estrogenic control of proliferation and cell phenotype. *Endocrinology, 144*(10), 4562-4574. doi:10.1210/en.2003-0567

Friedman, C. S., O'Donnell, M. A., Legarda-Addison, D., Ng, A., Cardenas, W. B., Yount, J. S., Moran, T. M., Basler, C. F., Komuro, A., Horvath, C. M., Xavier, R., & Ting, A. T. (2008). The tumour suppressor CYLD is a negative regulator of RIG-I-mediated antiviral response. *EMBO Rep, 9*(9), 930-936. doi:10.1038/embor.2008.136

Frith, J. E., Thomson, B., & Genever, P. G. (2010). Dynamic three-dimensional culture methods enhance mesenchymal stem cell properties and increase therapeutic potential. *Tissue Eng Part C Methods, 16*(4), 735-749. doi:10.1089/ten.TEC.2009.0432

Fu, S. L., & Lipsick, J. S. (1997). Constitutive expression of full-length c-Myb transforms avian cells characteristic of both the monocytic and granulocytic lineages. *Cell Growth Differ, 8*(1), 35-45.

Fuchs, E., & Raghavan, S. (2002). Getting under the skin of epidermal morphogenesis. *Nat Rev Genet, 3*(3), 199-209. doi:10.1038/nrg758

Fujii, A., Matsuyama, K., Mizutani, Y., Kanoh, H., Nakano, H., & Seishima, M. (2017). Multiple familial trichoepithelioma with a novel mutation of the CYLD gene. *J Dermatol*. doi:10.1111/1346-8138.13901

Furuta, Y., Aizawa, S., Suda, Y., Ikawa, Y., Nakasgoshi, H., Nishina, Y., & Ishii, S. (1993). Degeneration of skeletal and cardiac muscles in c-myb transgenic mice. *Transgenic Res, 2*(4), 199-207.

Fusco, N., Colombo, P. E., Martelotto, L. G., De Filippo, M. R., Piscuoglio, S., Ng, C. K., Lim, R. S., Jacot, W., Vincent-Salomon, A., Reis-Filho, J. S., & Weigelt, B. (2016). Resolving quandaries: basaloid adenoid cystic carcinoma or breast cylindroma? The role of massively parallel sequencing. *Histopathology, 68*(2), 262-271. doi:10.1111/his.12735

Gao, J., Huo, L., Sun, X., Liu, M., Li, D., Dong, J. T., & Zhou, J. (2008). The tumor suppressor CYLD regulates microtubule dynamics and plays a role in cell migration. *J Biol Chem, 283*(14), 8802-8809. doi:10.1074/jbc.M708470200

Gao, J., Sun, L., Huo, L., Liu, M., Li, D., & Zhou, J. (2010). CYLD regulates angiogenesis by mediating vascular endothelial cell migration. *Blood, 115*(20), 4130-4137. doi:10.1182/blood-2009-10-248526

Garcia-Suarez, O., Blanco-Gelaz, M. A., Lopez, M. L., Germana, A., Cabo, R., Diaz-Esnal, B., Silos-Santiago, I., Ciriaco, E., & Vega, J. A. (2002). Massive lymphocyte apoptosis in the thymus of functionally deficient TrkB mice. *J Neuroimmunol, 129*(1-2), 25-34.

Garcia-Suarez, O., Germana, A., Hannestad, J., Ciriaco, E., Laura, R., Naves, J., Esteban, I., Silos-Santiago, I., & Vega, J. A. (2000). TrkA is necessary for the normal development of the murine thymus. *J Neuroimmunol, 108*(1-2), 11-21.

Gees, M., Colsoul, B., & Nilius, B. (2010). The role of transient receptor potential cation channels in Ca2+ signaling. *Cold Spring Harb Perspect Biol, 2*(10), a003962. doi:10.1101/cshperspect.a003962

Geetha, T., Kenchappa, R. S., Wooten, M. W., & Carter, B. D. (2005). TRAF6-mediated ubiquitination regulates nuclear translocation of NRIF, the p75 receptor interactor. *EMBO J, 24*(22), 3859-3868. doi:10.1038/sj.emboj.7600845

Geetha, T., Seibenhener, M. L., Chen, L., Madura, K., & Wooten, M. W. (2008). p62 serves as a shuttling factor for TrkA interaction with the proteasome. *Biochem Biophys Res Commun, 374*(1), 33-37. doi:10.1016/j.bbrc.2008.06.082

Geetha, T., & Wooten, M. W. (2008). TrkA receptor endolysosomal degradation is both ubiquitin and proteasome dependent. *Traffic, 9*(7), 1146-1156. doi:10.1111/j.1600-0854.2008.00751.x

Geiger, T. R., Song, J. Y., Rosado, A., & Peeper, D. S. (2011). Functional characterization of human cancer-derived TRKB mutations. *PLoS One, 6*(2), e16871. doi:10.1371/journal.pone.0016871

Gentry, J. J., Rutkoski, N. J., Burke, T. L., & Carter, B. D. (2004). A functional interaction between the p75 neurotrophin receptor interacting factors, TRAF6 and NRIF. *J Biol Chem, 279*(16), 16646-16656. doi:10.1074/jbc.M309209200

George, O. L., & Ness, S. A. (2014). Situational awareness: regulation of the myb transcription factor in differentiation, the cell cycle and oncogenesis. *Cancers (Basel), 6*(4), 2049-2071. doi:10.3390/cancers6042049

Gerdes, J. M., Liu, Y., Zaghloul, N. A., Leitch, C. C., Lawson, S. S., Kato, M., Beachy, P. A., Beales, P. L., DeMartino, G. N., Fisher, S., Badano, J. L., & Katsanis, N. (2007). Disruption of the basal body compromises proteasomal function and perturbs intracellular Wnt response. *Nat Genet, 39*(11), 1350-1360. doi:10.1038/ng.2007.12

Gerretsen, A. L., Beemer, F. A., Deenstra, W., Hennekam, F. A., & van Vloten, W. A. (1995). Familial cutaneous cylindromas: investigations in five generations of a family. *J Am Acad Dermatol, 33*(2 Pt 1), 199-206.

Gerretsen, A. L., van der Putte, S. C., Deenstra, W., & van Vloten, W. A. (1993). Cutaneous cylindroma with malignant transformation. *Cancer, 72*(5), 1618-1623.

Ghosh, S., Spagnoli, G. C., Martin, I., Ploegert, S., Demougin, P., Heberer, M., & Reschner, A. (2005). Three-dimensional culture of melanoma cells profoundly affects gene expression profile: a high density oligonucleotide array study. *J Cell Physiol, 204*(2), 522-531. doi:10.1002/jcp.20320

Gilberto, S., & Peter, M. (2017). Dynamic ubiquitin signaling in cell cycle regulation. *J Cell Biol, 216*(8), 2259-2271. doi:10.1083/jcb.201703170

Goetz, S. C., & Anderson, K. V. (2010). The primary cilium: a signalling centre during vertebrate development. *Nat Rev Genet, 11*(5), 331-344. doi:10.1038/nrg2774

Gonda, T. J., Buckmaster, C., & Ramsay, R. G. (1989). Activation of c-myb by carboxy-terminal truncation: relationship to transformation of murine haemopoietic cells in vitro. *EMBO J, 8*(6), 1777-1783.

Gong, Y., Cao, P., Yu, H. J., & Jiang, T. (2008). Crystal structure of the neurotrophin-3 and p75NTR symmetrical complex. *Nature, 454*(7205), 789-793. doi:10.1038/nature07089

Gottardi, C. J., & Gumbiner, B. M. (2004). Distinct molecular forms of beta-catenin are targeted to adhesive or transcriptional complexes. *J Cell Biol, 167*(2), 339-349. doi:10.1083/jcb.200402153

Graham, F. L., Smiley, J., Russell, W. C., & Nairn, R. (1977). Characteristics of a human cell line transformed by DNA from human adenovirus type 5. *J Gen Virol, 36*(1), 59-74. doi:10.1099/0022-1317-36-1-59

Grasser, F. A., Graf, T., & Lipsick, J. S. (1991). Protein truncation is required for the activation of the c-myb proto-oncogene. *Mol Cell Biol, 11*(8), 3987-3996.

Greig, K. T., de Graaf, C. A., Murphy, J. M., Carpinelli, M. R., Pang, S. H., Frampton, J., Kile, B. T., Hilton, D. J., & Nutt, S. L. (2010). Critical roles for c-Myb in lymphoid priming and early B-cell development. *Blood, 115*(14), 2796-2805. doi:10.1182/blood-2009-08-239210

Grossmann, P., Vanecek, T., Steiner, P., Kacerovska, D., Spagnolo, D. V., Cribier, B., Rose, C., Vazmitel, M., Carlson, J. A., Emberger, M., Martinek, P., Pearce, R. L., Pearn, J., Michal, M., & Kazakov, D. V. (2013). Novel and recurrent germline and somatic mutations in a cohort of 67 patients from 48 families with Brooke-Spiegler syndrome including the phenotypic variant of multiple familial trichoepitheliomas and correlation with the histopathologic findings in 379 biopsy specimens. *Am J Dermatopathol, 35*(1), 34-44. doi:10.1097/DAD.0b013e31824e7658

Guiton, M., Gunn-Moore, F. J., Glass, D. J., Geis, D. R., Yancopoulos, G. D., & Tavare, J. M. (1995). Naturally occurring tyrosine kinase inserts block high affinity binding of phospholipase C gamma and Shc to TrkC and neurotrophin-3 signaling. *J Biol Chem, 270*(35), 20384-20390.

Haapasalo, A., Sipola, I., Larsson, K., Akerman, K. E., Stoilov, P., Stamm, S., Wong, G., & Castren, E. (2002). Regulation of TRKB surface expression by brain-derived neurotrophic factor and truncated TRKB isoforms. *J Biol Chem, 277*(45), 43160-43167. doi:10.1074/jbc.M205202200

Hadweh, P., Chaitoglou, I., Gravato-Nobre, MJ., Ligoxygakis, P., Mosialos, G., Hatzivassiliou, E. (2018). Functional analysis of the *C.elegans cyld-1* gene reveals extensive similarity with its human homolog. *PLoS One, 13*(2), e0191864. doi: 10.1371/journal.pone.0191864

Hagihara, K., Nishikawa, T., Sugamata, Y., Song, J., Isobe, T., Taga, T., & Yoshizaki, K. (2005). Essential role of STAT3 in cytokine-driven NF-kappaB-mediated serum amyloid A gene expression. *Genes Cells, 10*(11), 1051-1063. doi:10.1111/j.1365-2443.2005.00900.x

Haglund, K., & Dikic, I. (2005). Ubiquitylation and cell signaling. *EMBO J, 24*(19), 3353-3359. doi:10.1038/sj.emboj.7600808

Hamanoue, M., Middleton, G., Wyatt, S., Jaffray, E., Hay, R. T., & Davies, A. M. (1999). p75-mediated NF-kappaB activation enhances the survival response of developing sensory neurons to nerve growth factor. *Mol Cell Neurosci, 14*(1), 28-40. doi:10.1006/mcne.1999.0770

Hamburger, A. W., & Salmon, S. E. (1977). Primary bioassay of human tumor stem cells. *Science, 197*(4302), 461-463.

Harper, S., & Davies, A. M. (1990). NGF mRNA expression in developing cutaneous epithelium related to innervation density. *Development, 110*(2), 515-519.

Haycock, J. W. (2011). 3D cell culture: a review of current approaches and techniques. *Methods Mol Biol, 695*, 1-15. doi:10.1007/978-1-60761-984-0_1

He, X. L., & Garcia, K. C. (2004). Structure of nerve growth factor complexed with the shared neurotrophin receptor p75. *Science, 304*(5672), 870-875. doi:10.1126/science.1095190

Headington, J. T., Batsakis, J. G., Beals, T. F., Campbell, T. E., Simmons, J. L., & Stone, W. D. (1977). Membranous basal cell adenoma of parotid gland, dermal cylindromas, and trichoepitheliomas. Comparative histochemistry and ultrastructure. *Cancer, 39*(6), 2460-2469.

Hempstead, B. L., Martin-Zanca, D., Kaplan, D. R., Parada, L. F., & Chao, M. V. (1991). High-affinity NGF binding requires coexpression of the trk proto-oncogene and the low-affinity NGF receptor. *Nature, 350*(6320), 678-683. doi:10.1038/350678a0

Hetman, M., Cavanaugh, J. E., Kimelman, D., & Xia, Z. (2000). Role of glycogen synthase kinase-3beta in neuronal apoptosis induced by trophic withdrawal. *J Neurosci, 20*(7), 2567-2574.

Hijiya, N., Zhang, J., Ratajczak, M. Z., Kant, J. A., DeRiel, K., Herlyn, M., Zon, G., & Gewirtz, A. M. (1994). Biologic and therapeutic significance of MYB expression in human melanoma. *Proc Natl Acad Sci U S A, 91*(10), 4499-4503.

Ho, A. S., Kannan, K., Roy, D. M., Morris, L. G., Ganly, I., Katabi, N., Ramaswami, D., Walsh, L. A., Eng, S., Huse, J. T., Zhang, J., Dolgalev, I., Huberman, K., Heguy, A., Viale, A., Drobnjak, M., Leversha, M. A., Rice, C. E., Singh, B., Iyer, N. G., Leemans, C. R., Bloemena, E., Ferris, R. L., Seethala, R. R., Gross, B. E., Liang, Y., Sinha, R., Peng, L., Raphael, B. J., Turcan, S., Gong, Y., Schultz, N., Kim, S., Chiosea, S., Shah, J. P., Sander, C., Lee, W., & Chan, T. A. (2013). The mutational landscape of adenoid cystic carcinoma. *Nat Genet, 45*(7), 791-798. doi:10.1038/ng.2643

Hoesel, B., & Schmid, J. A. (2013). The complexity of NF-kappaB signaling in inflammation and cancer. *Mol Cancer, 12*, 86. doi:10.1186/1476-4598-12-86

Holgado-Madruga, M., Moscatello, D. K., Emlet, D. R., Dieterich, R., & Wong, A. J. (1997). Grb2-associated binder-1 mediates phosphatidylinositol 3-kinase activation and the promotion of cell survival by nerve growth factor. *Proc Natl Acad Sci U S A, 94*(23), 12419-12424.

Hongisto, V., Jernstrom, S., Fey, V., Mpindi, J. P., Kleivi Sahlberg, K., Kallioniemi, O., & Perala, M. (2013). High-throughput 3D screening reveals differences in drug sensitivities between culture models of JIMT1 breast cancer cells. *PLoS One, 8*(10), e77232. doi:10.1371/journal.pone.0077232

Hovelmeyer, N., Wunderlich, F. T., Massoumi, R., Jakobsen, C. G., Song, J., Worns, M. A., Merkwirth, C., Kovalenko, A., Aumailley, M., Strand, D., Bruning, J. C., Galle, P. R., Wallach, D., Fassler, R., & Waisman, A. (2007). Regulation of B cell homeostasis and activation by the tumor suppressor gene CYLD. *J Exp Med, 204*(11), 2615-2627. doi:10.1084/jem.20070318

Howe, K. M., Reakes, C. F., & Watson, R. J. (1990). Characterization of the sequence-specific interaction of mouse c-myb protein with DNA. *EMBO J, 9*(1), 161-169.

Huang, E. J., & Reichardt, L. F. (2001). Neurotrophins: roles in neuronal development and function. *Annu Rev Neurosci, 24*, 677-736. doi:10.1146/annurev.neuro.24.1.677

Huang, E. J., & Reichardt, L. F. (2003). Trk receptors: roles in neuronal signal transduction. *Annu Rev Biochem, 72*, 609-642. doi:10.1146/annurev.biochem.72.121801.161629

Huang, E. J., Wilkinson, G. A., Farinas, I., Backus, C., Zang, K., Wong, S. L., & Reichardt, L. F. (1999). Expression of Trk receptors in the developing mouse trigeminal ganglion: in vivo evidence for NT-3 activation of TrkA and TrkB in addition to TrkC. *Development, 126*(10), 2191-2203.

Huang, S. H., Zhao, L., Sun, Z. P., Li, X. Z., Geng, Z., Zhang, K. D., Chao, M. V., & Chen, Z. Y. (2009). Essential role of Hrs in endocytic recycling of full-length TrkB receptor but not its isoform TrkB.T1. *J Biol Chem, 284*(22), 15126-15136. doi:10.1074/jbc.M809763200

Huebner, K., Isobe, M., Chao, M., Bothwell, M., Ross, A. H., Finan, J., Hoxie, J. A., Sehgal, A., Buck, C. R., Lanahan, A., & et al. (1986). The nerve growth factor receptor gene is at human chromosome region 17q12-17q22, distal to the

chromosome 17 breakpoint in acute leukemias. *Proc Natl Acad Sci U S A, 83*(5), 1403-1407.

Hugo, H., Cures, A., Suraweera, N., Drabsch, Y., Purcell, D., Mantamadiotis, T., Phillips, W., Dobrovic, A., Zupi, G., Gonda, T. J., Iacopetta, B., & Ramsay, R. G. (2006). Mutations in the MYB intron I regulatory sequence increase transcription in colon cancers. *Genes Chromosomes Cancer, 45*(12), 1143-1154. doi:10.1002/gcc.20378

Hutti, J. E., Shen, R. R., Abbott, D. W., Zhou, A. Y., Sprott, K. M., Asara, J. M., Hahn, W. C., & Cantley, L. C. (2009). Phosphorylation of the tumor suppressor CYLD by the breast cancer oncogene IKKepsilon promotes cell transformation. *Mol Cell, 34*(4), 461-472. doi:10.1016/j.molcel.2009.04.031

Ibanez, C. F., & Simi, A. (2012). p75 neurotrophin receptor signaling in nervous system injury and degeneration: paradox and opportunity. *Trends Neurosci, 35*(7), 431-440. doi:10.1016/j.tins.2012.03.007

Ichaso, N., Rodriguez, R. E., Martin-Zanca, D., & Gonzalez-Sarmiento, R. (1998). Genomic characterization of the human trkC gene. *Oncogene, 17*(14), 1871-1875. doi:10.1038/sj.onc.1202100

Ikeda, F., & Dikic, I. (2008). Atypical ubiquitin chains: new molecular signals. 'Protein Modifications: Beyond the Usual Suspects' review series. *EMBO Rep, 9*(6), 536-542. doi:10.1038/embor.2008.93

Iliopoulos, D., Jaeger, S. A., Hirsch, H. A., Bulyk, M. L., & Struhl, K. (2010). STAT3 activation of miR-21 and miR-181b-1 via PTEN and CYLD are part of the epigenetic switch linking inflammation to cancer. *Mol Cell, 39*(4), 493-506. doi:10.1016/j.molcel.2010.07.023

Inagaki, N., Thoenen, H., & Lindholm, D. (1995). TrkA tyrosine residues involved in NGF-induced neurite outgrowth of PC12 cells. *Eur J Neurosci, 7*(6), 1125-1133.

Inoue, J., Gohda, J., Akiyama, T., & Semba, K. (2007). NF-kappaB activation in development and progression of cancer. *Cancer Sci, 98*(3), 268-274. doi:10.1111/j.1349-7006.2007.00389.x

Ip, N. Y., Stitt, T. N., Tapley, P., Klein, R., Glass, D. J., Fandl, J., Greene, L. A., Barbacid, M., & Yancopoulos, G. D. (1993). Similarities and differences in the way neurotrophins interact with the Trk receptors in neuronal and nonneuronal cells. *Neuron, 10*(2), 137-149.

Ishiguro, Y., Ishiguro, H., & Miyamoto, H. (2013). Epidermal growth factor receptor tyrosine kinase inhibition up-regulates interleukin-6 in cancer cells and induces subsequent development of interstitial pneumonia. *Oncotarget, 4*(4), 550-559. doi:10.18632/oncotarget.939

Islam, O., Loo, T. X., & Heese, K. (2009). Brain-derived neurotrophic factor (BDNF) has proliferative effects on neural stem cells through the truncated TRK-B receptor, MAP kinase, AKT, and STAT-3 signaling pathways. *Curr Neurovasc Res, 6*(1), 42-53.

Ivanov, S. V., Panaccione, A., Brown, B., Guo, Y., Moskaluk, C. A., Wick, M. J., Brown, J. L., Ivanova, A. V., Issaeva, N., El-Naggar, A. K., & Yarbrough, W. G. (2013). TrkC signaling is activated in adenoid cystic carcinoma and requires NT-3 to stimulate invasive behavior. *Oncogene, 32*(32), 3698-3710. doi:10.1038/onc.2012.377

Ivanova, O., Braas, D., & Klempnauer, K. H. (2007). Oncogenic point mutations in the Myb DNA-binding domain alter the DNA-binding properties of Myb at a

physiological target gene. *Nucleic Acids Res, 35*(21), 7237-7247. doi:10.1093/nar/gkm675

Jacobson, M. D., Weil, M., & Raff, M. C. (1997). Programmed cell death in animal development. *Cell, 88*(3), 347-354.

Jadhav, T., Geetha, T., Jiang, J., & Wooten, M. W. (2008). Identification of a consensus site for TRAF6/p62 polyubiquitination. *Biochem Biophys Res Commun, 371*(3), 521-524. doi:10.1016/j.bbrc.2008.04.138

Jeanneteau, F., Garabedian, M. J., & Chao, M. V. (2008). Activation of Trk neurotrophin receptors by glucocorticoids provides a neuroprotective effect. *Proc Natl Acad Sci U S A, 105*(12), 4862-4867. doi:10.1073/pnas.0709102105

Jin, W., Chang, M., Paul, E. M., Babu, G., Lee, A. J., Reiley, W., Wright, A., Zhang, M., You, J., & Sun, S. C. (2008). Deubiquitinating enzyme CYLD negatively regulates RANK signaling and osteoclastogenesis in mice. *J Clin Invest, 118*(5), 1858-1866. doi:10.1172/jci34257

Jin, Y. J., Wang, S., Cho, J., Selim, M. A., Wright, T., Mosialos, G., & Zhang, J. Y. (2016). Epidermal CYLD inactivation sensitizes mice to the development of sebaceous and basaloid skin tumors. *JCI Insight, 1*(11). doi:10.1172/jci.insight.86548

Johnson, D., Lanahan, A., Buck, C. R., Sehgal, A., Morgan, C., Mercer, E., Bothwell, M., & Chao, M. (1986). Expression and structure of the human NGF receptor. *Cell, 47*(4), 545-554.

Jones, P. H., & Watt, F. M. (1993). Separation of human epidermal stem cells from transit amplifying cells on the basis of differences in integrin function and expression. *Cell, 73*(4), 713-724.

Jono, H., Lim, J. H., Chen, L. F., Xu, H., Trompouki, E., Pan, Z. K., Mosialos, G., & Li, J. D. (2004). NF-kappaB is essential for induction of CYLD, the negative regulator of NF-kappaB: evidence for a novel inducible autoregulatory feedback pathway. *J Biol Chem, 279*(35), 36171-36174. doi:10.1074/jbc.M406638200

Jungehulsing, M., Wagner, M., & Damm, M. (1999). Turban tumour with involvement of the parotid gland. *J Laryngol Otol, 113*(8), 779-783.

Kallam, A. R., Satyanarayana, M. A., Aryasomayajula, S., & Krishna, B. A. (2016). Basal Cell Carcinoma Developing from Trichoepithelioma: Review of Three Cases. *J Clin Diagn Res, 10*(3), Pd17-19. doi:10.7860/jcdr/2016/15432.7464

Kanei-Ishii, C., MacMillan, E. M., Nomura, T., Sarai, A., Ramsay, R. G., Aimoto, S., Ishii, S., & Gonda, T. J. (1992). Transactivation and transformation by Myb are negatively regulated by a leucine-zipper structure. *Proc Natl Acad Sci U S A, 89*(7), 3088-3092.

Kanei-Ishii, C., Ninomiya-Tsuji, J., Tanikawa, J., Nomura, T., Ishitani, T., Kishida, S., Kokura, K., Kurahashi, T., Ichikawa-Iwata, E., Kim, Y., Matsumoto, K., & Ishii, S. (2004). Wnt-1 signal induces phosphorylation and degradation of c-Myb protein via TAK1, HIPK2, and NLK. *Genes Dev, 18*(7), 816-829. doi:10.1101/gad.1170604

Kanei-Ishii, C., Nomura, T., Takagi, T., Watanabe, N., Nakayama, K. I., & Ishii, S. (2008). Fbxw7 acts as an E3 ubiquitin ligase that targets c-Myb for nemo-like kinase (NLK)-induced degradation. *J Biol Chem, 283*(45), 30540-30548. doi:10.1074/jbc.M804340200

Kanei-Ishii, C., Yasukawa, T., Morimoto, R. I., & Ishii, S. (1994). c-Myb-induced trans-activation mediated by heat shock elements without sequence-specific DNA binding of c-Myb. *J Biol Chem, 269*(22), 15768-15775.

Kanning, K. C., Hudson, M., Amieux, P. S., Wiley, J. C., Bothwell, M., & Schecterson, L. C. (2003). Proteolytic processing of the p75 neurotrophin receptor and two homologs generates C-terminal fragments with signaling capability. *J Neurosci, 23*(13), 5425-5436.

Kaplan, D. R., Martin-Zanca, D., & Parada, L. F. (1991). Tyrosine phosphorylation and tyrosine kinase activity of the trk proto-oncogene product induced by NGF. *Nature, 350*(6314), 158-160. doi:10.1038/350158a0

Kaplan, D. R., Matsumoto, K., Lucarelli, E., & Thiele, C. J. (1993). Induction of TrkB by retinoic acid mediates biologic responsiveness to BDNF and differentiation of human neuroblastoma cells. Eukaryotic Signal Transduction Group. *Neuron, 11*(2), 321-331.

Kaplan, D. R., & Miller, F. D. (2000). Neurotrophin signal transduction in the nervous system. *Curr Opin Neurobiol, 10*(3), 381-391.

Kaptein, A., Paillard, V., & Saunders, M. (1996). Dominant negative stat3 mutant inhibits interleukin-6-induced Jak-STAT signal transduction. *J Biol Chem, 271*(11), 5961-5964.

Karin, M. (2009). NF-kappaB as a critical link between inflammation and cancer. *Cold Spring Harb Perspect Biol, 1*(5), a000141. doi:10.1101/cshperspect.a000141

Karin, M., Cao, Y., Greten, F. R., & Li, Z. W. (2002). NF-kappaB in cancer: from innocent bystander to major culprit. *Nat Rev Cancer, 2*(4), 301-310. doi:10.1038/nrc780

Kariya, Y., Moriya, T., Suzuki, T., Chiba, M., Ishida, K., Takeyama, J., Endoh, M., Watanabe, M., & Sasano, H. (2005). Sex steroid hormone receptors in human skin appendage and its neoplasms. *Endocr J, 52*(3), 317-325.

Kaspar, P., Zikova, M., Bartunek, P., Sterba, J., Strnad, H., Kren, L., & Sedlacek, R. (2015). The Expression of c-Myb Correlates with the Levels of Rhabdomyosarcoma-specific Marker Myogenin. *Sci Rep, 5*, 15090. doi:10.1038/srep15090

Kauraniemi, P., Hedenfalk, I., Persson, K., Duggan, D. J., Tanner, M., Johannsson, O., Olsson, H., Trent, J. M., Isola, J., & Borg, A. (2000). MYB oncogene amplification in hereditary BRCA1 breast cancer. *Cancer Res, 60*(19), 5323-5328.

Kazakov, D. V., Thoma-Uszynski, S., Vanecek, T., Kacerovska, D., Grossmann, P., & Michal, M. (2009). A case of Brooke-Spiegler syndrome with a novel germline deep intronic mutation in the CYLD gene leading to intronic exonization, diverse somatic mutations, and unusual histology. *Am J Dermatopathol, 31*(7), 664-673. doi:10.1097/DAD.0b013e3181a05dad

Kazakov, D. V., Zelger, B., Rutten, A., Vazmitel, M., Spagnolo, D. V., Kacerovska, D., Vanecek, T., Grossmann, P., Sima, R., Grayson, W., Calonje, E., Koren, J., Mukensnabl, P., Danis, D., & Michal, M. (2009). Morphologic diversity of malignant neoplasms arising in preexisting spiradenoma, cylindroma, and spiradenocylindroma based on the study of 24 cases, sporadic or occurring in the setting of Brooke-Spiegler syndrome. *Am J Surg Pathol, 33*(5), 705-719. doi:10.1097/PAS.0b013e3181966762

Kenchappa, R. S., Zampieri, N., Chao, M. V., Barker, P. A., Teng, H. K., Hempstead, B. L., & Carter, B. D. (2006). Ligand-dependent cleavage of the P75 neurotrophin receptor is necessary for NRIF nuclear translocation and apoptosis in sympathetic neurons. *Neuron, 50*(2), 219-232. doi:10.1016/j.neuron.2006.03.011

Khursigara, G., Bertin, J., Yano, H., Moffett, H., DiStefano, P. S., & Chao, M. V. (2001). A prosurvival function for the p75 receptor death domain mediated via the

caspase recruitment domain receptor-interacting protein 2. *J Neurosci, 21*(16), 5854-5863.

Khursigara, G., Orlinick, J. R., & Chao, M. V. (1999). Association of the p75 neurotrophin receptor with TRAF6. *J Biol Chem, 274*(5), 2597-2600.

Kim, C. J., Matsuo, T., Lee, K. H., & Thiele, C. J. (1999). Up-regulation of insulin-like growth factor-II expression is a feature of TrkA but not TrkB activation in SH-SY5Y neuroblastoma cells. *Am J Pathol, 155*(5), 1661-1670. doi:10.1016/s0002-9440(10)65481-8

Kim, D. J., Angel, J. M., Sano, S., & DiGiovanni, J. (2009). Constitutive activation and targeted disruption of signal transducer and activator of transcription 3 (Stat3) in mouse epidermis reveal its critical role in UVB-induced skin carcinogenesis. *Oncogene, 28*(7), 950-960. doi:10.1038/onc.2008.453

Kim, E., & Jeon, W. B. (2013). Gene expression analysis of 3D spheroid culture of human embryonic kidney cells. *Toxicol. Environ. Health Sci., 5*(2), 97-106. doi:10.1007/s13530-013-0160-y

Kim, J. B. (2005). Three-dimensional tissue culture models in cancer biology. *Semin Cancer Biol, 15*(5), 365-377. doi:10.1016/j.semcancer.2005.05.002

Kim, M. S., Lee, W. S., Jeong, J., Kim, S. J., & Jin, W. (2015). Induction of metastatic potential by TrkB via activation of IL6/JAK2/STAT3 and PI3K/AKT signaling in breast cancer. *Oncotarget, 6*(37), 40158-40171. doi:10.18632/oncotarget.5522

Kim, Y., & He, Y. Y. (2014). Ultraviolet radiation-induced non-melanoma skin cancer: Regulation of DNA damage repair and inflammation. *Genes Dis, 1*(2), 188-198. doi:10.1016/j.gendis.2014.08.005

Kimlin, L. C., Casagrande, G., & Virador, V. M. (2013). In vitro three-dimensional (3D) models in cancer research: an update. *Mol Carcinog, 52*(3), 167-182. doi:10.1002/mc.21844

Klein, R., Silos-Santiago, I., Smeyne, R. J., Lira, S. A., Brambilla, R., Bryant, S., Zhang, L., Snider, W. D., & Barbacid, M. (1994). Disruption of the neurotrophin-3 receptor gene trkC eliminates la muscle afferents and results in abnormal movements. *Nature, 368*(6468), 249-251. doi:10.1038/368249a0

Klein, R., Smeyne, R. J., Wurst, W., Long, L. K., Auerbach, B. A., Joyner, A. L., & Barbacid, M. (1993). Targeted disruption of the trkB neurotrophin receptor gene results in nervous system lesions and neonatal death. *Cell, 75*(1), 113-122.

Kleinman, H. K., & Martin, G. R. (2005). Matrigel: basement membrane matrix with biological activity. *Semin Cancer Biol, 15*(5), 378-386. doi:10.1016/j.semcancer.2005.05.004

Knudson, A. G., Jr. (1971). Mutation and cancer: statistical study of retinoblastoma. *Proc Natl Acad Sci U S A, 68*(4), 820-823.

Kobayashi, K., Ando, M., Saito, Y., Kondo, K., Omura, G., Shinozaki-Ushiku, A., Fukayama, M., Asakage, T., & Yamasoba, T. (2015). Nerve Growth Factor Signals as Possible Pathogenic Biomarkers for Perineural Invasion in Adenoid Cystic Carcinoma. *Otolaryngol Head Neck Surg, 153*(2), 218-224. doi:10.1177/0194599815584762

Koepp, D. M., Schaefer, L. K., Ye, X., Keyomarsi, K., Chu, C., Harper, J. W., & Elledge, S. J. (2001). Phosphorylation-dependent ubiquitination of cyclin E by the SCFFbw7 ubiquitin ligase. *Science, 294*(5540), 173-177. doi:10.1126/science.1065203

Komander, D., Lord, C. J., Scheel, H., Swift, S., Hofmann, K., Ashworth, A., & Barford, D. (2008). The structure of the CYLD USP domain explains its specificity for Lys63-

linked polyubiquitin and reveals a B box module. *Mol Cell, 29*(4), 451-464. doi:10.1016/j.molcel.2007.12.018

Komander, D., & Rape, M. (2012). The ubiquitin code. *Annu Rev Biochem, 81*, 203-229. doi:10.1146/annurev-biochem-060310-170328

Komander, D., Reyes-Turcu, F., Licchesi, J. D., Odenwaelder, P., Wilkinson, K. D., & Barford, D. (2009). Molecular discrimination of structurally equivalent Lys 63-linked and linear polyubiquitin chains. *EMBO Rep, 10*(5), 466-473. doi:10.1038/embor.2009.55

Kommaddi, R. P., Thomas, R., Ceni, C., Daigneault, K., & Barker, P. A. (2011). Trk-dependent ADAM17 activation facilitates neurotrophin survival signaling. *Faseb j, 25*(6), 2061-2070. doi:10.1096/fj.10-173740

Kostler, E., Schonlebe, J., Mentzel, T., Haroske, G., & Wollina, U. (2005). Psoriasis and Brooke-Spiegler syndrome with multiple malignancies. *J Eur Acad Dermatol Venereol, 19*(3), 380-381. doi:10.1111/j.1468-3083.2005.01037.x

Kovalenko, A., Chable-Bessia, C., Cantarella, G., Israel, A., Wallach, D., & Courtois, G. (2003). The tumour suppressor CYLD negatively regulates NF-kappaB signalling by deubiquitination. *Nature, 424*(6950), 801-805. doi:10.1038/nature01802

Kraemer, B. R., Yoon, S. O., & Carter, B. D. (2014). The biological functions and signaling mechanisms of the p75 neurotrophin receptor. *Handb Exp Pharmacol, 220*, 121-164. doi:10.1007/978-3-642-45106-5_6

Kryl, D., & Barker, P. A. (2000). TTIP is a novel protein that interacts with the truncated T1 TrkB neurotrophin receptor. *Biochem Biophys Res Commun, 279*(3), 925-930. doi:10.1006/bbrc.2000.4058

Kuklani, R. M., Glavin, F. L., & Bhattacharyya, I. (2009). Malignant cylindroma of the scalp arising in a setting of multiple cylindromatosis: a case report. *Head Neck Pathol, 3*(4), 315-319. doi:10.1007/s12105-009-0138-x

Kumar, A., Baker, S. J., Lee, C. M., & Reddy, E. P. (2003). Molecular mechanisms associated with the regulation of apoptosis by the two alternatively spliced products of c-Myb. *Mol Cell Biol, 23*(18), 6631-6645.

Kumar, V., Palermo, R., Talora, C., Campese, A. F., Checquolo, S., Bellavia, D., Tottone, L., Testa, G., Miele, E., Indraccolo, S., Amadori, A., Ferretti, E., Gulino, A., Vacca, A., & Screpanti, I. (2014). Notch and NF-kB signaling pathways regulate miR-223/FBXW7 axis in T-cell acute lymphoblastic leukemia. *Leukemia, 28*(12), 2324-2335. doi:10.1038/leu.2014.133

Kupferman, M. E., Jiffar, T., El-Naggar, A., Yilmaz, T., Zhou, G., Xie, T., Feng, L., Wang, J., Holsinger, F. C., Yu, D., & Myers, J. N. (2010). TrkB induces EMT and has a key role in invasion of head and neck squamous cell carcinoma. *Oncogene, 29*(14), 2047-2059. doi:10.1038/onc.2009.486

Kuphal, S., Shaw-Hallgren, G., Eberl, M., Karrer, S., Aberger, F., Bosserhoff, A. K., & Massoumi, R. (2011). GLI1-dependent transcriptional repression of CYLD in basal cell carcinoma. *Oncogene, 30*(44), 4523-4530. doi:10.1038/onc.2011.163

Lahortiga, I., De Keersmaecker, K., Van Vlierberghe, P., Graux, C., Cauwelier, B., Lambert, F., Mentens, N., Beverloo, H. B., Pieters, R., Speleman, F., Odero, M. D., Bauters, M., Froyen, G., Marynen, P., Vandenberghe, P., Wlodarska, I., Meijerink, J. P., & Cools, J. (2007). Duplication of the MYB oncogene in T cell acute lymphoblastic leukemia. *Nat Genet, 39*(5), 593-595. doi:10.1038/ng2025

Lai, Y., Wei, X., Lin, S., Qin, L., Cheng, L., Li, P. (2017). Current status and perspectives of patient-derived xenograft models in cancer research. *J Hematol Oncol, 10*(1), 106. doi: 10.1186/s13045-017-0470-7

Lang, G., White, J. R., Argent-Katwala, M. J., Allinson, C. G., & Weston, K. (2005). Myb proteins regulate the expression of diverse target genes. *Oncogene, 24*(8), 1375-1384. doi:10.1038/sj.onc.1208301

Lange, A. M., & Lo, H. W. (2018). Inhibiting TRK proteins in clinical cancer therapy. *Cancers (Basel), 10*(4), 105. doi: 10.3390/cancers10040105

Lauder, A., Castellanos, A., & Weston, K. (2001). c-Myb transcription is activated by protein kinase B (PKB) following interleukin 2 stimulation of Tcells and is required for PKB-mediated protection from apoptosis. *Mol Cell Biol, 21*(17), 5797-5805.

Le Bras, S., Loyer, N., & Le Borgne, R. (2011). The multiple facets of ubiquitination in the regulation of notch signaling pathway. *Traffic, 12*(2), 149-161. doi:10.1111/j.1600-0854.2010.01126.x

Leblebici, C., Pasaoglu, E., Kelten, C., Darakci, S., & Dursun, N. (2017). Cytokeratin 17 and Ki-67: Immunohistochemical markers for the differential diagnosis of keratoacanthoma and squamous cell carcinoma. *Oncol Lett, 13*(4), 2539-2548. doi:10.3892/ol.2017.5793

Lee, B. C., Miyata, M., Lim, J. H., & Li, J. D. (2016). Deubiquitinase CYLD acts as a negative regulator for bacterium NTHi-induced inflammation by suppressing K63-linked ubiquitination of MyD88. *Proc Natl Acad Sci U S A, 113*(2), E165-171. doi:10.1073/pnas.1518615113

Lee, D. A., Grossman, M. E., Schneiderman, P., & Celebi, J. T. (2005). Genetics of skin appendage neoplasms and related syndromes. *J Med Genet, 42*(11), 811-819. doi:10.1136/jmg.2004.025577

Lee, F. S., & Chao, M. V. (2001). Activation of Trk neurotrophin receptors in the absence of neurotrophins. *Proc Natl Acad Sci U S A, 98*(6), 3555-3560. doi:10.1073/pnas.061020198

Lee, F. S., Kim, A. H., Khursigara, G., & Chao, M. V. (2001). The uniqueness of being a neurotrophin receptor. *Curr Opin Neurobiol, 11*(3), 281-286.

Lee, H., Herrmann, A., Deng, J. H., Kujawski, M., Niu, G., Li, Z., Forman, S., Jove, R., Pardoll, D. M., & Yu, H. (2009). Persistently activated Stat3 maintains constitutive NF-kappaB activity in tumors. *Cancer Cell, 15*(4), 283-293. doi:10.1016/j.ccr.2009.02.015

Lee, H. J., Zhuang, G., Cao, Y., Du, P., Kim, H. J., & Settleman, J. (2014). Drug resistance via feedback activation of Stat3 in oncogene-addicted cancer cells. *Cancer Cell, 26*(2), 207-221. doi:10.1016/j.ccr.2014.05.019

Lee, K. F., Li, E., Huber, L. J., Landis, S. C., Sharpe, A. H., Chao, M. V., & Jaenisch, R. (1992). Targeted mutation of the gene encoding the low affinity NGF receptor p75 leads to deficits in the peripheral sensory nervous system. *Cell, 69*(5), 737-749.

Lee, K. H., Kim, J. E., Cho, B. K., Kim, Y. C., & Park, C. J. (2008). Malignant transformation of multiple familial trichoepithelioma: case report and literature review. *Acta Derm Venereol, 88*(1), 43-46. doi:10.2340/00015555-0322

Lee, R., Kermani, P., Teng, K. K., & Hempstead, B. L. (2001). Regulation of cell survival by secreted proneurotrophins. *Science, 294*(5548), 1945-1948. doi:10.1126/science.1065057

Lei, W., Rushton, J. J., Davis, L. M., Liu, F., & Ness, S. A. (2004). Positive and negative determinants of target gene specificity in myb transcription factors. *J Biol Chem, 279*(28), 29519-29527. doi:10.1074/jbc.M403133200

Leinonen, P. T., Hagg, P. M., Peltonen, S., Jouhilahti, E. M., Melkko, J., Korkiamaki, T., Oikarinen, A., & Peltonen, J. (2009). Reevaluation of the normal epidermal calcium gradient, and analysis of calcium levels and ATP receptors in Hailey-Hailey and Darier epidermis. *J Invest Dermatol, 129*(6), 1379-1387. doi:10.1038/jid.2008.381

Lenardo, M., & Siebenlist, U. (1994). Bcl-3-mediated nuclear regulation of the NF-kappa B trans-activating factor. *Immunol Today, 15*(4), 145-147.

Leprince, D., Gegonne, A., Coll, J., de Taisne, C., Schneeberger, A., Lagrou, C., & Stehelin, D. (1983). A putative second cell-derived oncogene of the avian leukaemia retrovirus E26. *Nature, 306*(5941), 395-397.

Lessmann, V., & Brigadski, T. (2009). Mechanisms, locations, and kinetics of synaptic BDNF secretion: an update. *Neurosci Res, 65*(1), 11-22. doi:10.1016/j.neures.2009.06.004

Leverson, J. D., & Ness, S. A. (1998). Point mutations in v-Myb disrupt a cyclophilin-catalyzed negative regulatory mechanism. *Mol Cell, 1*(2), 203-211.

Levi-Montalcini, R. (1987). The nerve growth factor 35 years later. *Science, 237*(4819), 1154-1162.

Levy, L., Broad, S., Diekmann, D., Evans, R. D., & Watt, F. M. (2000). beta1 integrins regulate keratinocyte adhesion and differentiation by distinct mechanisms. *Mol Biol Cell, 11*(2), 453-466.

Li, D., Gao, J., Yang, Y., Sun, L., Suo, S., Luo, Y., Shui, W., Zhou, J., & Liu, M. (2014). CYLD coordinates with EB1 to regulate microtubule dynamics and cell migration. *Cell Cycle, 13*(6), 974-983. doi:10.4161/cc.27838

Li, H. S., Xu, X. Z., & Montell, C. (1999). Activation of a TRPC3-dependent cation current through the neurotrophin BDNF. *Neuron, 24*(1), 261-273.

Li, Y., Jin, K., van Pelt, G. W., van Dam, H., Yu, X., Mesker, W. E., Ten Dijke, P., Zhou, F., & Zhang, L. (2016). c-Myb Enhances Breast Cancer Invasion and Metastasis through the Wnt/beta-Catenin/Axin2 Pathway. *Cancer Res, 76*(11), 3364-3375. doi:10.1158/0008-5472.can-15-2302

Liepinsh, E., Ilag, L. L., Otting, G., & Ibanez, C. F. (1997). NMR structure of the death domain of the p75 neurotrophin receptor. *EMBO J, 16*(16), 4999-5005. doi:10.1093/emboj/16.16.4999

Lieu, Y. K., & Reddy, E. P. (2009). Conditional c-myb knockout in adult hematopoietic stem cells leads to loss of self-renewal due to impaired proliferation and accelerated differentiation. *Proc Natl Acad Sci U S A, 106*(51), 21689-21694. doi:10.1073/pnas.0907623106

Lim, J. H., Ha, U. H., Woo, C. H., Xu, H., & Li, J. D. (2008). CYLD is a crucial negative regulator of innate immune response in Escherichia coli pneumonia. *Cell Microbiol, 10*(11), 2247-2256. doi:10.1111/j.1462-5822.2008.01204.x

Lim, X., & Nusse, R. (2013). Wnt signaling in skin development, homeostasis, and disease. *Cold Spring Harb Perspect Biol, 5*(2). doi:10.1101/cshperspect.a008029

Linggi, M. S., Burke, T. L., Williams, B. B., Harrington, A., Kraemer, R., Hempstead, B. L., Yoon, S. O., & Carter, B. D. (2005). Neurotrophin receptor interacting factor (NRIF) is an essential mediator of apoptotic signaling by the p75 neurotrophin receptor. *J Biol Chem, 280*(14), 13801-13808. doi:10.1074/jbc.M410435200

Liu, F., Lei, W., O'Rourke, J. P., & Ness, S. A. (2006). Oncogenic mutations cause dramatic, qualitative changes in the transcriptional activity of c-Myb. *Oncogene, 25*(5), 795-805. doi:10.1038/sj.onc.1209105

Liu, H. H., Xie, M., Schneider, M. D., & Chen, Z. J. (2006). Essential role of TAK1 in thymocyte development and activation. *Proc Natl Acad Sci U S A, 103*(31), 11677-11682. doi:10.1073/pnas.0603089103

Liu, N., Zhang, J., & Ji, C. (2013). The emerging roles of Notch signaling in leukemia and stem cells. *Biomark Res, 1*(1), 23. doi:10.1186/2050-7771-1-23

Liu, Y. Z., Boxer, L. M., & Latchman, D. S. (1999). Activation of the Bcl-2 promoter by nerve growth factor is mediated by the p42/p44 MAPK cascade. *Nucleic Acids Res, 27*(10), 2086-2090.

Lorenzo, P. I., Brendeford, E. M., Gilfillan, S., Gavrilov, A. A., Leedsak, M., Razin, S. V., Eskeland, R., Saether, T., & Gabrielsen, O. S. (2011). Identification of c-Myb Target Genes in K562 Cells Reveals a Role for c-Myb as a Master Regulator. *Genes Cancer, 2*(8), 805-817. doi:10.1177/1947601911428224

Lou, H., Kim, S. K., Zaitsev, E., Snell, C. R., Lu, B., & Loh, Y. P. (2005). Sorting and activity-dependent secretion of BDNF require interaction of a specific motif with the sorting receptor carboxypeptidase e. *Neuron, 45*(2), 245-255. doi:10.1016/j.neuron.2004.12.037

Lu, B., Pang, P. T., & Woo, N. H. (2005). The yin and yang of neurotrophin action. *Nat Rev Neurosci, 6*(8), 603-614. doi:10.1038/nrn1726

Luberg, K., Park, R., Aleksejeva, E., & Timmusk, T. (2015). Novel transcripts reveal a complex structure of the human TRKA gene and imply the presence of multiple protein isoforms. *BMC Neurosci, 16*, 78. doi:10.1186/s12868-015-0215-x

Luberg, K., Wong, J., Weickert, C. S., & Timmusk, T. (2010). Human TrkB gene: novel alternative transcripts, protein isoforms and expression pattern in the prefrontal cerebral cortex during postnatal development. *J Neurochem, 113*(4), 952-964. doi:10.1111/j.1471-4159.2010.06662.x

Luca, A. C., Mersch, S., Deenen, R., Schmidt, S., Messner, I., Schafer, K. L., Baldus, S. E., Huckenbeck, W., Piekorz, R. P., Knoefel, W. T., Krieg, A., & Stoecklein, N. H. (2013). Impact of the 3D microenvironment on phenotype, gene expression, and EGFR inhibition of colorectal cancer cell lines. *PLoS One, 8*(3), e59689. doi:10.1371/journal.pone.0059689

Luscher, B., Christenson, E., Litchfield, D. W., Krebs, E. G., & Eisenman, R. N. (1990). Myb DNA binding inhibited by phosphorylation at a site deleted during oncogenic activation. *Nature, 344*(6266), 517-522. doi:10.1038/344517a0

MacDonald, J. I., & Meakin, S. O. (1996). Deletions in the extracellular domain of rat trkA lead to an altered differentiative phenotype in neurotrophin responsive cells. *Mol Cell Neurosci, 7*(5), 371-390. doi:10.1006/mcne.1996.0027

MacPhee, I., & Barker, P. A. (1999). Extended ceramide exposure activates the trkA receptor by increasing receptor homodimer formation. *J Neurochem, 72*(4), 1423-1430.

Mahmoud, A., Hill, D. H., O'Sullivan, M. J., & Bennett, M. W. (2009). Cylindroma of the breast: a case report and review of the literature. *Diagn Pathol, 4*, 30. doi:10.1186/1746-1596-4-30

Makkerh, J. P., Ceni, C., Auld, D. S., Vaillancourt, F., Dorval, G., & Barker, P. A. (2005). p75 neurotrophin receptor reduces ligand-induced Trk receptor ubiquitination and delays Trk receptor internalization and degradation. *EMBO Rep, 6*(10), 936-941. doi:10.1038/sj.embor.7400503

Malaterre, J., Carpinelli, M., Ernst, M., Alexander, W., Cooke, M., Sutton, S., Dworkin, S., Heath, J. K., Frampton, J., McArthur, G., Clevers, H., Hilton, D., Mantamadiotis, T., & Ramsay, R. G. (2007). c-Myb is required for progenitor cell

homeostasis in colonic crypts. *Proc Natl Acad Sci U S A, 104*(10), 3829-3834. doi:10.1073/pnas.0610055104

Malaterre, J., Mantamadiotis, T., Dworkin, S., Lightowler, S., Yang, Q., Ransome, M. I., Turnley, A. M., Nichols, N. R., Emambokus, N. R., Frampton, J., & Ramsay, R. G. (2008). c-Myb is required for neural progenitor cell proliferation and maintenance of the neural stem cell niche in adult brain. *Stem Cells, 26*(1), 173-181. doi:10.1634/stemcells.2007-0293

Manzotti, G., Mariani, S. A., Corradini, F., Bussolari, R., Cesi, V., Vergalli, J., Ferrari-Amorotti, G., Fragliasso, V., Soliera, A. R., Cattelani, S., Raschella, G., Holyoake, T. L., & Calabretta, B. (2012). Expression of p89(c-Mybex9b), an alternatively spliced form of c-Myb, is required for proliferation and survival of p210BCR/ABL-expressing cells. *Blood Cancer J, 2*(5), e71. doi:10.1038/bcj.2012.16

Marconi, A., Panza, M. C., Bonnet-Duquennoy, M., Lazou, K., Kurfurst, R., Truzzi, F., Lotti, R., De Santis, G., Dumas, M., Bonte, F., & Pincelli, C. (2006). Expression and function of neurotrophins and their receptors in human melanocytes. *Int J Cosmet Sci, 28*(4), 255-261. doi:10.1111/j.1467-2494.2006.00321.x

Marconi, A., Terracina, M., Fila, C., Franchi, J., Bonté, F., Romagnoli, G., Maurelli, R., Failla, C. M., Dumas, M., & Pincelli, C. (2003). Expression and function of neurotrophins and their receptors in cultured human keratinocytes. *Journal of Investigative Dermatology, 121*(6), 1515-1521.

Marconi, A., Vaschieri, C., Zanoli, S., Giannetti, A., & Pincelli, C. (1999). Nerve growth factor protects human keratinocytes from ultraviolet-B-induced apoptosis. *Journal of Investigative Dermatology, 113*(6), 920-927.

Martin-Zanca, D., Hughes, S. H., & Barbacid, M. (1986). A human oncogene formed by the fusion of truncated tropomyosin and protein tyrosine kinase sequences. *Nature, 319*(6056), 743-748. doi:10.1038/319743a0

Martin-Zanca, D., Oskam, R., Mitra, G., Copeland, T., & Barbacid, M. (1989). Molecular and biochemical characterization of the human trk proto-oncogene. *Mol Cell Biol, 9*(1), 24-33.

Martinez, I., & Dimaio, D. (2011). B-Myb, cancer, senescence, and microRNAs. *Cancer Res, 71*(16), 5370-5373. doi:10.1158/0008-5472.can-11-1044

Martins, C., & Bartolo, E. (2000). Brooke-Spiegler syndrome: treatment of cylindromas with CO2 laser. *Dermatol Surg, 26*(9), 877-880; discussion 881.

Maruyama, H., Ishitsuka, Y., Fujisawa, Y., Furuta, J., Sekido, M., & Kawachi, Y. (2014). B-Myb enhances proliferation and suppresses differentiation of keratinocytes in three-dimensional cell culture. *Arch Dermatol Res, 306*(4), 375-384. doi:10.1007/s00403-014-1450-1

Massoumi, R., Chmielarska, K., Hennecke, K., Pfeifer, A., & Fassler, R. (2006). Cyld inhibits tumor cell proliferation by blocking Bcl-3-dependent NF-kappaB signaling. *Cell, 125*(4), 665-677. doi:10.1016/j.cell.2006.03.041

Massoumi, R., Kuphal, S., Hellerbrand, C., Haas, B., Wild, P., Spruss, T., Pfeifer, A., Fassler, R., & Bosserhoff, A. K. (2009). Down-regulation of CYLD expression by Snail promotes tumor progression in malignant melanoma. *J Exp Med, 206*(1), 221-232. doi:10.1084/jem.20082044

Massoumi, R., & Paus, R. (2007). Cylindromatosis and the CYLD gene: new lessons on the molecular principles of epithelial growth control. *Bioessays, 29*(12), 1203-1214. doi:10.1002/bies.20677

Massoumi, R., Podda, M., Fassler, R., & Paus, R. (2006). Cylindroma as tumor of hair follicle origin. *J Invest Dermatol, 126*(5), 1182-1184. doi:10.1038/sj.jid.5700218

Meakin, S. O., MacDonald, J. I., Gryz, E. A., Kubu, C. J., & Verdi, J. M. (1999). The signaling adapter FRS-2 competes with Shc for binding to the nerve growth factor receptor TrkA. A model for discriminating proliferation and differentiation. *J Biol Chem, 274*(14), 9861-9870.

Meldolesi, J. (2017). Neurotrophin receptors in the pathogenesis, diagnosis and therapy of neurodegenerative diseases. *Pharmacol Res, 121*, 129-137. doi:10.1016/j.phrs.2017.04.024

Melly, L., Lawton, G., & Rajan, N. (2012). Basal cell carcinoma arising in association with trichoepithelioma in a case of Brooke-Spiegler syndrome with a novel genetic mutation in CYLD. *J Cutan Pathol, 39*(10), 977-978. doi:10.1111/j.1600-0560.2012.01952.x

Menn, B., Timsit, S., Calothy, G., & Lamballe, F. (1998). Differential expression of TrkC catalytic and noncatalytic isoforms suggests that they act independently or in association. *J Comp Neurol, 401*(1), 47-64.

Mertsching, H., Weimer, M., Kersen, S., & Brunner, H. (2008). Human skin equivalent as an alternative to animal testing. *GMS Krankenhhyg Interdiszip, 3*(1), Doc11.

Meybehm, M., & Fischer, H. P. (1997). Spiradenoma and dermal cylindroma: comparative immunohistochemical analysis and histogenetic considerations. *Am J Dermatopathol, 19*(2), 154-161.

Michal, M. (1996). Spiradenoma associated with apocrine adenoma component. *Pathol Res Pract, 192*(11), 1135-1139; discussion 1140-1131. doi:10.1016/s0344-0338(96)80032-x

Michal, M., Lamovec, J., Mukensnabl, P., & Pizinger, K. (1999). Spiradenocylindromas of the skin: tumors with morphological features of spiradenoma and cylindroma in the same lesion: report of 12 cases. *Pathol Int, 49*(5), 419-425.

Michaud, E. J., & Yoder, B. K. (2006). The primary cilium in cell signaling and cancer. *Cancer Res, 66*(13), 6463-6467. doi:10.1158/0008-5472.can-06-0462

Miliani de Marval, P., Lutfeali, S., Jin, J. Y., Leshin, B., Selim, M. A., & Zhang, J. Y. (2011). CYLD inhibits tumorigenesis and metastasis by blocking JNK/AP1 signaling at multiple levels. *Cancer Prev Res (Phila), 4*(6), 851-859. doi:10.1158/1940-6207.capr-10-0360

Minichiello, L., Casagranda, F., Tatche, R. S., Stucky, C. L., Postigo, A., Lewin, G. R., Davies, A. M., & Klein, R. (1998). Point mutation in trkB causes loss of NT4-dependent neurons without major effects on diverse BDNF responses. *Neuron, 21*(2), 335-345.

Miranda, C., Fumagalli, T., Anania, M. C., Vizioli, M. G., Pagliardini, S., Pierotti, M. A., & Greco, A. (2010). Role of STAT3 in in vitro transformation triggered by TRK oncogenes. *PLoS One, 5*(3), e9446. doi:10.1371/journal.pone.0009446

Mitani, Y., Li, J., Rao, P. H., Zhao, Y. J., Bell, D., Lippman, S. M., Weber, R. S., Caulin, C., & El-Naggar, A. K. (2010). Comprehensive analysis of the MYB-NFIB gene fusion in salivary adenoid cystic carcinoma: Incidence, variability, and clinicopathologic significance. *Clin Cancer Res, 16*(19), 4722-4731. doi:10.1158/1078-0432.ccr-10-0463

Mitchison, T. J. (2012). The proliferation rate paradox in antimitotic chemotherapy. *Mol Biol Cell, 23*(1), 1-6. doi:10.1091/mbc.E10-04-0335

Mitra, P., Pereira, L. A., Drabsch, Y., Ramsay, R. G., & Gonda, T. J. (2012). Estrogen receptor-alpha recruits P-TEFb to overcome transcriptional pausing in intron 1 of the MYB gene. *Nucleic Acids Res, 40*(13), 5988-6000. doi:10.1093/nar/gks286

Miyoshi, K., Takaishi, M., Nakajima, K., Ikeda, M., Kanda, T., Tarutani, M., Iiyama, T., Asao, N., DiGiovanni, J., & Sano, S. (2011). Stat3 as a therapeutic target for the treatment of psoriasis: a clinical feasibility study with STA-21, a Stat3 inhibitor. *J Invest Dermatol, 131*(1), 108-117. doi:10.1038/jid.2010.255

Mo, X., Kowenz-Leutz, E., Laumonnier, Y., Xu, H., & Leutz, A. (2005). Histone H3 tail positioning and acetylation by the c-Myb but not the v-Myb DNA-binding SANT domain. *Genes Dev, 19*(20), 2447-2457. doi:10.1101/gad.355405

Molvaersmyr, A. K., Saether, T., Gilfillan, S., Lorenzo, P. I., Kvaloy, H., Matre, V., & Gabrielsen, O. S. (2010). A SUMO-regulated activation function controls synergy of c-Myb through a repressor-activator switch leading to differential p300 recruitment. *Nucleic Acids Res, 38*(15), 4970-4984. doi:10.1093/nar/gkq245

Montano, X., & Djamgoz, M. B. (2004). Epidermal growth factor, neurotrophins and the metastatic cascade in prostate cancer. *FEBS Lett, 571*(1-3), 1-8. doi:10.1016/j.febslet.2004.06.088

Moritz, A., Li, Y., Guo, A., Villen, J., Wang, Y., MacNeill, J., Kornhauser, J., Sprott, K., Zhou, J., Possemato, A., Ren, J. M., Hornbeck, P., Cantley, L. C., Gygi, S. P., Rush, J., & Comb, M. J. (2010). Akt-RSK-S6 kinase signaling networks activated by oncogenic receptor tyrosine kinases. *Sci Signal, 3*(136), ra64. doi:10.1126/scisignal.2000998

Moriwaki, K., Tsuruta, D., Sugawara, H., Kobayashi, H., Massoumi, R., & Ishii, M. (2007). A role of CYLD in hair cycling mouse. *Journal of Investigative Dermatology, 127*, S107.

Moser, J. J., Fritzler, M. J., & Rattner, J. B. (2009). Primary ciliogenesis defects are associated with human astrocytoma/glioblastoma cells. *BMC Cancer, 9*, 448. doi:10.1186/1471-2407-9-448

Mucenski, M. L., McLain, K., Kier, A. B., Swerdlow, S. H., Schreiner, C. M., Miller, T. A., Pietryga, D. W., Scott, W. J., Jr., & Potter, S. S. (1991). A functional c-myb gene is required for normal murine fetal hepatic hematopoiesis. *Cell, 65*(4), 677-689.

Mukai, J., Hachiya, T., Shoji-Hoshino, S., Kimura, M. T., Nadano, D., Suvanto, P., Hanaoka, T., Li, Y., Irie, S., Greene, L. A., & Sato, T. A. (2000). NADE, a p75NTR-associated cell death executor, is involved in signal transduction mediated by the common neurotrophin receptor p75NTR. *J Biol Chem, 275*(23), 17566-17570. doi:10.1074/jbc.C000140200

Murer, M. G., Yan, Q., & Raisman-Vozari, R. (2001). Brain-derived neurotrophic factor in the control human brain, and in Alzheimer's disease and Parkinson's disease. *Prog Neurobiol, 63*(1), 71-124.

Nagy, N., Farkas, K., Kemeny, L., & Szell, M. (2015). Phenotype-genotype correlations for clinical variants caused by CYLD mutations. *Eur J Med Genet, 58*(5), 271-278. doi:10.1016/j.ejmg.2015.02.010

Nagy, N., Rajan, N., Farkas, K., Kinyo, A., Kemeny, L., & Szell, M. (2013). A mutational hotspot in CYLD causing cylindromas: a comparison of phenotypes arising in different genetic backgrounds. *Acta Derm Venereol, 93*(6), 743-745. doi:10.2340/00015555-1590

Nakagawara, A., Azar, C. G., Scavarda, N. J., & Brodeur, G. M. (1994). Expression and function of TRK-B and BDNF in human neuroblastomas. *Mol Cell Biol, 14*(1), 759-767.

Nakagoshi, H., Takemoto, Y., & Ishii, S. (1993). Functional domains of the human B-myb gene product. *J Biol Chem, 268*(19), 14161-14167.

Nakajima, K., Yamanaka, Y., Nakae, K., Kojima, H., Ichiba, M., Kiuchi, N., Kitaoka, T., Fukada, T., Hibi, M., & Hirano, T. (1996). A central role for Stat3 in IL-6-induced regulation of growth and differentiation in M1 leukemia cells. *EMBO J, 15*(14), 3651-3658.

Nakamura, K., Martin, K. C., Jackson, J. K., Beppu, K., Woo, C. W., & Thiele, C. J. (2006). Brain-derived neurotrophic factor activation of TrkB induces vascular endothelial growth factor expression via hypoxia-inducible factor-1alpha in neuroblastoma cells. *Cancer Res, 66*(8), 4249-4255. doi:10.1158/0008-5472.can-05-2789

Nakano, K., Uchimaru, K., Utsunomiya, A., Yamaguchi, K., & Watanabe, T. (2016). Dysregulation of c-Myb Pathway by Aberrant Expression of Proto-oncogene MYB Provides the Basis for Malignancy in Adult T-cell Leukemia/lymphoma Cells. *Clin Cancer Res, 22*(23), 5915-5928. doi:10.1158/1078-0432.ccr-15-1739

Nakata, Y., Shetzline, S., Sakashita, C., Kalota, A., Rallapalli, R., Rudnick, S. I., Zhang, Y., Emerson, S. G., & Gewirtz, A. M. (2007). c-Myb contributes to G2/M cell cycle transition in human hematopoietic cells by direct regulation of cyclin B1 expression. *Mol Cell Biol, 27*(6), 2048-2058. doi:10.1128/mcb.01100-06

Nan, J., Du, Y., Chen, X., Bai, Q., Wang, Y., Zhang, X., Zhu, N., Zhang, J., Hou, J., Wang, Q., & Yang, J. (2014). TPCA-1 is a direct dual inhibitor of STAT3 and NF-kappaB and regresses mutant EGFR-associated human non-small cell lung cancers. *Mol Cancer Ther, 13*(3), 617-629. doi:10.1158/1535-7163.mct-13-0464

Narayanan, D. L., Saladi, R. N., & Fox, J. L. (2010). Ultraviolet radiation and skin cancer. *Int J Dermatol, 49*(9), 978-986. doi:10.1111/j.1365-4632.2010.04474.x

Nasti, S., Pastorino, L., Bruno, W., Gargiulo, S., Battistuzzi, L., Zavattaro, E., Leigheb, G., De Francesco, V., Tulli, A., Mari, F., Scarra, G. B., & Ghiorzo, P. (2009). Five novel germline function-impairing mutations of CYLD in Italian patients with multiple cylindromas. *Clin Genet, 76*(5), 481-485. doi:10.1111/j.1399-0004.2009.01259.x

Navarrete-Dechent, C., Bajaj, S., Marghoob, A. A., Gonzalez, S., & Munoz, D. (2016). Multiple familial trichoepithelioma: confirmation via dermoscopy. *Dermatol Pract Concept, 6*(3), 51-54. doi:10.5826/dpc.0603a10

Ness, S. A. (2003). Myb protein specificity: evidence of a context-specific transcription factor code. *Blood Cells Mol Dis, 31*(2), 192-200.

Ng, Y. P., Cheung, Z. H., & Ip, N. Y. (2006). STAT3 as a downstream mediator of Trk signaling and functions. *J Biol Chem, 281*(23), 15636-15644. doi:10.1074/jbc.M601863200

Nikolaou, K., Tsagaratou, A., Eftychi, C., Kollias, G., Mosialos, G., & Talianidis, I. (2012). Inactivation of the deubiquitinase CYLD in hepatocytes causes apoptosis, inflammation, fibrosis, and cancer. *Cancer Cell, 21*(6), 738-750. doi:10.1016/j.ccr.2012.04.026

Nilsson, M., Unden, A. B., Krause, D., Malmqwist, U., Raza, K., Zaphiropoulos, P. G., & Toftgard, R. (2000). Induction of basal cell carcinomas and trichoepitheliomas in mice overexpressing GLI-1. *Proc Natl Acad Sci U S A, 97*(7), 3438-3443. doi:10.1073/pnas.050467397

Ninkina, N., Grashchuck, M., Buchman, V. L., & Davies, A. M. (1997). TrkB variants with deletions in the leucine-rich motifs of the extracellular domain. *J Biol Chem, 272*(20), 13019-13025.

Nomoto, H., Takaiwa, M., Mouri, A., & Furukawa, S. (2007). Pro-region of neurotrophins determines the processing efficiency. *Biochem Biophys Res Commun, 356*(4), 919-924. doi:10.1016/j.bbrc.2007.03.059

Nomura, T., Sakai, N., Sarai, A., Sudo, T., Kanei-Ishii, C., Ramsay, R. G., Favier, D., Gonda, T. J., & Ishii, S. (1993). Negative autoregulation of c-Myb activity by homodimer formation through the leucine zipper. *J Biol Chem, 268*(29), 21914-21923.

Nowell, C., & Radtke, F. (2013). Cutaneous Notch signaling in health and disease. *Cold Spring Harb Perspect Med, 3*(12), a017772. doi:10.1101/cshperspect.a017772

Nykjaer, A., Lee, R., Teng, K. K., Jansen, P., Madsen, P., Nielsen, M. S., Jacobsen, C., Kliemannel, M., Schwarz, E., Willnow, T. E., Hempstead, B. L., & Petersen, C. M. (2004). Sortilin is essential for proNGF-induced neuronal cell death. *Nature, 427*(6977), 843-848. doi:10.1038/nature02319

Nykjaer, A., Willnow, T. E., & Petersen, C. M. (2005). p75NTR--live or let die. *Curr Opin Neurobiol, 15*(1), 49-57. doi:10.1016/j.conb.2005.01.004

O'Leary, R., Arrowsmith, M., & Wood, E. J. (2002). Characterization of the living skin equivalent as a model of cutaneous re-epithelialization. *Cell Biochem Funct, 20*(2), 129-141. doi:10.1002/cbf.965

O'Rourke, J. P., & Ness, S. A. (2008). Alternative RNA splicing produces multiple forms of c-Myb with unique transcriptional activities. *Mol Cell Biol, 28*(6), 2091-2101. doi:10.1128/mcb.01870-07

Obaidat, N. A., Alsaad, K. O., & Ghazarian, D. (2007). Skin adnexal neoplasms--part 2: an approach to tumours of cutaneous sweat glands. *J Clin Pathol, 60*(2), 145-159. doi:10.1136/jcp.2006.041608

Oh, I. H., & Reddy, E. P. (1998). The C-terminal domain of B-Myb acts as a positive regulator of transcription and modulates its biological functions. *Mol Cell Biol, 18*(1), 499-511.

Oh, I. H., & Reddy, E. P. (1999). The myb gene family in cell growth, differentiation and apoptosis. *Oncogene, 18*(19), 3017-3033. doi:10.1038/sj.onc.1202839

Ohira, K., Kumanogoh, H., Sahara, Y., Homma, K. J., Hirai, H., Nakamura, S., & Hayashi, M. (2005). A Truncated Tropo-Myosine-Related Kinase B Receptor, T1, Regulates Glial Cell Morphology via Rho GDP Dissociation Inhibitor 1. *The Journal of Neuroscience, 25*(6), 1343-1353. doi:10.1523/jneurosci.4436-04.2005

Ohyama, M. (2007). Hair follicle bulge: a fascinating reservoir of epithelial stem cells. *J Dermatol Sci, 46*(2), 81-89. doi:10.1016/j.jdermsci.2006.12.002

Okada, S., Yokoyama, M., Toko, H., Tateno, K., Moriya, J., Shimizu, I., Nojima, A., Ito, T., Yoshida, Y., Kobayashi, Y., Katagiri, H., Minamino, T., & Komuro, I. (2012). Brain-derived neurotrophic factor protects against cardiac dysfunction after myocardial infarction via a central nervous system-mediated pathway. *Arterioscler Thromb Vasc Biol, 32*(8), 1902-1909. doi:10.1161/atvbaha.112.248930

Oosterkamp, H. M., Neering, H., Nijman, S. M., Dirac, A. M., Mooi, W. J., Bernards, R., & Brummelkamp, T. R. (2006). An evaluation of the efficacy of topical application of salicylic acid for the treatment of familial cylindromatosis. *Br J Dermatol, 155*(1), 182-185. doi:10.1111/j.1365-2133.2006.07224.x

Oranje, A. P., Halley, D., den Hollander, J. C., Teepe, R. G., van de Graaf, R., van den Ouweland, A., & Wagner, A. (2008). Multiple familial trichoepithelioma and familial cylindroma: one cause! *J Eur Acad Dermatol Venereol, 22*(11), 1395-1396. doi:10.1111/j.1468-3083.2008.02648.x

Ouwens, D. M., de Ruiter, N. D., van der Zon, G. C., Carter, A. P., Schouten, J., van der Burgt, C., Kooistra, K., Bos, J. L., Maassen, J. A., & van Dam, H. (2002). Growth factors can activate ATF2 via a two-step mechanism: phosphorylation of Thr71 through the Ras-MEK-ERK pathway and of Thr69 through RalGDS-Src-p38. *EMBO J, 21*(14), 3782-3793. doi:10.1093/emboj/cdf361

Palazzo, E., Marconi, A., Truzzi, F., Dallaglio, K., Petrachi, T., Humbert, P., Schnebert, S., Perrier, E., Dumas, M., & Pincelli, C. (2012). Role of neurotrophins on dermal fibroblast survival and differentiation. *J Cell Physiol, 227*(3), 1017-1025. doi:10.1002/jcp.22811

Pandya, C., Kutiyanawalla, A., Turecki, G., & Pillai, A. (2014). Glucocorticoid regulates TrkB protein levels via c-Cbl dependent ubiquitination: a decrease in c-Cbl mRNA in the prefrontal cortex of suicide subjects. *Psychoneuroendocrinology, 45*, 108-118. doi:10.1016/j.psyneuen.2014.03.020

Pannem, R. R., Dorn, C., Hellerbrand, C., & Massoumi, R. (2014). Cylindromatosis gene CYLD regulates hepatocyte growth factor expression in hepatic stellate cells through interaction with histone deacetylase 7. *Hepatology, 60*(3), 1066-1081. doi:10.1002/hep.27209

Parren, L. J., Ferdinandus, P., van der Hulst, R., Frank, J., & Tuinder, S. (2014). A novel therapeutic strategy for turban tumor: scalp excision and combined reconstruction with artificial dermis and split skin graft. *Int J Dermatol, 53*(2), 246-249. doi:10.1111/ijd.12199

Pasini, L., Re, A., Tebaldi, T., Ricci, G., Boi, S., Adami, V., Barbareschi, M., & Quattrone, A. (2015). TrkA is amplified in malignant melanoma patients and induces an anti-proliferative response in cell lines. *BMC Cancer, 15*, 777. doi:10.1186/s12885-015-1791-y

Patapoutian, A., & Reichardt, L. F. (2001). Trk receptors: mediators of neurotrophin action. *Curr Opin Neurobiol, 11*(3), 272-280.

Penneys, N. S., & Kaiser, M. (1993). Cylindroma expresses immunohistochemical markers linking it to eccrine coil. *J Cutan Pathol, 20*(1), 40-43.

Pereira, L. A., Hugo, H. J., Malaterre, J., Huiling, X., Sonza, S., Cures, A., Purcell, D. F., Ramsland, P. A., Gerondakis, S., Gonda, T. J., & Ramsay, R. G. (2015). MYB elongation is regulated by the nucleic acid binding of NFkappaB p50 to the intronic stem-loop region. *PLoS One, 10*(4), e0122919. doi:10.1371/journal.pone.0122919

Persson, M., Andren, Y., Mark, J., Horlings, H. M., Persson, F., & Stenman, G. (2009). Recurrent fusion of MYB and NFIB transcription factor genes in carcinomas of the breast and head and neck. *Proc Natl Acad Sci U S A, 106*(44), 18740-18744. doi:10.1073/pnas.0909114106

Persson, M., Andren, Y., Moskaluk, C. A., Frierson, H. F., Jr., Cooke, S. L., Futreal, P. A., Kling, T., Nelander, S., Nordkvist, A., Persson, F., & Stenman, G. (2012). Clinically significant copy number alterations and complex rearrangements of MYB and NFIB in head and neck adenoid cystic carcinoma. *Genes Chromosomes Cancer, 51*(8), 805-817. doi:10.1002/gcc.21965

Peters, E. M., Hansen, M. G., Overall, R. W., Nakamura, M., Pertile, P., Klapp, B. F., Arck, P. C., & Paus, R. (2005). Control of human hair growth by neurotrophins:

brain-derived neurotrophic factor inhibits hair shaft elongation, induces catagen, and stimulates follicular transforming growth factor beta2 expression. *J Invest Dermatol, 124*(4), 675-685. doi:10.1111/j.0022-202X.2005.23648.x

Peters, E. M., Stieglitz, M. G., Liezman, C., Overall, R. W., Nakamura, M., Hagen, E., Klapp, B. F., Arck, P., & Paus, R. (2006). p75 Neurotrophin Receptor-Mediated Signaling Promotes Human Hair Follicle Regression (Catagen). *Am J Pathol, 168*(1), 221-234. doi:10.2353/ajpath.2006.050163

Petersen, O. W., Ronnov-Jessen, L., Howlett, A. R., & Bissell, M. J. (1992). Interaction with basement membrane serves to rapidly distinguish growth and differentiation pattern of normal and malignant human breast epithelial cells. *Proc Natl Acad Sci U S A, 89*(19), 9064-9068.

Petersson, F., Kutzner, H., Spagnolo, D. V., Bisceglia, M., Kacerovska, D., Vazmitel, M., Michal, M., & Kazakov, D. V. (2009). Adenoid cystic carcinoma-like pattern in spiradenoma and spiradenocylindroma: a rare feature in sporadic neoplasms and those associated with Brooke-Spiegler syndrome. *Am J Dermatopathol, 31*(7), 642-648. doi:10.1097/DAD.0b013e3181a1573e

Piccinini, F. (2015). AnaSP: a software suite for automatic image analysis of multicellular spheroids. *Comput Methods Programs Biomed, 119*(1), 43-52. doi:10.1016/j.cmpb.2015.02.006

Piccinini, F., Tesei, A., Arienti, C., & Bevilacqua, A. (2015). Cancer multicellular spheroids: volume assessment from a single 2D projection. *Comput Methods Programs Biomed, 118*(2), 95-106. doi:10.1016/j.cmpb.2014.12.003

Pickart, C. M., & Eddins, M. J. (2004). Ubiquitin: structures, functions, mechanisms. *Biochim Biophys Acta, 1695*(1-3), 55-72. doi:10.1016/j.bbamcr.2004.09.019

Pincelli, C., Sevignani, C., Manfredini, R., Grande, A., Fantini, F., Bracci-Laudiero, L., Aloe, L., Ferrari, S., Cossarizza, A., & Giannetti, A. (1994). Expression and function of nerve growth factor and nerve growth factor receptor on cultured keratinocytes. *Journal of Investigative Dermatology, 103*(1), 13-18.

Pincelli, C., & Yaar, M. (1997). Nerve growth factor: its significance in cutaneous biology. *J Investig Dermatol Symp Proc, 2*(1), 31-36.

Powell, B. C., Passmore, E. A., Nesci, A., & Dunn, S. M. (1998). The Notch signalling pathway in hair growth. *Mech Dev, 78*(1-2), 189-192.

Prinzhorn, W., Stehle, M., Kleiner, H., Ruppenthal, S., Muller, M. C., Hofmann, W. K., Fabarius, A., & Seifarth, W. (2016). c-MYB is a transcriptional regulator of ESPL1/Separase in BCR-ABL-positive chronic myeloid leukemia. *Biomark Res, 4*, 5. doi:10.1186/s40364-016-0059-2

Proenca, C. C., Song, M., & Lee, F. S. (2016). Differential effects of BDNF and neurotrophin 4 (NT4) on endocytic sorting of TrkB receptors. *J Neurochem, 138*(3), 397-406. doi:10.1111/jnc.13676

Qian, X., Riccio, A., Zhang, Y., & Ginty, D. D. (1998). Identification and characterization of novel substrates of Trk receptors in developing neurons. *Neuron, 21*(5), 1017-1029.

Quintana, A. M., Liu, F., O'Rourke, J. P., & Ness, S. A. (2011). Identification and regulation of c-Myb target genes in MCF-7 cells. *BMC Cancer, 11*, 30. doi:10.1186/1471-2407-11-30

Raff, M. C., Barres, B. A., Burne, J. F., Coles, H. S., Ishizaki, Y., & Jacobson, M. D. (1993). Programmed cell death and the control of cell survival: lessons from the nervous system. *Science, 262*(5134), 695-700.

Rajagopalan, H., Jallepalli, P. V., Rago, C., Velculescu, V. E., Kinzler, K. W., Vogelstein, B., & Lengauer, C. (2004). Inactivation of hCDC4 can cause chromosomal instability. *Nature, 428*(6978), 77-81. doi:10.1038/nature02313

Rajan, N., Andersson, M. K., Sinclair, N., Fehr, A., Hodgson, K., Lord, C. J., Kazakov, D. V., Vanecek, T., Ashworth, A., & Stenman, G. (2016). Overexpression of MYB drives proliferation of CYLD-defective cylindroma cells. *J Pathol, 239*(2), 197-205. doi:10.1002/path.4717

Rajan, N., & Ashworth, A. (2015). Inherited cylindromas: lessons from a rare tumour. *Lancet Oncol, 16*(9), e460-469. doi:10.1016/s1470-2045(15)00245-4

Rajan, N., Burn, J., Langtry, J., Sieber-Blum, M., Lord, C. J., & Ashworth, A. (2011). Transition from cylindroma to spiradenoma in CYLD-defective tumours is associated with reduced DKK2 expression. *J Pathol, 224*(3), 309-321. doi:10.1002/path.2896

Rajan, N., Elliott, R., Clewes, O., Mackay, A., Reis-Filho, J. S., Burn, J., Langtry, J., Sieber-Blum, M., Lord, C. J., & Ashworth, A. (2011). Dysregulated TRK signalling is a therapeutic target in CYLD defective tumours. *Oncogene, 30*(41), 4243-4260. doi:10.1038/onc.2011.133

Rajan, N., Elliott, R. J., Smith, A., Sinclair, N., Swift, S., Lord, C. J., & Ashworth, A. (2014). The cylindromatosis gene product, CYLD, interacts with MIB2 to regulate notch signalling. *Oncotarget, 5*(23), 12126-12140. doi:10.18632/oncotarget.2573

Rajan, N., Langtry, J. A., Ashworth, A., Roberts, C., Chapman, P., Burn, J., & Trainer, A. H. (2009). Tumor mapping in 2 large multigenerational families with CYLD mutations: implications for disease management and tumor induction. *Arch Dermatol, 145*(11), 1277-1284. doi:10.1001/archdermatol.2009.262

Rajan, N., Trainer, A. H., Burn, J., & Langtry, J. A. (2009). Familial cylindromatosis and brooke-spiegler syndrome: a review of current therapeutic approaches and the surgical challenges posed by two affected families. *Dermatol Surg, 35*(5), 845-852. doi:10.1111/j.1524-4725.2009.01142.x

Ramsay, R. G., & Gonda, T. J. (2008). MYB function in normal and cancer cells. *Nat Rev Cancer, 8*(7), 523-534. doi:10.1038/nrc2439

Ramsay, R. G., Ikeda, K., Rifkind, R. A., & Marks, P. A. (1986). Changes in gene expression associated with induced differentiation of erythroleukemia: protooncogenes, globin genes, and cell division. *Proc Natl Acad Sci U S A, 83*(18), 6849-6853.

Ramsay, R. G., Ishii, S., & Gonda, T. J. (1992). Interaction of the Myb protein with specific DNA binding sites. *J Biol Chem, 267*(8), 5656-5662.

Ramsay, R. G., Thompson, M. A., Hayman, J. A., Reid, G., Gonda, T. J., & Whitehead, R. H. (1992). Myb expression is higher in malignant human colonic carcinoma and premalignant adenomatous polyps than in normal mucosa. *Cell Growth Differ, 3*(10), 723-730.

Rao, D., Macias, E., Carbajal, S., Kiguchi, K., & DiGiovanni, J. (2015). Constitutive Stat3 activation alters behavior of hair follicle stem and progenitor cell populations. *Mol Carcinog, 54*(2), 121-133. doi:10.1002/mc.22080

Raschella, G., Cesi, V., Amendola, R., Negroni, A., Tanno, B., Altavista, P., Tonini, G. P., De Bernardi, B., & Calabretta, B. (1999). Expression of B-myb in neuroblastoma tumors is a poor prognostic factor independent from MYCN amplification. *Cancer Res, 59*(14), 3365-3368.

Rasmussen, C., Thomas-Virnig, C., & Allen-Hoffmann, B. L. (2013). Classical human epidermal keratinocyte cell culture. *Methods Mol Biol, 945*, 161-175. doi:10.1007/978-1-62703-125-7_11

Ravi, M., Paramesh, V., Kaviya, S. R., Anuradha, E., & Solomon, F. D. (2015). 3D cell culture systems: advantages and applications. *J Cell Physiol, 230*(1), 16-26. doi:10.1002/jcp.24683

Reddy, S., Andl, T., Bagasra, A., Lu, M. M., Epstein, D. J., Morrisey, E. E., & Millar, S. E. (2001). Characterization of Wnt gene expression in developing and postnatal hair follicles and identification of Wnt5a as a target of Sonic hedgehog in hair follicle morphogenesis. *Mech Dev, 107*(1-2), 69-82.

Reichardt, L. F. (2006). Neurotrophin-regulated signalling pathways. *Philos Trans R Soc Lond B Biol Sci, 361*(1473), 1545-1564. doi:10.1098/rstb.2006.1894

Reiley, W., Zhang, M., & Sun, S. C. (2004). Negative regulation of JNK signaling by the tumor suppressor CYLD. *J Biol Chem, 279*(53), 55161-55167. doi:10.1074/jbc.M411049200

Reiley, W., Zhang, M., Wu, X., Granger, E., & Sun, S. C. (2005). Regulation of the deubiquitinating enzyme CYLD by IkappaB kinase gamma-dependent phosphorylation. *Mol Cell Biol, 25*(10), 3886-3895. doi:10.1128/mcb.25.10.3886-3895.2005

Reiley, W. W., Jin, W., Lee, A. J., Wright, A., Wu, X., Tewalt, E. F., Leonard, T. O., Norbury, C. C., Fitzpatrick, L., Zhang, M., & Sun, S. C. (2007). Deubiquitinating enzyme CYLD negatively regulates the ubiquitin-dependent kinase Tak1 and prevents abnormal T cell responses. *J Exp Med, 204*(6), 1475-1485. doi:10.1084/jem.20062694

Reiley, W. W., Zhang, M., Jin, W., Losiewicz, M., Donohue, K. B., Norbury, C. C., & Sun, S. C. (2006). Regulation of T cell development by the deubiquitinating enzyme CYLD. *Nat Immunol, 7*(4), 411-417. doi:10.1038/ni1315

Ren, X., Duan, L., He, Q., Zhang, Z., Zhou, Y., Wu, D., Pan, J., Pei, D., & Ding, K. (2010). Identification of Niclosamide as a New Small-Molecule Inhibitor of the STAT3 Signaling Pathway. *ACS Med Chem Lett, 1*(9), 454-459. doi:10.1021/ml100146z

Renn, C. L., Leitch, C. C., & Dorsey, S. G. (2009). In vivo evidence that truncated trkB.T1 participates in nociception. *Mol Pain, 5*, 61. doi:10.1186/1744-8069-5-61

Rheinwald, J. G., & Green, H. (1975). Serial cultivation of strains of human epidermal keratinocytes: the formation of keratinizing colonies from single cells. *Cell, 6*(3), 331-343.

Ricci, A., Greco, S., Mariotta, S., Felici, L., Bronzetti, E., Cavazzana, A., Cardillo, G., Amenta, F., Bisetti, A., & Barbolini, G. (2001). Neurotrophins and neurotrophin receptors in human lung cancer. *Am J Respir Cell Mol Biol, 25*(4), 439-446. doi:10.1165/ajrcmb.25.4.4470

Riccio, A., Ahn, S., Davenport, C. M., Blendy, J. A., & Ginty, D. D. (1999). Mediation by a CREB family transcription factor of NGF-dependent survival of sympathetic neurons. *Science, 286*(5448), 2358-2361.

Rimann, M., & Graf-Hausner, U. (2012). Synthetic 3D multicellular systems for drug development. *Curr Opin Biotechnol, 23*(5), 803-809. doi:10.1016/j.copbio.2012.01.011

Rishikaysh, P., Dev, K., Diaz, D., Qureshi, W. M., Filip, S., & Mokry, J. (2014). Signaling involved in hair follicle morphogenesis and development. *Int J Mol Sci, 15*(1), 1647-1670. doi:10.3390/ijms15011647

Rittinger, K., & Ikeda, F. (2017). Linear ubiquitin chains: enzymes, mechanisms and biology. *Open Biol, 7*(4). doi:10.1098/rsob.170026

Rodriguez-Viciana, P., Warne, P. H., Dhand, R., Vanhaesebroeck, B., Gout, I., Fry, M. J., Waterfield, M. D., & Downward, J. (1994). Phosphatidylinositol-3-OH kinase as a direct target of Ras. *Nature, 370*(6490), 527-532. doi:10.1038/370527a0

Rose, C. R., Blum, R., Pichler, B., Lepier, A., Kafitz, K. W., & Konnerth, A. (2003). Truncated TrkB-T1 mediates neurotrophin-evoked calcium signalling in glia cells. *Nature, 426*(6962), 74-78. doi:10.1038/nature01983

Rossler, O. G., & Thiel, G. (2004). Brain-derived neurotrophic factor-, epidermal growth factor-, or A-Raf-induced growth of HaCaT keratinocytes requires extracellular signal-regulated kinase. *Am J Physiol Cell Physiol, 286*(5), C1118-1129. doi:10.1152/ajpcell.00301.2003

Roux, P. P., & Barker, P. A. (2002). Neurotrophin signaling through the p75 neurotrophin receptor. *Prog Neurobiol, 67*(3), 203-233.

Rushton, J. J., Davis, L. M., Lei, W., Mo, X., Leutz, A., & Ness, S. A. (2003). Distinct changes in gene expression induced by A-Myb, B-Myb and c-Myb proteins. *Oncogene, 22*(2), 308-313. doi:10.1038/sj.onc.1206131

Rushton, J. J., & Ness, S. A. (2001). The conserved DNA binding domain mediates similar regulatory interactions for A-Myb, B-Myb, and c-Myb transcription factors. *Blood Cells Mol Dis, 27*(2), 459-463. doi:10.1006/bcmd.2001.0405

Rutter, K. J., & Judge, M. R. (2009). Profuse congenital milia in a family. *Pediatr Dermatol, 26*(1), 62-64. doi:10.1111/j.1525-1470.2008.00824.x

Saikumar, P., Murali, R., & Reddy, E. P. (1990). Role of tryptophan repeats and flanking amino acids in Myb-DNA interactions. *Proc Natl Acad Sci U S A, 87*(21), 8452-8456.

Sakamoto, H., Dai, G., Tsujino, K., Hashimoto, K., Huang, X., Fujimoto, T., Mucenski, M., Frampton, J., & Ogawa, M. (2006). Proper levels of c-Myb are discretely defined at distinct steps of hematopoietic cell development. *Blood, 108*(3), 896-903. doi:10.1182/blood-2005-09-3846

Sakura, H., Kanei-Ishii, C., Nagase, T., Nakagoshi, H., Gonda, T. J., & Ishii, S. (1989). Delineation of three functional domains of the transcriptional activator encoded by the c-myb protooncogene. *Proc Natl Acad Sci U S A, 86*(15), 5758-5762.

Salehi, A. H., Roux, P. P., Kubu, C. J., Zeindler, C., Bhakar, A., Tannis, L. L., Verdi, J. M., & Barker, P. A. (2000). NRAGE, a novel MAGE protein, interacts with the p75 neurotrophin receptor and facilitates nerve growth factor-dependent apoptosis. *Neuron, 27*(2), 279-288.

Salhi, A., Bornholdt, D., Oeffner, F., Malik, S., Heid, E., Happle, R., & Grzeschik, K. H. (2004). Multiple familial trichoepithelioma caused by mutations in the cylindromatosis tumor suppressor gene. *Cancer Res, 64*(15), 5113-5117. doi:10.1158/0008-5472.can-04-0307

Samal, R., Ameling, S., Dhople, V., Sappa, P. K., Wenzel, K., Volker, U., Felix, S. B., Hammer, E., & Konemann, S. (2015). Brain derived neurotrophic factor contributes to the cardiogenic potential of adult resident progenitor cells in failing murine heart. *PLoS One, 10*(3), e0120360. doi:10.1371/journal.pone.0120360

Sampurno, S., Cross, R., Pearson, H., Kaur, P., Malaterre, J., & Ramsay, R. G. (2015). Myb via TGFbeta is required for collagen type 1 production and skin integrity. *Growth Factors, 33*(2), 102-112. doi:10.3109/08977194.2015.1016222

Sanchez-Sanchez, J., & Arevalo, J. C. (2017). A Review on Ubiquitination of Neurotrophin Receptors: Facts and Perspectives. *Int J Mol Sci, 18*(3). doi:10.3390/ijms18030630

Sandberg, M. L., Sutton, S. E., Pletcher, M. T., Wiltshire, T., Tarantino, L. M., Hogenesch, J. B., & Cooke, M. P. (2005). c-Myb and p300 regulate hematopoietic stem cell proliferation and differentiation. *Dev Cell, 8*(2), 153-166. doi:10.1016/j.devcel.2004.12.015

Sandberg, R., & Ernberg, I. (2005). The molecular portrait of in vitro growth by meta-analysis of gene-expression profiles. *Genome Biol, 6*(8), R65. doi:10.1186/gb-2005-6-8-r65

Sano, Y., & Ishii, S. (2001). Increased affinity of c-Myb for CREB-binding protein (CBP) after CBP-induced acetylation. *J Biol Chem, 276*(5), 3674-3682. doi:10.1074/jbc.M006896200

Saragovi, H. U., Zheng, W., Maliartchouk, S., DiGugliemo, G. M., Mawal, Y. R., Kamen, A., Woo, S. B., Cuello, A. C., Debeir, T., & Neet, K. E. (1998). A TrkA-selective, fast internalizing nerve growth factor-antibody complex induces trophic but not neuritogenic signals. *J Biol Chem, 273*(52), 34933-34940.

Sariola, H. (2001). The neurotrophic factors in non-neuronal tissues. *Cell Mol Life Sci, 58*(8), 1061-1066. doi:10.1007/pl00000921

Sato, M., Rodriguez-Barrueco, R., Yu, J., Do, C., Silva, J. M., & Gautier, J. (2015). MYC is a critical target of FBXW7. *Oncotarget, 6*(5), 3292-3305. doi:10.18632/oncotarget.3203

Sato, Y., Goto, E., Shibata, Y., Kubota, Y., Yamagata, A., Goto-Ito, S., Kubota, K., Inoue, J., Takekawa, M., Tokunaga, F., & Fukai, S. (2015). Structures of CYLD USP with Met1- or Lys63-linked diubiquitin reveal mechanisms for dual specificity. *Nat Struct Mol Biol, 22*(3), 222-229. doi:10.1038/nsmb.2970

Scala, S., Wosikowski, K., Giannakakou, P., Valle, P., Biedler, J. L., Spengler, B. A., Lucarelli, E., Bates, S. E., & Thiele, C. J. (1996). Brain-derived neurotrophic factor protects neuroblastoma cells from vinblastine toxicity. *Cancer Res, 56*(16), 3737-3742.

Schneider, L., Clement, C. A., Teilmann, S. C., Pazour, G. J., Hoffmann, E. K., Satir, P., & Christensen, S. T. (2005). PDGFRalphaalpha signaling is regulated through the primary cilium in fibroblasts. *Curr Biol, 15*(20), 1861-1866. doi:10.1016/j.cub.2005.09.012

Schulz, T., Proske, S., Hartschuh, W., Kurzen, H., Paul, E., & Wunsch, P. H. (2005). High-grade trichoblastic carcinoma arising in trichoblastoma: a rare adnexal neoplasm often showing metastatic spread. *Am J Dermatopathol, 27*(1), 9-16.

Schust, J., Sperl, B., Hollis, A., Mayer, T. U., & Berg, T. (2006). Stattic: a small-molecule inhibitor of STAT3 activation and dimerization. *Chem Biol, 13*(11), 1235-1242. doi:10.1016/j.chembiol.2006.09.018

Sclabas, G. M., Fujioka, S., Schmidt, C., Li, Z., Frederick, W. A., Yang, W., Yokoi, K., Evans, D. B., Abbruzzese, J. L., Hess, K. R., Zhang, W., Fidler, I. J., & Chiao, P. J. (2005). Overexpression of tropomysin-related kinase B in metastatic human pancreatic cancer cells. *Clin Cancer Res, 11*(2 Pt 1), 440-449.

Sellheyer, K. (2015). Spiradenoma and cylindroma originate from the hair follicle bulge and not from the eccrine sweat gland: an immunohistochemical study with CD200 and other stem cell markers. *J Cutan Pathol, 42*(2), 90-101. doi:10.1111/cup.12406

Serracino, H. S., & Kleinschmidt-Demasters, B. K. (2013). Skull invaders: when surgical pathology and neuropathology worlds collide. *J Neuropathol Exp Neurol, 72*(7), 600-613. doi:10.1097/NEN.0b013e318299c40f

Shao, H., Cheng, H. Y., Cook, R. G., & Tweardy, D. J. (2003). Identification and characterization of signal transducer and activator of transcription 3 recruitment sites within the epidermal growth factor receptor. *Cancer Res, 63*(14), 3923-3930.

Shelton, D. L., Sutherland, J., Gripp, J., Camerato, T., Armanini, M. P., Phillips, H. S., Carroll, K., Spencer, S. D., & Levinson, A. D. (1995). Human trks: molecular cloning, tissue distribution, and expression of extracellular domain immunoadhesins. *J Neurosci, 15*(1 Pt 2), 477-491.

Shibayama, E., & Koizumi, H. (1996). Cellular localisation of the Trk neurotrophin receptor family in human non-neuronal tissues. *American Journal of Pathology, 148*(6), 1807-1818.

Shih, V. F., Tsui, R., Caldwell, A., & Hoffmann, A. (2011). A single NFkappaB system for both canonical and non-canonical signaling. *Cell Res, 21*(1), 86-102. doi:10.1038/cr.2010.161

Shin, D. S., Kim, H. N., Shin, K. D., Yoon, Y. J., Kim, S. J., Han, D. C., & Kwon, B. M. (2009). Cryptotanshinone inhibits constitutive signal transducer and activator of transcription 3 function through blocking the dimerization in DU145 prostate cancer cells. *Cancer Res, 69*(1), 193-202. doi:10.1158/0008-5472.can-08-2575

Sicinska, J., Rakowska, A., Czuwara-Ladykowska, J., Mroz, A., Lipinski, M., Nasierowska-Guttmejer, A., Sikorska, J., Sklinda, K., Slowinska, M., Kowalska-Oledzka, E., Walecka, I., Walecki, J., & Rudnicka, L. (2007). Cylindroma transforming into basal cell carcinoma in a patient with Brooke-Spiegler syndrome. *J Dermatol Case Rep, 1*(1), 4-9. doi:10.3315/jdcr.2007.1.1002

Siddiquee, K., Zhang, S., Guida, W. C., Blaskovich, M. A., Greedy, B., Lawrence, H. R., Yip, M. L., Jove, R., McLaughlin, M. M., Lawrence, N. J., Sebti, S. M., & Turkson, J. (2007). Selective chemical probe inhibitor of Stat3, identified through structure-based virtual screening, induces antitumor activity. *Proc Natl Acad Sci U S A, 104*(18), 7391-7396. doi:10.1073/pnas.0609757104

Sinkevicius, K. W., Kriegel, C., Bellaria, K. J., Lee, J., Lau, A. N., Leeman, K. T., Zhou, P., Beede, A. M., Fillmore, C. M., Caswell, D., Barrios, J., Wong, K. K., Sholl, L. M., Schlaeger, T. M., Bronson, R. T., Chirieac, L. R., Winslow, M. M., Haigis, M. C., & Kim, C. F. (2014). Neurotrophin receptor TrkB promotes lung adenocarcinoma metastasis. *Proc Natl Acad Sci U S A, 111*(28), 10299-10304. doi:10.1073/pnas.1404399111

Skaper, S. D. (2012). The neurotrophin family of neurotrophic factors: an overview. *Methods Mol Biol, 846*, 1-12. doi:10.1007/978-1-61779-536-7_1

Skeldal, S., Sykes, A. M., Glerup, S., Matusica, D., Palstra, N., Autio, H., Boskovic, Z., Madsen, P., Castren, E., Nykjaer, A., & Coulson, E. J. (2012). Mapping of the interaction site between sortilin and the p75 neurotrophin receptor reveals a regulatory role for the sortilin intracellular domain in p75 neurotrophin receptor shedding and apoptosis. *J Biol Chem, 287*(52), 43798-43809. doi:10.1074/jbc.M112.374710

Smeyne, R. J., Klein, R., Schnapp, A., Long, L. K., Bryant, S., Lewin, A., Lira, S. A., & Barbacid, M. (1994). Severe sensory and sympathetic neuropathies in mice carrying a disrupted Trk/NGF receptor gene. *Nature, 368*(6468), 246-249. doi:10.1038/368246a0

Sorrell, J. M., & Caplan, A. I. (2004). Fibroblast heterogeneity: more than skin deep. *J Cell Sci, 117*(Pt 5), 667-675. doi:10.1242/jcs.01005

Spruck, C. H., Strohmaier, H., Sangfelt, O., Muller, H. M., Hubalek, M., Muller-Holzner, E., Marth, C., Widschwendter, M., & Reed, S. I. (2002). hCDC4 gene mutations in endometrial cancer. *Cancer Res, 62*(16), 4535-4539.

Srokowski, C. C., Masri, J., Hovelmeyer, N., Krembel, A. K., Tertilt, C., Strand, D., Mahnke, K., Massoumi, R., Waisman, A., & Schild, H. (2009). Naturally occurring short splice variant of CYLD positively regulates dendritic cell function. *Blood, 113*(23), 5891-5895. doi:10.1182/blood-2008-08-175489

Stefanato, C. M., Yaar, M., Bhawan, J., Phillips, T. J., Kosmadaki, M. G., Botchkarev, V., & Gilchrest, B. A. (2003). Modulations of nerve growth factor and Bcl-2 in ultraviolet-irradiated human epidermis. *J Cutan Pathol, 30*(6), 351-357.

Stegmeier, F., Sowa, M. E., Nalepa, G., Gygi, S. P., Harper, J. W., & Elledge, S. J. (2007). The tumor suppressor CYLD regulates entry into mitosis. *Proc Natl Acad Sci U S A, 104*(21), 8869-8874. doi:10.1073/pnas.0703268104

Stenman, G., Andersson, M. K., & Andren, Y. (2010). New tricks from an old oncogene: gene fusion and copy number alterations of MYB in human cancer. *Cell Cycle, 9*(15), 2986-2995. doi:10.4161/cc.9.15.12515

Stenman, G., Persson, F., & Andersson, M. K. (2014). Diagnostic and therapeutic implications of new molecular biomarkers in salivary gland cancers. *Oral Oncol, 50*(8), 683-690. doi:10.1016/j.oraloncology.2014.04.008

Stephens, P. J., Davies, H. R., Mitani, Y., Van Loo, P., Shlien, A., Tarpey, P. S., Papaemmanuil, E., Cheverton, A., Bignell, G. R., Butler, A. P., Gamble, J., Gamble, S., Hardy, C., Hinton, J., Jia, M., Jayakumar, A., Jones, D., Latimer, C., McLaren, S., McBride, D. J., Menzies, A., Mudie, L., Maddison, M., Raine, K., Nik-Zainal, S., O'Meara, S., Teague, J. W., Varela, I., Wedge, D. C., Whitmore, I., Lippman, S. M., McDermott, U., Stratton, M. R., Campbell, P. J., El-Naggar, A. K., & Futreal, P. A. (2013). Whole exome sequencing of adenoid cystic carcinoma. *J Clin Invest, 123*(7), 2965-2968. doi:10.1172/jci67201

Stoilov, P., Castren, E., & Stamm, S. (2002). Analysis of the human TrkB gene genomic organization reveals novel TrkB isoforms, unusual gene length, and splicing mechanism. *Biochem Biophys Res Commun, 290*(3), 1054-1065. doi:10.1006/bbrc.2001.6301

Stokes, A., Wakano, C., Koblan-Huberson, M., Adra, C. N., Fleig, A., & Turner, H. (2006). TRPA1 is a substrate for de-ubiquitination by the tumor suppressor CYLD. *Cell Signal, 18*(10), 1584-1594. doi:10.1016/j.cellsig.2005.12.009

Strohmaier, C., Carter, B. D., Urfer, R., Barde, Y. A., & Dechant, G. (1996). A splice variant of the neurotrophin receptor trkB with increased specificity for brain-derived neurotrophic factor. *EMBO J, 15*(13), 3332-3337.

Suhasini, M., & Pilz, R. B. (1999). Transcriptional elongation of c-myb is regulated by NF-kappaB (p50/RelB). *Oncogene, 18*(51), 7360-7369. doi:10.1038/sj.onc.1203158

Sun, L., Gao, J., Huo, L., Sun, X., Shi, X., Liu, M., Li, D., Zhang, C., & Zhou, J. (2010). Tumour suppressor CYLD is a negative regulator of the mitotic kinase Aurora-B. *J Pathol, 221*(4), 425-432. doi:10.1002/path.2723

Sun, S. C. (2010). CYLD: a tumor suppressor deubiquitinase regulating NF-kappaB activation and diverse biological processes. *Cell Death Differ, 17*(1), 25-34. doi:10.1038/cdd.2009.43

Swietach, P., Hulikova, A., Patiar, S., Vaughan-Jones, R. D., & Harris, A. L. (2012). Importance of intracellular pH in determining the uptake and efficacy of the weakly basic chemotherapeutic drug, doxorubicin. *PLoS One, 7*(4), e35949. doi:10.1371/journal.pone.0035949

Szepietowski, J. C., Wasik, F., Szybejko-Machaj, G., Bieniek, A., & Schwartz, R. A. (2001). Brooke-Spiegler syndrome. *J Eur Acad Dermatol Venereol, 15*(4), 346-349.

Tacconelli, A., Farina, A. R., Cappabianca, L., Cea, G., Panella, S., Chioda, A., Gallo, R., Cinque, B., Sferra, R., Vetuschi, A., Campese, A. F., Screpanti, I., Gulino, A., & Mackay, A. R. (2007). TrkAIII expression in the thymus. *J Neuroimmunol, 183*(1-2), 151-161. doi:10.1016/j.jneuroim.2006.12.005

Tacconelli, A., Farina, A. R., Cappabianca, L., Desantis, G., Tessitore, A., Vetuschi, A., Sferra, R., Rucci, N., Argenti, B., Screpanti, I., Gulino, A., & Mackay, A. R. (2004). TrkA alternative splicing: a regulated tumor-promoting switch in human neuroblastoma. *Cancer Cell, 6*(4), 347-360. doi:10.1016/j.ccr.2004.09.011

Tahirov, T. H., Sato, K., Ichikawa-Iwata, E., Sasaki, M., Inoue-Bungo, T., Shiina, M., Kimura, K., Takata, S., Fujikawa, A., Morii, H., Kumasaka, T., Yamamoto, M., Ishii, S., & Ogata, K. (2002). Mechanism of c-Myb-C/EBP beta cooperation from separated sites on a promoter. *Cell, 108*(1), 57-70.

Takahashi, M., Rapley, E., Biggs, P. J., Lakhani, S. R., Cooke, D., Hansen, J., Blair, E., Hofmann, B., Siebert, R., Turner, G., Evans, D. G., Schrander-Stumpel, C., Beemer, F. A., van Vloten, W. A., Breuning, M. H., van den Ouweland, A., Halley, D., Delpech, B., Cleveland, M., Leigh, I., Chapman, P., Burn, J., Hohl, D., Gorog, J. P., Seal, S., & Mangion, J. (2000). Linkage and LOH studies in 19 cylindromatosis families show no evidence of genetic heterogeneity and refine the CYLD locus on chromosome 16q12-q13. *Hum Genet, 106*(1), 58-65.

Takahashi, Y., Shimokawa, N., Esmaeili-Mahani, S., Morita, A., Masuda, H., Iwasaki, T., Tamura, J., Haglund, K., & Koibuchi, N. (2011). Ligand-induced downregulation of TrkA is partly regulated through ubiquitination by Cbl. *FEBS Lett, 585*(12), 1741-1747. doi:10.1016/j.febslet.2011.04.056

Takeuchi, T., Adachi, Y., & Ohtsuki, Y. (2005). Skeletrophin, a novel ubiquitin ligase to the intracellular region of Jagged-2, is aberrantly expressed in multiple myeloma. *Am J Pathol, 166*(6), 1817-1826. doi:10.1016/s0002-9440(10)62491-1

Tanaka, K., Okugawa, Y., Toiyama, Y., Inoue, Y., Saigusa, S., Kawamura, M., Araki, T., Uchida, K., Mohri, Y., & Kusunoki, M. (2014). Brain-derived neurotrophic factor (BDNF)-induced tropomyosin-related kinase B (Trk B) signaling is a potential therapeutic target for peritoneal carcinomatosis arising from colorectal cancer. *PLoS One, 9*(5), e96410. doi:10.1371/journal.pone.0096410

Tanaka, Y., Patestos, N. P., Maekawa, T., & Ishii, S. (1999). B-myb is required for inner cell mass formation at an early stage of development. *J Biol Chem, 274*(40), 28067-28070.

Tang, A., Gao, K., Chu, L., Zhang, R., Yang, J., & Zheng, J. (2017). Aurora kinases: novel therapy targets in cancers. *Oncotarget, 8*(14), 23937-23954. doi:10.18632/oncotarget.14893

Tauriello, D. V., Haegebarth, A., Kuper, I., Edelmann, M. J., Henraat, M., Canninga-van Dijk, M. R., Kessler, B. M., Clevers, H., & Maurice, M. M. (2010). Loss of the tumor suppressor CYLD enhances Wnt/beta-catenin signaling through K63-linked ubiquitination of Dvl. *Mol Cell, 37*(5), 607-619. doi:10.1016/j.molcel.2010.01.035

Teng, H. K., Teng, K. K., Lee, R., Wright, S., Tevar, S., Almeida, R. D., Kermani, P., Torkin, R., Chen, Z. Y., Lee, F. S., Kraemer, R. T., Nykjaer, A., & Hempstead, B. L. (2005). ProBDNF induces neuronal apoptosis via activation of a receptor complex of p75NTR and sortilin. *J Neurosci, 25*(22), 5455-5463. doi:10.1523/jneurosci.5123-04.2005

Tessarollo, L., Tsoulfas, P., Donovan, M. J., Palko, M. E., Blair-Flynn, J., Hempstead, B. L., & Parada, L. F. (1997). Targeted deletion of all isoforms of the trkC gene suggests the use of alternate receptors by its ligand neurotrophin-3 in neuronal development and implicates trkC in normal cardiogenesis. *Proc Natl Acad Sci U S A, 94*(26), 14776-14781.

Thiele, C. J., Li, Z., & McKee, A. E. (2009). On Trk--the TrkB signal transduction pathway is an increasingly important target in cancer biology. *Clin Cancer Res, 15*(19), 5962-5967. doi:10.1158/1078-0432.ccr-08-0651

Thoenen, H., & Barde, Y. A. (1980). Physiology of nerve growth factor. *Physiol Rev, 60*(4), 1284-1335.

Thompson, M. A., Rosenthal, M. A., Ellis, S. L., Friend, A. J., Zorbas, M. I., Whitehead, R. H., & Ramsay, R. G. (1998). c-Myb down-regulation is associated with human colon cell differentiation, apoptosis, and decreased Bcl-2 expression. *Cancer Res, 58*(22), 5168-5175.

Thorner, A. R., Hoadley, K. A., Parker, J. S., Winkel, S., Millikan, R. C., & Perou, C. M. (2009). In vitro and in vivo analysis of B-Myb in basal-like breast cancer. *Oncogene, 28*(5), 742-751. doi:10.1038/onc.2008.430

Thorner, A. R., Parker, J. S., Hoadley, K. A., & Perou, C. M. (2010). Potential tumor suppressor role for the c-Myb oncogene in luminal breast cancer. *PLoS One, 5*(10), e13073. doi:10.1371/journal.pone.0013073

Thurber, G. M., & Wittrup, K. D. (2008). Quantitative spatiotemporal analysis of antibody fragment diffusion and endocytic consumption in tumor spheroids. *Cancer Res, 68*(9), 3334-3341. doi:10.1158/0008-5472.can-07-3018

Tibbitt, M. W., & Anseth, K. S. (2009). Hydrogels as extracellular matrix mimics for 3D cell culture. *Biotechnol Bioeng, 103*(4), 655-663. doi:10.1002/bit.22361

Tomita, A., Towatari, M., Tsuzuki, S., Hayakawa, F., Kosugi, H., Tamai, K., Miyazaki, T., Kinoshita, T., & Saito, H. (2000). c-Myb acetylation at the carboxyl-terminal conserved domain by transcriptional co-activator p300. *Oncogene, 19*(3), 444-451. doi:10.1038/sj.onc.1203329

Tong, X., & Coulombe, P. A. (2006). Keratin 17 modulates hair follicle cycling in a TNFalpha-dependent fashion. *Genes Dev, 20*(10), 1353-1364. doi:10.1101/gad.1387406

Toscani, A., Mettus, R. V., Coupland, R., Simpkins, H., Litvin, J., Orth, J., Hatton, K. S., & Reddy, E. P. (1997). Arrest of spermatogenesis and defective breast development in mice lacking A-myb. *Nature, 386*(6626), 713-717. doi:10.1038/386713a0

Tournier, C., Dong, C., Turner, T. K., Jones, S. N., Flavell, R. A., & Davis, R. J. (2001). MKK7 is an essential component of the JNK signal transduction pathway activated by proinflammatory cytokines. *Genes Dev, 15*(11), 1419-1426. doi:10.1101/gad.888501

Trauth, K., Mutschler, B., Jenkins, N. A., Gilbert, D. J., Copeland, N. G., & Klempnauer, K. H. (1994). Mouse A-myb encodes a trans-activator and is expressed in mitotically active cells of the developing central nervous system, adult testis and B lymphocytes. *EMBO J, 13*(24), 5994-6005.

Tripathy, S. M., Somu, T. N., Sundaram, M., & Sadhiya, S. (2015). Malignant Cylindroma of Post Aural Region Involving the Temporal Bone. *J Clin Diagn Res, 9*(7), Md01-02. doi:10.7860/jcdr/2015/13682.6232

Trompouki, E., Hatzivassiliou, E., Tsichritzis, T., Farmer, H., Ashworth, A., & Mosialos, G. (2003). CYLD is a deubiquitinating enzyme that negatively regulates NF-kappaB activation by TNFR family members. *Nature, 424*(6950), 793-796. doi:10.1038/nature01803

Trompouki, E., Tsagaratou, A., Kosmidis, S. K., Dolle, P., Qian, J., Kontoyiannis, D. L., Cardoso, W. V., & Mosialos, G. (2009). Truncation of the catalytic domain of the cylindromatosis tumor suppressor impairs lung maturation. *Neoplasia, 11*(5), 469-476.

Troyanovsky, S. M., Guelstein, V. I., Tchipysheva, T. A., Krutovskikh, V. A., & Bannikov, G. A. (1989). Patterns of expression of keratin 17 in human epithelia: dependency on cell position. *J Cell Sci, 93 (Pt 3)*, 419-426.

Truzzi, F., Marconi, A., Atzei, P., Panza, M. C., Lotti, R., Dallaglio, K., Tiberio, R., Palazzo, E., Vaschieri, C., & Pincelli, C. (2011). p75 neurotrophin receptor mediates apoptosis in transit-amplifying cells and its overexpression restores cell death in psoriatic keratinocytes. *Cell Death Differ, 18*(6), 948-958. doi:10.1038/cdd.2010.162

Truzzi, F., Marconi, A., Lotti, R., Dallaglio, K., French, L. E., Hempstead, B. L., & Pincelli, C. (2008). Neurotrophins and their receptors stimulate melanoma cell proliferation and migration. *J Invest Dermatol, 128*(8), 2031-2040. doi:10.1038/jid.2008.21

Tsai, Y. F., Tseng, L. M., Hsu, C. Y., Yang, M. H., Chiu, J. H., & Shyr, Y. M. (2017). Brain-derived neurotrophic factor (BDNF) -TrKB signaling modulates cancer-endothelial cells interaction and affects the outcomes of triple negative breast cancer. *PLoS One, 12*(6), e0178173. doi:10.1371/journal.pone.0178173

Tsao, M. C., Walthall, B. J., & Ham, R. G. (1982). Clonal growth of normal human epidermal keratinocytes in a defined medium. *J Cell Physiol, 110*(2), 219-229. doi:10.1002/jcp.1041100217

Tsoulfas, P., Soppet, D., Escandon, E., Tessarollo, L., Mendoza-Ramirez, J. L., Rosenthal, A., Nikolics, K., & Parada, L. F. (1993). The rat trkC locus encodes multiple neurogenic receptors that exhibit differential response to neurotrophin-3 in PC12 cells. *Neuron, 10*(5), 975-990.

Tu, K., Liu, Z., Yao, B., Xue, Y., Xu, M., Dou, C., Yin, G., & Wang, J. (2016). BCL-3 promotes the tumor growth of hepatocellular carcinoma by regulating cell proliferation and the cell cycle through cyclin D1. *Oncol Rep, 35*(4), 2382-2390. doi:10.3892/or.2016.4616

Tunggal, L., Ravaux, J., Pesch, M., Smola, H., Krieg, T., Gaill, F., Sasaki, T., Timpl, R., Mauch, C., & Aumailley, M. (2002). Defective laminin 5 processing in cylindroma cells. *Am J Pathol, 160*(2), 459-468. doi:10.1016/s0002-9440(10)64865-1

Uede, K., Yamamoto, Y., & Furukawa, F. (2004). Brooke-Spiegler syndrome associated with cylindroma, trichoepithelioma, spiradenoma, and syringoma. *J Dermatol, 31*(1), 32-38.

Ultsch, M. H., Wiesmann, C., Simmons, L. C., Henrich, J., Yang, M., Reilly, D., Bass, S. H., & de Vos, A. M. (1999). Crystal structures of the neurotrophin-binding domain of TrkA, TrkB and TrkC. *J Mol Biol, 290*(1), 149-159. doi:10.1006/jmbi.1999.2816

Underwood, C. K., & Coulson, E. J. (2008). The p75 neurotrophin receptor. *Int J Biochem Cell Biol, 40*(9), 1664-1668. doi:10.1016/j.biocel.2007.06.010

Urbanik, T., Kohler, B. C., Boger, R. J., Worns, M. A., Heeger, S., Otto, G., Hovelmeyer, N., Galle, P. R., Schuchmann, M., Waisman, A., & Schulze-Bergkamen, H. (2011). Down-regulation of CYLD as a trigger for NF-kappaB activation and a mechanism of apoptotic resistance in hepatocellular carcinoma cells. *Int J Oncol, 38*(1), 121-131.

Uren, R. T., & Turnley, A. M. (2014). Regulation of neurotrophin receptor (Trk) signaling: suppressor of cytokine signaling 2 (SOCS2) is a new player. *Front Mol Neurosci, 7*, 39. doi:10.3389/fnmol.2014.00039

Urfer, R., Tsoulfas, P., O'Connell, L., Shelton, D. L., Parada, L. F., & Presta, L. G. (1995). An immunoglobulin-like domain determines the specificity of neurotrophin receptors. *EMBO J, 14*(12), 2795-2805.

Uttarkar, S., Dukare, S., Bopp, B., Goblirsch, M., Jose, J., & Klempnauer, K. H. (2015). Naphthol AS-E Phosphate Inhibits the Activity of the Transcription Factor Myb by Blocking the Interaction with the KIX Domain of the Coactivator p300. *Mol Cancer Ther, 14*(6), 1276-1285. doi:10.1158/1535-7163.mct-14-0662

Uttarkar, S., Frampton, J., & Klempnauer, K. H. (2017). Targeting the transcription factor Myb by small-molecule inhibitors. *Exp Hematol, 47*, 31-35. doi:10.1016/j.exphem.2016.12.003

Uttarkar, S., Piontek, T., Dukare, S., Schomburg, C., Schlenke, P., Berdel, W. E., Muller-Tidow, C., Schmidt, T. J., & Klempnauer, K. H. (2016). Small-Molecule Disruption of the Myb/p300 Cooperation Targets Acute Myeloid Leukemia Cells. *Mol Cancer Ther, 15*(12), 2905-2915. doi:10.1158/1535-7163.mct-16-0185

Vaillant, A. R., Mazzoni, I., Tudan, C., Boudreau, M., Kaplan, D. R., & Miller, F. D. (1999). Depolarization and neurotrophins converge on the phosphatidylinositol 3-kinase-Akt pathway to synergistically regulate neuronal survival. *J Cell Biol, 146*(5), 955-966.

Valdez, G., Akmentin, W., Philippidou, P., Kuruvilla, R., Ginty, D. D., & Halegoua, S. (2005). Pincher-mediated macroendocytosis underlies retrograde signaling by neurotrophin receptors. *J Neurosci, 25*(21), 5236-5247. doi:10.1523/jneurosci.5104-04.2005

Valdez, G., Philippidou, P., Rosenbaum, J., Akmentin, W., Shao, Y., & Halegoua, S. (2007). Trk-signaling endosomes are generated by Rac-dependent macroendocytosis. *Proc Natl Acad Sci U S A, 104*(30), 12270-12275. doi:10.1073/pnas.0702819104

Valenta, T., Hausmann, G., & Basler, K. (2012). The many faces and functions of beta-catenin. *EMBO J, 31*(12), 2714-2736. doi:10.1038/emboj.2012.150

Valenzuela, D. M., Maisonpierre, P. C., Glass, D. J., Rojas, E., Nunez, L., Kong, Y., Gies, D. R., Stitt, T. N., Ip, N. Y., & Yancopoulos, G. D. (1993). Alternative forms of rat TrkC with different functional capabilities. *Neuron, 10*(5), 963-974.

Valley, M., Zimprich, C. A., & Lazar, D. F. (2014, May 2014). CellTiter-Glo® 3D: A Sensitive, Accurate Viability Assay for 3D Cell Cultures. Retrieved from http://www.promega.co.uk/resources/pubhub/a-cell-viability-assay-for-3d-cultures/

van Andel, H., Kocemba, K. A., de Haan-Kramer, A., Mellink, C. H., Piwowar, M., Broijl, A., van Duin, M., Sonneveld, P., Maurice, M. M., Kersten, M. J., Spaargaren, M., & Pals, S. T. (2017). Loss of CYLD expression unleashes Wnt signaling in multiple

myeloma and is associated with aggressive disease. *Oncogene, 36*(15), 2105-2115. doi:10.1038/onc.2016.368

van Balkom, I. D., & Hennekam, R. C. (1994). Dermal eccrine cylindromatosis. *J Med Genet, 31*(4), 321-324.

van der Putte, S. C. (1995). The pathogenesis of familial multiple cylindromas, trichoepitheliomas, milia, and spiradenomas. *Am J Dermatopathol, 17*(3), 271-280.

van Dijk, M., Goransson, S. A., & Stromblad, S. (2013). Cell to extracellular matrix interactions and their reciprocal nature in cancer. *Exp Cell Res, 319*(11), 1663-1670. doi:10.1016/j.yexcr.2013.02.006

Vanecek, T., Halbhuber, Z., Kacerovska, D., Martinek, P., Sedivcova, M., Carr, R. A., Slouka, D., Michal, M., & Kazakov, D. V. (2014). Large germline deletions of the CYLD gene in patients with Brooke-Spiegler syndrome and multiple familial trichoepithelioma. *Am J Dermatopathol, 36*(11), 868-874. doi:10.1097/dad.0000000000000068

Vanhecke, E., Adriaenssens, E., Verbeke, S., Meignan, S., Germain, E., Berteaux, N., Nurcombe, V., Le Bourhis, X., & Hondermarck, H. (2011). Brain-derived neurotrophic factor and neurotrophin-4/5 are expressed in breast cancer and can be targeted to inhibit tumor cell survival. *Clin Cancer Res, 17*(7), 1741-1752. doi:10.1158/1078-0432.ccr-10-1890

Vega, J. A., Garcia-Suarez, O., Hannestad, J., Perez-Perez, M., & Germana, A. (2003). Neurotrophins and the immune system. *J Anat, 203*(1), 1-19.

Verhoeft, K. R., Ngan, H. L., & Lui, V. W. Y. (2016). The cylindromatosis (CYLD) gene and head and neck tumorigenesis. *Cancers of the Head & Neck, 1*(1), 10. doi:10.1186/s41199-016-0012-y

Vernon, H. J., Olsen, E. A., & Vollmer, R. T. (1988). Autosomal dominant multiple cylindromas associated with solitary lung cylindroma. *J Am Acad Dermatol, 19*(2 Pt 2), 397-400.

Vesela, B., Svandova, E., Smarda, J., & Matalova, E. (2014). Mybs in mouse hair follicle development. *Tissue Cell, 46*(5), 352-355. doi:10.1016/j.tice.2014.06.006

Vicario, A., Kisiswa, L., Tann, J. Y., Kelly, C. E., & Ibanez, C. F. (2015). Neuron-type-specific signaling by the p75NTR death receptor is regulated by differential proteolytic cleavage. *J Cell Sci, 128*(8), 1507-1517. doi:10.1242/jcs.161745

Vijg, J., & Dolle, M. E. (2002). Large genome rearrangements as a primary cause of aging. *Mech Ageing Dev, 123*(8), 907-915.

Vijg, J., & Suh, Y. (2013). Genome instability and aging. *Annu Rev Physiol, 75*, 645-668. doi:10.1146/annurev-physiol-030212-183715

Vilar, M., Charalampopoulos, I., Kenchappa, R. S., Simi, A., Karaca, E., Reversi, A., Choi, S., Bothwell, M., Mingarro, I., Friedman, W. J., Schiavo, G., Bastiaens, P. I., Verveer, P. J., Carter, B. D., & Ibanez, C. F. (2009). Activation of the p75 neurotrophin receptor through conformational rearrangement of disulphide-linked receptor dimers. *Neuron, 62*(1), 72-83. doi:10.1016/j.neuron.2009.02.020

Virtanen, C., Ishikawa, Y., Honjoh, D., Kimura, M., Shimane, M., Miyoshi, T., Nomura, H., & Jones, M. H. (2002). Integrated classification of lung tumors and cell lines by expression profiling. *Proc Natl Acad Sci U S A, 99*(19), 12357-12362. doi:10.1073/pnas.192240599

Vollmers, A., Wallace, L., Fullard, N., Hoher, T., Alexander, M. D., & Reichelt, J. (2012). Two- and three-dimensional culture of keratinocyte stem and precursor cells

derived from primary murine epidermal cultures. *Stem Cell Rev, 8*(2), 402-413. doi:10.1007/s12015-011-9314-y

von Schack, D., Casademunt, E., Schweigreiter, R., Meyer, M., Bibel, M., & Dechant, G. (2001). Complete ablation of the neurotrophin receptor p75NTR causes defects both in the nervous and the vascular system. *Nat Neurosci, 4*(10), 977-978. doi:10.1038/nn730

Wagner, N., Wagner, K. D., Theres, H., Englert, C., Schedl, A., & Scholz, H. (2005). Coronary vessel development requires activation of the TrkB neurotrophin receptor by the Wilms' tumor transcription factor Wt1. *Genes Dev, 19*(21), 2631-2642. doi:10.1101/gad.346405

Wakahara, R., Kunimoto, H., Tanino, K., Kojima, H., Inoue, A., Shintaku, H., & Nakajima, K. (2012). Phospho-Ser727 of STAT3 regulates STAT3 activity by enhancing dephosphorylation of phospho-Tyr705 largely through TC45. *Genes Cells, 17*(2), 132-145. doi:10.1111/j.1365-2443.2011.01575.x

Wallace, L., & Reichelt, J. (2013). Using 3D culture to investigate the role of mechanical signaling in keratinocyte stem cells. *Methods Mol Biol, 989*, 153-164. doi:10.1007/978-1-62703-330-5_13

Wang, C., Deng, L., Hong, M., Akkaraju, G. R., Inoue, J., & Chen, Z. J. (2001). TAK1 is a ubiquitin-dependent kinase of MKK and IKK. *Nature, 412*(6844), 346-351. doi:10.1038/35085597

Wang, L., Baiocchi, R. A., Pal, S., Mosialos, G., Caligiuri, M., & Sif, S. (2005). The BRG1- and hBRM-associated factor BAF57 induces apoptosis by stimulating expression of the cylindromatosis tumor suppressor gene. *Mol Cell Biol, 25*(18), 7953-7965. doi:10.1128/mcb.25.18.7953-7965.2005

Wang, S., Bray, P., McCaffrey, T., March, K., Hempstead, B. L., & Kraemer, R. (2000). p75(NTR) mediates neurotrophin-induced apoptosis of vascular smooth muscle cells. *Am J Pathol, 157*(4), 1247-1258. doi:10.1016/s0002-9440(10)64640-8

Wang, X., Sun, L., Maffini, M. V., Soto, A., Sonnenschein, C., & Kaplan, D. L. (2010). A complex 3D human tissue culture system based on mammary stromal cells and silk scaffolds for modeling breast morphogenesis and function. *Biomaterials, 31*(14), 3920-3929. doi:10.1016/j.biomaterials.2010.01.118

Watson, F. L., Heerssen, H. M., Bhattacharyya, A., Klesse, L., Lin, M. Z., & Segal, R. A. (2001). Neurotrophins use the Erk5 pathway to mediate a retrograde survival response. *Nat Neurosci, 4*(10), 981-988. doi:10.1038/nn720

Watt, F. M., Mattey, D. L., & Garrod, D. R. (1984). Calcium-induced reorganization of desmosomal components in cultured human keratinocytes. *J Cell Biol, 99*(6), 2211-2215.

Weber, L., Wick, G., Gebhart, W., Krieg, T., & Timpl, R. (1984). Basement membrane components outline the tumour islands in cylindroma. *Br J Dermatol, 111*(1), 45-51.

Weber, L. V., Al-Refae, K., Wolk, G., Bonatz, G., Altmuller, J., Becker, C., Gisselmann, G., & Hatt, H. (2016). Expression and functionality of TRPV1 in breast cancer cells. *Breast Cancer (Dove Med Press), 8*, 243-252. doi:10.2147/bctt.s121610

Wei, W., Jin, J., Schlisio, S., Harper, J. W., & Kaelin, W. G., Jr. (2005). The v-Jun point mutation allows c-Jun to escape GSK3-dependent recognition and destruction by the Fbw7 ubiquitin ligase. *Cancer Cell, 8*(1), 25-33. doi:10.1016/j.ccr.2005.06.005

Welch, J. P., Wells, R. S., & Kerr, C. B. (1968). Ancell-Spiegler cylindromas (turban tumours) and Brooke-Fordyce Trichoepitheliomas: evidence for a single genetic entity. *J Med Genet, 5*(1), 29-35.

Welcker, M., & Clurman, B. E. (2008). FBW7 ubiquitin ligase: a tumour suppressor at the crossroads of cell division, growth and differentiation. *Nat Rev Cancer, 8*(2), 83-93. doi:10.1038/nrc2290

Wen, Z., Zhong, Z., & Darnell, J. E., Jr. (1995). Maximal activation of transcription by Stat1 and Stat3 requires both tyrosine and serine phosphorylation. *Cell, 82*(2), 241-250.

Weskamp, G., Schlondorff, J., Lum, L., Becherer, J. D., Kim, T. W., Saftig, P., Hartmann, D., Murphy, G., & Blobel, C. P. (2004). Evidence for a critical role of the tumor necrosis factor alpha convertase (TACE) in ectodomain shedding of the p75 neurotrophin receptor (p75NTR). *J Biol Chem, 279*(6), 4241-4249. doi:10.1074/jbc.M307974200

Wickstrom, S. A., Masoumi, K. C., Khochbin, S., Fassler, R., & Massoumi, R. (2010). CYLD negatively regulates cell-cycle progression by inactivating HDAC6 and increasing the levels of acetylated tubulin. *EMBO J, 29*(1), 131-144. doi:10.1038/emboj.2009.317

Wiedemann, F. R., Siemen, D., Mawrin, C., Horn, T. F., & Dietzmann, K. (2006). The neurotrophin receptor TrkB is colocalized to mitochondrial membranes. *Int J Biochem Cell Biol, 38*(4), 610-620. doi:10.1016/j.biocel.2005.10.024

Wiese, S., Digby, M. R., Gunnersen, J. M., Gotz, R., Pei, G., Holtmann, B., Lowenthal, J., & Sendtner, M. (1999). The anti-apoptotic protein ITA is essential for NGF-mediated survival of embryonic chick neurons. *Nat Neurosci, 2*(11), 978-983. doi:10.1038/14777

Wiesmann, C., Ultsch, M. H., Bass, S. H., & de Vos, A. M. (1999). Crystal structure of nerve growth factor in complex with the ligand-binding domain of the TrkA receptor. *Nature, 401*(6749), 184-188. doi:10.1038/43705

Wilczek, C., Chayka, O., Plachetka, A., & Klempnauer, K. H. (2009). Myb-induced chromatin remodeling at a dual enhancer/promoter element involves non-coding rna transcription and is disrupted by oncogenic mutations of v-myb. *J Biol Chem, 284*(51), 35314-35324. doi:10.1074/jbc.M109.066175

Williams, S. E., Beronja, S., Pasolli, H. A., & Fuchs, E. (2011). Asymmetric cell divisions promote Notch-dependent epidermal differentiation. *Nature, 470*(7334), 353-358. doi:10.1038/nature09793

Wilson, A., & Radtke, F. (2006). Multiple functions of Notch signaling in self-renewing organs and cancer. *FEBS Lett, 580*(12), 2860-2868. doi:10.1016/j.febslet.2006.03.024

Wilson, W. R., & Hay, M. P. (2011). Targeting hypoxia in cancer therapy. *Nat Rev Cancer, 11*(6), 393-410. doi:10.1038/nrc3064

Wong, A. L., Soo, R. A., Tan, D. S., Lee, S. C., Lim, J. S., Marban, P. C., Kong, L. R., Lee, Y. J., Wang, L. Z., Thuya, W. L., Soong, R., Yee, M. Q., Chin, T. M., Cordero, M. T., Asuncion, B. R., Pang, B., Pervaiz, S., Hirpara, J. L., Sinha, A., Xu, W. W., Yuasa, M., Tsunoda, T., Motoyama, M., Yamauchi, T., & Goh, B. C. (2015). Phase I and biomarker study of OPB-51602, a novel signal transducer and activator of transcription (STAT) 3 inhibitor, in patients with refractory solid malignancies. *Ann Oncol, 26*(5), 998-1005. doi:10.1093/annonc/mdv026

Wong, A. L. A., Hirpara, J. L., Pervaiz, S., Eu, J. Q., Sethi, G., & Goh, B. C. (2017). Do STAT3 inhibitors have potential in the future for cancer therapy? *Expert Opin Investig Drugs, 26*(8), 883-887. doi:10.1080/13543784.2017.1351941

Wong, J., & Garner, B. (2012). Evidence that truncated TrkB isoform, TrkB-Shc can regulate phosphorylated TrkB protein levels. *Biochem Biophys Res Commun, 420*(2), 331-335. doi:10.1016/j.bbrc.2012.02.159

Woo, C. H., Sopchak, L., & Lipsick, J. S. (1998). Overexpression of an alternatively spliced form of c-Myb results in increases in transactivation and transforms avian myelomonoblasts. *J Virol, 72*(8), 6813-6821.

Wooten, M. W., Seibenhener, M. L., Mamidipudi, V., Diaz-Meco, M. T., Barker, P. A., & Moscat, J. (2001). The atypical protein kinase C-interacting protein p62 is a scaffold for NF-kappaB activation by nerve growth factor. *J Biol Chem, 276*(11), 7709-7712. doi:10.1074/jbc.C000869200

Wright, A., Reiley, W. W., Chang, M., Jin, W., Lee, A. J., Zhang, M., & Sun, S. C. (2007). Regulation of early wave of germ cell apoptosis and spermatogenesis by deubiquitinating enzyme CYLD. *Dev Cell, 13*(5), 705-716. doi:10.1016/j.devcel.2007.09.007

Xia, Z. P., Sun, L., Chen, X., Pineda, G., Jiang, X., Adhikari, A., Zeng, W., & Chen, Z. J. (2009). Direct activation of protein kinases by unanchored polyubiquitin chains. *Nature, 461*(7260), 114-119. doi:10.1038/nature08247

Xie, S., Chen, M., Gao, S., Zhong, T., Zhou, P., Li, D., Zhou, J., Gao, J., & Liu, M. (2017). The B-box module of CYLD is responsible for its intermolecular interaction and cytoplasmic localization. *Oncotarget, 8*(31), 50889-50895. doi:10.18632/oncotarget.15142

Yaar, M., Eller, M. S., DiBenedetto, P., Reenstra, W. R., Zhai, S., McQuaid, T., Archambault, M., & Gilchrest, B. A. (1994). The trk family of receptors mediates nerve growth factor and neurotrophin-3 effects in melanocytes. *J Clin Invest, 94*(4), 1550-1562. doi:10.1172/jci117496

Yacoubian, T. A., & Lo, D. C. (2000). Truncated and full-length TrkB receptors regulate distinct modes of dendritic growth. *Nat Neurosci, 3*(4), 342-349. doi:10.1038/73911

Yamada, M., Ohnishi, H., Sano, S., Nakatani, A., Ikeuchi, T., & Hatanaka, H. (1997). Insulin receptor substrate (IRS)-1 and IRS-2 are tyrosine-phosphorylated and associated with phosphatidylinositol 3-kinase in response to brain-derived neurotrophic factor in cultured cerebral cortical neurons. *J Biol Chem, 272*(48), 30334-30339.

Yamashita, T., & Tohyama, M. (2003). The p75 receptor acts as a displacement factor that releases Rho from Rho-GDI. *Nat Neurosci, 6*(5), 461-467. doi:10.1038/nn1045

Yamashita, T., Tucker, K. L., & Barde, Y. A. (1999). Neurotrophin binding to the p75 receptor modulates Rho activity and axonal outgrowth. *Neuron, 24*(3), 585-593.

Yang, Y., Liu, M., Li, D., Ran, J., Gao, J., Suo, S., Sun, S. C., & Zhou, J. (2014). CYLD regulates spindle orientation by stabilizing astral microtubules and promoting dishevelled-NuMA-dynein/dynactin complex formation. *Proc Natl Acad Sci U S A, 111*(6), 2158-2163. doi:10.1073/pnas.1319341111

Yang, Y., Ran, J., Liu, M., Li, D., Li, Y., Shi, X., Meng, D., Pan, J., Ou, G., Aneja, R., Sun, S. C., & Zhou, J. (2014). CYLD mediates ciliogenesis in multiple organs by deubiquitinating Cep70 and inactivating HDAC6. *Cell Res, 24*(11), 1342-1353. doi:10.1038/cr.2014.136

Yang, Y., & Zhou, J. (2016). CYLD - a deubiquitylase that acts to fine-tune microtubule properties and functions. *J Cell Sci, 129*(12), 2289-2295. doi:10.1242/jcs.183319

Yano, H., Cong, F., Birge, R. B., Goff, S. P., & Chao, M. V. (2000). Association of the Abl tyrosine kinase with the Trk nerve growth factor receptor. *J Neurosci Res, 59*(3), 356-364.

Yau, R., & Rape, M. (2016). The increasing complexity of the ubiquitin code. *Nat Cell Biol, 18*(6), 579-586. doi:10.1038/ncb3358

Yeiser, E. C., Rutkoski, N. J., Naito, A., Inoue, J., & Carter, B. D. (2004). Neurotrophin signaling through the p75 receptor is deficient in traf6-/- mice. *J Neurosci, 24*(46), 10521-10529. doi:10.1523/jneurosci.1390-04.2004

Yin, B., Ma, Z. Y., Zhou, Z. W., Gao, W. C., Du, Z. G., Zhao, Z. H., & Li, Q. Q. (2015). The TrkB+ cancer stem cells contribute to post-chemotherapy recurrence of triple-negative breast cancers in an orthotopic mouse model. *Oncogene, 34*(6), 761-770. doi:10.1038/onc.2014.8

Yokouchi, M., Kondo, T., Houghton, A., Bartkiewicz, M., Horne, W. C., Zhang, H., Yoshimura, A., & Baron, R. (1999). Ligand-induced ubiquitination of the epidermal growth factor receptor involves the interaction of the c-Cbl RING finger and UbcH7. *J Biol Chem, 274*(44), 31707-31712.

Yoon, S. O., Casaccia-Bonnefil, P., Carter, B., & Chao, M. V. (1998). Competitive signaling between TrkA and p75 nerve growth factor receptors determines cell survival. *J Neurosci, 18*(9), 3273-3281.

York, R. D., Molliver, D. C., Grewal, S. S., Stenberg, P. E., McCleskey, E. W., & Stork, P. J. (2000). Role of phosphoinositide 3-kinase and endocytosis in nerve growth factor-induced extracellular signal-regulated kinase activation via Ras and Rap1. *Mol Cell Biol, 20*(21), 8069-8083.

Yoshida, H., Jono, H., Kai, H., & Li, J. D. (2005). The tumor suppressor cylindromatosis (CYLD) acts as a negative regulator for toll-like receptor 2 signaling via negative cross-talk with TRAF6 AND TRAF7. *J Biol Chem, 280*(49), 41111-41121. doi:10.1074/jbc.M509526200

Yu, H., Lee, H., Herrmann, A., Buettner, R., & Jove, R. (2014). Revisiting STAT3 signalling in cancer: new and unexpected biological functions. *Nat Rev Cancer, 14*(11), 736-746. doi:10.1038/nrc3818

Yu, T., Calvo, L., Anta, B., Lopez-Benito, S., Lopez-Bellido, R., Vicente-Garcia, C., Tessarollo, L., Rodriguez, R. E., & Arevalo, J. C. (2014). In vivo regulation of NGF-mediated functions by Nedd4-2 ubiquitination of TrkA. *J Neurosci, 34*(17), 6098-6106. doi:10.1523/jneurosci.4271-13.2014

Yu, T., Calvo, L., Anta, B., Lopez-Benito, S., Southon, E., Chao, M. V., Tessarollo, L., & Arevalo, J. C. (2011). Regulation of trafficking of activated TrkA is critical for NGF-mediated functions. *Traffic, 12*(4), 521-534. doi:10.1111/j.1600-0854.2010.01156.x

Yuan, X. B., Jin, M., Xu, X., Song, Y. Q., Wu, C. P., Poo, M. M., & Duan, S. (2003). Signalling and crosstalk of Rho GTPases in mediating axon guidance. *Nat Cell Biol, 5*(1), 38-45. doi:10.1038/ncb895

Zamansky, G. B., Nguyen, U., & Chou, I. N. (1991). An immunofluorescence study of the calcium-induced coordinated reorganization of microfilaments, keratin intermediate filaments, and microtubules in cultured human epidermal keratinocytes. *J Invest Dermatol, 97*(6), 985-994.

Zanoni, M., Piccinini, F., Arienti, C., Zamagni, A., Santi, S., Polico, R., Bevilacqua, A., & Tesei, A. (2016). 3D tumor spheroid models for in vitro therapeutic screening: a

systematic approach to enhance the biological relevance of data obtained. *Sci Rep, 6*, 19103. doi:10.1038/srep19103

Zegers, M. M., O'Brien, L. E., Yu, W., Datta, A., & Mostov, K. E. (2003). Epithelial polarity and tubulogenesis in vitro. *Trends Cell Biol, 13*(4), 169-176.

Zhan, T., Rindtorff, N., & Boutros, M. (2017). Wnt signaling in cancer. *Oncogene, 36*(11), 1461-1473. doi:10.1038/onc.2016.304

Zhang, J., Stirling, B., Temmerman, S. T., Ma, C. A., Fuss, I. J., Derry, J. M., & Jain, A. (2006). Impaired regulation of NF-kappaB and increased susceptibility to colitis-associated tumorigenesis in CYLD-deficient mice. *J Clin Invest, 116*(11), 3042-3049. doi:10.1172/jci28746

Zhang, M., Wu, X., Lee, A. J., Jin, W., Chang, M., Wright, A., Imaizumi, T., & Sun, S. C. (2008). Regulation of IkappaB kinase-related kinases and antiviral responses by tumor suppressor CYLD. *J Biol Chem, 283*(27), 18621-18626. doi:10.1074/jbc.M801451200

Zhang, Q., Lenardo, M. J., & Baltimore, D. (2017). 30 Years of NF-kappaB: A Blossoming of Relevance to Human Pathobiology. *Cell, 168*(1-2), 37-57. doi:10.1016/j.cell.2016.12.012

Zhang, X. J., Liang, Y. H., He, P. P., Yang, S., Wang, H. Y., Chen, J. J., Yuan, W. T., Xu, S. J., Cui, Y., & Huang, W. (2004). Identification of the cylindromatosis tumor-suppressor gene responsible for multiple familial trichoepithelioma. *J Invest Dermatol, 122*(3), 658-664. doi:10.1111/j.0022-202X.2004.22321.x

Zhang, Y., Moheban, D. B., Conway, B. R., Bhattacharyya, A., & Segal, R. A. (2000). Cell surface Trk receptors mediate NGF-induced survival while internalized receptors regulate NGF-induced differentiation. *J Neurosci, 20*(15), 5671-5678.

Zhao, H., Kalota, A., Jin, S., & Gewirtz, A. M. (2009). The c-myb proto-oncogene and microRNA-15a comprise an active autoregulatory feedback loop in human hematopoietic cells. *Blood, 113*(3), 505-516. doi:10.1182/blood-2008-01-136218

Zhao, L., Glazov, E. A., Pattabiraman, D. R., Al-Owaidi, F., Zhang, P., Brown, M. A., Leo, P. J., & Gonda, T. J. (2011). Integrated genome-wide chromatin occupancy and expression analyses identify key myeloid pro-differentiation transcription factors repressed by Myb. *Nucleic Acids Res, 39*(11), 4664-4679. doi:10.1093/nar/gkr024

Zhong, Z., Wen, Z., & Darnell, J. E., Jr. (1994). Stat3: a STAT family member activated by tyrosine phosphorylation in response to epidermal growth factor and interleukin-6. *Science, 264*(5155), 95-98.

Zhou, Y., & Ness, S. A. (2011). Myb proteins: angels and demons in normal and transformed cells. *Front Biosci (Landmark Ed), 16*, 1109-1131.

Zuo, Y. G., Xu, Y., Wang, B., Liu, Y. H., Qu, T., Fang, K., & Ho, M. G. (2007). A novel mutation of CYLD in a Chinese family with multiple familial trichoepithelioma and no CYLD protein expression in the tumour tissue. *Br J Dermatol, 157*(4), 818-821. doi:10.1111/j.1365-2133.2007.08081.x